LAMP Final report

Low Altitude Modular Platform: A small satellite platform for earth observation in a VLEO orbit.

DSE Group 23

Delft University of Technology

TU Delft

LAMP Final report

Low Altitude Modular Platform: A small satellite platform for earth observation in a VLEO orbit.

by

DSE Group 23

Student Name	Student Number
Lodewijk Bakker	5001285
Tim Hogenelst	5084334
Thomas de Jong	4825136
Bastiaan Deul	5056608
Miquel Rull Trinidad	4852575
José Cunha	5216087
Calvin Grootenboer	5208599
Boyan Kolev	5243416
Dragomir Nikolov	5216915
Kamalesh Sriram Ganapathy	5331951

Tutors:	Dr. ir. J. Bouwmeester
Coaches:	Dr. ir. E.J.O. Schrama
	ir. D.J. Groot
Project Duration:	24 April , 2023 - 30 June, 2023
Faculty:	Faculty of Aerospace Engineering, Delft

TU Delft

Executive Summary

Introduction

This summary is about the highlights of the final design of the LAMP (Low Altitude Modular Platform). This report follows the project plan, baseline report and midterm report. This report presents the market analysis for the platform followed by the detailed design of the platform. The design of each subsystem is treated on its own after which the integration, manufacturing and operations of all subsystems are discussed.

The low-altitude modular platform is a versatile satellite platform with a wide range of capabilities. It bridges the gap between small CubeSats and high-end Earth observational satellites, while also flying at 300 Km, enabling higher resolutions in a small form factor.

While the market share of CubeSats has grown a lot in recent years, their capabilities are still limited. Due to practical constraints of miniaturisation, the spacecraft bus platform typically occupies approximately 50% to 80% of the total satellite internal volume. This problem is however remedied with the use of larger satellites, which is the market gap LAMP tries to occupy. It has both the advantages of standardisation, ease of production, and low cost of CubeSats, while also possessing a large payload fraction and the bus capabilities to accommodate a high-end earth observation payload.

LAMP is also innovative in its communication capabilities: It is planned to be the first satellite platform to use the SpaceX Starlink constellation. This gives LAMP unparalleled communication capabilities for an earth observational satellite in its class. LAMP is capable of sending all the information of its design payload (the DST) in livelink. In certain orbits, it is even capable of streaming 1080p 60fps video live to Earth. This opens it for a great number of new applications related to civil, law enforcement, and military surveillance.
The LAMP mission need statement and project objective statements are as follows:

Mission Need Statement

Create a cost-competitive, modular satellite platform for Very Low Earth Orbit observation payloads.

Project Objective Statement

Design a 27U micro-satellite platform which can host different Earth observation payloads from a very low altitude (300 km), cost-effectively.

DSE Objective Statement

Construct a preliminary design of a 27U micro-satellite platform which can host different Earth observation payloads from a very low altitude (300 km), by 10 students in 10 weeks.

Final design

Figure 1 shows a render of LAMP in the configuration for a 9h local time of acsending node sun synchronous orbit. The view looks at the back panel with the cut-out for the thruster. The Deployable Space Telescope (DST) points in the nadir direction and is mounted below the primary structure. On the left hand side of the structure, the Earth shield is deployed which shields the radiator attached.

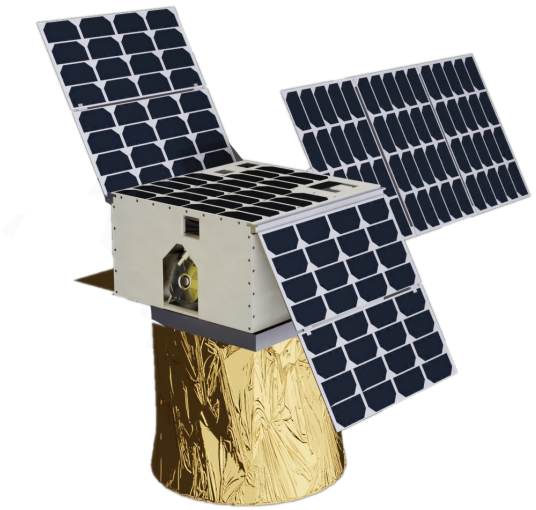

Figure 1: *External view of LAMP with DST payload*

Payload analysis

As a modular Earth observation platform, LAMP will have to be able to accommodate different types of payloads. To achieve this, specifications and requirements of different types of suitable payloads need to be gathered. This was done in three ways: a general payload study, a specific payload study, and a case study of the DST.

It was found that over 90% of Earth observation satellites fly between 90 and 100 degrees inclination, corresponding to a sun-synchronous orbit. The satellite shall thus be designed for such an orbit. Furthermore, the payload volume requirement of at least 16U was deemed reasonable based on smaller CubeSat payload volumes.

From studying the DST, a plastic monitoring payload, a SPEXone-like payload and the Terrahertz payload, the technical requirements on LAMP for the payload were set up. The mass LAMP should be able to carry was put at 30 kg, which aligns with the mass of the DST. In terms of power, three operational modes were decided upon based both upon the analysed payloads and an investigation by the EPS. The modes were divided up into continuous operation and inactive during eclipse. For inactive during eclipse 25 W is available for the payload. Continuous operation is divided into either 5 W or 10 W available to the payload. For the thermal requirement, a range from 200 to 295 K was used. The platform should be able to accommodate this by slight variations in the TCS for different payloads and configurations.

Astrodynamic characteristics

As mentioned above LAMP was designed to fly in sun-synchronous orbits of an inclination 96.7°, and an average altitude of 300 km. The satellite is able to operate in an orbit with any local time of ascension. The aerodynamic properties of LAMP were simulated using a numerical model. The results are compiled in Table 1.

Table 1: *Results of drag simulation for LAMP*

Total ΔV (SF=1.2 + 0.1 for manoeuvres) [m/s]	$F_{aero_{mean}}$ [mN]	$F_{aero_{max}}$ [mN]	Mean duty cycle	Fuel mass [kg]	Fuel volume [U]
1093.5	0.277	0.346	0.0336	4.894	1.00

Guidance, navigation and control subsystem

After choosing an elevation mask and compiling a corresponding link budget it was determined that LAMP will use a miniaturised single frequency single point GPS receiver and a corresponding GPS antenna. The GNS will consist of a Celest GPS receiver and Celest passive L1 GPS patch antenna. The system will use C/A code for tracking, which is expected to significantly outperform the coarse positioning requirement for LAMP. The GNS receiver will need to be integrated on top of a printed circuit board (PCB) in the electronics stack together with the communications transceiver, the on-board computer (OBC) and the power control and distribution unit (PCDU).

Attitude determination and control subsystem

The ADCS consists of a set of sensors and actuators in order to provide attitude determination and control capabilities. After considering multiple combinations of different sensors and actuators the final design will consist of the components that are shown in Table 2. For the sizing of the actuators, an iterative tool was created to help optimise the consecutive sizing of the magnetorquers and the Control Moment Gyros (CMGs) in terms of mass.

Table 2: *List of ADCS components*

ADCS Components	Number
Sensors	
Star Tracker	2
Magnetometer	2
Actuators	
CMG	4
Magnetorquer	3

Thermal control subsystem

For the TCS, a thermal analysis model was created, integrating a radiation simulation from ESATAN-TMS and an in-house built thermal tool. Using this tool, the temperature of spacecraft components was calculated throughout an orbit, summarised in Figure 2. Through an iterative process of updating the thermal model, the TCS strategy was developed and sized, to ensure that the different operating temperatures are met. The TCS contains a mix of passive and active components, with the cooling down of components being done passively through radiation to space, and the heating of the propellant tank and lines being done actively. The components used in the TCS are: white and black paints, Multi Layer Insulation (MLI), thermal tape, a radiator, an Earth-shield, electric heaters, and a heat strap.

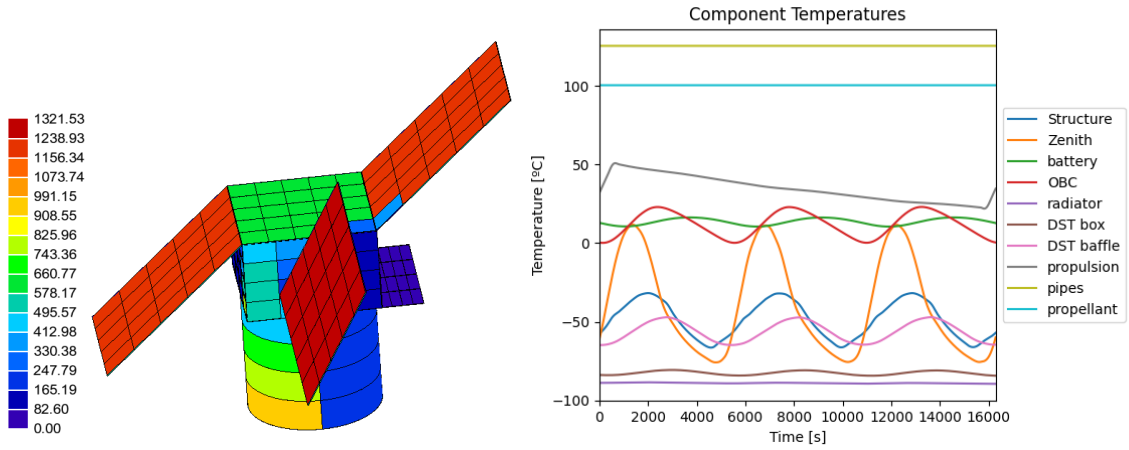

Figure 2: *Radiation analysis (in* $\mathrm{W/m^2}$*) from ESATAN (left) and component temperatures throughout three orbits, calculated using the Python model (right).*

Electric power subsystem

The EPS subsystem sizing has been sized based on continuous and peak power needs of the other subsystems during sun and eclipse. A summary of the sizing results is presented in Table 3 and Table 4:

Table 3: *Summary of EPS component performance*

Item	**Capacity [Wh]**	**Cost [€]**	**Mass [kg]**	**Volume [U]**
Battery 1	155	16250	1.24	0.88
Battery 2	77	10000	0.61	0.44
Item	**Mass [kg]**	**Number of cells**	**Max. P Generated [W]**	**Cost [€] (cell + structure)**
Top Panel	0.689	26	35.8	5200 + 1733
Side Panels	1.696	64	88.3	12 800 + 4000
Side Panels	1.590	60	82.8	12 000 + 4267
Item	**Mass [kg]**	**Efficiency [%]**	**Volume [U]**	**Output blocks support**
PCDU	0.3	96	0.2	Supports [3.3V, 5V, 12V, (4-28V)], max 8A

Table 4: *Series(S)/Parallel(P) cells architecture using IMM-*α*V*$_{mpp}$ = $4.28\,\text{V}$ *and max power per cell P*$_{mpp}$ = $1.38\,\text{V}$*,* $\eta_{cell} = 0.32$

Item	**Cell Configuration**	**Max. Voltage [V]**	**Max. Current [A]**
Side fold	4P, 4S	17.12	1.288
Side array	2 folds in P	17.12	2.576
Front fold	4P, 5S	21.4	1.288
Front array	3 folds in P	21.4	3.864
Top panel con.1	(4P, 3S)	12.84	1.288
Top panel con.2	(3S, (2x5P, 1x4P))	12.84	1.485
Top array	2 connections in P	12.84	2.773

The Power Control and Distribution Unit (PCDU) used is the pumpkin EPMS1, battery 1 is in charge of eclipse operations, while battery 2 is in charge of propulsion operations.

The solar panel deployment angle is dependent on the local time of ascending node for the chosen sun-synchronous orbit with inclination $96.7°$. The deployment angle can be either $0°$, $46°$, $61°$, $72°$, $80°$ or $83°$ with respect to the top panel. The different deployment angles are determined by a retainer in the deployment hinges.

Communications subsystem

A decision was made to use Starlink satellites as a relay system in combination with a high-gain patch antenna placed on the top of the satellite. This decision was made due to the high data throughput and the simplicity and low volume requirement of having a high-gain patch antenna on the top-side of the satellite. To transmit the data, a QPSK 13/45 modulation and a 14.5GHz transmit frequency will be used. The use of Starlink satellites gives a near constant connection, a peak data rate of 180Mbit/s and a stable data rate of 46Mbit/s. This would equate to the ability to stably send 55 lossless compressed images from the DST per second or around two lossless-compressed 4k-images per second. A CubeSat-format Ku-band transceiver that adheres to the requirements generated by the antenna and Starlink connection will be developed in-house.

Software and data handling

For the software and data handling subsystem, it has been decided that the on board computer will be developed and build in-house. Some of the things the on board computer (OBC) needs to do is run algorithms for the ADCS and be able to compute and distribute data and commands for and to all subsystems. Table 5 gives an overview of the components and properties of the OBC that will be built.

Table 5: *OBC overview*

OBC Parameters	
CPU 1	ARM Cortex-A9
CPU 2-4	ARM Cortex-A7
Storage	2TB SSD
Available interfaces	I2C, RS-232, RS-422, RS-485, RJ45 (Ethernet)
Volume	<0.25 U
Mass	<250 [g]
Normal operations Power	2 [W]
Peak Power	4 [W]

Structures

For the structural subsystem, a monocoque concept was selected which consists of load carrying aluminium panels reinforced with stiffeners. The structures interact with the deployer which constraints the geometry and center of gravity location. The width of the structure is equal to 326 mm which is 27 mm less than the maximum allowable width to allow for the solar panels to be folded along the side of the structure. The deployer contains tabs which are used to clamp the satellite during launch and act as a guide when deploying the satellite. These tabs limited the available area for solar array folds to 366$\times$170mm.

To determine the wall thickness and the most suitable aluminium alloy, structural analyses have been performed based on, compression buckling, shear buckling, axial and lateral natural vibration, and thermal expansion. It was found that AL 6061-T6 with a panel thickness of 1.2 mm was sufficient to meet all requirements.

Propulsion

The thruster BHT-100 from Busek has been selected for LAMP. It can operate with both xenon and iodine. The system mass, volume, thrust/power and energy per burn were compared by performing a trade-off, which resulted in selecting iodine as a fuel. The advantages of iodine over the traditional xenon propellant is that it is stored in a solid, powdered form, and is three times denser than xenon. Furthermore, since the fuel does not need to be pressurised, the tanks need not have hemispherical end-caps, which increases the over-all packing efficiency of the platform. The downsides of iodine are the need for active heating to sublime the fuel, as well as its corrosive properties. This limits the choice of materials, as well as the solar panel placement.

System design

To validate the volume budget and to determine the internal configuration of all parts, a CAD model was created. Important considerations for the internal configuration was internal heating by the subsystems, accessibility during assembly and the location of the centre of gravity.

The centre of gravity (c.g.) was estimated to be below the working line of the thruster which would result in a disturbance torque when thrusting. To limit this moment, heavy components like the batteries and propellant tanks were mounted to the zenith panel. Additionally, the thruster is angled by 10.6° which results in an equal moment arm for beginning-of-life and end-of-life centres of gravity.

Technical risk analysis

To increase reliability, a risk analysis has been performed where risks were identified and mitigated. In total 48 risks have been identified, and after applying both likelihood and severity mitigation, no critical risks are present within the design.

Sustainable development

Having a focus on sustainability is a growing trend in the space industry, especially regarding the reduction of space debris. Due to the chosen low-altitude orbital environment, orbits are much less crowded by other spacecraft than slightly higher orbits such as Low Earth Orbit (LEO). Therefore, the occurrence of collisions with existing space debris is considerably lower. This, in combination with the use of natural deorbiting into the atmosphere, greatly decreases the amount of space debris created, improving the sustainability of the mission. Other aspects of sustainable development are also considered, with respect to compliance with UN regulations/recommendations (UNOOSA) but also with existing sustainability rankings such as the Space Sustainability Ranking.

Manufacturing, operations and logistics

The production method chosen is in-demand batch manufacturing, this is due to the number of platforms that are expected to be produced (50+) are more akin to the aircraft industry than the custom spacecraft industry. The assembly will consists of three stations, each station holding a platform for two months, before moving to the next station. This means each platform will be worked on for six months, and the delivery interval will be two months, with a total throughput of six platforms per year.

Product verification, certification and validation

Product tests that are performed include analysis, structural, integration, functional, qualification, payload, environmental and full product launch. Some of these tests, such as the environmental tests, are necessary to be able to launch the platforms. Finally, a demonstration mission is used to validate the whole spacecraft, which can be used to cut back in expensive testing on ground.

Financial analysis

The profitability of the LAMP platform was based on a cost per unit of 300k € with a selling price of 500k €, this results in a break-even point after the sale of 50 platforms after taking development costs into account. The cost of the platform is based upon the cost of commercial of the shelve products of similar capabilities, the working hours put into it, and the money for a demonstration mission. The price per unit was estimated by this approach to be 400k €, which is above the required cost per unit. By upping the selling price to 600k €, the company could break even after 8.3 years by selling 6 platforms per year.

Future recommendations

For the future, a more detailed cost analysis is recommended to be done. This determines whether or not the project is viable or not and it is thus of great importance to the project. Since the approach of using Starlink is novel, it is recommended to contact SpaceX to further work out the details on how this will work. For the thruster assembly, it is recommended to further analyse the internal pressures and the effect of deposition of the iodine in the pipes.

Contents

Nomenclature

ADCS Attitude Determination & Control Subsystem

BRWA Biased Reaction Wheel Assembly

CMG Control Moment Gyroscope

COMMS Communication Subsystem

CoM Centre of Mass

COTS Commercial of the Shelf

DST Deployable Space Telescope

EO Earth Observation

EPS Electrical Power Subsystem

FBS Functional Breakdown Structure

FFD Functional Flow Diagram

FPGA Field Programmable Gate Arrays

GDOP Geometric Dilution of Precision

GNSS Global Navigation Satellite System

GNS Guidance & Navigation Subsystem

HDRM Hold Down & Release Mechanism

LAMP Low Altitude Modular Platform

LEO Low Earth Orbit

LNA Low Noise Amplifier

LTAN Local Time of Ascending Node

MLI Multi-Layer Insulation

OBC Onboard Computer

PCDU Power Conditioning & Distribution Unit

PFCV Proportional Flow Control Valve

RUD Rapid Unscheduled Disassembly

SDH Software & Data Handling

SLI Single-Layer Insulation

SNR Signal-to-noise ratio

SP Solar Panels

SSD Solid State Drive

SSR Space Sustainability Rating

STR Structures

SupMCU Supervisor Micro Controller Unit

TCS Thermal Control Subsystem

TIR Thermal Infrared

TT&C Tracking telemetry & Control

UNOOSA United Nations Office of Outer Space Affairs

VLEO Very Low Earth Orbit

1 Introduction

This chapter contains an introduction to the mission and the design solution. First the mission and project objectives are discussed. Next, the configuration of the platform and the subsystems are introduced. Finally, the structure of this report is presented.

The Mission

The aim of the mission is to unite high-end Earth observation with the growing market trends of miniaturisation of components and the trend towards larger size CubeSats (6u, 12u, and 27u) [1]. For this, a design study of a 27u modular satellite will be done, where the modular part refers to that it should be able to accommodate different high-end Earth observation payloads without significant alterations to the design. To achieve the required performance for high-end Earth observation a very low Earth orbit (VLEO) at 300 km, is needed to compensate for the smaller instrument size [1, 2]. Furthermore, the platform should be cost-competitive to promote adoption of it. All this shall be achieved by LAMP (Low Altitude Modular Platform). From this mission description, the mission need statement, the project objective statement and DSE Objective Statement follow as:

Mission Need Statement

Create a cost-competitive, modular satellite platform for Very Low Earth Orbit observation payloads.

Project Objective Statement

Develop a 27U micro-satellite platform which can host different Earth observation payloads from a very low altitude (300 km), cost-effectively.

DSE Objective Statement

Develop a preliminary design of a 27U micro-satellite platform which can host different Earth observation payloads from a very low altitude (300 km), by 10 students in 10 weeks.

Platform Configuration

A satellite mission is typically split up into two parts, the space segment and the ground segment. These two parts are further divided, with the ground segment being split into the ground station and operations, and the space segment being split between platform and payload. LAMP differs from this norm since it only consists of the platform. However, the potential payloads it will carry and the ground segment need to be taken into account during the design. For the payload, different Earth observation instruments have been researched to establish a set of user and system requirements in terms of mass, power and thermal control to ensure that LAMP can host a variety of payloads.
The purpose and reasons for the inclusion of each subsystem in the platform are as follows:

- **Thermal Control Subsystem (TCS):** subsystem to manage the heat received and emitted by the spacecraft to ensure components and the payload stay within their operating temperature range.
- **Structures and Mechanisms (Str):** subsystem to provide connection points, support and protection from the environment for subsystems and payloads. Environmental hazards could include debris and radiation in VLEO. Mechanisms are moving structures used to deploy or manipulate subsystems such as potential solar panels or antennas.
- **Attitude Determination & Control (ADCS):** Subsystem to provide de-tumbling after deployment, determination of the attitude of the spacecraft, and control of the attitude of the spacecraft. This system includes both sensors and actuators to perform these tasks. This system is needed for the pointing of the payload.
- **Propulsion (Prop):** Subsystem to provide orbit maintenance and control. With the propulsion subsystem, the altitude of the spacecraft can be manipulated. For the VLEO environment, the drag can be very significant, therefore, the propulsion system is crucial to prevent early de-orbit. The propulsion subsystem can also be used to perform potential formation/constellation flying of a spacecraft.
- **Guidance and Navigation (GNS)**: the Navigation (GNS) subsystem is responsible for providing the spacecraft with navigational capabilities. This includes determining the position and velocity of the spacecraft in its orbit. In combination with the propulsion subsystem, it is responsible for maintaining the orbit and determining the manoeuvres needed for the potential formation/constellation flying of a spacecraft.
- **Communication (Comms):** The Communication (Comms) subsystem is responsible for providing the spacecraft with the ability to communicate with other segments of the mission. This includes transmitting payload data to ground stations, receiving telecommands from ground stations and providing a link for spacecraft telemetry.
- **Electrical Power Subsystem (EPS):** Provides the power necessary to supply all other subsystem's power needs. For this, it has to provide power management, storage, and generation.
- **Software & Data Handling (SDH):** The onboard software is responsible for the control of the subsystems and the payloads, management of the communication channels, telemetry generation and telecommand handling, and failure detection, isolation and recovery. On the other hand, onboard data handling is responsible for the storage and distribution of the data.

Report lay-out

First, a functional analysis is performed in Chapter 2 in order to establish system requirements. The user requirements are presented in Chapter 3 after which the market analysis is performed in Chapter 4 to research the use of the platform. Chapter 5 presents the final design including the external and internal configuration, engineering budgets and cost breakdown. Chapter 6 discusses the impact of the VLEO environment on the design. The detailed design of each subsystem is discussed in Chapter 7 to Chapter 14. Thereafter, the complete platform design and integration is presented in Chapter 15. Next, the risk analysis is performed in Chapter 16. Finally, the total system in terms of sustainbility, integration, verification and validation, and financial analysis is discussed in Chapter 17 to Chapter 19.

2

Functional Analysis

The focus of this chapter is dividing and establishing a proper link between all the functions that the spacecraft must perform during it's mission. Functional analysis flows from the user and stakeholder's requirements as stated in Mission Need Statement in Chapter 1. In Section 2.1, the Functional Flow Diagram is presented. In Section 2.2, the Functional Breakdown Diagram is presented.

2.1. Functional Flow Diagram

Throughout its mission lifetime, a spacecraft goes through various mission phases, and during each one, it has to fulfill specific functions. Hence, it is important to identify and organise these functions in order to successfully complete the mission. For this, a functional flow diagram (FFD) is created. FFDs are multi-tiered, time-sequenced, step-by-step graphical representations of the functions that need to be performed.

The whole mission, from development to end of life, is detailed in the FFD. Since the launch and injection into orbit are separate from the mission and will be performed by a different launcher, they are not explained in detail. The FFD additionally includes logic that describes flow control using conditional statements. In the figure, there are other feedback logic loops as well, for instance, when sub-systems are initiated, a system check must be performed to ensure their appropriate operation. If a fault is discovered in their functioning, the sub-system must then be initiated again and re-calibrated. The FFD structure is presented in Figure 2.1.

2.2. Functional Breakdown Structure

A Functional Breakdown Structure (FBS) is an additional tool for outlining the functions of the spacecraft in addition to the FFD. The FBS is an "AND-tree" where each element of the tree is the sum of the components below it which gives a more detailed overview of the functions and corresponding subfunctions. The FBS provides a hierarchical overview of all the processes needed to support the functions above. The IDs for each block are used to link and compare the FFD and FBS. Once again the launch and inject to orbit phases are not included in FBD as it will be performed by a third-party launcher and out of scope for this report. The FBS structure is presented in Figure 2.2.

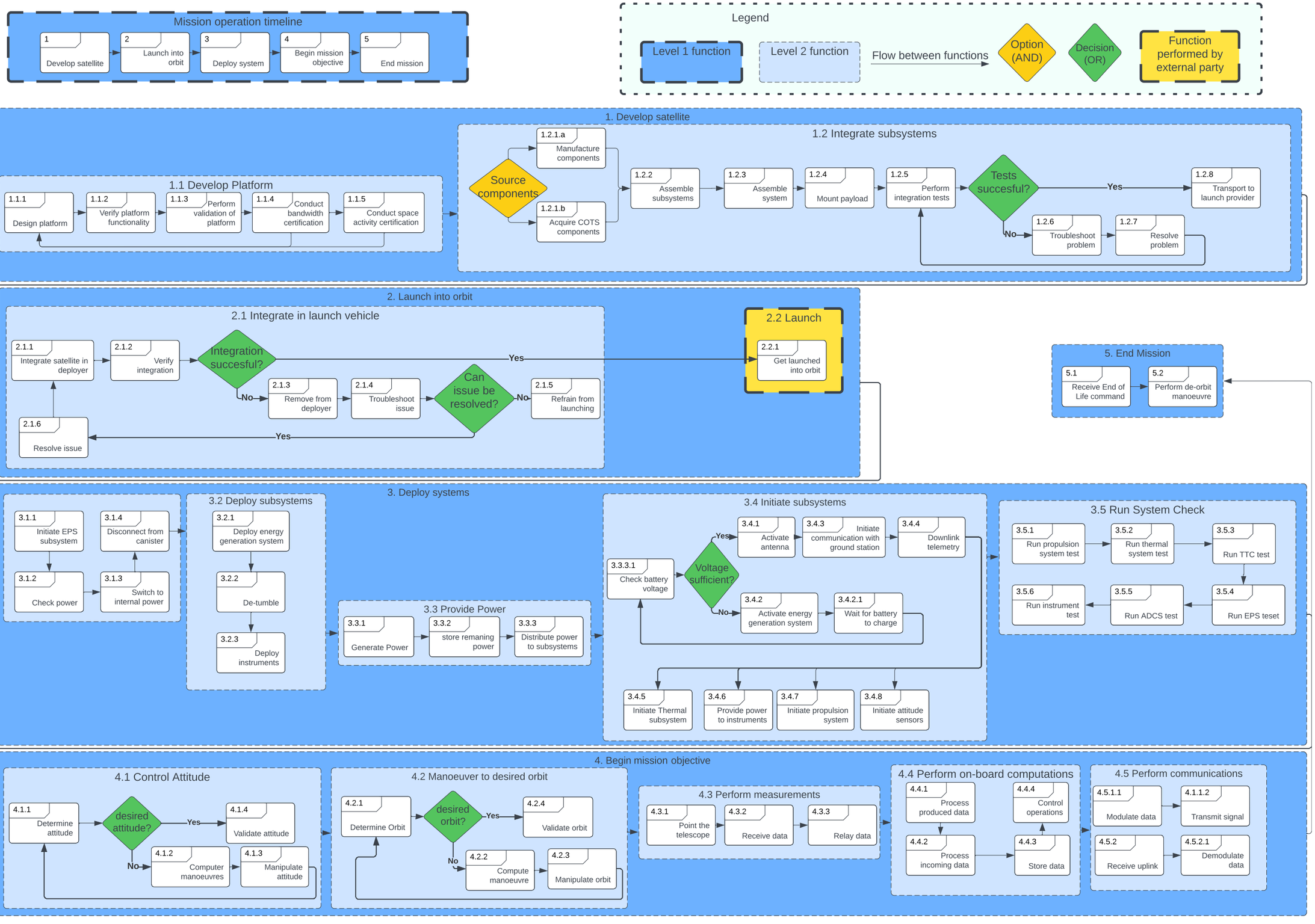

Figure 2.1: *Functional Flow Diagram*

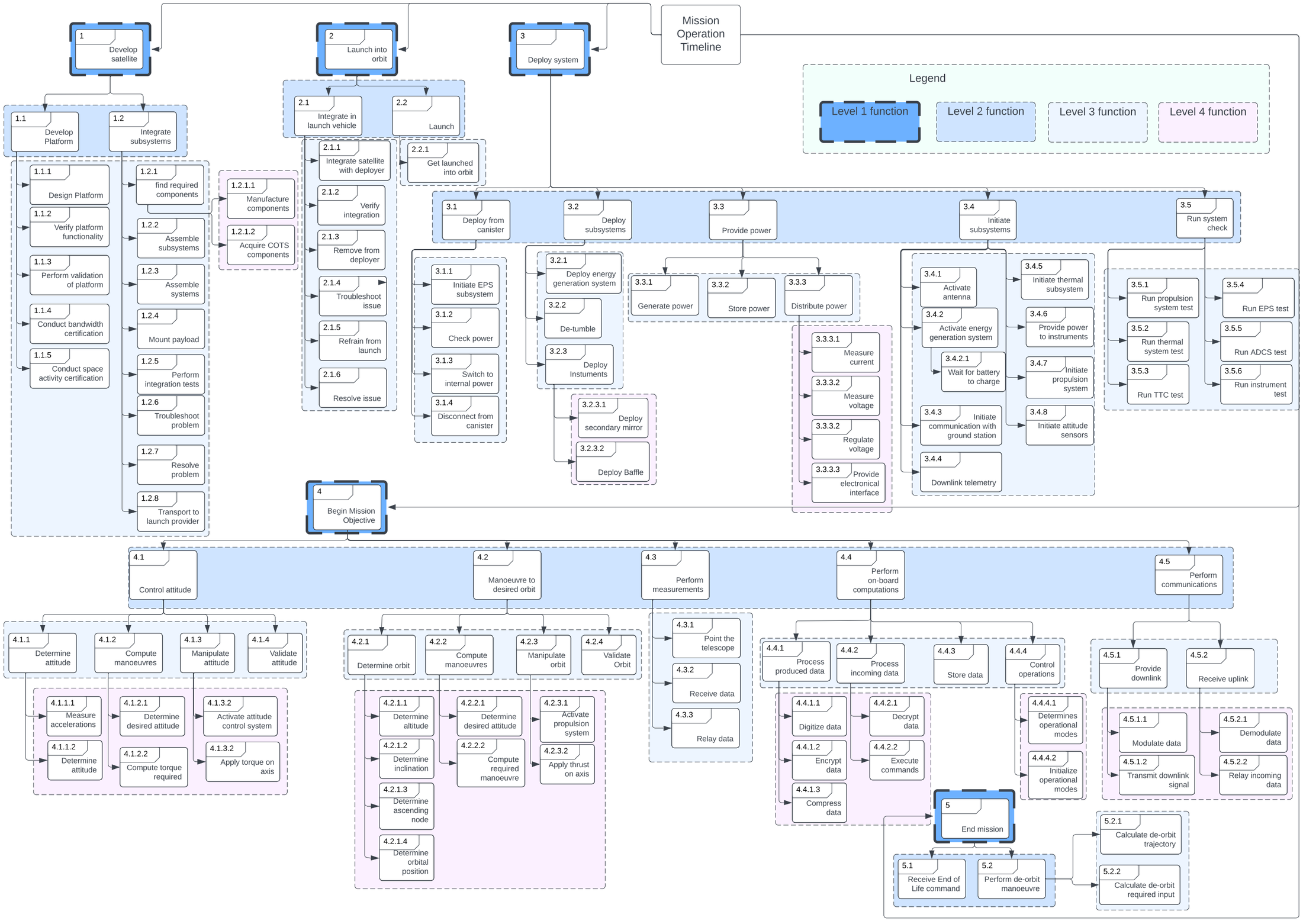

Figure 2.2: *Functional Breakdown Structure*

3 Requirements

In this chapter, LAMP's user requirements are presented as derived from [1]. Some user requirements have already been linked to related subsystems following the abbreviations as presented in Chapter 1. Additionally, requirements related to overall reliability and safety are identified by *ReS*. Each requirement can be verified by different verification methods (Verif. M), either by demonstrating (Demo), analysis (Ana), inspection (Insp) or testing (Test).

Compliance legend

The user requirements, as well as the system requirements in their own subsections, are marked with a colour to represent their compliance/non-compliance or non investigated status.

✓	**Compliant**	Compliance confirmed through investigation
○	**Not investigated**	No investigation was carried out
×	**Non-compliant**	Investigation indicates non-compliance
-	**Not Applicable**	Req. removed or not applicable to current design

Table 3.1: *User requirements for LAMP*

ID	Description	Rationale	Verif. M	
U-Ops-01	The satellite bus platform shall be operational for at least 5 years.	Sets the mission duration and platform lifetime.	Demo	✓
U-Ops-02	The satellite shall be able to operate the payload(s) continuously over its operational life time.	Indicates that the payload has to be operational both for day/eclipse time over the entire mission duration.	Ana	✓
U-Ops-03	The satellite platform shall cost no more than 500 k€ (2023), based on a financial break-even point after 50 satellites.	Constraints the financial budget for the development and production of the platform.	Ana, Demo	×
U-Ops-04	The total cost up to and including a first single-satellite demonstrator mission shall cost no more than 5 M€.	Provides a financial budget constraint for the first satellite platform demonstrator.	Ana	✓
U-Ops-05	The satellite design shall take series production and modularity towards different Earth Observation into account.	Modularity and series production are required to incorporate in the design of a platform which can accommodate d○ifferent payloads.	Demo	✓

U-Ops-06	A first demonstrator mission shall occur within five years after the investment cost has been secured.	Provides a timeline goal for the first launch.	Demo	○
U-GNS-01	The satellite shall fly at an altitude of 300 km with a maximum offset of 10 km.	Provides the operational altitude range for which the satellite platform is intended.	Demo	✓
U-ADCS-01	The satellite shall be able to point its payload in nadir direction and an off-nadir pointing of +/- 30 degrees.	Provides the pointing range for which the ADCS shall be able to orient the platform. A wide pointing range increases the width of the ground area which can be observed by the payload.	Insp	✓
U-ADCS-02	The satellite shall be able to point its payloads with a maximum offset of 5% from its swath width.	Provides pointing control accuracy the ADCS subsystem should be able to provide. Accurate control is required to point the payload to objects of interest.	Ana	○
U-ADCS-03	The satellite shall be able to determine its attitude which yields a maximum determination error of 50% of the ground sampling distance	Provides the determination accuracy which the ADCS should be able to achieve. Accurate determination is required in order to point the payload to objects of interest.	Ana	✓
U-ADCS-04	The satellite shall have an attitude stability which yields a maximum shift of 25% of the ground sampling distance over the integration time of one ground sample.	Provides the pointing stability that the ADCS should be able to achieve. If the pointing fluctuates too much during sampling time, images and measurements become blurry.	Test	○
U-COMMS-01	The satellite shall be able to downlink at least 20% of generated payload data when operated continuously plus a continuous set of housekeeping data.	Provides information on the amount of data to be transmitted to Earth which in terms will affect the link budget.	Test	✓
U-COMMS-02	The satellite shall be able to downlink data real-time when a ground station link is available.	Implies that data should be downlinked immediately when the ground station link is available.	Demo	✓
U-COMMS-03	The satellite downlink communication shall not interrupt the payload operation, including its attitude pointing.	Has an impact on the antenna design and operational modes of the spacecraft as Comms and payload operations can take place simultaneously.	Ana, Test	✓
U-Str-01	The satellite shall comply with the 27U CubeSat dimensions (36 cm x 35 cm x 34 cm).	Constraints the geometry, and volume available for the platform design.	Insp	✓
U-Str-02	The satellite shall fit within a commercially available deployer for 27U CubeSats and comply to their mass budget.	The deployer should not be developed in-house. Using commercially available deployers constraints the mass budget and allowable center of mass range[3].	Insp	✓
U-Str-03	The satellite shall have a payload volume of at least 16U in total.	Constraints the volume of the subsystems of the bus.	Insp	✓

U-Str-04	As a modular option, the full lower (Earth-facing) side half of the satellite's main body (13.5U) shall be available for the payload.	Constraints the location of the payload volume.	Insp	✓
U-Str-05	The satellite bus platform shall provide the option to replace the outer structure of the lower payload half with a fully dedicated payload structure.	Allows for improved accessibility to the payload.	Insp	✓
U-Str-06	The satellite bus platform shall provide the structural option to integrate one or more payloads of an integer number of CubeSat units enclosed by a (modular) external structure.	Implicates the necessity to develop a modular design.	Demo	✓
U-ReS-01	The reliability of the platform shall be 95% or higher for a mission lifetime of 5 years.	Indicates the minimum acceptable reliability for the platform including all its subsystems.	Ana	✓
U-ReS-02	The satellite shall not disintegrate during the orbital lifetime (down to 150 km) with a 99% certainty.	Provides minimum reliability for which the platform should not disintegrate under a certain altitude, in consideration of the VLEO at which the platform will operate.	Ana	○
U-ReS-03	The satellite shall be de-orbited in the atmosphere using natural decay.	No additional systems or operations should be specifically designed/used to decommission the platform.	Ana	✓
U-ReS-04	De-orbiting of the satellite shall result in a complete burn-up of all components.	Prevent hazardous situations on Earth due to falling debris.	Ana	○
U-SDH-01	The satellite shall be able to store all generated data with a minimum retention time of 1 month.	Within a month, data can be transmitted again in case the received data is compromised, distorted or no downlink channel is available.	Test	✓
U-Pay-01	The compliance of the platform for high-end Earth Observation missions of the satellite platform shall be proven by two different Earth Observation payload case studies: The satellite platform shall be able to host the 30 cm thermal infrared deployable space telescope developed by TU Delft.	Indicates how the modularity of the satellite platform is to be demonstrated.	Demo	✓
U-Thm-01	The satellite platform shall include a thermal radiator for the payload, compliant to the temperature and heat flows of the selected payloads.	Indicates the need for thermal control for different payloads.	Insp	✓

Table 3.2: *Other requirements for LAMP*

ID	Description	Rationale	Verif. M	
CON-Sus-01	The spacecraft structure shall use 20% of recycled materials	Ecological considerations	Demo	○
CON-Res-Tp-01	The satellite shall have a maximum mass of 54 kg	Dictated by commercially available CubeSat deployers	Insp	✓
CON-Res-Tp-02	The satellite shall be able to withstand the g loads during launch	Structural integrity needed for the satellite platform to survive launch	Ana	✓
CON-Res-Tp-03	The eigenfrequency of the satellite shall be higher than 35 Hz	Safety constraints for the satellite platform to survive induced vibrations.	Ana	-
CON-Res-Tp-05	The satellite volume shall fit within the deployment mechanism prescribed by the deployer system	This is a constraint to the outer dimensions of the CubeSat.	Insp	✓
CON-Res-Tp-06	The satellite shall be able to withstand the g loads during transportation to the launch provider	Structural integrity constraint.	Ana	○
CON-Res-Fc-01	The satellite shall be developed using TU Delft facilities	All the development up until the preliminary design are executed using TU Delft facilities	Demo	○
CON-Leg-Nt-01	The satellite data bandwidth shall be registered/licensed in the Master International Frequency Register managed by the International Telecommunication Union and the Dutch Rijksinspectie Digitale Infrastructuur.	Legal requirement.	Demo	✓
CON-Leg-Nt-02	~~The telemetry shall transmit at a power lower than <*TBD*>~~	Legal requirement stated by the ITU to minimise the interference with other services.	Test	-
CON-Leg-Pp-01	The satellite ISO cleanliness shall be above <*TBD*>.	Legal and ecological requirements.	Test	○
CON-Leg-Ng-01	The satellite mission should get a license on space activities from Netherlands Space Office (NSO).	Legal requirement	Demo	○
CON-UN-01	The satellite should be registered on the United Nations Register of Objects Launched into Outer Space.	Legal requirement.	Demo	○
CON-Fe-01	The satellite shall de-orbit within 5 years of mission completion.	Legal requirement United Nations Space Debris Mitigation Guidelines, though the platform will de-orbit in a matter of months.	Ana	○

4

Market Analysis

In order to ensure competitiveness of the product and to determine an initial financial budget it is important to do proper research on the available market. For a design to be viable, it must be competitive with the current offerings or fill a yet unexplored market gap. The trends in satellite designs are described and analysed in Section 4.1. Then, noteworthy competitors to our design are presented in Section 4.2. Based on the competitors identified, some of the competitive advantages of our design over the existing ones are mentioned in Section 4.3. After which, potential customers who might be interested in our design are analysed in Section 4.4. The market size and future prospects are analysed in Section 4.5. A mission Strengths, Weaknesses, Opportunities, and Threats (SWOT) analysis was performed and is described in Section 4.6. Finally, an analysis of the required specifications for the platform payloads is described in Section 4.7.

4.1. Satellite trends

The proliferation of commercial satellites began with the first communications satellites in the 1960s. Soon after, governments joined the market with satellites used for remote sensing and meteorology. It has been only in the past few years that a steady commercial market for satellites has established itself. However, that market is still heavily dependent on governmental and military contracts.

Since the first CubeSats were launched in the 2000s, the market for standardised micro-satellites such as CubeSats, has been steadily increasing [4]. There are several reasons for this trend. First, universities have started developing CubeSats as a means to conduct affordable research and engineering education. These satellites would ride along bigger satellites or be launched from the ISS to save on launch costs. Later, in the 2010s, specialised ride-share missions were specifically designed to launch 100+ CubeSats at a time. This further decreased the cost of satellite launch costs and opened an even wider market to not only universities but any commercial entity that wanted to send a payload cheaply to space [5].

Another market was also emerging, not due to the low cost, but due to the standard form of CubeSats. Some companies, like ISISpace and Endurosat, started selling CubeSat buses based on 1U to 6U and beyond. They provide quick and reliable access to a proven platform, cutting the development of such elements from interested customers, so they can integrate the payload and launch not long after. LAMP will try to penetrate the market with a new 27U platform, providing an economical and reliable bus to interested customers.

During 2019 and 2020, the space industry had a slowdown due to Covid-19, as there was a shortage of liquid oxygen, as well as a switch of government and companies budgets from the space industry to the health industry. This trend, however, has ceded and now the previous growing trend has been

re-established [1].

The market demand for LAMP will be defined by the LEO payload market and its most common customers. In 2020, out of a total of 4550 satellites, by far the largest number of in-orbit satellites, are used for communication (63%), followed by Earth observation (EO) (22.1%), Technology Development (7.8%), Global Positioning (3.6%) and other scientific purposes ($\approx$1.5%) [2] . CubeSats as a whole aim at the earth observation and scientific markets. LAMP specifically is developed with the use of multiple payload types in mind. The comparatively large VLEO platform will be beneficial to Scientific and Intelligence optical observation, as well as other earth science applications [6].

4.2. Competition

The first notable aspect of LAMP is that it is breaking into a market that does not yet have significant competition. A few 27U CubeSat platforms are in development but there have not been any launched yet.

The Italian Argotec is developing a 27U platform with capabilities similar to LAMP but with a focus on higher LEO orbits and deep space. Their platform is developed and tested entirely in-house and offered with both chemical and electric propulsion options [3]. The company makes no claims about its platform's VLEO capabilities, however, Argotech should be looked closely for future updates, as it could be possible that they could do VLEO with the electric propulsion they offer. No information about pricing is publicly available.

Space information laboratories is a US company offering a satellite platform with sizes between 3 and 27U [7]. Their platforms are qualified for LEO and can host any type of payload. However, their pointing accuracy would not be enough to host the DST. Furthermore, no mention of VLEO could be found on their website or official press releases[4]

According to NASA's State-of-the-Art Small Spacecraft Technology report [7] there are 3 more companies developing 27U satellite platforms - SpaceManic, Pumpkin Space and Orbital Astronautics. None of them have publicly available information or data sheets about the performance of their platforms. The report claims that they are all developed for LEO or MEO orbits and seem to be in the early stages of development [5] [6] [7].

It has to be noted that all companies mentioned above, except Argotec, don't sell the platform, but instead want able to adapt their 16U designs to a 27U if they can get enough resources for it. This presents a market opportunity that is explained in Section 4.3.
This leaves the 16U platforms as the main competitors, being developed by some companies like ISISpace. They are well-established companies that could accommodate a wide arrange of payloads. They, however, lack the capabilities of a bigger satellite. A comparison of some competitors can be seen in Table 4.1. The 16U platforms can fit a lot of payloads that a 27U platform could, but the capabilities in terms of ADCS and propulsion are either low or non-existent, as well as not being able to fit the apertures that a 27U platform could (from 20cm to 30cm) None of the companies claim VLEO capabilities, but due to the propulsion and ADCS capabilities, it can be inferred if it is VLEO capable or not.

[1] www.imarcgroup.com/cubesat-market, last accessed on 19/06/2023
[2] dewesoft.com , last accessed on 21/06/2023
[3] www.argotecgroup.com/wp-content, last accessed on 19/06/2023
[4] www.spaceinformationlabs.com/product-brochures, last accessed on 19/06/2023
[5] www.pumpkinspace.com/store, last accessed on 19/06/2023
[6] https://www.nanosats.eu/org/orbastro, last accessed on 19/06/2023
[7] www.spacemanic.com/cubesat-platforms, last accessed on 19/06/2023

Name	Payload Mass [kg]	Impulse [Ns] or ΔV [m/s]	Pointing accuracy/-knowledge [°]	Payload average power [W]	VLEO capability	Status
LAMP 27U	30	50000 [Ns]	0.002/ 0.0014	up to 25	Yes	Under development
ISISpace	N/A	2000 [Ns]	0.05/0.02	up to 40	No (inferred)	Under development
SPACE Inventor 16U satellite	10-12	0 [-]	1 (uncertain)	30-150	No (inferred)	Flight tested
OrbAstro 16U	19	16560 [Ns]	0.05/0.01	8.3, upgradable to 64.7	No (inferred)	In production
Argotec 27U	30	3500 [m/s]	N/A	25	N/A	Under development
GOMspace	13	10800 [Ns]	0.07/0.056	N/A	No (inferred)	Qualified LEO
BerlinSpace LEOS-100	15-30	N/A	N/A	25	Unknown	N/A
Sierra Nevada: SN-30L	20	270 [m/s]	0.02	No (inferred)	N/A	
Blue Canyon Technologies: X-Sat Mercury-class	40	N/A	0.002	-	No (inferred)	Under development

Table 4.1: *LAMP Competitors and their characteristics [N/A]- not mentioned and [-] - no propulsion. The VLEO capabilities were inferred on the basis of the fact that drag compensation ΔV scales linearly with the area. Thus 16 U platforms should provide ΔV similar to that of LAMP to maintain the orbit. Additionally, some systems have undersized ADCS subsystems for VLEO.*

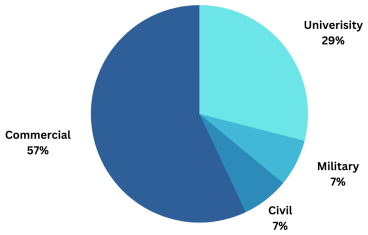

Figure 4.1: *Distribution of CubeSats by end user [9]*

4.3. Competitive advantage

LAMP will provide a service for customers that would previously have had to launch on a non-standardised satellite. This means that in the past, a complete satellite would have to be designed around the payload, whereas with LAMP, the customer is able to buy an economic, reliable platform to integrate their payload into. In contrast to other CubeSats, LAMP will be able to accommodate advanced scientific and remote sensing payloads.

There has also been an increase in interest into bigger CubeSats. The most popular CubeSat form factor right now is 3U[8], however, there is a trend for bigger satellites [8]. Most of the current research is still on 16U (see Section 4.2). This also means LAMP has a competitive advantage by existing on its own for some period of time before many competitors emerge (a market gap). Subsequently, customers that were waiting for an opportunity to buy a bigger CubeSat platform will finally be presented with an option that didn't exist before.

One of the main advantage of LAMP is the Starlink uplink capability. Due to the continuous Starlink coverage, it is possible to upload a continuous stream of data. This could for example be used as a video feed. Compared to the traditional ground stations, LAMP is capable of sending a larger amount of data over time. Another advantage is the radiator and earth shield, which can cool temperature sensitive payloads.

The other main advantage of LAMP is the VLEO capability. None of the available platforms researched claim to be able to operate on VLEO. However, LAMP is designed to fly at 300 Km for 5 years. Due to this driving design choice, the platform is capable of obtaining better resolutions than higher orbits, while still providing the modularity of cubesats. By being able to fly at 300 km (instead of more popular orbits like 600 km), and having a 50% bigger aperture than 16U platforms, the GSD can be improved by three fold.

4.4. Potential customers

As with any other product, the driving for LAMP's marketability and success will be the opinion and needs of potential customers. The potential customers for satellite buses can be divided into 4 separate groups: Military customers, Civil customers, Commercial customers and Science institutions. Figure 4.1 shows the market share of each customer in the CubeSat market [9].

Military

Earth observational instruments have many applications in the sphere of military intelligence. Because of LAMP's VLEO orbit, it should be capable of taking higher-resolution images than other CubeSats and Smallsats of similar size, flying at higher orbits. Militaries of smaller nation-states, that do not have the funding to develop their own satellites, are expected to have a particular interest in the platform. With LAMP's livelink capabilities, there is a use case for live tracking of combat theatres. The temporal resolution of the Earth observations provided by LAMP can be increased by

[8] airtable.com, last accessed on 19/06/2023

placing several satellites in a constellation.

A limitation for military customers would be the use of Starlink. SpaceX is a United States-based company and thus is subject to government limitations in the use of its technology. Additionally, there are limitations on the willingness of SpaceX management to allow the use of its constellation by military users[9].

The military satellite share is not the highest Figure 4.1, however, they usually require certain capabilities that result in lucrative projects. It is possible, for example, to adapt LAMP to be able to work in constellation flight, in order to get very high spatial resolution imaging. LAMP could provide such a service, but it would be outside the 50+ mission scope of the current design.

Civil

National governments are the third biggest customer of Earth observation satellites, tied with military as can be seen in Figure 4.1. Their interest can vary widely, they can range from intelligence services which is more related to military interest, to environmental monitoring which aligns with scientific institutes. The different use cases for satellites have to be investigated to understand LAMP's relevancy for them.

It has to be noted that 95% of currently operational civil Earth observation satellites fly in a sun-synchronous orbit[10], which places LAMP at an ideal spot for this customer base.

Figure 4.2 shows the most optimal ground sampling distance (GSD) ranges for cost efficiency of different remote sensing applications. To give an approximation of what GSD LAMP payloads would be capable of the DST as a study case. The DST is a payload on the limits of LAMP's capabilities and thus the estimations made considering its size in Figure 4.3 should be representative of the payloads with the smallest GSDs that LAMP is able to carry. From Figure 4.3 it is clearly visible that at lower wavelengths LAMP payloads can have GSDs of less than a meter and even at higher wavelengths the minimum GSD only reaches values of approximately $15\,\mathrm{m}$. Those values were then compared with the optimal ranges presented in Figure 4.2. The results are summarised in Table 4.2. From the table, it is clearly visible that based on GSD LAMP is a versatile platform with a multitude of applications of interest to civil customers.

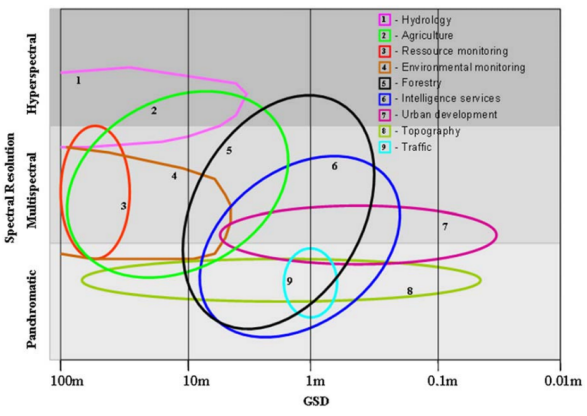

Figure 4.2: *Most optimal ground sampling distance ranges for different remote sensing applications[6]*

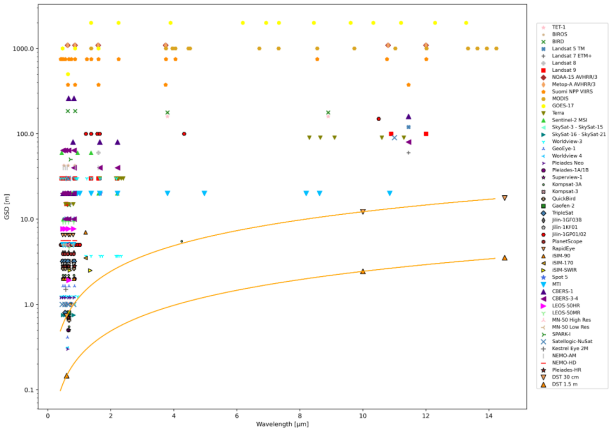

Figure 4.3: *Satellite Ground sampling distance (GSD) vs wavelength for the DST at 300km [10]*

Out of the payload instrument technologies investigated up until now, Thermal infrared (TIR) telescopes, like the DST, have a wide range of uses for civil applications. They can be used for monitoring

[9] www.economist.com/europe, last accessed 20/6/2023
[10] calval.cr.usgs.gov, last acessed on 20/06/2023

Application	Panchromatic	Multispectral	Hyperspectral
Hydrology	-	Well suited	Good for some applications
Agriculture	Not cost optimal	Well suited	Good for some applications
Resource monitoring	Not cost optimal	Not cost optimal	Not cost optimal
Environmental monitoring	Well suited	Good for some applications	
Forestry	Well suited	Good for some applications	Too small
Intelligence services	Good for some applications	Too small	-
Urban environment	Good for some applications	Too small	-
Topography	Good for some applications	-	-
Traffic	Too small	-	-

Table 4.2: *Summary of the suitability of LAMP for different applications*

high-temperature events like volcano eruptions and fires.

A constellation of LAMP satellites will be particularly suited for live monitoring natural disasters in a given area. Multiple countries have already launched constellations of sun-synchronous small satellites for observations of specific regions [11].

Commercial

Commercial satellite companies can be split up into two categories, satellite communication providers and Earth imaging companies. The former is disregarded since the focus of LAMP is Earth observation.

This market is already established, with big players like Spire[11], Planet[12], and Spot Image[13] Whilst Spire and Planet mainly operate constellations of hundred 3u CubeSats with GSD of $3.7\,\mathrm{m}$ [14], Spot Image operates a smaller constellation of bigger satellites, with the most recent version of their satellites coming in at about $700\,\mathrm{kg}$, a payload mass of about $60\,\mathrm{kg}$ and Panchromatic GSD of $2.19\,\mathrm{cm}$[15].

For commercial customers, there is a potential gap in the market for a constellation of higher-performance satellites. The constellations of Spire and Planet offer high temporal resolution due to the number of satellites in them, but the 3u form factor limit resolution. Spot Image's constellation has lower temporal resolution due to the limited amount of satellites in the constellation but can achieve higher resolution due to the larger satellite mass. LAMP could potentially bridge this gap by offering an affordable platform with high-performance capabilities. It is however not certain if customers would buy the platform since the aforementioned companies either build their own satellites or are subsidiaries of those that do.

[11] spire.com/, last accessed on 21/06/2023
[12] www.planet.com/, last accessed on 21/06/2023
[13] intelligence-airbusds.com/, last accessed on 21/06/2023
[14] assets.planet.com, last accessed on 27/06/2023
[15] eoportal.org

Science institutions

LAMP is designed around a scientific payload case study and with multiple other scientific payloads in mind [12] and thus it is important to look further into Science institutions as potential customers. While universities are not a large customer in the overall EO market they make up a significant part of the CubeSat market [13]. They are usually government funded under I&D and provide research on cutting-edge technologies. The findings can then develop into newer companies. Since these institutions usually don't have money to spare, LAMP can provide an economic platform for high-end instruments.

Universities are another civil organisation that could be interested in LAMP. They are mainly involved in research and are also interested in training their students with real-life missions. In terms of money, they are not a sizeable part of the space industry, however, they are a sizeable share of the total CubeSats launched [5].
The 4 payloads investigated during the previous design stages: DST, SPEXone, Terraherz and Plastic monitoring payloads are all designed for scientific purposes. Thus the institutions developing the payloads may have a high interest in purchasing a LAMP unit. Those institutions are TU Delft, Airbus DS NL, SRON and TNO. Before the start of production, further contact shall be made with these institutions to evaluate their interest in purchasing the platform.

4.5. Future market capitalisation

One of the main objectives of this chapter is to establish the current and future size of the large Cube Satellite market and estimate the share LAMP will obtain in it. Since LAMP will try to establish itself in a presently virtually non-existent market, estimations will need to be made on the basis of the current size of the satellite industry. An overview of it is presented in Figure 4.4.

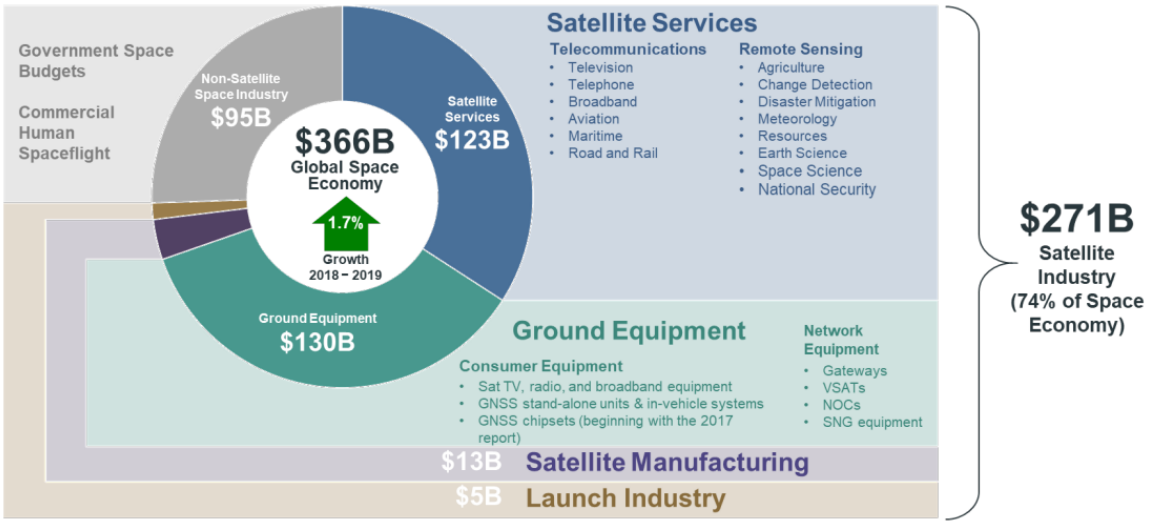

Figure 4.4: *Satellite industry size in 2019 [14]*

CubeSats account for approximately 18% of all satellites currently in orbit[16]. However, they had only $277M or 1%[17] share of the total market. That number is expected to grow rapidly by on average 18.3% per year until 2028[1]. The size of the market is expected to be $860M in 2028.

The target break-even point for LAMP is 50 units at a price of 500 000 € each. This adds up to a total sales revenue of 25M €. The team anticipates hitting the break-even point 8.5 years after the start of production. This means that on average 6 satellite platforms will be sold each year. If that is

[16] celestrak.org, last accessed on 19/06/2023
[17] www.thebusinessresearchcompany.com, last accessed on 27/06/2023

the case in 2028 LAMP will account for 0.35% of the total CubeSat market. With the trend of increasing CubeSat sizes [7], the team expects that the number of sales for LAMP and its future iterations will increase over time, possibly reducing the break-even point.

4.6. SWOT Analysis

SWOT - Strength, Weakness, Opportunity and Threat analysis is a project management technique that aims to assess internal and external factors that can influence the success of the venture. Based on this information management staff can make decisions on the financial and technical direction of the project. The 4 characteristics have the following meaning.

- Strength - The positive internal attributes of the project related to the product and organisation
- Weakness - The negative internal attributes of the project related to the product and organisation
- Opportunity - External factors that could positively influence the project's success. Often related to competition.
- Threat - External factors that could negatively influence the project's success.Often related to competition.

The SWOT analysis for LAMP can be found in Figure 4.5. Some of the more notable aspects of these are:

- VLEO: One of the biggest strengths is how low LAMP is designed to operate at, this provides a good opportunity for observation payloads.
- Livelink capabilities: Through the use of Starlink the satellite can cheaply communicate large amounts of data., which is not a common capability of LEO SmallSats.
- Faster development than the competition: Competition is mainly focused on delivering 16U CubeSats [7].
- Competitors launching new platforms: Some companies have 27U concepts or have plans to scale their existing platforms to 27U.

Figure 4.5: *SWOT analysis*

4.7. Payload Analysis

During the baseline (see [15]) and midterm (see [12]) phase, an analysis of Earth observation payloads was performed. This analysis served to set the required capabilities of LAMP. This section summarises the most important findings.

In the midterm report, it was found that the vast majority (>90%) of operational Earth observation satellites fly in an orbit with an inclination between 90°and 100°. During the detailed design stage, this conclusion was further examined and it was determined that virtually all of those satellites fly in Sun-synchronous orbit (90.8% of all commercial and civil EO satellites[18]) and thus the decision was made to design for this.

The team looked further into also constraining the operational orbits to only some local hours of ascension. However, after some data analysis of already existing missions, it was determined that EO satellite orbits are well spread over the different LTANs. The team concluded that LAMP will be designed for all circular Sun-synchronous 300 km orbits.

Furthermore, from the same analysis in [12] of payloads designed for bigger CubeSat formats (12u, 16u, 27u), the mass, power, and thermal range requirements that LAMP should be able to accommodate were set up. These can be found in Table 4.3.

Table 4.3: *Payload requirements on LAMP*

Parameter	Value	Unit
Mass	30	kg
Power	5 (A1), 10 (A2), 25 (B)	W
Thermal	200-295	K

For the mass, the value is an upper limit. Any payload that is below this value could be accommodated if it meets the other requirements. Power is split into three cases: 5 W continuously (A1), 10 W continuously (A2), and 25 W operating only during sunlight (B). In the midterm only the cases of 10 W and 25 W were set up, however after analysis from the EPS (see Chapter 10), it was found that 10 W continuously was too constraining depending on the local time of ascension of the orbit. 5 W continuously was thus added for these orbits (A1), whilst 10 W continuously is used for orbits where more power is available (A2) (see Chapter 10). The thermal range is unchanged from the midterm. LAMP should be able to maintain a payload at approximately any temperature within this range. This will require customisation between different LAMPs. However, in this report, it is shown that LAMP could cool down the payload to 200 K by the inclusion of a radiator (see Chapter 10), the upper limit does require further analysis.

Lastly, from the payload market analysis the user requirements for payload volume, *U-Str-03*, was deemed reasonable.

4.7.1. Deployable Space Telescope

To further ensure that the LAMP platform can accommodate payloads, a case study was performed using the Deployable Space Telescope (DST). This case study used the specifications of the DST to ensure that when more information was needed for the integration of a subsystem with the rest of the spacecraft or to what standards it should comply.

One of the subsystems the DST had big consequences on was the ADCS subsystem (see Chapter 8). The pointing knowledge, accuracy, and stability requirements were in the user requirements (see Chapter 3) given relative to payload specifications such as swath width and ground sample distance. Using the DST the subsystem requirements for the ADCS system were set up in the baseline

[18] calval.cr.usgs.gov, last accessed on 21/06/2023

[15] and refined in the midterm [12], which can be found in Table 8.1. Furthermore, the DST had consequences for both the ADCS and propulsion subsystems due to it being able to deploy. By extending the baffle, the centre of gravity of the satellite is moved down significantly which causes a torque. How this is dealt with is explained in Figure 14.3 and subsection 15.2.1.

The subsystem which used the DST the most to confirm that it could comply with the requirements put onto it was TCS. Previously the thermal requirement range of 200 to 295 K. For the DST, the inside of the instrument box (inner side box, optics and detector) has a maximum temperature requirement of 200 K whilst inside the baffle (inner side baffle, M2 suspensions, M1 and M2[19]) has a maximum temperature requirement of 280 K[20]. During the case study, these values and the geometry of the DST were used to confirm that the TCS (see Chapter 9 could regulate the temperature of a payload within the required values.

The last subsystem which had significant consequences from the DST is the structures subsystem which includes the placement of components. As stated in the user requirements (see Chapter 3), about 16u of payload volume needs to be available and also the full lower half (13.5u) has to be reserved for payload. This leaves 2.5u unaccounted for, which needs to be placed somewhere. This was placed using the DST instrument box, which sticks out of the lower half reserved for the payload. For this box, a cutout was made in the lower structure panel (see Figure 13.2a through which the instrument box can pass. For other payloads, it is the place where the 13.5u and the remaining volume can be connected to each other. With this information, the internal components could also be placed in the remaining volume, as seen in Figure 15.2.

For GNS, the DST specifications determined the accuracy required based upon the user requirements, as explained in Chapter 7. For the communications subsystem, the DST was first leading in the required data rate but with the current solution much higher data rates can be reached than needed for the DST specifically (see Chapter 11). The power subsystem is sized according to the requirements set up in Table 4.3, which exceeds that of the DST and thus the DST was not leading for EPS. For the software and data handling subsystem (see Chapter 12) the DST served as an indication of approximately how much data rate it should be able to handle, but also which connectors would be required for a payload.

These results assure that it is feasible for LAMP to accommodate different payloads designed for it. Some of the specifications have to match that of LAMP or be less, like volume or mass. Whilst specifications like power consumption and data rate can be much higher.

[19] M1 and M2 stand for the primary and secondary mirror respectively

[20] From ”DST Key Specifications (v2)”, internal communication with J. Bouwmeester

5

Final Design

This chapter is an overview of the final design of LAMP covering the general details of the different subsystems and how they are integrated. The overall mass, volume and power budgets are also shown in Section 5.2 and 5.4.

5.1. Configuration

The external and internal layout of LAMP can be seen in Figure 5.1 and Figure 15.2 respectively.

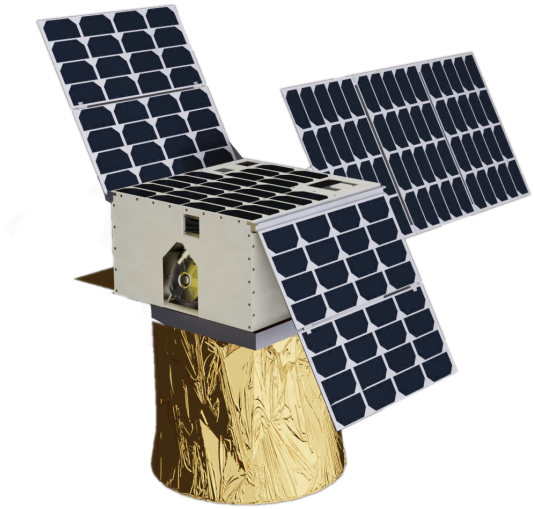

Figure 5.1: *External view of LAMP with DST payload*

(a) *Internal view of LAMP from thruster side (back)*

(b) *Internal view of LAMP from front side*

Figure 5.2: *Internal views of LAMP*

Guidance and Navigation Subsystem

The guidance and navigation subsystem (GNS) is tasked with determining the orbital position. It consists of a passive patch antenna placed on top of LAMP. The patch antenna connects to a global navigation satellite system such as GPS. With this connection, the satellite is able to estimate its position in orbit when in connection with 4 satellites or more. The patch antenna is internally connected to a receiver, which in turn is connected to the central computer. Finally, the in-depth design of the GNS is discussed in Chapter 7.

Attitude Determination and Control Subsystem

Attitude determination is done by star trackers and magnetometers. Star trackers are needed since they are the only sensors which can fulfil the determination requirements. Magnetometers are used when the star trackers are unavailable, to improve the determination sampling rate, and to improve the performance of the magnetorquers. Attitude control is achieved by control moment gyroscopes. These are needed since they are the only control actuators which can achieve both the pointing accuracy and the stability accuracy requirements. Since control moment gyroscopes cannot dump momentum, magnetorquers are included to achieve this. Finally, the in-depth design of the ADCS is discussed in Chapter 8.

Thermal Control Subsystem

The thermal control subsystem (TCS) is tasked with maintaining the temperature of the components of the platform. It achieves this by applying a white coating on the outside structure to manage the absorptivity and emissivity of the platform. Furthermore, patch heaters and pipe heaters are used to heat up the propellant tanks and piping respectively, which need to maintain a temperature higher than the rest of the platform. For the study with the deployable space telescope, an external radiator and Earth-shield were included to cool down the instrument box. Other payloads with similar thermal requirements can use the same solution, whilst payloads which need to maintain a higher temperature do not need it. Lastly, multi-layer insulation is used internally between components to thermally isolate them from each other. Finally, the in-depth design of the TCS is discussed in Chapter 9.

Electrical Power Subsystem

The electrical power subsystem (EPS) is tasked with generating, storing and distributing power for the satellite. Power generation is done using solar cells. The solar cells are mounted on top of the spacecraft and on three arrays. Of these arrays, two are mounted on the side whilst the third one is mounted on the front. The placement of the front-mounted array is such as placing it on the back would cause the array to suffer from corrosion due to the plume of the thruster. Power from the solar panels goes to the power control and distribution unit, which converts it to the correct voltages and distributes it to where it is needed. Two battery packs are used to store power. One is responsible only for the propulsion peak operations, while the other is for eclipse operations. Finally, the in-depth design of the EPS is discussed in Chapter 10.

Communications subsystem

The communications subsystem is tasked with establishing a communications link with a ground station to send down the payload data and telemetry of the satellite, and to receive commands from the ground. This is achieved by establishing an inter-satellite link with the Starlink constellation. This link is established using a patch antenna mounted on top of the spacecraft. This patch antenna is internally connected to a transceiver, which in turn is connected to the central computer. Finally, the in-depth design of the Comms is discussed in Chapter 11.

Software and Data Handling subsystem

The software and data handling (SDH) subsystem is tasked with commanding the spacecraft, monitoring the telemetry of the spacecraft, storing the payload data, and computing internal algorithms. This is achieved by the onboard computer, different interfaces and data cables, and internal storage. In the case study with the DST, it is assumed that the DST does its own pre-processing before sending

the data to the onboard computer. Finally, the in-depth design of the SDH is discussed in Chapter 12.

Structures subsystem

The structures subsystem is tasked with providing stiffness, protecting the internals, and providing mounting for the components. To achieve this, a monocoque structure made of aluminium was designed. The structure is split up into two parts, one for the platform and the other for the payload. For the platform structure, the zenith (top) panel is used to mount the electronics stack, GNS and Comms patches, star trackers, batteries, and fuel tanks. The nadir panel is used to mount the CMGs and thruster assembly. One of the side panels contains the radiator, if necessary, build into it. In the nadir (bottom) panel a hole is present to allow for access between the platform and the payload. The payload can either be mounted in a provided payload structure or in its own structure. Finally, the in-depth design of the structures subsystem is discussed in Chapter 13.

Propulsion subsystem

The propulsion subsystem is tasked with maintaining the orbital altitude of the satellite. This is achieved by the Hall effect iodine propellant thruster. To neutralise the iodine-ion flow, a cathode is included to release the freed electrons back into the flow. The iodine is stored in fuel tanks which are connected to the propellant flow control valve (PFCV), managing the flow of propellant. The thruster is angled such that the thrust goes through the centre of gravity when the fuel tanks are half full, this is done to minimise the torque during thruster operation. Finally, the in-depth design of the propulsion subsystem is discussed in Chapter 14.

5.2. Mass and volume budget

The mass and volume have also been updated. LAMP is under the maximum allowable 54 kg mass, while the volume of all of the components combined is considerably under 27U. The reason for the reduction is mainly due to the change in fuel type to iodine, with the addition of the cumulative savings of all the subsystems.

Table 5.1: *Mass and volume budget breakdown for LAMP*

Subsystem	Mass [kg]	Volume (Units)
Thermal [5]	1.731	0.430
Electrical	7.698	1.328
Propulsion	7.651	1.752
Structures	3.123	-
ADCS	2.233	2.512
Comms	0.259	0.308
GNS	0.035	0.202
OBC& CDHS	0.250	0.250
Payload	30.000	16.055
Total	52.98$\pm$15%	22.84$\pm$15%
Remaining	1.02	4.16

5.3. Astrodynamical budget

LAMP is going to fly in an inclination 96.7°orbit with no fixed local time of ascension. Table 5.2 presents the final astrodynamical properties of LAMP.

Table 5.2: *Astrodynamic properties of LAMP*

Total ΔV (SF=1.2 + 0.1 for manoeuvres) [m/s]	$F_{aero_{mean}}$ [mN]	$F_{aero_{max}}$ [mN]	Mean duty cycle	Fuel mass [kg]	Fuel volume [U]
1093.5	0.277	0.346	0.0336	4.894	1.00

5.4. Power budget

In this section, the power needs of LAMP's subsystems are presented. Subsequently, an operational timeline is created to distribute the peak power usage over the orbit in order to design to optimise the electric power subsystem (EPS) for efficiency in terms of power generation and storage.

Table 5.3 presents the continuous and peak power consumption of each subsystem based on the selected components.

Table 5.3: *Power budget of LAMP*

Subsystem	**Cont. Power [W]**	**Peak Power [W]**	**Subsystem**	**Cont. Power [W]**	**Peak Power [W]**
Str	0	0	Payload Sc.1	5	5
ADCS	14.4	14.4	Payload Sc.2	10	10
TCS	3.5	3.5	Payload Sc.3	0	25
SDH	2	4	Propulsion	0	121
EPS	3	3	$P_{max_{Sun}} =$	173	[W]
Comms	1.8	1.8	$P_{max_{eclipse}} =$	158	[W]
GNS	0.3	0.3	$E_{max_{eclipse}} \approx$	50	[W h]

Note that the payload scenarios are distributed among the local times of ascension as follows - for $LTAN = 6$ h payload scenarios 2 and 3 apply with a possibility to increase the continuous power by a margin of 8W, for $LTAN < 9$ h payload scenarios 2 and 3 apply, and for $LTAN < 12$ h payload scenarios 1 and 3 apply.

5.4.1. Operational timeline

Below is the operational timeline presented which indicates when which system will operate at peak power throughout the duration of six orbits, after which the cycle will repeat itself. This is the nominal operational timeline of LAMP. A distinction is made between continuous and discontinuous payload operations, for which the payload is only active when the satellite is in sunlight. The peaks in Figure 5.4 and Figure 5.5 relate to the activation of the thruster which is activated once in sunlight and once in eclipse to maintain a circular orbit for 870 s, and shows a general overview of the timeline. The eclipse period is highlighted by a bold line on the time axis. The middle of the thrusting time corresponds to the middle of the sun period as power generation is maximal at this point and with the middle of the eclipse for the next thrusting period. On the other hand, a per subsystem representation may be found in Figure 5.3.

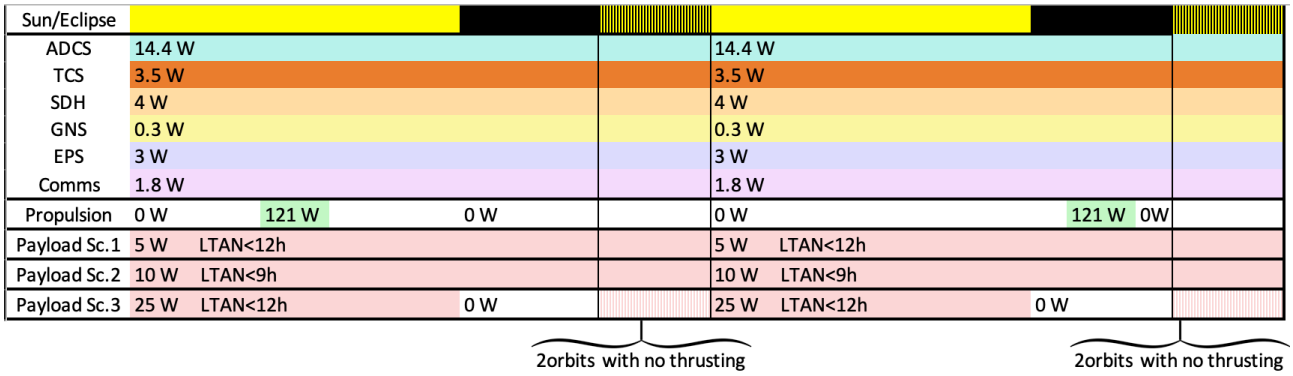

Figure 5.3: *Power consumption map over the nominal operational timeline*

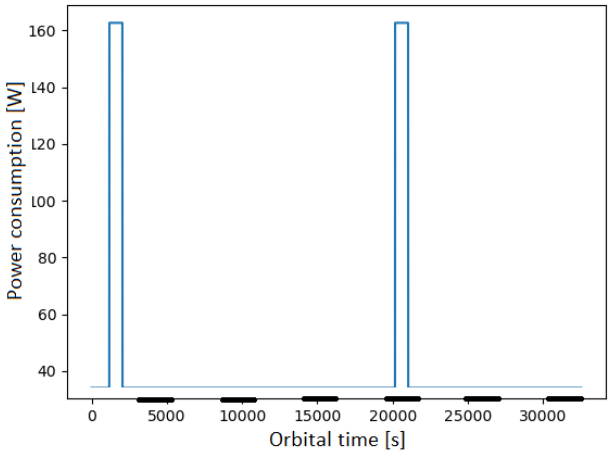

Figure 5.4: *Operational timeline for continuous payload operations*

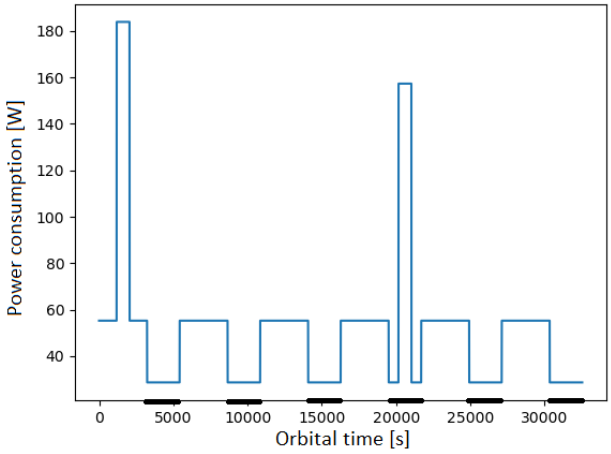

Figure 5.5: *Operational timeline for discontinuous payload operations*

Furthermore, the beginning-of-life operations order is described chronologically, but not quantitatively. After the deployment of LAMP from the deployer, the LAMP's EPS will activate the ADCS in order to stabilise itself and detumble. Furthermore, the GNS and COMMS antennae will activate, and SDH-OBC will activate. These operations will entirely rely on the 2 battery packs. After this initial phase, the TCS will activate and the deployment of the Earth-shield and deployable solar panels will begin. After full deployment, the battery will be charged to nominal values, before the payload is activated. Once, this happens LAMP will enter its nominal 6-orbit operational timeline.
On the other hand, at end-of-life, LAMP will reach a $125\,\mathrm{km}$ orbit within 4 weeks as derived in the Midterm report [12].

6

Environmental characteristics

6.1. Stability and control characteristics

For the stability and control characteristics, a simulation was made combining a panel method calculation for aerodynamic torques with simplified calculations for thruster, gravity gradient and radiation torques. With the torques given as an absolute value in roll, pitch and yaw (or rather around the body axis of the satellite) defined in Figure 6.1. The magnetic moment is omitted from this simulation and instead added later. This is because the ADCS sizing also requires disturbance torques free of magnetic moments for its sizing (the particular sizing approach is given in Chapter 8).

The panel method calculation was performed through the use of ADBsat, which is able to calculate aerodynamic moment coefficients of a provided 3D model excluding the effects of the spacecraft that are not in the flow, using a shadow analysis algorithm and a selectable single gas-surface interaction model (GSIM). The GSIM used in the simulation is the Sentman model, which uses an assumption of complete diffuse re-emission which holds true for VLEO [16].

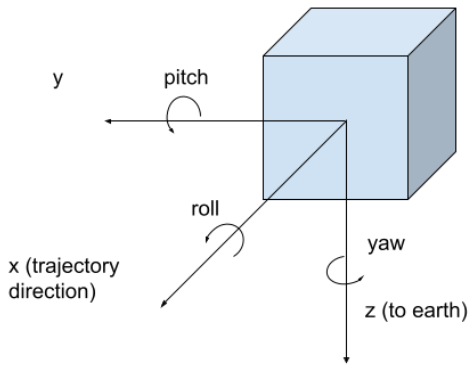

Figure 6.1: *Body axes and rotations of the spacecraft*

The aerodynamic torque calculation using this GSIM requires density and temperature of the flow, a thermal accommodation coefficient and a wall temperature. The accommodation coefficient varies around 0.9-1 [17]. 0.9 was selected, as this consistently resulted in the maximum torques for our simulation. The wall temperature of $250\,\mathrm{K}$ was obtained from subsection 9.2.4. The flow temperature and density of the flow were calculated using ADBsat's provided environment calculator based on MATLAB's implementation of atmosnrlmsise00.

The simulation calculates the disturbance torques in 2 modes: A nominal pointing mode and a thrusting mode depicted in Figure 6.2. The simulation iterates through different model possibilities outlined in Chapter 10 and cg's outlined in Chapter 13. The side slip angle and angle of attack ranges that are used in the simulation are based on common wind speeds experienced at $300\,\mathrm{km}$ altitude. With side slip angle and angle of attack being the spacecraft rotations in respect to the orbit trajectory in pitch and yaw respectively in accordance with Figure 6.1.
At $7730\,\mathrm{m/s}$ orbital speed and $600\,\mathrm{m/s}$ horizontal wind speeds [18] (Mean speeds over the poles at $400\,\mathrm{km}$) a side slip angle of approximately -5°to 5°can be expected. The vertical wind speed of $150\,\mathrm{m/s}$

that have been observed [19] result in an approximate angle of attack ranges of -1°to 1°.

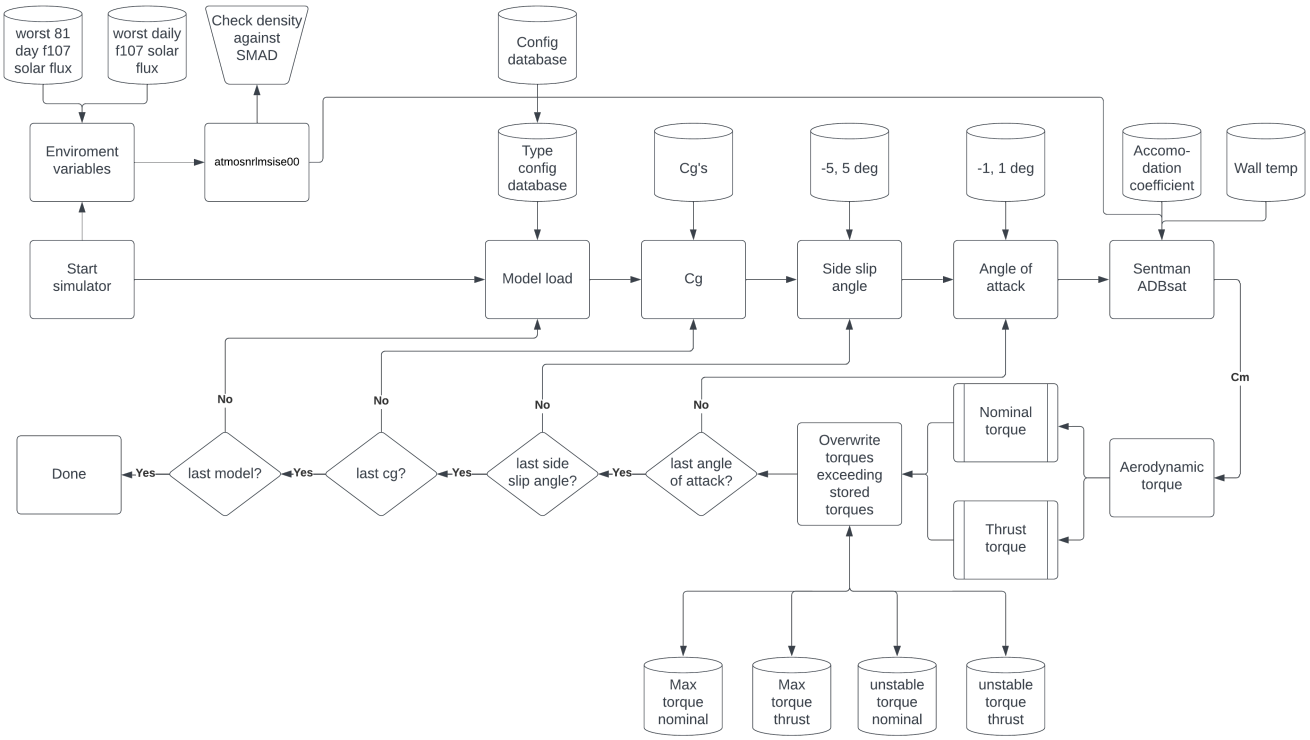

Figure 6.2: *Flow chart of torque simulation*

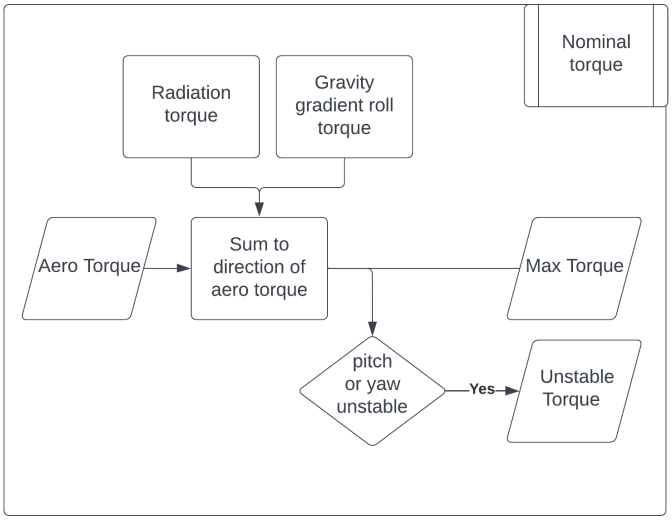

Figure 6.3: *Flow chart of the nominal sub-routine torque calculation*

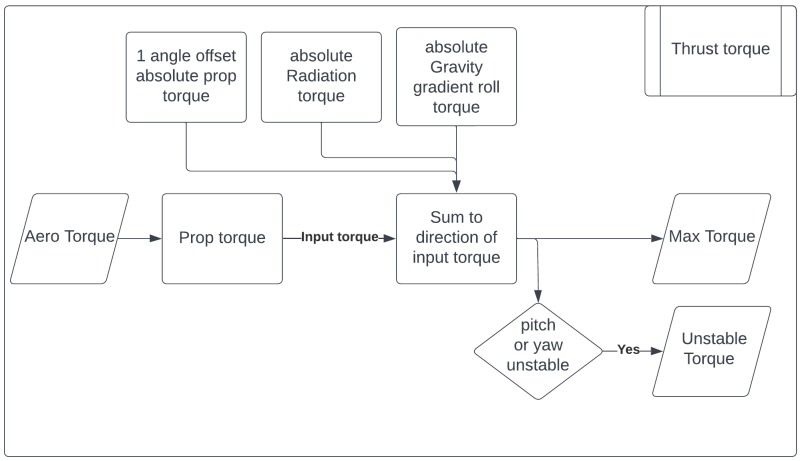

Figure 6.4: *Flow chart of the sub-routine thrust torque calculation*

For the thrusting mode, the nominal propulsion torque was combined with aerodynamic torque for a provided position and nominal inclination of the thruster. The nominal propulsion torque using this information is calculated with Equation 6.1, where r is the arm from the placement of the thruster from a given cg and F_{thrust} the force of the thruster. To take into account a potential offset of the propulsion, a 1°maximum offset in any direction is assumed. This contribution can either add or reduce the maximum torque in different situations in different axes. However, for conservative ADCS sizing, the limiting case is the situation where the offset torque adds up to the total torque. To calculate this resulting torque, the secondary torque (offset thrusting) was added in the direction of the primary torque (nominal thrusting plus aerodynamic torque).

The other torques are similarly summed in both nominal pointing and thrusting mode. To comply with *Sys-ADCS-05*, a gravitational torque where μ is the gravitational parameter of earth, a the radius of the orbit and I_{zz}, I_{yy} the moments of inertia around the z and y-axis respectively.

Lastly the radiation torque was added in a highly conservative manner. As was observed in the Baseline report [15], this torque is significantly lower than other torques. To account for its influence while refraining from using extensive analysis Equation 6.3 was used. In this equation $\dot{q_{\odot}}_{max}$ is taken as the combination of maximum solar heat flux and albedo of the earth at around $1700\,\mathrm{w/m^2}$ [20]. The projected area or S_{max} is taken as $0.7\,\mathrm{m}^2$ (approximate value of the maximum projected area for the configuration calculated with the process outlined in the baseline report [15]), with the arm length $(C_g - C_p)$ equal to $0.35\,\mathrm{m}$. This arm length is is equal to the entire width of the spacecraft, which is a value that is taken to represent the influence of the front panel to a shift in centre of pressure. The equation itself also assumes perfect reflection of all radiation, which creates a higher torque compared to deflection due to a higher force being applied.

The resulting total torques were assessed for pitch and yaw instability. Unstable torques are produced when the direction of the torque along the pitch and yaw directions correspond to the direction of the angle of attack or side slip angle respectively. The roll torque was not considered here as there is a range of roll positions that the spacecraft should be able to point to according to *Sys-ADCS-05*, as such any such roll torque was deemed destabilising.

With this analysis, the maximum torques (both stable and unstable) were calculated for a variety of spacecraft configurations that were encountered during the design process. These maximum torques are what the spacecraft systems are designed for. In particular the adcs system uses these torques to determine the size of their control components Chapter 8. Providing the spacecraft system with maximum torques opposed to average or nominal torques ensures a conservative sizing increasing the reliability of the satellite. For future calculations, if these torques become too limiting average or

nominal torques could instead be used to reduce the size of the spacecraft subsystem at a certain cost of reliability in orbit.
In Table 6.1 and Table 6.2 the result for nominal mode and thrusting mode are outlined for the 2 main configurations that were considered. The first configuration is CIII-Bf$_{h_i}$-Sf$_i$, this represents a spacecraft with a trailing solar panel and 2 side panels while CIV-Ff$_{h_i}$-Sf$_i$ represents a spacecraft with a forward solar panel. A visual representation of both configurations can also be seen in Figure 10.3. The cgs that were used to assess the maximum torques for these configurations are presented in Section 15.2 with the moment of inertia presented in subsection 15.2.2.
The results are presented without magnetic moment and with an angled propulsion unit. The 2 configurations represent desirable options for EPS where the first configuration is when the larger solar panel is pointed in the direction of flow and the second configuration points away from the direction of flow. The difference in torque between these two configurations is of particular interest to the design as it was expected that the destabilizing torque is higher for a front-facing solar panel due to a weathervane effect. However, if this effect was not impossible to overcome it would have several benefits for the design to have the solar panel pointed into the trajectory of the orbit, in particular reducing the risk of the propulsion unit depositing ions of fuel on the solar panel Section 10.2. As can be seen in the Table 6.1 and Table 6.2 this effect is minimal.

$$T_{thrust} = r_{cg-to-prop} \times F_{thrust} \tag{6.1}$$

$$T_{grav} = \frac{3}{2}\frac{\mu}{a^3}(I_{zz} - I_{yy})sin(2\frac{30\phi}{180}) \tag{6.2}$$

$$T_{sun} = \frac{\dot{q_{\odot max}}}{c} \cdot 2S_{max}(C_g - C_p) \tag{6.3}$$

Table 6.1: *Maximum torques in nominal mode for two configurations.*

Nominal mode	Max. torque [Nm]			Max. unstable torque [Nm]	
Configuration	Roll	Pitch	Yaw	Pitch	Yaw
CIV-Ff$_{h_i}$-Sf$_i$	1.43×10^{-5}	7.74×10^{-5}	2.73×10^{-5}	7.74×10^{-5}	2.38×10^{-5}
CIII-Bf$_{h_i}$-Sf$_i$	1.48×10^{-5}	7.69×10^{-5}	2.80×10^{-5}	7.63×10^{-5}	2.24×10^{-5}

Table 6.2: *Maximum torques in thrusting mode for two configurations.*

Thrusting mode	Max. torque [Nm]			Max. unstable torque [Nm]	
Configuration	Roll	Pitch	Yaw	Pitch	Yaw
CIV-Ff$_{h_i}$-Sf$_i$	1.46×10^{-5}	3.49×10^{-5}	2.46×10^{-5}	3.50×10^{-5}	2.10×10^{-5}
CIII-Bf$_{h_i}$-Sf$_i$	1.52×10^{-5}	3.49×10^{-5}	2.52×10^{-5}	3.48×10^{-5}	1.97×10^{-5}

This magnetic moment and its resulting instability to the spacecraft was estimated using a process outlined in the Baseline report [15]. For an overview of the absolute maximum torques that need to be counteracted this torque is added upon the maximum torque per axis for both nominal and thrusting mode. The maximum torques for the two configurations along each axes are given in Table 6.3.

Table 6.3: *Total maximum torques for two configurations.*

Configuration	Roll [Nm]	Pitch [Nm]	Yaw [Nm]
CIV-Ff$_{h_i}$-Sf$_i$	2.54×10^{-5}	3.60×10^{-5}	3.81×10^{-5}
CIII-Bf$_{h_i}$-Sf$_i$	2.59×10^{-5}	3.60×10^{-5}	3.88×10^{-5}

6.1.1. Verification

As previously mentioned the simulation interfaces with ADBsat code. The ADBsat aerodynamic coefficient and shadow analysis have already been verified and validated in literature [21]. In addition to simple unit tests of the simulation, additional verification tests were performed, to check the validity of our simulation around ADBsat. For this, three tests were performed to check the actual aerodynamic moment compared to simple aerodynamic calculations by hand. The three tests were performed on each of the body axis: roll, pitch and yaw. Based on blocks with a moment arm of $1\,\mathrm{m}$, a frontal area of $1\,\mathrm{m}^2$ and positioned such that it produces a torque around a desired body axis while keeping the block faces perpendicular to the flow. For this simple calculation, Equation 6.4 is used. The drag coefficient C_d is taken as 2.2 a common value used for this coefficient [12]. ρ is taken from simulation and $v_{trajectory}$ is the orbital speed of $7730\,\mathrm{m/s}$. When compared with ADBsat, the results match closely: $3.40\,\mathrm{mNm}$ for ADBsat and $3.49\,\mathrm{mNm}$ for the simple evaluation. This can most likely be attributed to small deviations in C_d estimation but it verifies the correct usage of ADBsat.

$$T_{aerodynamic} = 0.5 \cdot \rho \cdot c_d \cdot r_{arm} \cdot A_{frontal} \cdot v_{trajectory}^2 \tag{6.4}$$

6.2. Astrodynamical characteristics

The orbit of each LAMP platform mission is a key characteristic that determines several budgets and establishes minimum requirements for the design. As described in previous work [12], the team developed a numerical model that simulates the VLEO environment and gives important inputs to multiple subsystems. The model simulates the movement of the satellite over the orbital time, estimates of the aerodynamic drag, the effects of thrust on the orbit, the thermal radiation inputs as well as the orientation and incidence angle of the solar rays to the solar panels (SP). This section details the structure of the numerical model, its outputs and the verification performed on it, furthermore, it gives reference to its use in the design of the individual subsystems.

The model is a simple Newtonian force model which uses the explicit Runge-Kutta method of order 5(4) [22] for the time integration. All forces are calculated in the ECI (Earth-centered inertial) reference frame that has its centre at the Earth's centre of mass. Since the goal of the model is to give a preliminary estimation of the aforementioned budgets and not a precise orbit determination, it considers the effects of only three forces - the radial force of gravity, the aerodynamic drag and the thrust. In this stage of development, the model is intended for short simulations whose results are extrapolated and thus it ignores nodal precession (J_2 effect). It is assumed that the Earth is an ellipsoid with a polar radius of $6.357\,\mathrm{km}$ and equatorial radius $6.378\,\mathrm{km}$ [23]. The model state vector q and its derivative take the following form:

$$\vec{q} = [x, y, z, V_x, V_y, V_z, m]^T \tag{6.5}$$

$$\dot{\vec{q}} = [V_x, V_y, V_z, F_x, F_y, F_z]^T = [q_4, q_5, q_6, G_x + F_{aero_x} + T_x, G_y + F_{aero_y} + T_y, G_z + F_{aero_z} + T_z, \dot{m}]^T, \tag{6.6}$$

where G_i is the component of the force of gravity and F_{aero_i} is the component of the aerodynamic force, both in the $\vec{i}$ direction. To calculate the orientation of the satellite, it is assumed that the DST points constantly in the Nadir direction and that one of the cube's sides is constantly perpendicular to the velocity vector.

The force of gravity acting on an object in a given location can be calculated as follows:

$$\vec{G} = -\frac{m\mu}{|\vec{r}|^3}\vec{r}, \tag{6.7}$$

where G is the force of gravity, μ is the gravitational parameter of the central body, r is the position of the satellite with respect to the central body's centre of mass and m is the satellite mass.

The aerodynamic force acting on the satellite is estimated using the drag equation:

$$F_{aero} = 0.5 C_d \rho |\vec{V_r}|^2 S, \tag{6.8}$$

where C_d is the drag coefficient, V_r is the speed of the satellite in relation to the aerodynamic flow, and S is the satellite cross-section. The model assumes that the effects of skin friction and viscous drag are negligible [22].

Two different approaches were used to give an estimate on the value for C_d. Setman's model equations were used with some standard values [24]. This gave an estimate of $C_d = 2.0278$. The model however proved to be highly sensitive on input parameters with drag values varying between $C_d = 1.93$ and $C_d = 3.18$, which indicates significant uncertainty in the drag values which is to be later examined in subsection 6.2.2. Further work was done by using a standard value of $C_d = 2.2$ [25, 22, 5].

The cross-section of the satellite depends on its size and the position and orientation of external surfaces like the SPs. Since the DST LAMP case study is expected to fly in extended DST configuration for most of its mission the area of the body was considered constant $S = 0.196\,\text{m}^2$ [15].

In addition to this, the contribution of the SPs to the overall frontal area was considered. The SPs were split into 4 types - Fixed SPs, SPs rotatable around an axis pointing in the direction of travel, rotatable SPs around an axis pointing right of the direction of travel and SPs rotatable around 2 axes. Each type of solar panel is prescribed an area. Then the orientation of the given solar panel is calculated. The solar panel surface normal vector as defined in Figure 6.6 and the aerodynamic flow velocity vector is used to calculate the contribution of each SP wing to the overall frontal area. When the satellite is in eclipse, the Sun-facing rotatable external bodies can be rotated to a minimum-drag configuration where only their thickness contributes to the satellite cross-section. External bodies constantly positioned behind the satellite are assumed to have an insignificant effect on drag. During previous design stages, it was determined that two-axis rotational solar panels would be discounted from further consideration[15, 12]

The implementation of a full atmospheric model could not be justified at this preliminary design stage. Thus a simple exponential model of Earth's atmospheric density based around an altitude of $300\,\text{km}$ was considered:

$$\rho = \rho_{300km} * exp((300 - h)/H), \tag{6.9}$$

where ρ_{300km} is the mean density at $300\,\text{km}$, h is the height above the earth's reference ellipsoid in km and H is the atmospheric scale height. The model can run in two density configurations [5]:

- Normal mode - $\rho_{300km_{mean}}$=$2.3 \times 10^{-11}\,\text{kg}\,\text{m}^3$ and H=$45.8\,\text{km}$
- Maximum drag mode - $\rho_{300km_{max}}$=$4.39 \times 10^{-11}\,\text{kg}\,\text{m}^3$ and H=$54.5\,\text{km}$

It has to be noted that the drag estimations of the model are highly sensitive to the atmospheric density and that furthermore the density itself is heavily influenced by the solar cycles [22]. This sensitivity will be elaborated upon further in subsection 6.2.2.

Finally the satellite velocity relative to the incoming flow depends on the state of the dynamics of the atmosphere in high Earth orbit. To simplify those, it was assumed that the atmosphere co-rotates with earth [22] and thus the relative velocity is:

$$\vec{V_r} = \vec{V} - \vec{\omega_e} \times \vec{r}, \tag{6.10}$$

where $\vec{V}$ and $\vec{r}$ are the velocity and position of the satellite in an inertial reference frame and $\vec{\omega}$ is the rotational vector of Earth. This approximation leads to uncertainties in the drag force of less than 5% [22].

The last force considered in the simulation is the thrust force. During the detailed design stage, it was discovered that there is a need for the satellite thrusting to be angled by 10.6°in the zenith direction

in order to reduce the torques acting on the satellite during thrusting (Section 15.2). The thrust vector also has a component pointing to the side of the satellite that is meant to counteract the average effects of wind's side-ward drag on the orbital inclination (Figure 14.3). The remaining thrust is assumed to point in a direction opposite the direction of travel. Additionally, the model accounts for a pre-specified pointing accuracy of 1°. The thrust vector is defined in Equation 6.11.

$$\vec{T} = T(\vec{u_V} \cos\alpha_t \cos\alpha_w + \vec{u_R} \sin\alpha_t \cos\alpha_w + \vec{u_R} \times \vec{u_V} \cos\alpha_t \sin\alpha_w) \tag{6.11}$$

where $\vec{u_V}$ and $\vec{u_R}$ are respectively the satellite velocity and position vectors, T is the magnitude of the propulsion system thrust, α_t=10.6°is the angle at which the thruster is pointed in the zenith direction and α_w=0.14°is the thruster stewards pointing andgle for wing drag compensation.

During previous design stages it was determined that the satellite would thrust on average once every 3 orbital periods [12]. This was done to reduce the effects of excessive lower altitude drag and to reduce the thrusting time in consideration of the EPS. However, if LAMP performs thrusting manoeuvres at an integer number of orbital periods they will always occur on the same side of the orbit, which will lead to an increase of orbital eccentricity and eventual orbital decay. To combat this issue the team devised a thrusting timeline where the satellite first thrust at the middle of the orbital day (when it is oriented so that it generates maximum power). Then 3.5 orbits later it thrusts again in the middle of the orbital eclipse period.

Using Equation 6.12 the mass flow rate can be calculated from the thruster-specific impulse and thrust.

$$\dot{m} = \frac{T}{I_{sp} g_0} \tag{6.12}$$

Equation 6.13 defines the propulsion system duty cycle.

$$D = \frac{F_{drag}}{T \cos 10.6^\circ \cos 0.14^\circ} \tag{6.13}$$

Estimating solar panel incidence angle efficiency

The average incidence angle between the sun vector and the LAMP solar panels stays constant over the year since LAMP flies in a sun-synchronous orbit with an inclination of 96.7°. This means that by simulating only one orbital period with a fixed position of the orbital plane with respect to the sun, the team was able to deduce the efficiency of the fixed and one-axis rotatable solar panels at any given point within the orbit. The way those efficiencies were estimated is described below.

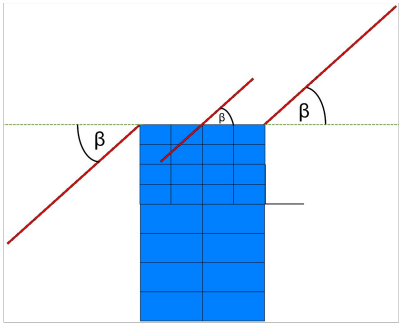

Figure 6.5: *Definition of the angle between the top plate of LAMP and the SP wings (β). Image in front view*

First the case of solar panels rotatable around one axis will be examined. A visualisation of a front rotatable panel is presented in Figure 6.6.
Figure 6.6 shows that the back solar panel is most efficient in case, its normal vector lies in the plane defined by its rotation axis vector (orange) and the sun vector (red). The maximum efficiency of the solar panel is given by Equation 6.14.

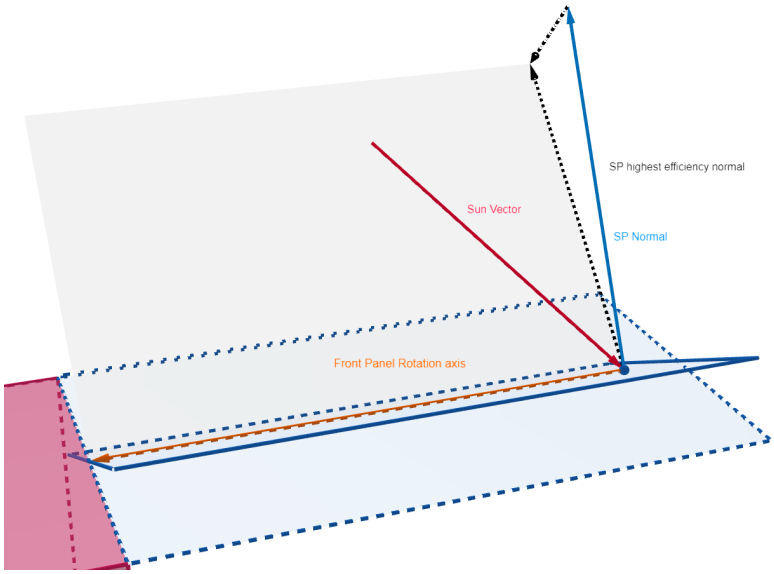

Figure 6.6: *Visualization of relevant vectors for the rotatable solar panel. Orange: Front panel rotation axis, Red: Sun vector, Blue: Solar Panel normal vector, Black: Solar panel highest efficiency normal vector*

$$\cos\theta = \sqrt{1 - (u_{\vec{Sun}} \cdot u_{\vec{Rot}})^2} \tag{6.14}$$

Additionally, the model needs to account for the uncertainty in the sun vector knowledge and the accuracy of the rotation of the solar panels. The angle offsets due to sun vector knowledge(5°3σ [26]) are modelled as bivariate normal distributions - one variable for the angle in-plane with the front panel rotation axis and one perpendicular to the plane with the front panel rotation axis. The second angle offset is due to the solar panel rotation accuracy (1°3σ [26]). For a rotatable side solar panel, the efficiency estimation procedure is equivalent, only in this case, the rotation axis vector is pointed to the right of LAMP. It is important to note that rotatable solar panels are operational during the whole sun day. The model makes the important assumption that LAMP's shadow does not affect solar panel efficiency.

The second type of panel examined are SPs at a fixed angle. The angle that provides the highest average efficiency over a full orbit is a non-trivial calculation to make. To simplify the design process the team calculated the average efficiency of SPs rotated, at any β (as defined in Figure 6.5) angle between 0°and 360°, for different local times of ascension. Using those results the team determined the β angle that would give the highest average solar panel efficiency over an orbital period accounting for both eclipse times and the orientation of the solar cells. The results are summarised in Table 10.3 and Figure 10.2. Fixed solar panels are sometimes oriented in a direction opposite the sun and are thus operated for less than the whole orbital day.

Model outputs

The model outputs were used at different places throughout the design process as they are important for multiple subsystems:

- The estimated ΔV with consideration for safety factors and thrust vectoring is used in subsection 14.2.2 to size the propulsion system. Those results are tabulated in tab Table 6.5 and Table 6.4.
- The estimated SP efficiencies for different configurations are used in Section 10.2 as a consideration for the SP external configuration and as input for the EPS numerical model. Additionally, the duty fraction is used to calculate the amount of time the propulsion subsystem stays active. An overview of the efficiencies can be found in subsection 10.2.1.
- The exact state of the satellite including if it is in eclipse or not was used as input for the TCS numerical model in Section 9.2.

The ΔV budget for LAMP is divided into 5 parts as described in Table 6.4. Further detail about the exact magnitude of the thruster angling component is given in Figure 14.3.

Table 6.4: *Lamp's ΔV budget for a 5 year mission*

Source	**ΔV required [m/s]**
Drag compensation	806.1
Initial orbital manoeuvres (10% [5])	80.6
Thruster angling losses	16.5
Orbit correction and debris avoidance	8.1
Safety factor (20%)	182.2
Total	1093.5

Table 6.5: *Results of drag simulation for LAMP*

Total ΔV (SF=1.2 + 0.1 for manoeuvres) [m/s]	$F_{aero_{mean}}$ [mN]	$F_{aero_{max}}$ [mN]	Mean duty cycle	Fuel mass [kg]	Fuel volume [U]
1093.5	0.277	0.346	0.0336	4.894	1.00

6.2.1. Sensitivity analysis

Several assumptions were made in the development of the model. To account and quantify for the effect of those the team performed a sensitivity analysis. This was done in two ways: First initial conditions were varied to check if a small variation in the initial conditions would result in a large change in the outputs and secondly the most uncertain assumptions expected to have the largest impact on the result were looked into.

Varying each model input (the 6 Keplerian elements, the environmental parameters, such as mean density, and the satellite parameters,e.g. the drag coefficient and the SP area) by 1% resulted in no divergence of the model over 30 orbits.

Three assumptions which are most likely to significantly affect the satellite design were identified. Those are the assumed value of C_d, the assumed mean density and the assumption that the satellite shadow does not affect the solar panels.

Due to Equation 6.8 the assumed value of C_d and the assumed density have a linear relationship with the calculated ΔV. As mentioned in Section 6.2 Setman's model equations were tested as an alternative to determine the satellite drag coefficient, but those were found to be highly dependent on external conditions. If the maximum drag coefficient calculated by the model (3.18) is used for the simulation, the total satellite propellant mass would increase by approximately 2.2 kg or 46%. This would exceed the system's mass budget and would make requirement *Sys-Prop-01* a driving one. This is a significant difference that could lead to serious changes in the overall design. In further design stages, this estimate can be looked into using more sophisticated software. Some literature indicates that the 2.2 value is close to reality for certain satellites [16, 27].

The second significant assumption is the average and maximum density models. The atmospheric density in VLEO is dependent on solar activity and is affected by the 11-year solar cycles [28]. To check the validity of this assumption the average density over the 5 most active years of solar cycle 20 was calculated using the NRLMSISE-00 Empirical Atmospheric model [28, 29]. The average density over this worst-case scenario was found to be 17.4% higher than the mean density estimate. The highest drag value estimated through NRLMSISE-00 was $5.11\,\mathrm{kg\,m^{-3}}$ which is only 16.4% higher than the one used in the model.

The last assumption is related to the effect of the satellite shadow on the active solar panel area. It has the largest effect in the LTAN 12h orbit where the shadow of the satellite falls directly on the panels. If it is assumed that the satellite shadows cover the whole back solar panel during 5% of the orbital period (half of the time the satellite is on the opposite side of the earth to the sun and not in eclipse) the decrease in total power generation would still not be that significant as this is the period when the panel is least efficient.

To account for the effects of those assumptions safety factors of 1.2 for the ΔV and 1.05 for the solar panel area were used.

6.2.2. Model Verification and validation

The model was verified in two steps: first through code and then through model verification. Code verification is the process of confirming that a section of code or an application functions according to the intended design specifications, while model verification is the process of confirming that the numerical model itself is accurate and reliable.

The code verification process followed the standard procedure of combining static code verification (through the use of Pylint [1]) with active unit, subsystem and system tests. Additionally, the code was explained to and tested by different members of the group to tackle the personal blind spots of the programmer.

Simple model verification was performed on the basis of several theoretical results:

- The eclipse fraction fits the one calculated based on a simple 2D model.
- The average velocity and drag values of the satellite in specific setups fit the ones estimated through theory.
- The average fixed and rotatable SP panel efficiencies of in the LTAN 6h, 9h and 12h orbits fit the theoretical results from previous design stages[12].
- If the effects of aerodynamic drag are turned off the model conserves its specific orbital energy.
- The total increase/decrease of the orbital energy from the effects of thrusting and aerodynamic drag fits theoretical results [22].

Further model verification was done using ESA's DRAMA tool [30]. A deorbiting manoeuvre was simulated starting at a standard starting orbital semi-major axis of 6371.8 km. Given 10 simulations of the different configurations the estimated semi-major axis decrease rate had an RMS deviation of 12.3% from ESA DRAMA's results.

To finally complete the verification of the model additional verification was done using Python's sgp4 library [2]. The SGP4 model is expected to give a large variation in the orbital position of the satellite compared to reality(in the order of 500 m radial displacement [31]), still over a day the deviation between the teams numerical model and SGP propagated position stayed below 739 m, or below a second in orbital time.

Further verification and validation of the model were not done due to time and software availability constraints. The validation of the model with real-world data is left for further analysis. A simple next step would be to improve the accuracy of the ΔV estimation using Ansys ODTK [3].

6.3. Effects of thruster angling on orbit

The addition of a component of thrust pointing in the zenith direction will affect the orbit of LAMP. The component of thrust acting in the zenith direction would not affect the semi-major axis or the

[1] https://pypi.org, last accessed on 21/06/2023
[2] pypi.org, last accessed on 21/06/2023
[3] www.ansys.com, last accessed on 21/06/2023

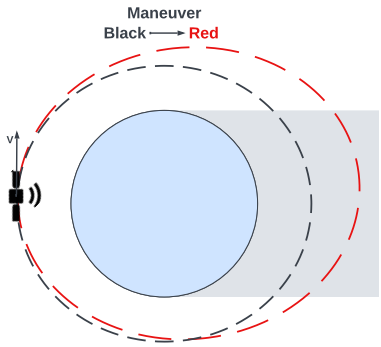

Figure 6.7: *Exaggerated view of a LAMP orbital maneuver*

inclination of the orbit however it will affect its eccentricity vector and thus lead to an increase in the nodal precession rate due to the J2 effect [32]. An exaggerated visualisation of the effects can be found in Figure 6.7. The combined effect of the zenith thrust over two manoeuvres will be 0 so the thruster angling would not lead to an increase in the eccentricity over time. However, the increase in average eccentricity will lead to a higher average nodal procession and disturb the sun-synchronicity of LAMP's orbit. To compensate for this effect the satellite will have to stay in orbit with an inclination slightly lower than 96.7°or execute periodical correction manoeuvres. The magnitude of this effect is excessively slow (each manoeuvre is $<0.1\,\mathrm{m\,s^{-1}}$). The ΔV budget of LAMP has 1% margin allocated for those and other miscellaneous orbit maintenance manoeuvres.

6.4. End of life deorbiting

To confirm that LAMP is able to fulfil the deorbiting requirement *U-ReS-03*, the end of life was simulated using ESA's DRAMA tool[30]. A 50% confidence interval was taken on the solar flux data predictions to simulate the slowest deorbiting scenario. For the simulation, it is assumed that the satellite will be tumbling at its EOL. Still, the satellite is predicted to deorbit to an altitude of $125\,\mathrm{km}$ in less than 22 days. The next report will further consider the process of atmospheric burnup of the satellite once it gets to altitudes of below $125\,\mathrm{km}$.

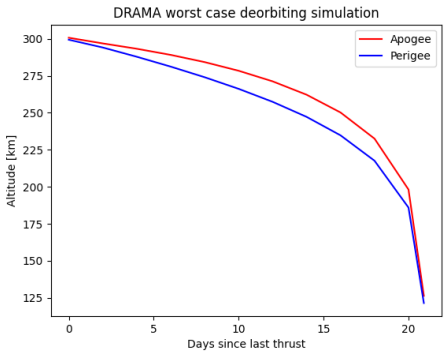

Figure 6.8: *EOL Deorbiting simulation result from ESA DRAMA. The simulation was taken for the period between 24/5/2023 and 13/6/2023.*

7

Guidance and Navigation subsystem

The Guidance, navigation and control subsystem is tasked with determining and predicting the position and orbit of the satellite at any given point in time. This chapter details the design process of LAMP's GNS. First in Section 7.1 the requirements derived during previous deign stages are given [12]. The sizing and the choice of components for the GNS are given in Section 7.2. Finally the subsystem architecture and performance specifications are given in Section 7.3 and Section 7.4.

7.1. GNS requirements

Table 7.1 presents all the system requirements applied to the Guidance and Navigation subsystem (GNS).

Table 7.1: *List of GNS system requirements. Description of the requirement with a specific ID, a rationale and the verification method are provided*

ID	Description	Rationale	Verif. M	
Sys-GNS-01	The GNS shall provide tracking of the satellite	Functional requirement of the GNS	Ana, Test	✓
Sys-GNS-01-I	The GNS shall provide the position of the satellite with an accuracy better than 368 m (3 standard deviations).	Functional requirement of the GNS, needed to determine the platform's position with sufficient accuracy.	Ana, Test	✓

U-GNS-01-I is the only performance requirement applied to LAMP's GNS. It is derived on the basis of based on the maximum allowed swath width deviation and some corrections applied due to pointing accuracy (*U-ADCS-02*,*SYS-ADCS-07* and *SYS-ADCS-08*).
The verification of both requirements can be accomplished using a combination of analysis and testing. It is a standard procedure for an engineering model to be used during verification. The GNS receiver will be tested using an RF vector signal generator that is capable of simulating GPS signals.

7.2. GNS design

This section contains a description of the GNS subsystem design process from the derivation of requirements and selection of settings to choice of components.

7.2.1. GNS choice of technology

During the preliminary development phase, ground station and GNSS positioning were investigated as possible technologies to be used in LAMP's GNS. After performing a trade-off between these options, it was concluded that the investigated ground station technologies do not provide the required positioning accuracy. Out of the GNSS positioning options the decision came down to a choise between

single-point single-frequency GNSS positioning and differential single-frequency GNSS positioning (using SBAS [33]). While differential GNSS provides higher accuracy, that accuracy is not required and is accompanied by higher system complexity. Thus it was decided that the best available technology for LAMP is single-point single-frequency GNSS positioning. With consideration of the limited power budget (Section 10.2), the use of miniaturised satellite GNSS receivers was researched.

An alternative option that received some attention during the detailed stage of design is navigation using LEO satellites, specifically the Starlink constellation. The gain of the main satellite communication patch antenna (Table 11.3) at low elevation angles however was found to be insufficient for such an operation. In case a separate GNS antenna is required, GNSS is far easier to implement and benefits from decades of LEO applications.

During this design phase, a passive or active GNSS antenna has to be selected. Active GNSS antennas use an integrated low-noise amplifier (LNA) to increase the power of the signal and noise after reception. This means that the losses after the amplifier will be drowned out and won't affect the overall noise figure. Additionally, the LNA by itself reduces the overall noise figure and results in better system sensitivity. The disadvantage is that it requires high amounts of power and is generally more expensive. If the GNSS link budget allows for it, a passive antenna is preferred. The choice of antenna is entirely dependent on the sensitivity of the receiver and thus its type will be chosen based on the choice of specific receiver and the GNSS link budget .

7.2.2. GNS sizing

To select a component combination capable of fulfilling LAMP's requirements, the GNSS link budget at LAMP's sun-synchronous orbit was calculated. The boundary case of the link budget is highly dependent on the selected elevation mask which first has to be chosen.

The choice of elevation mask will be based on the number of visible GNSS satellites during the orbit, the Geometric Dilution of Precision (GDOP) allowed by the satellites, and the gain of an average GNSS antenna at an equivalent beam width. The following calculations are performend based on an GNSS antenna placed on the top face of the satellite (Section 7.3). A numerical model provided by the DLR's Galileo competence centre[1] was used to simulate the GNSS satellite visibility and GDOP over the period: 30/05/2023 to 20/06/2023. The simulation considers only the worst-case satellite visibility and GDOP. Since GPS and Galileo satellites fly at an inclination of 55° and 56° respectively this occurs at the highest and lowest latitudes. The highest latitude of LAMP during orbit is 83.3°. The results for different elevation masks for a theoretical stationary antenna at an altitude of 309km(Section 6.2), latitude 83.3°and longitude 0°are presented in Table 7.2.

Table 7.2: *Elevation masks*

Elevation mask [deg]	GPS satellites visible	GALILEO satellites visible	GPS GDOP(Max)	GALILEO GDOP(Max)	Gain of reference antenna[2]
5°	11.3	9.4	2.3(3.99)	2.41(4.01)	-3 dB
10°	10.6	8.4	2.9 (5.0)	3.7(9.3)	-1.8 dB
15°	9.5	7.1	3.7 (5.6)	4.2 (14.3)	0 dB

The required GDOP for good connection is hard to quantify accurately. In general, GDOPs below 4 are considered sufficient for the relatively imprecise positioning requirements [34] (Section 7.1). For the number of satellites available the only requirement is that more than 4 satellites stay visible at all

[1] gnss-monitoring.dlr.de, last accessed on 21/06/2023

[2] anywaves.eu/products, last accessed on 21/06/2023

times[35]. Based on these results an elevation mask of 10°was decided on, as it provides sufficient GDOP and has more than four satellites visible at all times while not requiring the system to receive signals at very low antenna gain.

The link budget for a worst-case scenario of a GNSS satellite visible at 10°elevation angle is presented in Table 7.3.

Table 7.3: *GNSS link budget for 2 different satellite constellations.*

Source	GPS	GALILEO
GNSS transmitter EIRP	26.8 dB (L1)	35.1 dB(E1)
Atmospheric Attenuation	-2.0 dB	-2.0 dB
Free space loss	-184.2 dB	-185.3 dB
Receiver Antenna Gain (80°Beamwidth)	-1.8 dB	-1.8 dB
Noise	-202.9 dB	-202.9 dB
Line, connector & surge protector losses	-1.0 dB	-1.0 dB
Margin	3.0 dB	3.0 dB
Signal power at receiver passive	-163.4 dB	-155.6 dB
Signal to noise power density passive	36.2 dBc $-$ Hz	44.3 dBc $-$ Hz
Signal power at receiver active	-162.4 dB	-154.6 dB
Signal to noise power density active	35.5 dBc $-$ Hz	44.3 dBc $-$ Hz

7.2.3. GNS subsystem component selection

Commercial off-the-shelf single-point single frequency GNSS receivers compatible with either the GALILEO or GPS constellations were researched. Since there are options available that fulfil all GNS requirements, a trade-off has to be performed.

Trade-off criteria

The trade-off for selecting the best receiver was based on the following criteria:

- Power (40%) - The power required for the whole system if it was to use the specific receiver. The power required by an active antenna, if one is required due to insufficient sensitivity, is included in this parameter. The power budget from previous design stages allows 0.5 W of power for the subsystem.
- Cold start sensitivity (40%) - A higher sensitivity improves the robustness of the system. In general, the sensitivity should be at least 3dB below the calculated signal power or signal-to-noise ratio at the receiver. Reference minimum values can be found in Table 7.3.
- Ease of integration (20%) - during the development process it was discovered that the easiest place to position the GNSS receiver would be somewhere within the electronics stack. For this, the receiver needs to have a standard 1U plate shape. For the receivers that do not, a small integration plate or board needs to be included. Both options were considered of low enough complexity to be nominal in this criterion.

The power and cold start sensitivity were each given 40% of the total importance. This is because cold start sensitivity is the only criterion that considers the performance of the system. The power on the other hand, is the only external consideration that significantly limits the choice of components. Ease of integration was given the remaining 20% due to its lower relative importance.

The mass and volume were not included as criteria as all the considered receivers are well within the volume and mass budget (estimated 0.07% of the dry mass and 0.9% of the total volume Section 5.2). Additionally, volume-wise all, receivers will have approximately the same size as they will need to conform to the 1U plate shape to fit in the electronics stack.

7.2.4. Trade-off

The trade-off between the Comercial off the shelf (COTS) options is presented in Table 7.4 based on the aforementioned criteria. The goal of this trade-off is only to simplify the choice between multiple requirement fulfilling options.

Table 7.4: *GNS receiver trade-off table*

Criteria / Options	Power [40%]	Cold start sensitivity [40%]	Ease of integration [20%]
Spacemanic: Celeste The GNSS receiver[3]	0.100 W(Passive antenna)$^{\text{Green}}$	-178 dB$^{\text{Green}}$	Requires an additional board to integrate$^{\text{Yellow}}$
Skyfox Labs: PiNAV-NG[4]	0.124 W(Passive antenna)$^{\text{Green}}$	35 dBc $-$ Hz$^{\text{Yellow}}$	Requires an additional board to integrate$^{\text{Yellow}}$
SURREY: SGR-Ligo[5]	0.500 W(Active antenna) Yellow	33 dBc $-$ Hz$^{\text{Yellow}}$	Standard CubeSat board shape$^{\text{Green}}$
Accord: Navika-251[6]	0.595 W (Active antenna) Yellow	-166 dB$^{\text{Yellow}}$	Can be integrated in OBC$^{\text{Green}}$

Table 7.5: *Trade-off Legend*

Green	**Excellent**	Exceeds requirements
Yellow	**Nominal**	Meets requirements
Orange	**Correctable deficiency**	Can meet requirements with modification
Red	**Unacceptable**	Does not meet requirements

From the trade-off table, it can be seen that two options do not rely on active antennas which is beneficial for the power budget. This leaves only two receivers in consideration: the PiNAV-NG and Celeste. The two receivers are comparable in power consumption and ease of integration, however, Celeste allows for a significantly higher link margin both during initial position acquisition and normal operations. Thus, the Celeste GNSS receiver is selected for LAMP. The chosen receiver can operate with the GPS, Beidou and Glonass GNSS constellations. Out of those it was decided that LAMP will use the L1 GPS band at a frequency of 1575.42 MHz using only Coarse/acquisition(C/A) code ranging [36].

In general patch antennas are most commonly used in satellite applications [37]. The Spacemanic: GNSSANT GNSS antenna[7] was selected as it has already been tested flight tested with the Celeste receiver and provides sufficient gain both at zenith (4 dBi) and at 80°beamwidth (-2 dBi).

To integrate the receiver in the standard electronics CubeSat stack it will need an additional board to convert both the communication and power interfaces to the PC104 standard. The receiver is to be connected through an I2C interface to the connector board. As specified by the receiver manufacturer the connector board will have to also include a $3\,\text{k}\Omega$ resistor and an I2C separator (e.g. NXP PCA9507

[3] spacemanic.com, last accessed on 16/06/2023
[4] satcatalog.com, last accessed on 16/06/2023
[5] sstl.co.uk, last accessed on 16/06/2023
[6] satsearch.co/products, last accessed on 16/06/2023
[7] www.spacemanic.com, last accessed on 16/06/2023

2-wire serial bus extender[8]).

7.2.5. Trade-off sensitivity analysis

To access the validity of the results from the previous section a sensitivity analysis of the trade-off in Table 7.4 was performed consisting of two phases - first by looking into the confidence intervals of the numbers in the table and then by varying the weights of the different criteria. Since the data for power and cold-start sensitivity are based on manufacturer datasheets they are considered to be of high precision. The ease of integration grades, however, are based on engineering judgement. A case when the outcome would be different is one when the development of an integration PCB turns out to be costly in human and time recourses. In such case the Surrey: SGR-Ligo and the Accord: Navica-251 would be the preferred options. The Celeste GNSS receiver outperforms all its competitors in both terms of power and sensitivity. This means that the ease of integration is the only criterion that could change the outcome of the trade-off. The Skyfox Labs: PiNAV-NG, the closest competitor to the Celeste GNSS receiver, suffers from the same integration issues as the chosen option and thus even if the weight of the ”Ease of integration” was increased, it would not influence the result.

Since the trade-off is a comparison between different options that all fulfill the technical requirements, the grading of the different options was entirely subjective, despite using objective values. For example the difference between 0.1 W and 0.5 W power consumption represents only approximately 1% of the entire continuous power budget (Table 5.3). Thus it should be noted that the decision is also sensitive to the choice of grades. In case that all options were graded yellow in power consumption, the two active antenna options would become significantly more attractive due to their low ease of integration. However the better sensitivity of Spacemanics's Celeste GNSS receiver would still make it the best option in the trade-off.

7.2.6. GNS operations

The subsystem has 3 operational modes:

- Cold start: At the start of a LAMP mission the receiver will need to acquire a connection with GNSS satellites and calculate GPS lock. This mode lasts 35 s on average and consumes 1 W of power.
- Hot start: This mode occurs when the receiver has been connected to an insufficient number of satellites and has some estimation of where it is positioned. This mode lasts 30 s on average and consumes 0.3 W of power.
- Nominal operations: The receiver operates continuously and sends live data about the position of the satellite to the OBC. In this mode, it consumes on average 0.1 W of power.

Additional information about the planned operations of those modes is included in Chapter 5.

In case of a minor failure or unexpected behaviour during operations the operations team will be able to use the debug mode of the Celeste GNSS receiver to carry out investigation and implement software updates.

7.3. GNS architecture

The subsystem consists of a passive antenna, receiver and connector board. The layout of all the components and their sub-components can be seen in Figure 7.1.

The GNSS receiver is attached directly to the connector board. The connector board itself with a 1U area is placed in the electronics stack. It is connected through a PC104 connector block to the rest of the boards to avoid the use of tangled cables.

[8]www.nxp.com, last accessed on 16/06/2023

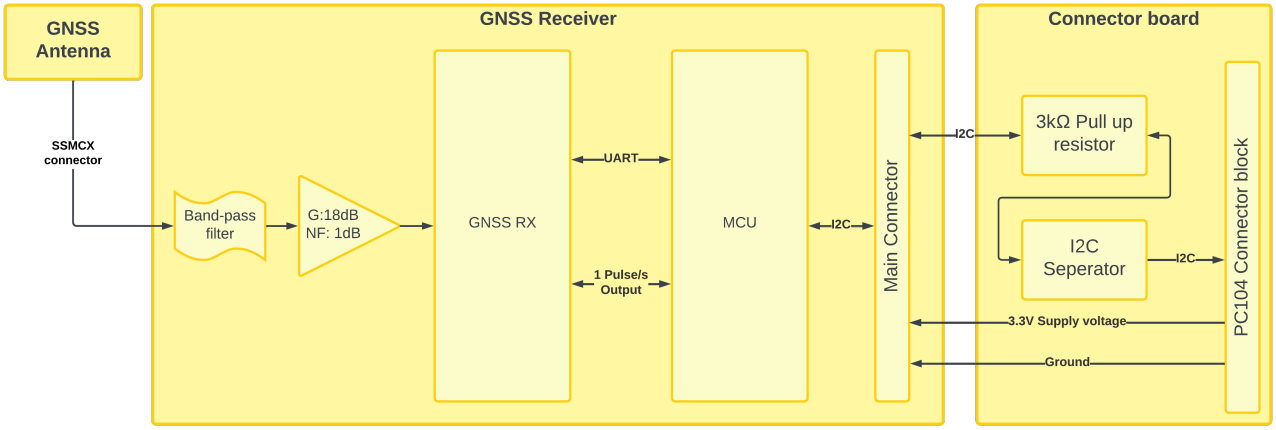

Figure 7.1: *GNS block diagram*

The GNSS antenna is positioned on the top face of the satellite, pointing in the zenith direction as recommended by the manufacturer, removed as far as possible from the main communications antenna to reduce the interference between the 2 antennas. The antenna is connected through a coaxial cable with two SSMCX RF connectors as specified in the receiver and antenna datasheets.

7.4. GNS performance

Table 7.6 presents the specifications of the GNS systems. Values from the manufacturer datasheets[9][10] are used for the GNSS antenna and receiver. A standard estimation of a GNSS system's performance analysis would include an estimation of the system's positioning accuracy. This analysis however was considered redundant as the coarse positioning requirement of LAMP will not be exceeded in continuous GPS operations [36] during operations.

Property	Value
Subsystem Mass	35 g
Subsystem Volume	0.202 U
Subsystem Price	€7767
Average Subsystem power	0.100 W
GNS system Sensitivity	182.1 dB
Elevation mask	10°
Positioning accuracy (C/A code)	2m CEP

Table 7.6: *GNS performance parameters*

[9] www.spacemanic.com/Antenna, last accessed on 16/06/2023
[10] www.spacemanic.com/Receiver, last accessed on 16/06/2023

8

Attitude Determination and Control Subsystem

In this chapter, the design and final sizing for the ADCS are performed. First, a newly updated trade-off table is presented, after this the sizing and selection for the new actuators are performed, followed by an architecture, performance and operations overview.

8.1. ADCS requirements

From the Midterm report [12], a series of subsystem requirements for ADCS was generated. These are tabulated in Table 8.1, along with their rationale and respective verification method.

Table 8.1: *ADCS requirements.*

ID	Description	Rationale	Verif. M.	
Sys-ADCS-01	The ADCS shall provide attitude determination ability to the satellite throughout the system's lifetime.	Functional requirement of the ADCS.	Ana	✓
Sys-ADCS-01-I	The satellite shall be able to determine its attitude during tumbling at 200 °/sec.	The ADCS needs to be able to measure rotational rates to determine attitude control.	Ana	✓
Sys-ADCS-01-I-1	The satellite tumbling sensor shall have an update time of 1.1 hz. when measuring	The ADCS needs to be able to measure in time otherwise you don't know which way you are spinning and might make the assumption you are spinning to opposite way.	Ana	✓
Sys-ADCS-02	The ADCS shall provide attitude control to the satellite throughout the system's lifetime.	Functional requirement of the ADCS.	Ana	✓
Sys-ADCS-02-I	The satellite shall be able to recover from tumbling at 200 °/sec in 40 orbits	Expected disturbance scenario which the ADCS needs to handle (e.g. in case of collisions with debris) and max time without propulsion burn.	Ana	✓
Sys-ADCS-02-II	~~The satellite shall be able to provide a maximum TBD Nm of torque for TBD amount of time.~~	~~Torque required to meet~~ *Sys-ADCS-02*.	~~Test~~	-

Sys-ADCS-02-III	The satellite shall be able to provide a minimum < *2.59E-05, 3.60E-04, 3.88E-05*> Nm of torque for the roll pitch and yaw body axis for the entire mission duration.	Torque required to meet *Sys-ADCS-02*.	Ana	✓
Sys-ADCS-03	The satellite shall be able to store <*30.1, 61.5, 12.4*> mNms moment impulse for the roll pitch and yaw body axis.	Necessary for momentum dumping.	Test	✓
Sys-ADCS-04	~~The satellite shall be able to provide TBD Nms momentum dumping.~~	~~Momentum dumping is required when momentum or reaction wheels are used.~~	~~Test~~	-
Sys-ADCS-05	The ADCS shall change the pointing direction of the satellite platform by 30° in one orbit.	The attitude should be changed within a certain time span to avoid overshooting the payload objects on the ground.	Ana	○
Sys-ADCS-06	The ADCS shall be capable of mitigating disturbance torques.	The ADCS has to be able to restore the original attitude after disturbances have been imposed.	Ana, Demo	✓
Sys-ADCS-06-I	The satellite shall have a dipole moment below 0.27 A/m in all body axes.	Constraints magnetic disturbance torques imposed by external magnetic field.	Ana, Demo	○
Sys-ADCS-06-II	~~The satellite center of mass shall be TBD m from center of pressure in nominal and thrusting modes~~	~~Constraints aerodynamic disturbance torques.~~	~~Test, Ana~~	-
Sys-ADCS-07	The ADCS shall provide a pointing accuracy of $\pm\ 0.002°$.	Pointing accuracy required to meet U-ADCS-02 combined with DST specifications.	Ana	○
Sys-ADCS-08	The ADCS shall provide a pointing knowledge of 5 arcsec.	Pointing knowledge required to meet *U-ADCS-03* combined with DST specifications.	Ana	✓
Sys-ADCS-09	The ADCS shall provide a pointing stability of 2.4 arcsec/s.	Pointing stability required to meet *U-ADCS-04* combined with DST specifications.	Ana	✓

Requirement *Sys-ADCS-02-II* has been removed from the list of system requirements because it the torque was to be determined over the mission duration not over a TBD amount of time. Requirement *Sys-ADCS-04* was removed as it was phrased incorrectly and because of this was not discussed further. Lastly, requirement *Sys-ADCS-06-II* was removed because getting the final value for the center of pressure was found to depend on more than initially expected resulting in it not being possible to give a reasonably supported value.

8.2. ADCS design

In the following subsections, the final design for the ADCS will be discussed and elaborated with the use of calculations, estimations and examples. As discussed in Section 6.1 two configurations were considered for the sizing of the ADCS. The final design selection the ADCS is sized for is the CIV-Ff$_{h_i}$-Sf$_i$ configuration as can be seen in Table 10.5.

8.2.1. ADCS choice of technology

The initial selection for the sensors and actuators for the ADCS was performed in the midterm report [12], this trade-off determined that using two star trackers alongside one single magnetometer would adequately fulfil the requirements on ADCS sensors for LAMP. For the actuators, the trade-off concluded that the biased reaction wheel assembly (BRWA) was the best option. In this section

the trade-off table for both the sensors and actuators will be shown again. This is because there have been some changes due to the in depth analysis performed for the final report that revealed the necessity of reviewing the midterm trade-offs.

ADCS sensors

Starting with the sensor trade-off, a more detailed investigation of the selected sensors demonstrated that the two star trackers and one 3-axis magnetometer do not provide satisfactory redundancy. Therefore a more extensive and detailed trade-off is repeated and shown in this section.
The updated version of the trade-off only includes magnetometers, gyroscopes, sun sensors, and earth sensors. The reason for this is that star trackers have not been re-added to the trade-off. Star trackers are the only sensors that can achieve the determination precision needed to comply with requirement *Sys-ADCS-08*. With the precision determination requirement met by adding two star trackers to LAMP, this criterion and the option were removed in order to provide a better focused trade-off on the remaining sensors.

Table 8.2: *ADCS sensor trade-off [38, 7, 5, 39]*

	Mass [14%]	**Volume [24%]**	**Slew rate [24%]**	**Drift [24%]**	**Availability [14%]**
Magnetometer	Green 0.008-0.22 kg	Yellow Nominal	Yellow High	Green None	Yellow Short singularity at poles
Gyroscope	Yellow <0.1-2.36 kg	Yellow Nominal	Green Very high	Red 0.003-1 deg/h	Yellow Nominal
Sun sensor	Green 0.1-2 kg	Yellow Nominal	Orange Moderate	Green None	Orange Fails out of sunlight
Earth sensor	Green 0.03-1.5 kg	Yellow Nominal	Orange Moderate	Green None	Orange Fails in direct sunlight

From this newly revised trade-off it becomes clear magnetometers are still the best option. However, this time redundancy was considered, such that the final selection consisted of two star trackers and two magnetometers (instead of one).

ADCS actuators

As explained in subsection 8.2.1 a previous actuator trade-off concluded that BRWA are the best actuator option. This was mainly caused by a favourable volume, higher accuracy and higher reliability of the option. Following this selection, for the final report, an in depth analysis for the final sizing of the BRWA was performed. This analysis concluded that the selection in the midterm report was incorrect. The reason for which was a much lower allowable RPM for the reaction wheels in turn enlarging the reaction wheel to an unreasonable mass and size. Therefore the use of control moment gyroscopes (CMGs) had to be reconsidered for the trade-off. The calculation for this updated RPM is given in subsection 8.2.2 with the result of the new sizing given in the updated actuator trade-off table Table 8.3.

Table 8.3: *ADCS actuator trade-off*

	Mass [16%]	**Volume [16%]**	**Jitter [27%]**	**Pointing accuracy [21%]**	**Roll Axis Control [10%]**	**Reliability [10%]**
Control Moment Gyroscopes	Yellow ∼500g	Yellow 0.4-0.8 U	Green low, due to gyroscopic effect	Orange 0.05-0.1 deg (0.001 deg feasible)	Green Fast control	Orange has singularity points
Biased Reaction Wheels 3-Axis	Red 35 kg	Red ∼ 16U	Red RPM range too low	Green 0.0001 deg, constraint depends on attitude sensors	Green Fast control	Yellow Nominal

With the newly updated values for the trade-off criteria, the new best option is the CMGs as they are the only available option that complies with the criteria, for the rest of the report the sizing and final component selection will be worked out.
For both trade-offs the sensitivity analysis performed in the midterm report [12] remains valid as the criteria are the same. The only thing that can be noted is that for the actuator trade-off, the BRWA scores substantially lower now when compared to the midterm making CMGs the only viable option thus decreasing the sensitivity of the trade-off.

8.2.2. ADCS sizing

Now that both the trade-off for the sensors and actuators have been finalised the ADCS can be sized and selected. Starting with the sensor selection and followed by the actuator sizing and selection.

Sensor sizing

For the sensor trade-off performed in subsection 8.2.1 the final selection is to have two star trackers and two magnetometers placed inside LAMP. These sensors will be, as explained in the midterm report [12], COTS products. The selected sensors are two Sagitta star trackers[1] and two NewSpace Systems magnetometers[2] which have an update rate of 25 Hz. The combination of these two types of sensors means that LAMP meets all requirements regarding the sensors, and includes redundancy in case of a magnetometer failure.

Actuator sizing

In this subsection, the sizing of the CMGs and magnetorquers will be discussed. First, the magnetic moment and angular momentum calculations are discussed. These are followed by an explanation of how the jitter analysis was performed and the BRWA jitter results are shown. Lastly, the actual sizing and component selection of the magnetorquers and CMGs is done.

Magnetic moment calculations

In order to size the magnetorquers, the magnetic environment in which the spacecraft orbits must be known. A tool was created to calculate the magnetic moment on the spacecraft throughout multiple orbits. Firstly, a pre-existing MATLAB tool to calculate the vector of the magnetic field strength[3] that uses the International Geomagnetic Reference Field[4] (in terms of intensity, inclination and declination)

[1] arcsec.space, last accessed on 19/06/2023
[2] cubesatshop.com, last accessed on 19/06/2023
[3] github.com, last accessed 20/06/2023
[4] ncei.noaa.gov, last accessed on 20/06/2023

was adapted into Python and integrated into the rest of the ADCS tools. These values are thence transformed from an ECEF reference frame into the body axis system of the spacecraft to output the magnetic field strength in the pitch, roll and yaw axis respectively, using the transformation matrix described in Equation 8.1, where λ is the longitude, ϕ the latitude and μ the magnetic field strength in the respective axis.

$$\begin{bmatrix} B_{yaw} \\ B_{pitch} \\ B_{roll} \end{bmatrix} = \begin{bmatrix} -cos(\lambda)sin(\phi) & -sin(\lambda)sin(\phi) & cos(\phi) \\ -sin(\lambda) & cos(\lambda) & 0 \\ -cos(\lambda)cos(\phi) & -sin(\lambda)cos(\phi) & -sin(\phi) \end{bmatrix} \begin{bmatrix} B_x \\ B_y \\ B_z \end{bmatrix}_{ECEF} \tag{8.1}$$

With the magnetic field vector calculated, the minimum dipole moment around each axis can also be calculated, to be used later to size the magnetorquers. This can be done by considering the scalar equation for the magnetic moment, seen in Equation 8.2, where m is the magnetic moment, τ the torque and B the average magnetic field strength for a body axis. Using an average disturbance torque, the minimum dipole moment can be estimated such that the angular momentum does not continuously grow, but stabilizes. The magnitude of this averaged torque was calculated by considering times that certain modes and their corresponding torques outlined in Section 6.1 are active over a certain amount of orbits (excluding however the spacecraft magnetic torques). An added step of analysis compares this value to the nominal mode and takes for the new averaged torque the highest torque for each axis. This ensures that when the thrusting mode occurs later than expected that no unaccounted build up of angular momentum occurs.

$$m = \frac{\tau}{B} \tag{8.2}$$

The magnetic moment created by the magnetorquer at a certain dipole moment is also used for detumbling. To satisfy the requirement of detumbling $200\,\mathrm{deg/s}$ detumbling speed in 40 orbit, a dipole moment was calculated such that in 40 orbits at a average magnetic field this angular rate was removed. The maximum dipole moment for an axis for both detumbling and desaturation was then used as the minimum dipole needed to be provided by the magnetorquer. This dipole moment was then used to calculate the torque that can be provided by the magnetorquers due to a certain magnetic field. This calculation was done for each body axis for any time during 30 orbits. Where 30 orbits is the approximate time to return to the same orbit due to orbital precession.

Angular momentum calculation

The magnetorquer torques list was converted to the angular momentum, this was done by subtracting a magnetorquer torque from an input torque for each point of time per axis. Following this, by integrating these torques the angular momentum envelope can be created, it must be noted that this envelope can contain both positive and negative angular momentum. The negative angular momentum corresponds to the situation where a magnetorquer creates too much torque and creates angular momentum in the opposite direction of the applied disturbance torque. Within the model, the direction of the disturbance torques around a specific axis is not evaluated, making it possible that a disturbance torque acts in an opposite direction. This exacerbates these negative angular momentum torques above the maximum calculated angular momentum.

To prevent this and contain the analysis in one direction only, the angular momentum values are looped through. If the angular momentum increases at a point in the analysis while the angular momentum is negative, the graph is shifted from this point upward such that this increase is visible above the x-axis. Lastly, the values below 0 are clipped to become 0 so there are no remaining negative values.

The input torques that were used for the analysis were the averaged torques described in the section above Equation 8.2. This does take the average effect of thrust into account, however, the assumption that the average torques are perfectly distributed can deviate from actual results. Concentrated torques that take place seldom occur and are significantly higher than other torques and can create areas of higher angular momentum that need to be stored. Due to the fact that the torques are relatively similar in both nominal and thrusting mode for the CIV-Ff$_{h_i}$-Sf$_i$ configuration selected in Section 6.1 this effect was neglected.

Jitter calculations

In this section, jitter analysis will be presented which also includes the calculations performed for the BRWA prior to selecting the CMGs as the findings from the jitter analysis for the BRWA resulted in the need to redo the actuator trade-off. The equations used for the jitter analysis are split into a static unbalance jitter Equation 8.3 Equation 8.4 Equation 8.5 and dynamic unbalance jitter Equation 8.6 Equation 8.7 Equation 8.8 [40]. Where mr equals the static unbalance, mrd equals the dynamic unbalance, ω is the angular velocity of the wheel, c is the wheel distance to the spacecraft centre of mass (CoM) in meters and Ixx/yy is the spacecraft moment of inertia.

The value used for spacecraft moment of inertia, was the minimum value derived from all axis from subsection 15.2.2. This value imposed the largest constraint on the design of the BRWA as a smaller value of moment of inertia means that the spacecraft can move around easier. It is important to note however that subsection 15.2.2 states that the moment of inertia is underestimated. This consequently means that when calculating jitter at a certain RPM the result is overestimated.

The wheel distance to the centre of mass has been derived from the 3D model that was made of LAMP and is approximately From the model 0.1 m, The values for the static and dynamic unbalances are taken from 3×10^{-6} kg/m^2 for the static and 1.4×10^{-6} kg/m^2 for the dynamic unbalance[5].

$$F_{su} = mr\omega^2 \tag{8.3}$$

$$\dot{\omega}_{x/y} = \frac{cF_{su}}{I_{XX/YY}} \tag{8.4}$$

$$\left|\omega_{x/y\,static}\right| = \frac{\left|\dot{\omega}_{x/y}\right|}{\omega} \tag{8.5}$$

$$|N_{du}| = mrd\omega^2 \tag{8.6}$$

$$\left|\dot{\omega}_{x/y}\right| = \frac{|N_{du}|}{I_{XX/YY}} \tag{8.7}$$

$$\left|\omega_{x/y\,dynamic}\right| = \frac{\left|\dot{\omega}_{x/y}\right|}{\omega} \tag{8.8}$$

To find the maximum RPM possible, the dynamic unbalance equations Equation 8.6 - Equation 8.8 have been rewritten with the jitter requirement of maximum 2.4 arcsec/s or 1.164×10^{-5} rad/sec (*Sys-ADCS-09*) filling in these values result in Equation 8.9

$$\omega_{max} = \frac{I_{XX/YY} \cdot \omega_{x/y\,dynamic}}{mrd} = \frac{0.62 \cdot 1.164 \cdot 10^{-5}}{1.4 \cdot 10^{-6}} = 5.153\,rad/s = 49.22\,RPM \tag{8.9}$$

Using these values a maximum angular rate of 49 RPM was calculated for the BRWA due to the occurrence of excessive jitter caused by dynamic unbalance. Moreover, the presence of static unbalance further diminishes the potential RPM range. Additionally, it is typical for BRWA systems to be continuously spinning, resulting in a narrower effective RPM range.

It should be noted that the limited RPM range is influenced by the underestimation of moment of inertia, as mentioned earlier, underestimating the maximum angular rate. However, due to the linear relation between moment of inertia and maximum angular rate the maximum estimated error rate of about 9% does not significantly, the size of a BRWA would have to be at such a small range of RPM. At the size needed for this RPM range, it is impossible to fit the wheels inside LAMP. As opposed to BRWAs, CMG jitter was possible for miniaturised CMGs at around 0.72 arcsec/s [41].

Magnetorquer and CMG sizing and selection

The sizing of the magnetorquers and the CMGs is done with the use of a process that combines the iterative and optimization process for both designs such that mass is minimised. These calculations are closely related to each other as a change in the sizing of one results in a different sizing of the other. A larger magnetorquer means that at lower magnetic fields it may be more capable to counteract disturbance torques meaning that it does not have to be stored by the CMGs. Alternatively if the CMG can be sized larger to store more angular momentum without a large penalty of weight the magnetorquer can be sized smaller.

This can be transformed in an iterative sizing process where the dipole moment is used as the variable to adjust (keeping above the minimum dipole moment stated in subsection 8.2.2) to get an overall

[5] cubespace.co.za, last accessed on 20/06/2023

minimum mass. The dipole moment itself is used as an input for the sizing of the magnetometers and the CMG. The magnetorquers are sized on a dipole moment which is the result of a summation of the dipole moment together with the spacecraft specific dipole moment (such that magnetic torques are also taken into account). Next to this, as magnetorquers can not operate while the magnetometers are measuring, a cycle time of 0.9 sec for the magnetorquer and 0.1 sec for the magnetometer per second[42] was assumed to be used for the sizing. This results in a factor of 1.11. Lastly, a safety factor of 1.5 was also included. The mass was then sized based on statistical values to provide a continuous space of dipole moment to mass/volume and power.
The final sizing results for the magnetorquers resulted in the following minimum required values for electric current density $\mathrm{A/m^2}$, For yaw $2.2\,\mathrm{A/m^2}$ is needed, for pitch $18\,\mathrm{A/m^2}$ is needed and for roll $10\,\mathrm{A/m^2}$ is needed.
With the required values for the electric current density known for every axis it is possible to select suitable COTS magnetorquers. The magnetorquers have been selected so that their performance closely relates to the required electric current density. This was decided as sizing them this way will ensure they are not oversized in performance or mass. For the yaw axis, the best available magnetorquer is the GMAT-1[6]. For the roll axis, the best available magnetorquer is the MTQ[7]. For the Pitch axis, the best available magnetorquer is the MTQ800[8].

During the final stages of the design a large amount of available space inside LAMP indicated that the CMGs could take up more volume than initially expected increasing the potential wheel radius. This is efficient for the mass of the CMGs as a mass farther away from an origin creates a higher moment of inertia meaning that when rotating it can store more angular momentum, more mass efficiently. This mass for the CGMs in the iterative process was calculated using the process outlined in [12], which sizes the CMG based on the angular momentum required. Several minor variables were edited including a new wheel radius of 35 mm and a safety factor of 1.5.
The angular momentum itself was based on the input dipole moment of the magnetorquers and the calculation from Equation 8.2.2 and a particular mounting strategy of the CMGs. There are two main configurations to mount CMGs inside a spacecraft, a rooftop cluster (CMG at every corner) and as a pyramid cluster (CMG in the middle of each side)[43]. A visual representation of both can be observed in Figure 8.1. The axis in this image corresponds to the body axis outlined in Section 6.1.
Each configuration has advantages and disadvantages, in the case of LAMP it has been decided to mount the CMGs in a rooftop cluster formation. The reason for this was primarily because the cross position of the pyramid cluster requires a non optimal placing due to propulsion and the instrument box of the DST being in the way. An added benefit to this type of mounting is that it reduces the severity of the singularity points [43].

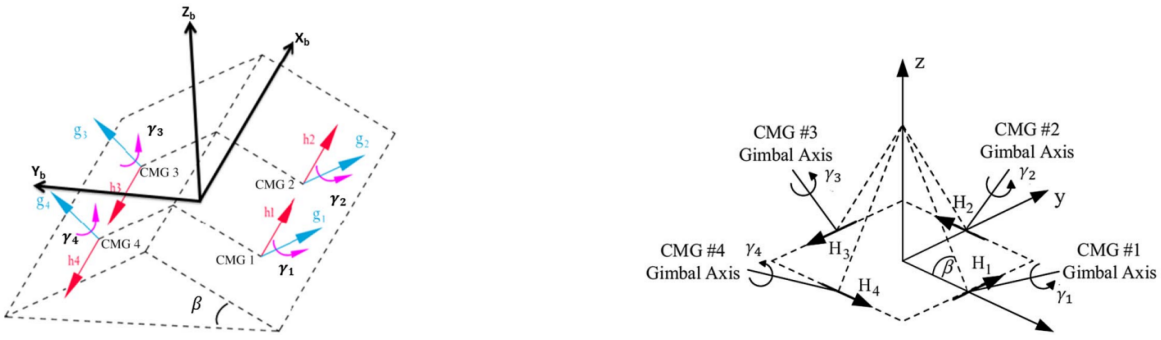

(a) *Example of a rooftop cluster* **(b)** *Example of a pyramid cluster*

Figure 8.1: *CMG Cluster configurations [43]*

As such the angular momentum that was required to be produced by each of the four CMGs was calculated with Equation 8.10 and Equation 8.11 [43]. In these equations H_{body} is the angular momen-

[6] cubesatshop.com, last accessed on 14/06/2023
[7] satcatalog.com, last accessed on 14/06/2023
[8] satsearch.co, last accessed on 14/06/2023

tum for a certain body axis specified after a colon and H_{sizing} the angular momentum that one of the CMGs have to deliver.

$$\tan\beta = \frac{H_{body}:yaw}{H_{body}:pitch} \quad (8.10) \qquad H_{sizing} = max(\frac{H_{roll}}{4}, \frac{H_{pitch}}{4 \cdot \cos\beta}) \quad (8.11)$$

In order to be able to estimate the final volume, a value of $0.8989\,\mathrm{U/kg}$ was used. This value was estimated using the mass averages of statistical data from COTS CMGs. For the peak power the same method was used to find a value of $5.36\,\mathrm{W/kg}$. The final result for a singular CMG is a mass of $116\,\mathrm{g}$, a volume of $0.104\,\mathrm{U}$ and a peak power consumption of $0.622\,\mathrm{W}$. A rooftop mounted cluster of 4 CMGs (mounted in the at an angle of $22\,\mathrm{deg}$) will be capable of providing an angular momentum of $15.69\,\mathrm{nNms}$. The torque that the CMG's can produce is left for further study but it should exceed the torques in the requirement *Sys-ADCS-02-III*

While looking at and designing for different RPM values of the CMGs it is important to consider at what maximum speed a wheel can spin before it would be destroyed by the stress caused by the rotation. This was calculated with the use of Equation 8.12. Which for an aluminium wheel that is slightly larger than the ones in the CMGs, with an average yield stress of 270MPA, a density of 2700$kg/m3$ and a radius of 5cm (sized for the absolute maximum space available in LAMP for four CMGs) would result in a maximum of over 100,000 RPM showing that the rotational speed is likely not a limiting factor as typical CMGs spin in the range of 8000-30000 RPM.

$$\sigma_z = \omega^2 r^2 \frac{\rho}{3} \quad (8.12)$$

8.3. ADCS component overview

In Table 8.4, a complete overview of the components that make up the ADCS is presented. These components are the ones described in the sections above in this chapter.

Table 8.4: *List of ADCS components*

ADCS Components	Number
Sensors	
Star Tracker [Sagitta]	2
Magnetometer [NewSpace Systems]	2
Actuators	
CMG [Built in house]	4
Magnetorquer 1 [GMAT-1]	1
Magnetorquer 2 [MTQ]	1
Magnetorquer 3 [MTQ800]	1

8.4. ADCS operations

In Figure 8.2, the ADCS control architecture can be found. This diagram shows the interaction between platform subsystems, the internal algorithms of the ADCS subsystem, and external disturbances on the LAMP platform.

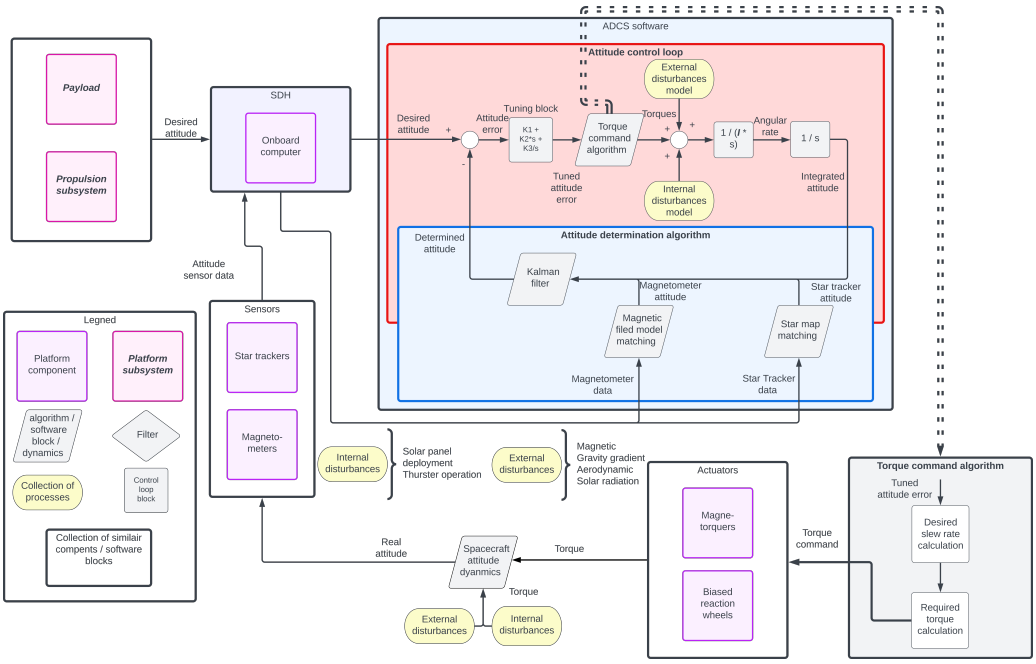

Figure 8.2: *ADCS control architecture*

Figure 8.2 starts off with the groups which require attitude control, namely the payload and propulsion subsystem. These pointing requirements are known by the onboard computer, which uses its software to command the spacecraft. The software starts with the ADCS control loop[9], in which the error between the determined attitude and the required attitude is computed. This is then put through a tuning block, in which s is the complex frequency domain variable. The tuning block ensures that the control loop is proportional-integral-differential and thus both drift and steady-state error can be eliminated. The tuned attitude is then put through an algorithm which calculated the required torques. This signal is both kept internally for the control loop and sent to the actuators to operate. Internally in the control loop, the actuator torques and the modelled disturbance torques are added together to compute the spacecraft dynamics. In the second block, I is the spacecraft inertia tensor. In this block, the torques are converted into angular rates to angular rates by computing the spacecraft dynamics. The angular rates are then converted back into the attitude by integrating them in the following block. This integrated attitude is combined with both the star tracker and magnetometer attitude data to get an estimated attitude which is used as feedback in the control loop.

Going back to the torque calculation block, from this block, the ADCS software sends commands to the actuators which apply torque on the spacecraft. The actuator torques and the disturbance torques change the attitude of the spacecraft. The new attitude is measured by the sensors which sent the attitude data to the central computer. In the central computer, the attitude data is processed to determine the attitude by matching the magnetometer measurement to a model of the magnetic field and matching the Star Tracker images to models of the sky map. The sensor-based attitude is then passed through a Kalman filter with the attitude that was integrated in the control loop to determine an estimated attitude. Subsequently, this estimated attitude is then utilised as feedback within the control loop, as mentioned previously.

[9]The control loop is based upon material of the AE2235-I course by Dr.ir. C.C. de Visser

9 Thermal Control Subsystem

Throughout the mission, LAMP will be exposed to a harsh and constantly changing thermal environment, due to the change in solar radiation during the orbit. To ensure that all of the components in LAMP can operate and survive within this harsh environment, a thermal control subsystem (TCS) must be designed. The TCS can have the functions of both protecting the spacecraft from radiation, cooling it down, but also to heat up components.

Section 9.1 introduces the requirements of the TCS and the need for thermal control. subsection 9.2.2 refers back to the Midterm report's TCS trade-off and which components were selected. subsection 9.2.1 to 9.2.5 introduce the thermal modelling and analysis software, as well as the sizing of the selected TCS components, and the performance of the chosen TCS strategy. Subsequently, the verification and validation of the model used is done in subsection 9.2.6.

9.1. TCS requirements

From the Midterm report [12], a number of system and subsystem requirements were identified. For the TCS, the requirements generated are tabulated in Table 9.1, along with the rationale for each requirement.

Table 9.1: *Thermal control subsystem requirements.*

ID	Description	Rationale	Verif. M.	
U-Thm-01	The satellite platform shall include a thermal radiator for the payload, compliant with the temperature and heat flows of the selected payloads	Indicates the need for thermal control for different payloads	Insp	✓
Sys-TCS-01	The satellite shall be capable of withstanding the expected thermal environments that it could encounter	Maintaining all subsystems and payload at their operational temperature ranges	Demo	✓
Sys-TCS-01-I	The TCS shall keep the payload below $200\,\mathrm{K}$	The payload has a certain operational temperature range to properly function	Ana	✓
Sys-TCS-01-II	All components shall be able to withstand at last 30000 thermal cycles	Derived from the number of orbits over the satellite's lifetime (sunlight-eclipse cycle)	Ana	✓

Sys-TCS-02	The TCS shall keep the temperature gradient for the structure below $20\,\mathrm{K/mm}$	Functional requirement to maintain operational temperature of structure		○
CON-Res-Tp-04	The satellite shall withstand fairing heat loads of $500\,\mathrm{W/m^2}$	Structural integrity constraint dictated by launch provider	Ana	✓
Sys-Gen-01	All the subsystems shall comply with the power budget	Constrain the individual power requirements of the subsystems	Test	✓
Sys-Gen-02	All the subsystems shall comply with the mass budget	Constrain the individual mass of the subsystems	Test	✓
Sys-Gen-03	All the subsystems shall comply with the volume budget	Constrain the individual volume of the subsystems	Test	✓

The main requirement for the TCS is to maintain all the components of the spacecraft at their required operating temperature ranges (requirement *Sys-TCS-01*), throughout the changing thermal environment during each orbit. For the main components of the spacecraft, their operational temperature ranges can be seen in Table 9.2.

Table 9.2: *Required operating temperature ranges of the different satellite components.*

Component	Min. temperature [°C]	Max. temperature [°C]
DST [1]	-	7
DST instrument box [1]	-	-73
Batteries [44]	25	40
OBC [45]	-25	65
Solar array [5]	-150	100
Propellant tank [46]	90	100
Propellant lines [46]	120	150
Thruster [46]	-5	200
Structure [47]	-100	100
Control moment gyro [1]	-20	60

From Table 9.2, one can observe that one of the most constraining components is the DST instrument box, which has a maximum operating temperature of $-73\,$°C, as compared to most other components, which have much higher maximum temperatures, hinting at some cooling strategy being required for the instrument box. Similarly, the propellant tanks and lines have high minimum temperatures of $90\,$°C and $120\,$°C respectively, mainly due to the choice of iodine propellant, which must be kept at high temperatures (for further considerations, refer to Chapter 14). This hints at the need for some heating strategy for these components.

9.2. TCS design

In this section, the TCS strategy will be designed. This shall be done iteratively with the use of a thermal model described in subsection 9.2.1, whose results (shown in subsection 9.2.4) are used to size the different TCS components and analyse their performance.

9.2.1. Thermal model

To design the TCS, the thermal environment where the spacecraft orbits in must be described, yielding the radiation incident on the spacecraft throughout the orbit. Moreover, the thermal transport phenomena (namely conduction as well as the aforementioned radiation) within the spacecraft must be described and studied. For this purpose, a thermal analysis tool was developed [2], wherein the spacecraft is described as a group of nodes, and the thermal interactions between those nodes and

[1] satcatalog.com, last accessed 16/06/2023
[2] github.com, last accessed 13/06/2023

with the environment are modelled.

To simplify the model, a series of assumptions were taken. Firstly, a small number of nodes were used, where only the more temperature-critical components (namely the ones mentioned in Table 9.2) were analysed. This was done to reduce development, computation and testing times, as well as to keep the modelling within the scope of the project. Another major simplifying assumption is that the radiation between internal components of the spacecraft is neglected. Even though there is some radiation emission from the internal components (especially coming from the propulsion system), strategies can be employed to thermally isolate the nodes from each other [48], causing the impact of internal radiation on other internal components to be small enough to be neglected. Moreover, a relatively simplified conduction model between components is used. As components are described as nodes and not three-dimensional objects, the distance that the heat travels within the material is not taken into consideration, and instead, nodes can be connected through Fourier's law of conduction seen in Equation 9.5 [47]. Another assumption comes from the incident environmental heat flux values for solar, albedo and Earth IR radiation. From the Midterm's implementation of the model, a coarse assumption of heat fluxes was used, where several unrealistic worse-case scenarios were chosen. However, due to the relatively high sensitivity of the model to changes in these heat fluxes, more accurate values should be used. Thus, a radiative model was also created in ESATAN-TMS [3], where the incident radiation with respect to the Earth and the Sun could be calculated for each exterior face of the spacecraft and any exterior components. These heat values could then be used in the thermal model herein developed, increasing its accuracy and validity.

To begin describing the thermal distribution of the spacecraft, the sources of heat must be analysed, and then related to a change in temperature of the different components. From the environment, there are three sources of external heat: solar, albedo and Earth IR. These are shown in Equation 9.1, 9.2 and 9.3 respectively. In these equations, A_{in} corresponds to the effective area that receives the incoming radiation, α the absorptivity, ϵ the emissivity, a_s the albedo factor of the Earth ($a_s = 0.309$), and J_s and J_{IR} are the incoming heat flows from the Sun and Earth respectively.

$$Q_{solar} = \alpha J_s A_{in}, \tag{9.1}$$

$$Q_{albedo} = \alpha a_s J_s A_{in}, \tag{9.2}$$

$$Q_{EarthIR} = \epsilon J_{IR} A_{in}. \tag{9.3}$$

These three equations can be then combined into the total absorbed heat, which must be calculated for each node in the model, seen in Equation 9.4. Another source of heat is the heat generated by the components, symbolised by Q_{gen}. The final source of heat to a node comes from conduction due to contact with other nodes. This is described by Fourier's law of conduction, seen in Equation 9.5, where k_{ij} is the conductivity between nodes i and j, A_{ij} is the area of contact between the nodes, and T_i and T_j are the temperatures of the two nodes respectively. As a node can be connected to multiple other nodes, the total conductive heat is the sum of the heat from each node.

$$Q_{in,i} = A_{in,i} J_{s,i} \alpha_i + A_{in,i} a_s J_{s,i} \alpha_i + A_{in,i} J_{IR,i} \epsilon_i \tag{9.4}$$

$$Q_{cond,i} = \sum_{j}^{N} k_{ij} A_{ij} (T_j - T_i) \tag{9.5}$$

Knowing the heat sources for each node, the temperature of each node can be calculated. This is done by applying a heat balance equation, seen in Equation 9.6. In this equation, m is the mass of

[3] esatan-tms.com, last accessed 13/06/2023

the node, C_i the specific heat capacity of the node's material and A_{rad} the radiation emission area of the node.

$$mC_i\frac{dT}{dt} = Q_{in,i} + Q_{gen,i} + \sum_{j}^{N} k_{ij}A_{k,i}(T_j - T_i) - A_{rad,i}\varepsilon_i\sigma T_i^4 \tag{9.6}$$

To then solve this equation to find the temperature of each node throughout an orbit, a solver was implemented in Python, which allows for the definition of any number of nodes and the connections between them, as well as the definition of either steady-state or transient heat sources. An assumption the solver has is that the geometric, material and optical properties of each node remain unchanged throughout the orbit, which in turn should be designed for, as these will slightly change during the lifetime of the mission (notably for optical properties of some materials). Results from this model will be used in Section 9.2 to choose and size the TCS strategy, and to analyse the performance of the subsystem.

As previously mentioned in the assumptions of the model, the incident heat fluxes from the environment are considered coarse (as no view factors are considered between faces), and thus a more accurate radiative model was created in ESATAN-TMS. For this model, the orbital characteristics specified in Section 6.2 were used, and a preliminary geometry of the spacecraft was created. With these specified, ESATAN-TMS is able to calculate the radiation incident on each exterior face of the spacecraft, and with the optical properties of the surfaces defined, the absorbed and emitted radiation can be calculated (which will later be chosen in Section 9.2).

9.2.2. Choice of components

From the Midterm report, a trade-off was performed between possible thermal control options, using the criteria of mass, power, environmental vulnerability and thermal controllability. This trade-off resulted in the following best options: surface coatings, radiators, baffles and MLI (for passive), and electric heaters (for active). It is an aim of the TCS to use as minimal amount of power as possible, hence fully passive options should be preferred, however, this may not be possible, as some components may need to be heated up, wherein the electric heaters can be useful. From the Midterm, it was also shown that using solely one of the passive options was not sufficient to keep all components within their operating temperatures, hence a combination must be used.

Using the combination of the different thermal control strategies mentioned above, the model was updated to include the geometries and optical properties of the selected TCS components. Considering the preliminary results from the Midterm phase, the components that would be needed are listed below:

- **Surface coatings:** surface coatings are used to control the amount of radiation absorbed and emitted by a component of the spacecraft. They will be applied to the exterior of the spacecraft's structure (all faces), the outward-facing surface of the radiator, the Earth-facing surface of the Earth-shield, and the bottom surface of the solar panels. For the purposes of this mission, high emissions and low absorptivity coatings can be used to cool down the surfaces exposed to space. The DST baffle will also require a high absorptivity coating on the inside face of the baffle, to reduce reflections onto the M1 mirror.
- **Radiator:** radiators are used to reject heat from the spacecraft, to cool down components. The radiator is placed on the side of the spacecraft facing space, and placed in such a way to receive the lowest amount of radiation possible. It is also painted with high a emissivity coating, to increase the amount of heat rejection.
- **Earth-shield:** radiation shields are used to block radiation from reaching a component, by providing a physical barrier. The Earth-shield is used to prevent the heating of components that need to stay cool, namely the radiator (and consequently the DST instrument box). It is made of a thin sheet of aluminium and covered in MLI and a high emissivity coating.

- **MLI/SLI:** multi and single-layer insulation are used to reduce the amount of heat transfer between radiating components. They are characterised by low absorptivity, emissivity and conductivity. They can be made of a single layer of material (for example a thick insulating tape) or multiple layers of thin sheets of aluminium and polymide. MLI will be applied to the interior surfaces of the spacecraft, to reduce the amount of internal radiation (to help comply with model assumptions), but also to the exterior of the DST baffle, while thermal tape will be applied to the OBC and batteries to reduce heat emission.
- **Electric heaters:** electric heaters can be used to heat up components that need to stay warm. Electric heaters shall be placed around the propellant pipes and tanks, to prevent solidification of the iodine propellant. This is the only active thermal control strategy proposed.

These strategies were put into the models (both ESATAN and own Python model) with initial preliminary values, followed by a more extensive TCS sizing, to choose the actual optical properties of the coatings, the size of the radiator and Earth-shield, and the power required for the electric heaters.

9.2.3. ESATAN-TMS model results

A simplified geometry of the satellite was created in ESATAN, using the components mentioned above, namely surface coatings (white paint and optical solar reflectors), a radiator, an Earth-shield, MLI and SLI (thermal tape). The geometry and the distribution of the external optical elements can be seen in Figure 9.1a.

Having generated the geometry and described the optical properties of the external surfaces, the radiation incident on each face can be calculated. First, the orbital characteristics were defined, according to Section 6.2, and the optical/material properties are applied, so that the absorbed radiation can be calculated (according to Equation 9.4). This results in an accurate description of the heat over an orbit, which can be seen in Figure 9.1b for one point in the orbit, and in Figure 9.2 for a description of the heat throughout the orbit.

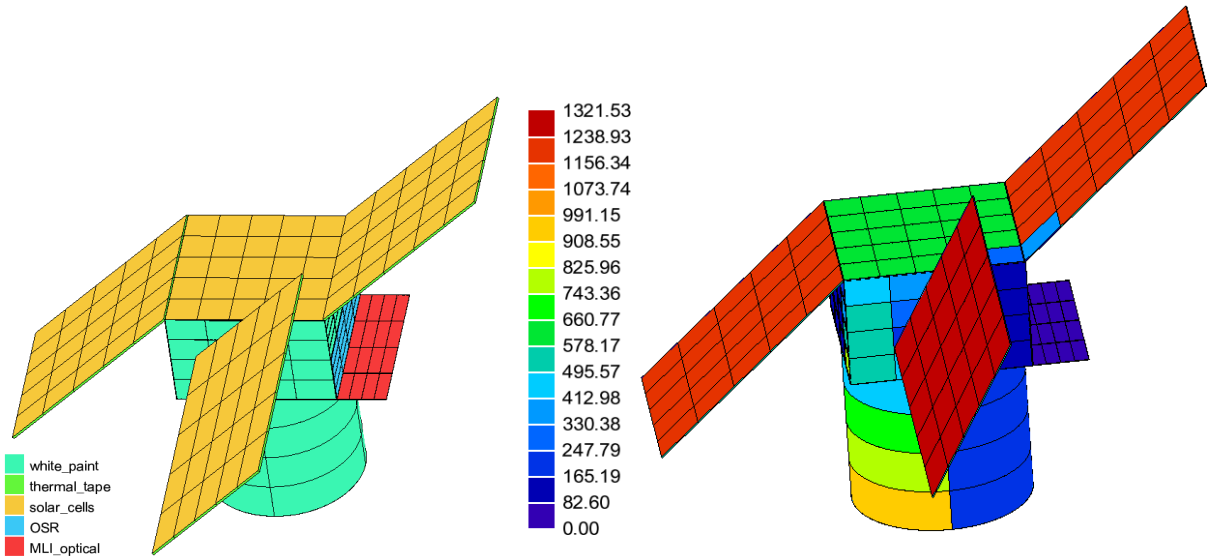

(a) *Geometry and optical properties of the thermal control subsystem.*

(b) *Incident radiation on the external surfaces of the satellite using ESATAN in* $\mathrm{W/m^2}$.

Figure 9.1: *ESATAN model of the incident and absorbed radiation.*

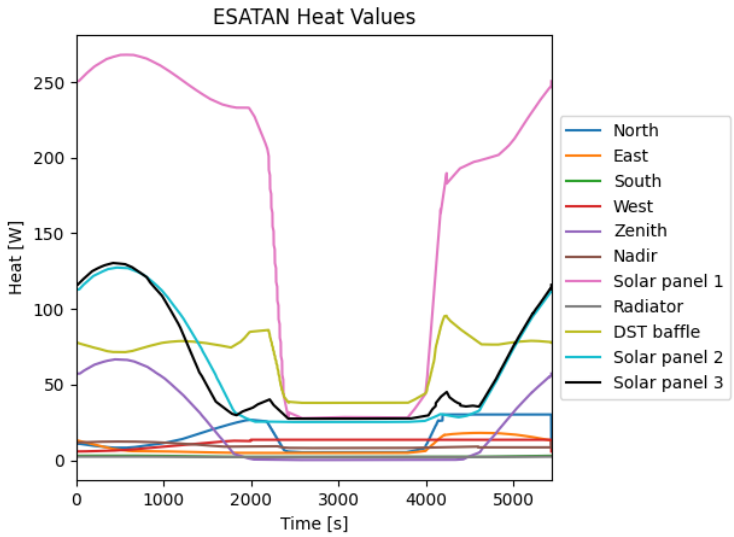

Figure 9.2: *Heat absorbed by the external surfaces of the satellite over the course of an orbit, calculated using ESATAN.*

From Figure 9.2, one can note that the radiator receives a very low amount of heat, which is beneficial, as it is the component that needs to be kept cool. This can be attributed to both the solar panel and the Earth-shield, as the solar panel blocks the solar radiation, and the Earth-shield blocks the Earth-IR and albedo radiation. Therefore, the radiator is considered to be mostly in shadow. One can also see the effect of the eclipse, where the absorbed radiation drops considerably (between around 2500 and 4000 seconds). The high heat on the solar panels is also expected, as they are rotated to a specific angle to increase the solar radiation incident on them. Regarding the internal components of the spacecraft (e.g. OBC, batteries, propellant tanks, etc) the incident environmental heat can be considered to be zero, as the structure mostly completely blocks the radiation. These values can then be input into the Python simulation, greatly increasing its validity (due to the high accuracy and validity of the ESATAN model).

Another type of radiative case that should be considered relates to requirement *CON-Res-Tp-04* - the satellite should be able to withstand a heat load of $500\,\mathrm{W/m^2}$ from the fairing during launch. As the satellite will be in its stowed configuration, and placed within the deployer, it will be protected from most of that radiation. Nonetheless, the solar panels (which are the surfaces which would receive most of the fairing heat load) will be exposed to considerably larger amounts of radiation when in orbit, therefore, they should be able to withstand the $500\,\mathrm{W/m^2}$ for the relatively short amount of time during launch.

9.2.4. Python model results

Using the values from the ESATAN model, the Python implementation of Equation 9.6 can be completed. First, the heat generated by each component is input, namely for the OBC [45], batteries [49], and DST instrument box [50]. Following this, the heat transfer between the components is calculated, by defining which parts are connected to each other, and the heat transfer coefficient between them. Finally, the optical properties of each component are defined, and the heat transfer between the components and the environment is calculated. This results in a change in temperature, which can be used by the simulation to calculate the temperature at each point in the orbit. The results of the simulation can be seen in Figure 9.3. As this model was created in-house the validity and accuracy of the results should be questioned. This shall be expanded upon in subsection 9.2.6.

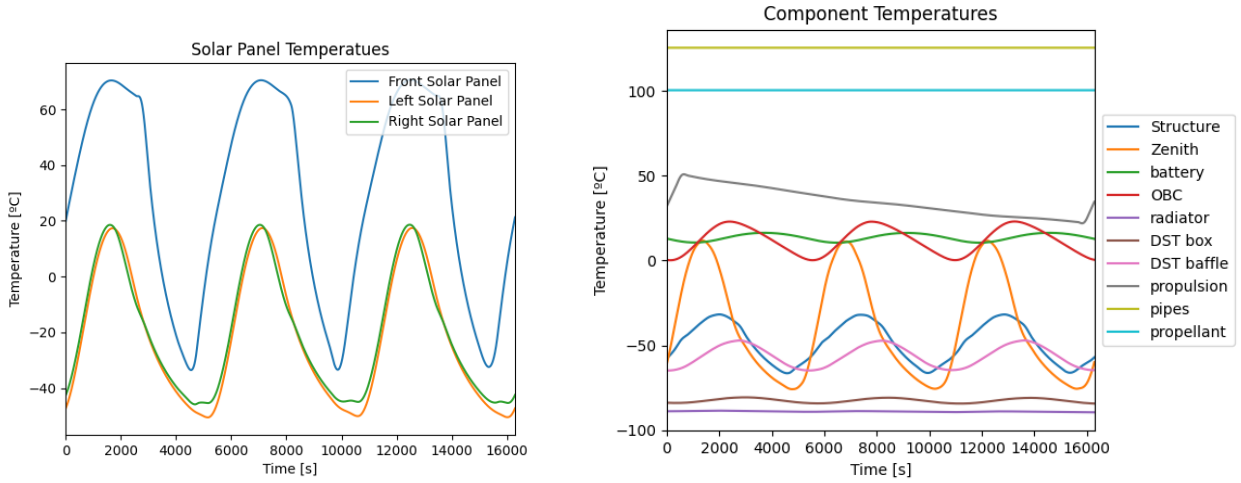

Figure 9.3: *Component temperatures throughout three orbits, calculated using the Python model.*

As can be seen from Figure 9.3, the temperatures of all components are within the acceptable operating temperature ranges, tabulated in Table 9.2. Considering the solar panels, one can see that due to their high emissivity and absorptivity, as well as the fact that they are rotated to increase the exposure to solar radiation, the temperature range is significantly greater than other exterior components of the satellite. Regarding the structural components, as they are placed on the exterior of the satellite and are subjected to transient thermal loads, their temperature also ranges around $50\,°C$ at maximum. The effect of the Earth-shield on the radiator (and consequently the DST's instrument box) can be clearly seen in Figure 9.2 and 9.3, as the incident radiation on the radiator is significantly low, lowering the temperature of the radiator to on average $-83\,°C$ and the temperature of the instrument box to $-78\,°C$ (below the maximum required operating of $-73\,°C$). Notably, other internal components are also within their operating temperatures, and the relatively constant temperature of the propellant pipes, tanks and batteries can be explained by the assumption of no radiation between internal components. This assumption is met by covering these components in MLI and thermal tape, which keep the heat of the component within the component, reducing radiation.

The sizing of the components was done in an iterative process, where the optical and conductive properties of the materials used in the thermal control strategy were changed in the models, and the temperatures of each component were analysed to assure that they complied with the operating temperature ranges. Further details regarding sizing can be seen in subsection 9.2.5.

9.2.5. Component sizing

With the model defined, and the temperatures of each component calculated, proper sizing of the components can take place. This was done as an iterative process, wherein components were sized and replaced in the model to assure that the temperatures of the satellite were within acceptable ranges. The components that were sized are summarised in Table 9.4. COTS solutions were chosen for most components, while the radiator and Earth-shield were designed in-house. The white paint was chosen for its high emissivity and some absorptivity to slightly increase the internal temperature of the satellite. The MLI and thermal tape were also chosen for their optical properties and low conductivity. The heaters were chosen for their small form factor and low mass, as well as good physical resistance to the environment. The heat strap is sized differently from COTS solutions, though Thermal Management Technologies offers customisation of their existing heat straps[51].

Regarding the sizing of the radiator and Earth-shield, the radiator was sized to have an area of $0.04\,m^2$ with a thickness of $2.5\,mm$ [52], enough to dissipate the heat generated by the DST instrument box. This area corresponds to about half the area of the left side of the satellite. It is also covered in white paint to increase its emissivity. The Earth-shield was sized to have the same shape as the radiator, though with a lower thickness of $1\,mm$ as it is only used to block heat not radiate it away. It is covered

with white paint on its Earth-facing side to reduce absorptivity, and with MLI on its top face, to reduce radiation towards the radiator. It should be noted, that the bottom side of the solar panel above the radiator is covered in MLI, to reduce the emitted radiation of the hot towards the radiator. Another consideration of the Earth-shield is its deployment strategy. A passive deployment mechanism could be employed using shape memory alloys springs[4] or tape springs [53], which would be activated by the heat incident on the satellite. The heat straps were also somewhat sized, starting from an existing COTS solution, and then resizing it such that it fits into the satellite, which can be seen in Section 9.3.

Furthermore, the heaters must be sized, by calculating the power required to keep the propellant tanks and lines at their high operating temperatures. This was done by calculating the heat loss of the propellant tanks with the thermal model, and then calculating the required heat. This led to the need for $1.35\,\mathrm{W}$ for each propellant tank, and $0.8\,\mathrm{W}$ for the propellant lines. The physical size of the heaters was chosen by looking at available COTS solutions and resizing them to fit the specified needs. To ensure minimal loss of heat from the propellant tanks and pipes (and also to prevent heating up of other internal components), the tanks, pipes and heaters were covered in an insulating layer of low emissivity thermal tape ($\varepsilon = 0.035, \alpha = 0.14$) [54].

9.2.6. Model verification and validation

As previously stated in Section 9.2, to assure that the results are sufficiently accurate, the model must be both verified and validated. With regards to verification of the software of the Python model, several unit tests were performed to assure that the functions used in the model were working as intended[2]. Following this, a visual inspection of the model was performed by multiple team members to assure that the model was working as intended. During this process, several errors were corrected, namely regarding the incident solar radiation on the satellite, leading to the use of ESATAN as the source of the incident/absorbed heat flows.

After verifying that the model was working correctly, the model must be validated to assure that it reflects the physical process of heat transfer by radiation and conduction. This was mainly done by comparing the results of the Python model to the results of an existing ESATAN model of the satellite[5]. ESATAN-TMS is an already-validated software package for thermal analysis, making it a valid form of validation for the in-house-designed Python model. It should be noted that the configurations of the provided model, and the one created in this project differ to some degree (e.g. the provided model does not include solar panels, which block radiation to the radiator, and the internal heat generations are different), hence it was slightly modified to better reflect the satellite designed in this project. A simplified ESATAN model of the satellite was created in subsection 9.2.3, but the full capabilities of ESATAN to model the temperatures of the satellite were not used, as they lie beyond the scope of this project.

The geometry and results of the validation model can be seen in Figure 9.4. As can be seen, some components are missing in the validation model, but also the internal components are not modelled. Hence, an internal temperature can be extracted to be compared with the Python model.

[4] dcubed.space, last accessed 19/06/2023

[5] A similar detailed ESATAN model of the satellite and DST was generously provided by Frank Eshuis (F.Eshuis@student.tudelft.nl), a Master's student at TU Delft, for the purposes of validation of the thermal control subsystem herein designed.

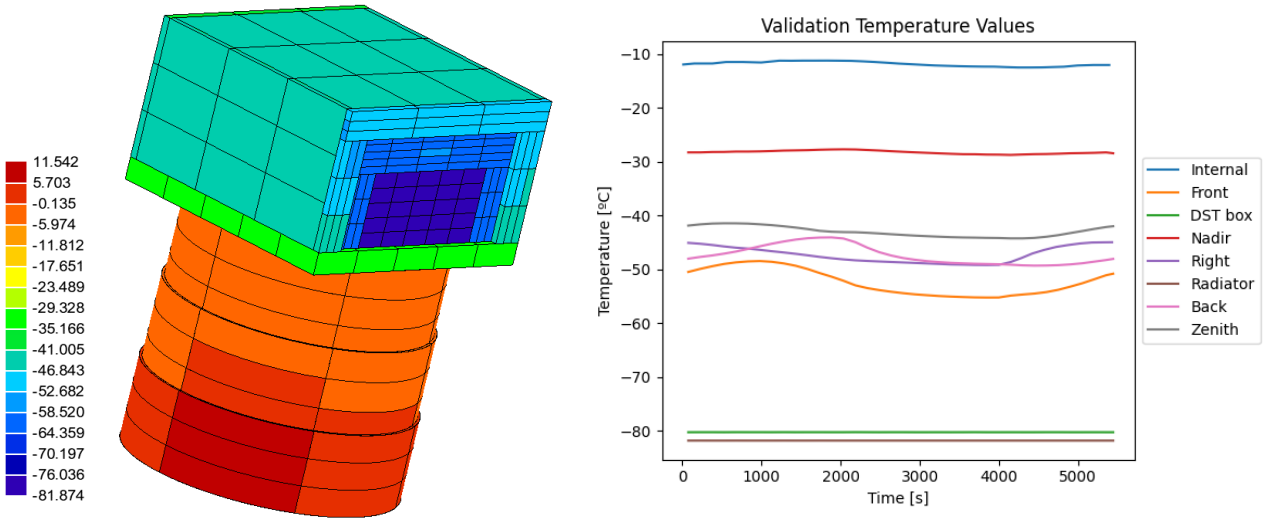

(a) *ESATAN validation model of the satellite with surface temperatures in °C.*

(b) *Temperature results of the validation model for some of the similar components.*

Figure 9.4: *Validation model of the satellite.*

Comparing Figure 9.4b to Figure 9.3, it can be seen that the temperatures of the radiator and DST instrument box are similar, with the Python model predicting lower temperatures than the validation model, likely due to the presence of a solar panel in the Python model, which blocks solar radiation to the radiator, cooling it down. Considering the Zenith panel, The Python model predicts both higher temperatures, and a higher temperature range throughout an orbit, while the validation model predicts a more stable, lower temperature. This can also be attributed to the differences in configuration between the two models, where the Zenith of the Python model contains solar cells with different optical properties. Taking onto account the internal temperature of the satellite, The validation model predicts a stable temperature around $-10\,°C$, while the Python model predicts temperatures for the batteries and OBC closer to $28\,°C$ and $20\,°C$ respectively. This can be attributed to the heat generation of these components, and the inclusion of insulation around the components in the Python model, heating the batteries and OBC.

A limitation of the Python model which can be seen in the validation model is the differences in temperature range over an orbit between them. This can be mainly attributed to the simplification of heat conduction between nodes in the Python model and the small number of nodes used, leading to a less accurate representation of the heat transfer between components. Moreover, comparing the validation model to other literature, it should be expected that the temperature range (especially for exterior components) be larger [55], contradicting the results of the validation set. Nonetheless, as the average temperatures of components/structures are similar across models, the Python model can still be considered accurate.

With these considerations in mind, the Python model can be considered sufficiently accurate for the purposes of this report, and the results of the model can be used to design the thermal control subsystem of the satellite.

9.2.7. Sensitivity analysis

To analyse the validity of the thermal analysis, and consequently the design choices made, a sensitivity analysis was performed. For this purpose, the optical properties of some TCS components were varied. White paint is one of the most critical components of the TCS, as it covers the entire spacecraft and is used to cool it down to an acceptable range. During the lifetime of the mission, the absorptivity of surface coatings tends to increase (decreasing the ε / α value), due to the effects of solar radiation, so the sensitivity of the design to an increase in absorptivity should be analysed. From the manufacturer of the white paint, the absorptivity is expected to increase by 0.013 in LEO [56], while the emissivity

is not expected to change. Thus, keeping the emissivity constant, the absorptivity of the white paint was varied from 0.06 to 0.08. Such a change would mostly affect the temperature of the radiator and the structure as they are the ones coated in the white paint. The changes caused by this change in absorptivity are tabulated in Table 9.3.

Table 9.3: *Comparison of the maximum temperature of the radiator and structure for different absorptivities of the white paint.*

Absorptivity	Radiator temperature [°C]	Structure temperature [°C]
0.06	-87	-33
0.08	-78	-26

As can be seen from Table 9.3, the maximum temperatures of the radiator and structure increase with the change in absorptivity, showing some sensitivity, though the altered temperatures are still within the allowable temperature ranges of the components. The maximum radiator temperature is however very similar to the maximum allowable temperature of the DST instrument box, leaving little margin for any spikes in temperature. This shows some sensitivity in the design, as the radiator could include larger margins or the Earth-shield could be re-designed to better protect the radiator. These are possible recommendations for further analysis into the design of the TCS.

9.3. TCS architecture

The thermal control subsystem was integrated into the satellite model as shown in Figure 9.5, with detail given to the placement of the radiator and Earth-shield, as well as the heat strap. The radiator is integrated into the face structure of the satellite, with a marginally larger thickness than the structure, which protrudes into the inside of the satellite for better clearance with the deployment mechanism of the spacecraft. The Earth-shield can also be seen in its deployed configuration, where its deployment mechanism is attached just below the radiator. The heat strap provides a high conductivity connection between the radiator and the DST instrument box, where a thermal interface material is placed between the heat strap blocks and the metal surfaces for better conduction.

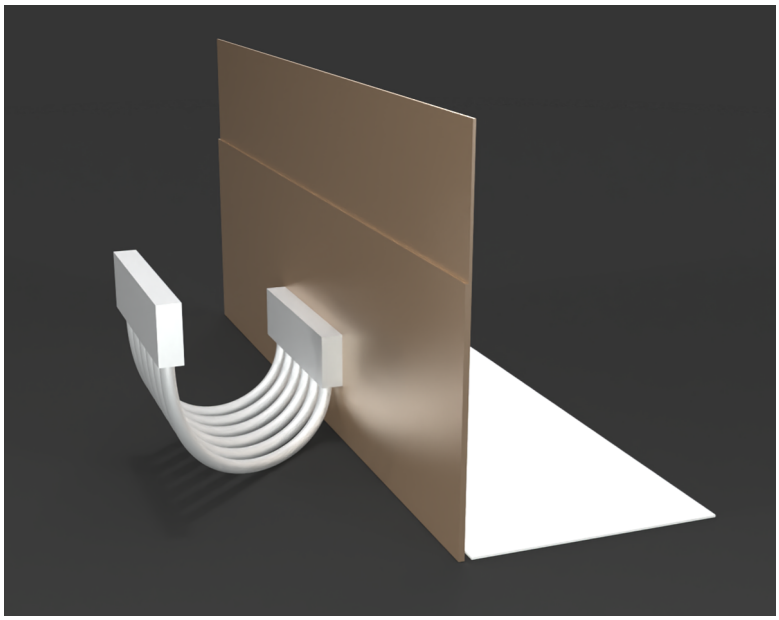

Figure 9.5: *Architecture of radiator, Earth-shield and heat strap.*

9.4. TCS performance

With the thermal control subsystem sized and integrated into the rest of the satellite, the performance characteristics of the TCS can be tabulated in Table 9.4. For many components, the cost is not stated as no resources regarding cost could be found for those components. As can be seen, most of the TCS strategy involves passive components, except for the heaters, which require a power input to heat up the propellant tanks and lines.

Table 9.4: *Properties of the selected components for the thermal control subsystem.*

Type	Component	α [-]	ε [-]	Mass [g]	Volume [U]	Power [W]	Cost [$]
White paint[6]	MAP® PCBE (K)	0.19	0.88	90	0.04	0	1200
Black paint[7]	MAP® PU1 (K)	0.96	0.88	30	0.02	0	750
MLI [54]	Sheldahl® Gold coated Polymide	0.3	0.03	90	0.06	0	-
Thermal tape [54]	Sheldahl® Gold coated Polymide tape with acrylic adhesive	0.3	0.03	50	0.03	0	-
Radiator [52]	In-house design	-	-	260	0.1	0	-
Earth-shield [57]	In-house design	-	-	150	0.05	0	-
Electric heater[8]	Minco Thermofoil™ HAP6749	-	-	10	0.01	2.7	506
Pipe heater[9]	Minco HR6851A	-	-	90	0.01	0.8	122
Heat strap [51]	Custom TMT010-420	-	-	340	0.04	0	-

Table 9.5: *Operating temperature ranges of spacecraft components after applying TCS strategy.*

Component	Min. temperature [°C]	Max. temperature [°C]
DST	-62	-44
DST instrument box	-83	-74
Radiator	-87	-78
Batteries	25	31
OBC	11	28
Solar panels	-51	70
Propellant tanks	97	97
Propellant lines	125	125
Thruster	11	55
Structure	-63	-33

[6] map-coatings.com, last accessed 19/06/2023
[7] map-coatings.com, last accessed 19/06/2023
[8] minco.com, last accessed 19/06/2023
[9] minco.com, last accessed 19/06/2023

10

Electrical Power Subsystem

The electrical power subsystem (EPS) is charged with generating, storing, and distributing power throughout LAMP's mission. In this chapter, all the information with regard to the EPS design is gathered.

Section 10.1 introduces the requirements of the EPS and the power needs of the system. Follows Section 10.2 in which the design of the EPS is presented, expending on the work performed in the midterm phase [12]. In Section 10.3 an overview of the EPS architecture is discussed. Followed by a discussion on the EPS performance in Section 10.4. Finally, in Section 10.5 a brief mention of the verification process and observations of the numerical model is provided.

10.1. Electrical power subsystem requirements

From the Midterm report [12], a number of subsystem requirements were identified. For the EPS the requirements generated are tabulated in Table 10.1, along with their rationale and verification method. Furthermore, some of the requirements were modified and adjusted. On the other hand, in Table 10.2 the power needs of all the subsystems are presented, and an example of the operational timeline and power need map is present in Figure 10.1.

Table 10.1: *Electrical power subsystem requirements*

ID	Description	Rationale	Verif. M.	
Sys-EPS-01	The EPS shall provide energy storage for the satellite.	Functional requirement of the EPS.	Demo	✓
Sys-EPS-01-I	The EPS shall be able to store at least 50 W h at EOL	Energy storage capacity of the EPS to cover for the eclipse time at EOL for idealised conditions. The individual storage capacity varies depending on the battery technology, and the power need scenario of the payload. (Table 10.2).	Ana, Test	✓
Sys-EPS-02	The EPS shall provide energy generation for the satellite.	Functional requirement of the EPS.	Demo	✓
Sys-EPS-03	The EPS shall be able to distribute power to all subsystems throughout the satellite's lifetime.	Functional requirement of the EPS.	Demo	✓
Sys-EPS-03-I	~~The EPS shall provide at least 51 W of average power during nominal mode at EOL~~.	~~Power needed for nominal mode~~ Nominal mode case has been changed.	Ana	-

Sys-EPS-03-II	The EPS shall be able to provide a peak power of at least 158 W at EOL during eclipse.	Maximum power needed during eclipse orbit at end-of-life.	Ana	✓
Sys-EPS-03-III	The EPS shall be able to provide a peak power of at least 173 W at EOL during sun.	Maximum required power needed during sun orbit at end-of-life.	Test	✓
Sys-EPS-03-IV	The EPS shall provide telemetry data on its health/status throughout the satellite's lifetime.	Needed for continuous monitoring of the EPS status.	Test	✓
Sys-EPS-03-V	The EPS shall be able to control the power distributed to all subsystems throughout the satellite's lifetime.	This requirement relates to the ability of the EPS to control the amplitude of the power distributed over the subsystems.	Demo	✓
Sys-EPS-03-VI	The EPS shall be able to switch on & off all subsystems throughout the satellite's lifetime.	The EPS has to be capable of activating operational modes when a command is issued from the SDH by powering different subsystems.	Demo	✓
Sys-EPS-04	The EPS shall be able to regulate voltages up to 28VDC	Safety measure to protect against overvoltages, and needed for the distribution of power for the various subsystems	Test	✓

Table 10.2: *Power needs of LAMP*

Subsystem	Cont. Power [W]	Peak Power [W]	Subsystem	Cont. Power [W]	Peak Power [W]
Str	0	0	Payload Sc.1	5	5
ADCS	14.4	14.4	Payload Sc.2	10	10
TCS	3.5	3.5	Payload Sc.3	0	25
SDH	2	4	Propulsion	0	121
EPS	3	3	$P_{max_{Sun}} =$	173	[W]
Comms	1.8	1.8	$P_{max_{eclipse}} =$	158	[W]
GNS	0.3	0.3	$E_{max_{eclipse}} \approx$	50	[W h]

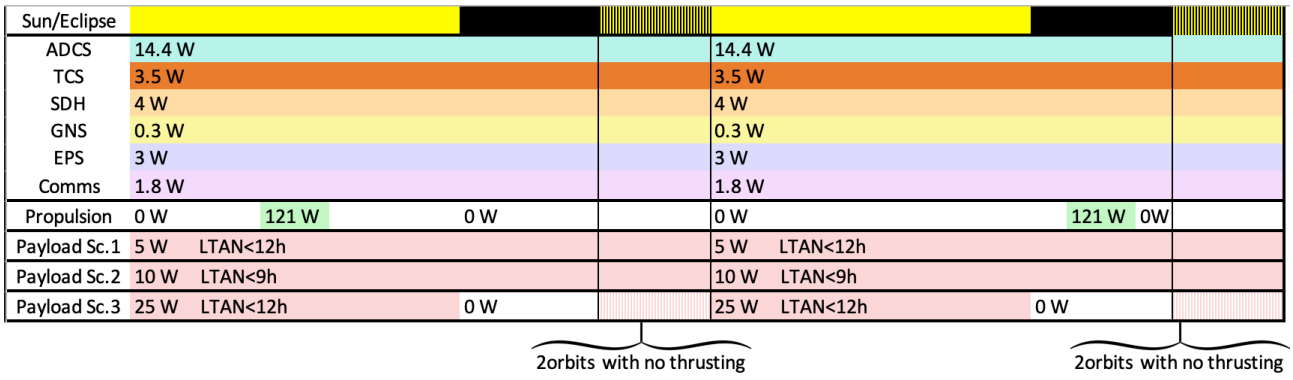

Figure 10.1: *Power consumption map over the nominal operational timeline*

In Table 10.2 the power needs per subsystem is presented. Detailed information about where the values originate is present in the subsystem's respective chapters, (from Chapter 7 to Chapter 14). For EPS the 3 W continuous power is taken from the chosen power conditioning and distribution (PCDU) system presented in Section 10.2.

Note that in Figure 10.1, all the subsystems except for propulsion and payload scenario 3 have a continuous duty cycle. For, propulsion the duty cycle is $870\,\mathrm{s}$, once every three orbits. On the other hand, for payload scenario 3, the duty cycle is associated with the sun-illuminated portion of the orbit which is variable depending on the eclipse fraction of the different LTAN's as can be seen from Figure 10.2.

10.2. EPS design

The EPS design is split into power generation sizing, power storage sizing, and power distribution sizing. First, in subsection 10.2.1 the chosen technologies from the midterm report [12] are reviewed with the updated data. Thereafter, in subsection 10.2.2 all the important sizing parameters are mentioned. subsection 10.2.3 introduces the sizing methodology and results for the solar panels and battery. Additionally, the component selection is discussed in subsection 10.2.4. Finally, in subsection 10.2.5 the sensitivity analysis is conducted.

10.2.1. Choice of technology & midterm configuration review

In the midterm report [12], an analysis of the choice of technologies available and feasible was performed, yielding:

- Solar cell technology: Solar cells of efficiency above 30% (inverted metamorphic, multi-junction solar cells - typically triple junction).
- Solar panel configuration: Body fixed top panel (305x360x2.5)mm, 2x1.5 deployed (fixed) side panels (200x360x2.5)mm, 3 back deployed ($\pm\ 180^\circ$ rotatable) panels (220x350x2.5)mm.
- Battery technology: *Li-Ion* batteries - one battery pack.

The battery cell technology remains $Li-Ion$, however noticeable changes to the solar panel and some changes to the battery configuration, have been performed since. First, after the nominal operational timeline for LAMP was designed as presented in subsection 5.4.1, it was decided to split the battery pack into two packs. The first, is responsible for the propulsion operations during eclipse/sun, with a duty cycle of 10,000 cycles, using the thrusting once every three orbits scheme from Chapter 14. The second is responsible for all the other subsystems during eclipse operations, with a duty cycle of 30,000 cycles. Doing so eases the charging/discharging profile computations for the EPS simulation (i.e. eases the sizing of the batteries), and eases the placement of the batteries within the structure. Additionally, the splitting of the batteries into two packs, also allows for LAMP to continue its mission in case of complete failure of one of the packs, thus mitigating a single point of failure. However, further investigation of the operations with one battery pack in-operational is left for a future stage.

On the other hand, further insight into the orbital efficiency parameters was gained, once the sun-synchronous orbit with an inclination of 96.7° was chosen (Section 4.7). Thus, it was decided to explore the options in which the deployed panels are fixed under the most efficient angle depending on the local time of ascending node.

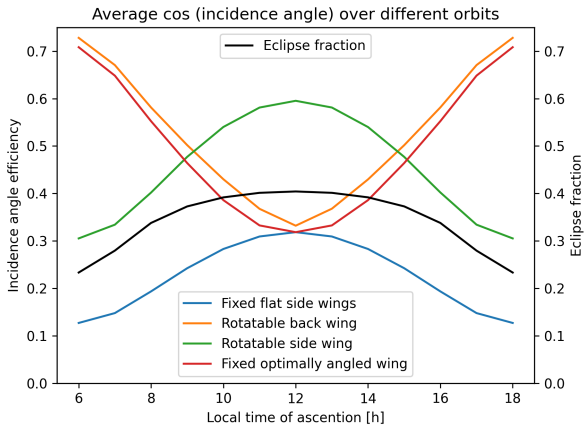

Figure 10.2: *Comparison between average incidence angle efficiencies over 1 orbit, for different types of solar panels, over different local times of ascension of the* 96.6° *sun-synchronous orbit.*

From, Figure 10.2, it can be seen that the difference between the fully rotatable deployed back (or front) panels, incidence angle efficiency, and the deployed at a fixed angle back (or front) panels, is marginal on average ($< 5\%$). Thus it is worth investigating replacing the rotatable system with a system that deploys under an angle β_i, which is defined as in Figure 6.5. This will be discussed in Section 10.2. Furthermore, the most efficient β_i angles for the different local times of ascending nodes are gathered in Table 10.3. Finally, it should be noted that the method for computing the results displayed in Figure 10.2 and Table 10.3 are explained in Section 6.2.

Table 10.3: β_i *against local times of acsensions for the* 96.6° *sun-synchronous orbit*

LTAN [h]	6	7	8	9	10	11	12
β_i **[°]**	83	80	72	61	46	12	0

Furthermore, as will be further detailed in Chapter 14, the propulsion subsystem uses Iodine as the propellant, which is corrosive and can damage the solar panels when they are angled on the back. Two solutions were investigated. First, keeping the panels at the back but offsetting the hinge location depending on the LTAN scenario, in order for the propellant to not hit the panels. This also requires the panels to be hinged on the side array of the back for LTAN between 6h-10h and on the top array for 11h - 12h. In addition to needing drastic changes in the deployment and hinge design, fixing the panels on the back also requires their along the flight centre of gravity to be more offset from the geometrical middle axis of LAMP along the direction of flight. Considering, all these constraints linked to accommodating the 3 panels on the back, with the propulsion subsystem, the option of placing them on the front was investigated.

For the EPS, placing them on the front or on the back has no effect on the overall produced power and efficiency of the panels. Moreover, after an investigation of the effect of such changes, it was found that there is no major conflict with any other subsystems. Only a star tracker and the GNS antenna were placed on the front. Both can easily be changed locations, with the star tracker placement being moved to the back or sides (90° angle needed from the top plane where the second tracker is, as elaborated in Chapter 8) and the GNS antenna moved to the top side. Furthermore, the aerodynamics, thermal, stability and control characteristics were analysed by the environmental model (Chapter 6) and the ADCS model (Chapter 8), and no changes were observed for the thermal and aerodynamics, while only marginal changes in the stability and control characteristics as shown in Table 6.1 to Table 6.3.

Moreover, the COMMS antenna, GNS antenna, star tracker placement and constraints from the deployer have also been updated in their respective chapters, and the area of the back and side folds as well as the top area for SPs has been reduced accordingly. Thus, the final solar panel configuration

considered can be seen in Figure 10.3. The angle i in the configurations stands for the β_i as defined in Figure 6.5.

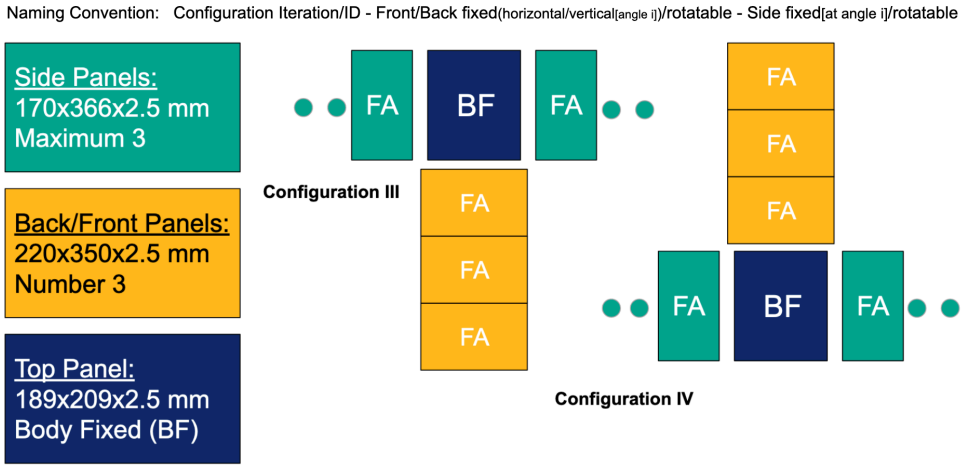

Figure 10.3: *SP configuration CIV-Ff$_{h_i}$-Sf$_i$ (Front fixed horizontally at angle i, Sides fixed at angle i) in comparison to CIII-Bf$_{h_i}$-Sf$_i$ (back fixed)*

10.2.2. Parameters overview

An overview of all the parameters, efficiencies, constants and their origin, used in the sizing of the EPS is provided in Table 10.4.

Table 10.4: *Overview of parameters used for the EPS sizing and their origin*

Symbol	Description	Source
L	Mission lifetime of 5 years	*U-Ops-01*
T_o	Orbital period of LAMP ≈ 5423 s at 300 km altitude	Section 6.2
$LTAN$	Local time of ascending node in hours	[-]
$r_{e_{LTAN}}$	Eclipse fraction as a function of $LTAN$; [6 h, 9 h, 12 h] $\rightarrow$ [0.23, 0.37, 0.404]	Section 6.2
$T_{e_{LTAN}}$	Eclipse time in seconds $\cong T_{e_{LTAN}} = T_o \cdot r_{e_{LTAN}}$	[-]
N_{b1c}	Number of cycles of battery 1 (i.e. in charge of eclipse/sun operations with no propulsion) $\cong N_{b1c} = L{\cdot}3.1536{\times}10^7/T_o \approx 30000$	subsection 10.2.1
N_{b2c}	Number of cycles of battery 2 (i.e. in charge of propulsion eclipse / sun operations). Propulsion once every three orbits $\rightarrow N_{b2c} = N_{b1c}/3 = 10000$	Chapter 14
η_{bat_c}	$Li-ion$ battery efficiency of charge $\cong 0.96$	[7, 58, 5]
η_{bat_d}	$Li-ion$ battery efficiency of discharge $\cong 0.98$	[7, 58, 5]
DOD_{nc}	Depth of Discharge as a function of the number of cycles for $Li-Ion$; [10 000, 30 000] $\rightarrow$ [50 %, 20 %]	[59, 5]
E_{sp}	Typical specific energy of $Li-Ion \cong E_{sp} = 150\,\mathrm{W\,h\,kg^{-1}}$	[7]
ρ_{sp}	Typical energy density of $Li-Ion \cong \rho_{sp} = 210\,\mathrm{W\,h\,L^{-1}}$	[7]
S_{flux}	Solar flux $\cong S_{flux} = 1322\,\mathrm{W/m^2}$, minimal value taken for worst case scenario analysis	[20]
η_{cell}	Solar cell efficiency chose for the sizing $\cong \eta_{cell} = 32.0\,\%$	[7]
D	Solar cell degradation per year $\cong D = 0.5\,\%$	[7]
I_d	Total inherent degradation of the cells accounting for design & assembly, temperature of array and shadowing of cells $\cong I_d = 0.88$	[5]

m_{cs}	Combined mass of cell & structure around per cell $\cong m_{cs} = 26.5\,\text{g/cell}$	[7], COTS[1]
A_{cell}	Typical dimensions of solar cell $4\,\text{cm}$ x $8\,\text{cm} \rightarrow A_{cell} = 32\,\text{cm}^2$	[7], COTS[2]
A_{top}	Maximum area of top body fixed panel, assuming it is fully covered with solar cell area; $A_{top} = (329-140)$ mm x $(349-140)$ mm x 2.5 mm, subtractions are to allow for the COMMS, GNS antennas and one ADCS star tracker	Chapter 7, Chapter 11, Chapter 13
A_{front}	Maximum area of front solar panel (1 fold), assuming it is fully covered with solar cell area; $A_{front} = 220$ mm x 350 mm x 2.5 mm	Chapter 13
A_{side}	Maximum area of side solar panel (1 fold), assuming it is fully covered with solar cell area; $A_{front} = 170$ mm x 3 mm x 2.5 mm	Chapter 13
η_{PCD}	Efficiency of power conditioning and distribution, using the efficiencies of the PCD unit and the harness; $\eta_{PCD} = \eta_{PCDU} \cdot \eta_{harness} = 0.96 \cdot 0.98 = 0.9408$	[60, 61]

10.2.3. Solar panel & battery sizing

The solar panel & battery sizing method has been improved from the 'one orbit averaging energy method' presented in the midterm report [12], to a discrete simulation of step size 1 s over the 6 orbits nominal operational timeline as defined in Chapter 5.

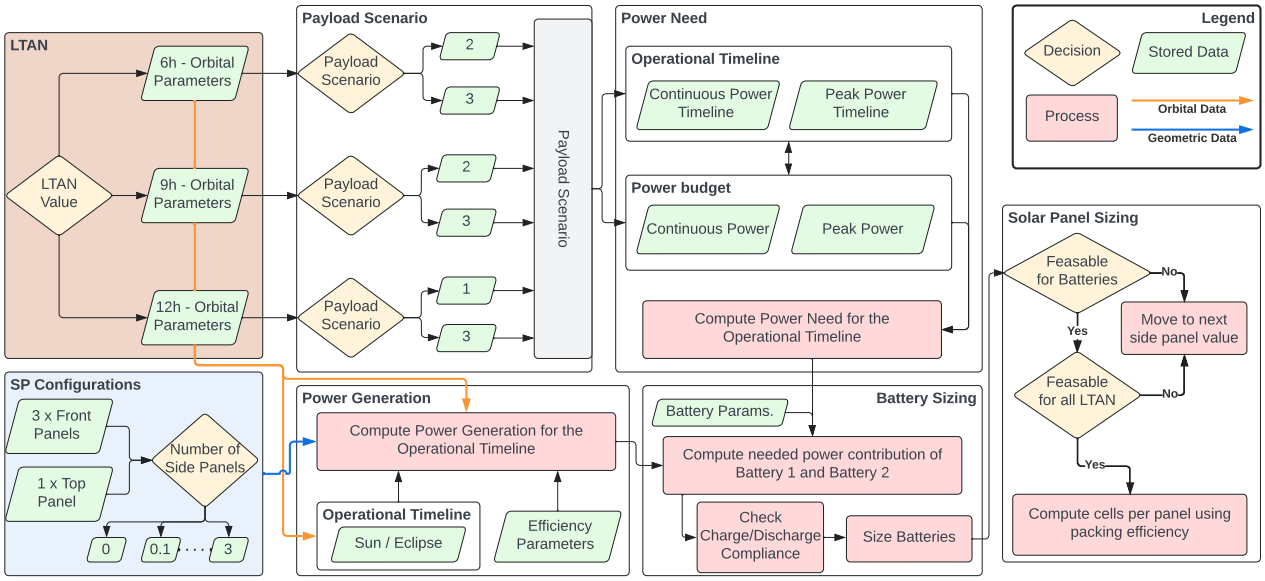

Figure 10.4: *Simplified panels and battery sizing methodology flow diagram*

The sizing methodology and the EPS model logic are depicted in Figure 10.4. Five main portions can be identified. First, the inputs are gathered from the geometrical properties of the considered SP configurations, and the orbital parameters (i.e. eclipse fraction and incidence angle efficiencies) from the astrodynamical model (Section 6.2).

The second step consists of assembling the power needed per second, from the operational timeline (subsection 5.4.1) and the power budget (Table 10.2).

[1] endurosat.comlast accessed 19/06/2023
[2] azurspace.comlast accessed 19/06/2023

The third step computes the power generation capability per second of the tested configuration using the SP configuration geometrical data as well as the orbital parameters. This is done using Equation 10.1, where $N_sf \in (0, 3)$ is the number of side folds.

$$P_{in}(t, LTAN) = (N_{sf} \cdot A_{side} \cdot \cos\theta_{side} + 3A_{front} \cdot \cos\theta_{front} + A_{top} \cdot \cos\theta_{top}) \cdot S_{flux} \cdot I_d \cdot (1-D)^L \cdot \eta_{cell} \quad (10.1)$$

Thus, the battery power contribution at a given second can be computed using Equation 10.2.

$$P_{bat} = P_{in} - P_{need} \begin{cases} \text{if < 0 : Battery is discharging} \\ \text{if > 0 : Battery is charging (overcharge sensors active)} \\ \text{if = 0 : Battery is idle} \end{cases} \quad (10.2)$$

Visual results of this method are presented in Figure 10.5 for different SP configurations, payload configurations and $LTAN$, in which 2 out of the 30 tested side folds configurations, the 3 different power need/consumption profiles related to the payload scenarios are depicted, as well as the 3 power generation profiles related to the 6,9,12 h $LTAN$. Furthermore, from the power generation profiles, it can be concluded that for the same power consumption scenario, if the EPS is sized for $LTAN = 12$ h then it will be able to exceed the requirements of the power consumption scenario for $LTAN \in [6, 12]$ h.

During the fourth step the model computes the sizing of the batteries, based on the output from the previous step. Some side panels configuration can already be discarded if the total discharge of the battery (i.e. the sum of the negative values of the battery contribution curve in Figure 10.5) is larger than the total charge of the battery (i.e. the sum of the negative values of the battery contribution curveFigure 10.5) scaled with η_{bat_c}. Thus, for the sizing of the batteries, first, the total energy needed for propulsion during the eclipse and the energy deficit (i.e. in case the solar panel power generation is lower than the power needed) associated with propulsion during sun are added in order to obtain battery energy needed for propulsion (i.e. E_{bat_2}). Hence, the energy needed for battery 1 E_{bat_i} is the total discharge of the battery, to which the propulsion contribution is subtracted, and normalised for one orbit. Hence, to size the capacity of the batteries Equation 10.3 is used. Note that a safety factor $SF = 1.2$ is used in order to account for unexpected operational events.

$$C_{bat_1}(LTAN) = SF \cdot \frac{E_{bat_1}}{\eta_{bat_1} \cdot DOD_{10000}} \qquad C_{bat_2}(LTAN) = SF \cdot \frac{E_{bat_2}}{\eta_{bat_2} \cdot DOD_{30000}} \quad (10.3)$$

Using the computed capacities the mass and volume of the batteries are obtained using E_{sp} and ρ_{sp} respectively. Furthermore, if the combined mass or volume of the batteries exceeds, respectively, 2 kg or 1.5 U, which are the allocated budgets for the battery from the midterm report [12], then the configuration is excluded.

The final step consists of finding the optimal solar panel-battery configuration. This corresponds to the smallest side panel configuration for which the three analysed $LTAN$ configurations, [6, 9, 12] h, all yield feasible battery sizing within the design space. This happens to occur for 1.5 side folds, per side. The power generation and battery charge/discharge profiles for the selected side panels configuration and some payload scenarios can be seen in Figure 10.6. The payload scenarios are explained in Chapter 5.

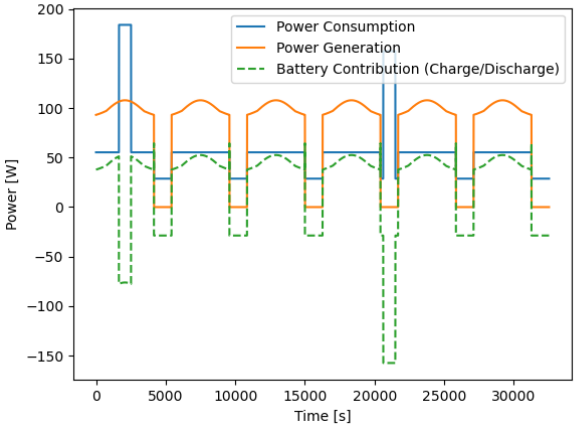

(a) *0.5 side folds per side,* $LTAN = 6\,\text{h}$*, payload scenario 3*

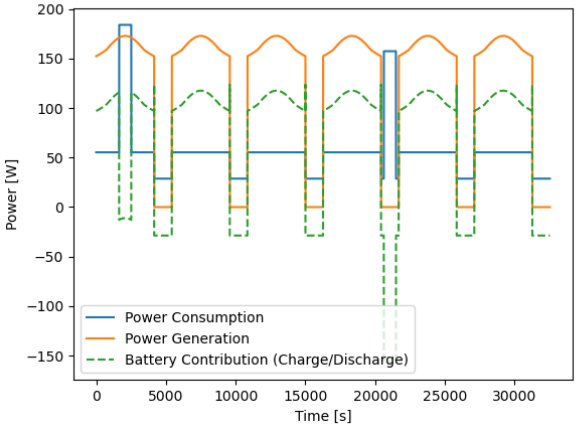

(d) *2 side folds per side,* $LTAN = 6\,\text{h}$*, payload scenario 3*

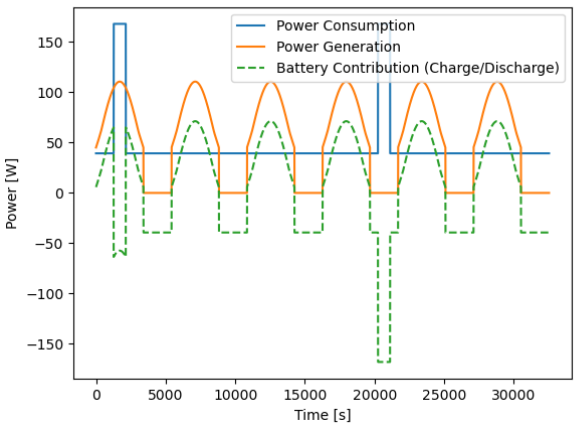

(b) *0.5 side folds per side,* $LTAN = 9\,\text{h}$*, payload scenario 2*

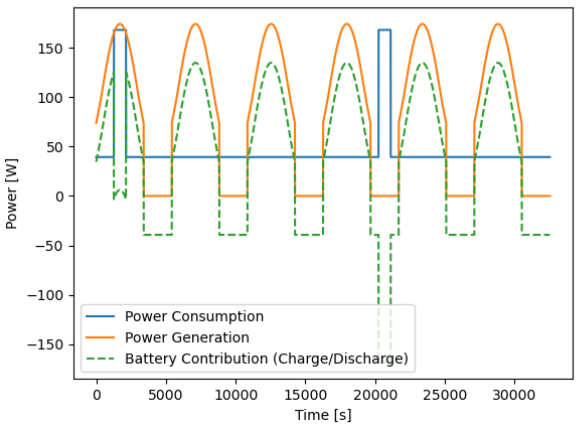

(e) *2 side folds per side,* $LTAN = 9\,\text{h}$*, payload scenario 2*

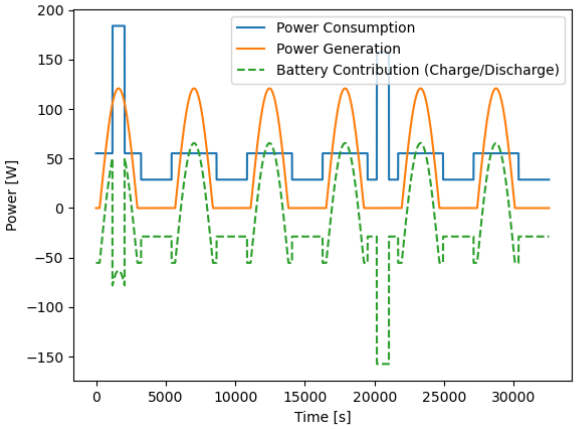

(c) *0.5 side folds per side,* $LTAN = 12\,\text{h}$*, payload scenario 1*

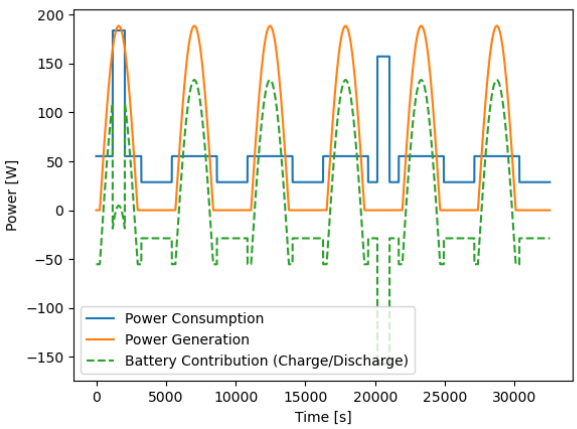

(f) *2 side folds per side,* $LTAN = 12\,\text{h}$*, payload scenario 1*

Figure 10.5: *Output graphs of the EPS simulation model for different SP configurations, LTAN, and side folds*

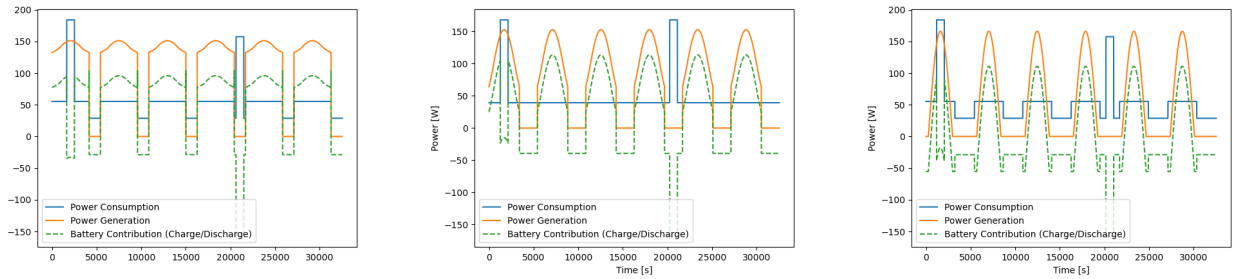

(a) $LTAN = 6\,\text{h}$, *payload scenario 3* **(b)** $LTAN = 9\,\text{h}$, *payload scenario 2* **(c)** $LTAN = 12\,\text{h}$, *payload scenario 1*

Figure 10.6: *Optimal side panels configuration (1.5 folds per side) EPS simulation profiles*

Nonetheless, the 1.5 side folds per side assume that the entirety is covered by solar cell area. Thus, the total number of solar cells required num_{cell_t} is computed with Equation 10.4.

$$num_{cell_t} = \frac{3 \cdot A_{front} + 2 \cdot 1.5 \cdot A_{side} + A_{top}}{A_{cell}} \tag{10.4}$$

Thus, $num_{cell_t} = 143$ cells (rounded up). Moreover, considering the cell dimensions $4\,\text{cm}$ x $8\,\text{cm}$ and the geometry of the panels, it has been derived that 20 cells may be placed on each of the front folds, 26 cells fit on the top side, hence leaving 57 cells to be distributed over the side panels, which can each fit a maximum of 16 cells. For ease of manufacturability, it has been decided to make use of 2 side panel folds on each side adding up to 64 cells, leaving 7 redundant extra cells on the sides. Thus, the estimated mass of the panels can be computed using m_{cs} from Table 10.4.

On the other hand, since the sized capacity of the batteries is dependent on the $LTAN$ the largest mass and volume are selected for battery 1, and battery 2, which do not necessarily occur at the same $LTAN$. A general overview of the battery and solar panel sizings is presented in Table 10.5.

Table 10.5: *General overview of SP and battery sinzing*

Component	**Total Mass [kg]**	**Num. Folds**	**Num. Cells/fold**
Top	0.689	1	26
Front	1.590	3	20
Right side	0.848	2	16
Left side	0.848	2	16
Total SP	3.975	7	150
Component	**Total Mass [kg]**	**Volume U**	**Capacity [W h]**
Battery 1	1.24	0.88	155
Battery 2	0.61	0.44	77
Total Batteries	1.85	1.32	232

10.2.4. Component selection

The component selection is split between the PCDU, batteries, solar cells and solar panel release mechanism.

The PCDU selection was performed only with COTS components. The following criteria were used:

- At least 4 solar array inputs (i.e. at least one per array).
- Preferably 2 battery blocks, with a battery management system, batteries can connect/disconnect.

Figure 10.7: *EPMS1*

- Charging support for $Li - Ion$ batteries.
- Compatible with output voltages ranging from 3.3V DC to 28V DC, necessary for the different subsystem components.
- Efficiency above 90%.
- As light and small as possible.

The PCDU determined to best fit these criteria was the Pumpkin Electrical Power System Module 1 (EPSM1)[3] which can be seen in Figure 10.7 and which main characteristics are presented in Table 10.6. Other microsatellite and CubeSat PCDUs such as Gauss PCDU[4], Starckbuck Nano[5] or PCU-110[6] were considered. However, they either did not have enough output power (or the required output voltage blocks) to match the needs of LAMP or were performing within the same parameters as EPSM1 but with increased mass and volume budgets.

Table 10.6: *EPMS1 Main Parameters*

Mass	0.3 kg	6 SP input blocks	(8-28V, 2A/4A)
Volume	< 0.3 U	2 battery blocks ($Li - Ion$)	(16.8V, 8A)
Power	< 3 W	3 regulated outputs	(3.3/5.0/12V, 5-8A)
Efficiency	96%	switchable regulated output	(4-28V, 8A)
Battery blocks	2	Battery management system	Included

For the battery packs cell selection, or entire battery module selection, the battery packs must comply with the capacity sizing presented in Table 10.5 as well as be able to provide sufficient discharge/charge capabilities to follow the battery contribution profiles as presented in Figure 10.6. EPMS1 already has the option of already integrated battery modules which can be used, namely the Intelligent Protected Lithium Battery Module with SoC Reporting (BM2)[7] from Pumpkin. BM2 can provide up to 160 W of power and store up to 100 W h of energy with 8 high-current 18650-size Li-Ion cells, each with an individual cell capacity of 3500 mAh. This configuration needs to be up-scaled in order to fit the needs of battery 1, by increasing the number of cells in the pack to 13 or increasing the cell capacity to 3700mAh. On the other hand, BM2 provides meets the needs of battery 2, with its 86 W h configuration of 8 x 3000 mAh cells.

The solar cell selection is done on the basis of assumed sizing cell efficiency of 32%. Solar cells such as the XTE series from SpectroLab[8] or the IMM-α from Rocket Lab[9], meet the requirements for efficiency. However, IMM-α presents better $V_{mpp} = 4.28$ V and $P_{mp} = 433.1$ W/m^2(compared to XTE series < 3 V, $P_{mp} = 427.1$ W/m^2), and is thus selected.

Finally, the hold down and release mechanism (HDRM) for the solar panels is inspired by the HDRM of Delfi-n3Xt [62] and the HDRM advanced by F.Santoni [63]. The idea is to have the solar panels pack simultaneously deploy at the required angle β and open to release the panels into their final configuration. The process is controlled by a fibre wire and thermal cutters, and the power consumption occurs only once during the beginning of life operations and typically ranges from $\mathcal{O}(10^{-1})$ - $\mathcal{O}(10^{0})$W. The process is entirely controlled by the batteries. However, a more detailed design of the mechanism is left for a future phase.

Similarly the detailed harness design is left for a future phase. The mass of the harness is approximated by statistical relations, using harness mass ($10\% - 25\%$) of EPS total mass [64, 65]). Using the upper bound it is obtained that $m_{harness} = 1.53$ kg.

[3] pumpkin EPMS1 last accessed 10/06/2023
[4] Gauss PCDU last accessed 24/06/2023
[5] www.aac-clyde.space/StarbuckNano last accessed 24/06/2023
[6] www.berlin-space-tech last accessed 24/06/2023
[7] Pumpkin BM2 last accessed 20/07/2023
[8] spectrolab.com last accessed 15/03/2023
[9] rocketlab.com last accessed 15/03/2023

10.2.5. Sensitivity analysis

The sensitivity analysis is performed on the input parameters of the simulation. The most uncertain parameters which have the potential to vary and affect the design negatively are the yearly cell degradation D, the inherent degradation I_d, and the combined mass estimate for the solar panels m_{cs}. Other parameters are either taken from COTS, which increases the confidence level in the value, derived from simulations (such as the eclipse fractions) or if they vary they are only expected to affect the design positively (e.g. the depth of discharge of 20% for 30,000 cycles is only expected to increase, similarly the harness mass fraction of 25% is expected to decrease).

Thus first the inherent degradation $I_d = 0.88$ is made gradually less efficient until 3 side folds per side are needed (i.e. 1.7 fully solar cell covered folds), and then until more than 3 side folds per side are needed (i.e. 2.6 fully solar cell covered folds). The maximum theoretical decrease achievable is 20% or $I_d = 0.704$ [5] for which the design is completely unfeasible. On the other hand, if the decrease of efficiency is 10% i.e. $I_d = 0.792$ the design is feasible but the side panels require 3 folds of 16 cells each and a new overall EPS mass of $8.57\,\text{kg}$ or a 10% increase in the EPS mass. In case of a 5% decline in the inherent degradation i.e. $I_d = 0.836$, the resulting configuration only requires one extra cell of area $32\,\text{cm}^2$. The chance of the value changing by more than 5% is relatively low, thus the design is not very sensitive to a change in the inherent degradation factor.

The same sort of analysis is performed on the yearly degradation factor D. However, even if the degradation factor per year is quadrupled, the overall EPS design is not modified, for noticeable design changes to be observed the original value needs to be multiplied tenfold.

Finally the sensitivity of m_{cs} is analysed. This parameter affects the overall expected mass of the EPS with a one-on-one relation with the mass of the panels i.e. 1% increase in m_{cs} results in a 1% increase in the SPs mass. Thus, the mass budget for the EPS is very sensitive to m_{cs}. The mass budget allocated to EPS will be exceeded if the solar cell mass m_{cs} is increased by more than 10%.

10.3. EPS architechture

The EPS architecture is split into two main parts: The solar panel architecture and the electrical block diagram. The solar panel architecture shows how the selected cells are fitted on the 3 types of panels, side folds in Figure 10.8a, front folds in Figure 10.8b and top panel in Figure 10.9.

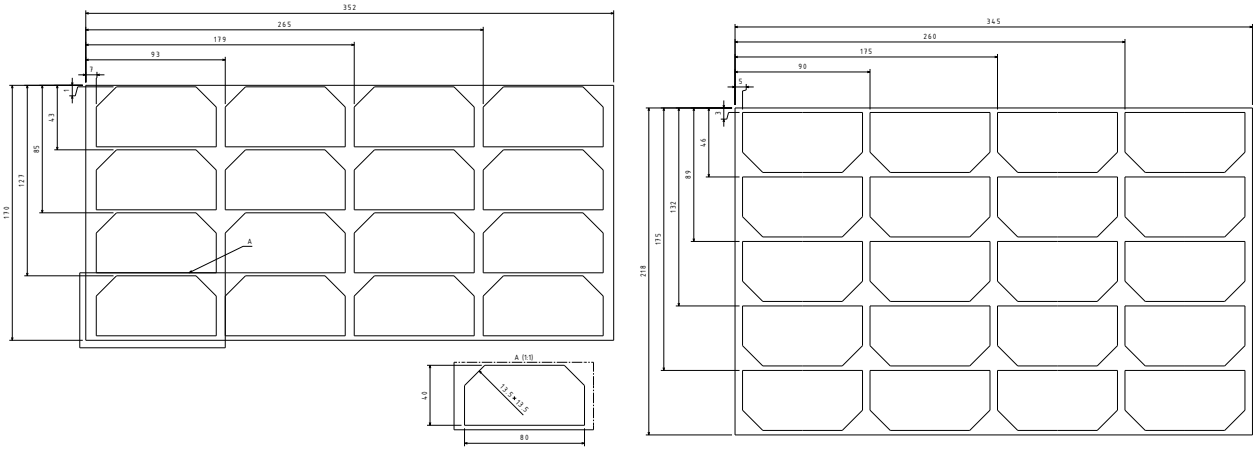

(a) *Solar cell configuration on the side folds panels* **(b)** *Solar cell configuration on the front folds panels*

Figure 10.8: *Technical drawings for the deployable panels*

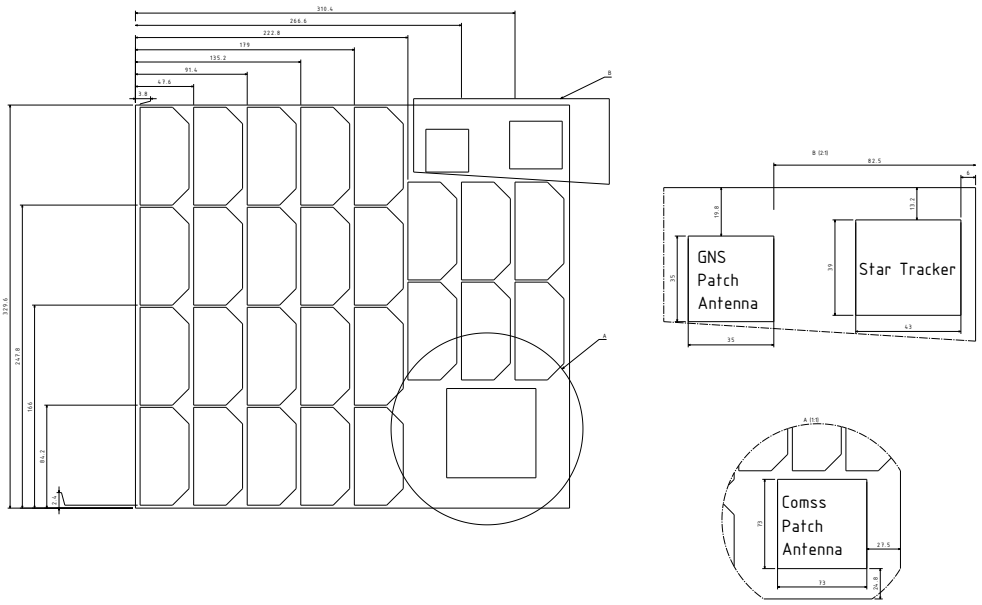

Figure 10.9: *Solar cell configuration on the top panel*

The architecture of the cells over all the folds is summarised in Table 10.7. The allowable PCDU solar array input block accepts a voltage range between 8-28 V and a maximum of 2A/4A, as described in Table 10.6. It should be noted that the proposed architecture of the top panel is more complex than for the side and front folds. If needed it is possible to simplify it to a 5P (Parallel), 5S (series), architecture by removing one of the 7 redundant solar cells of the design.

Table 10.7: *Series (S) / Parallel (P) cells architecture using IMM-α V_{mpp} = $4.28\,\mathrm{V}$ and max power per cell P_{mpp} = $1.38\,\mathrm{V}$ [7]*

Item	Cell Configuration	Max. Voltage [V]	Max. Current [A]
Side fold	4P, 4S	17.12	1.288
Side array	2 folds in P	17.12	2.576
Front fold	4P, 5S	21.4	1.288
Front array	3 folds in P	21.4	3.864
Top panel con.1	(4P, 3S)	12.84	1.288
Top panel con.2	(3S, (2x5P, 1x4P))	12.84	1.485
Top array	2 connections in P	12.84	2.773

The EPS block diagram is presented in Figure 10.10. Note that the PCDU portion is taken from the datasheet[10] of EPMS1.

[10]datasheet EPMS1 last accessed 10/06/2023

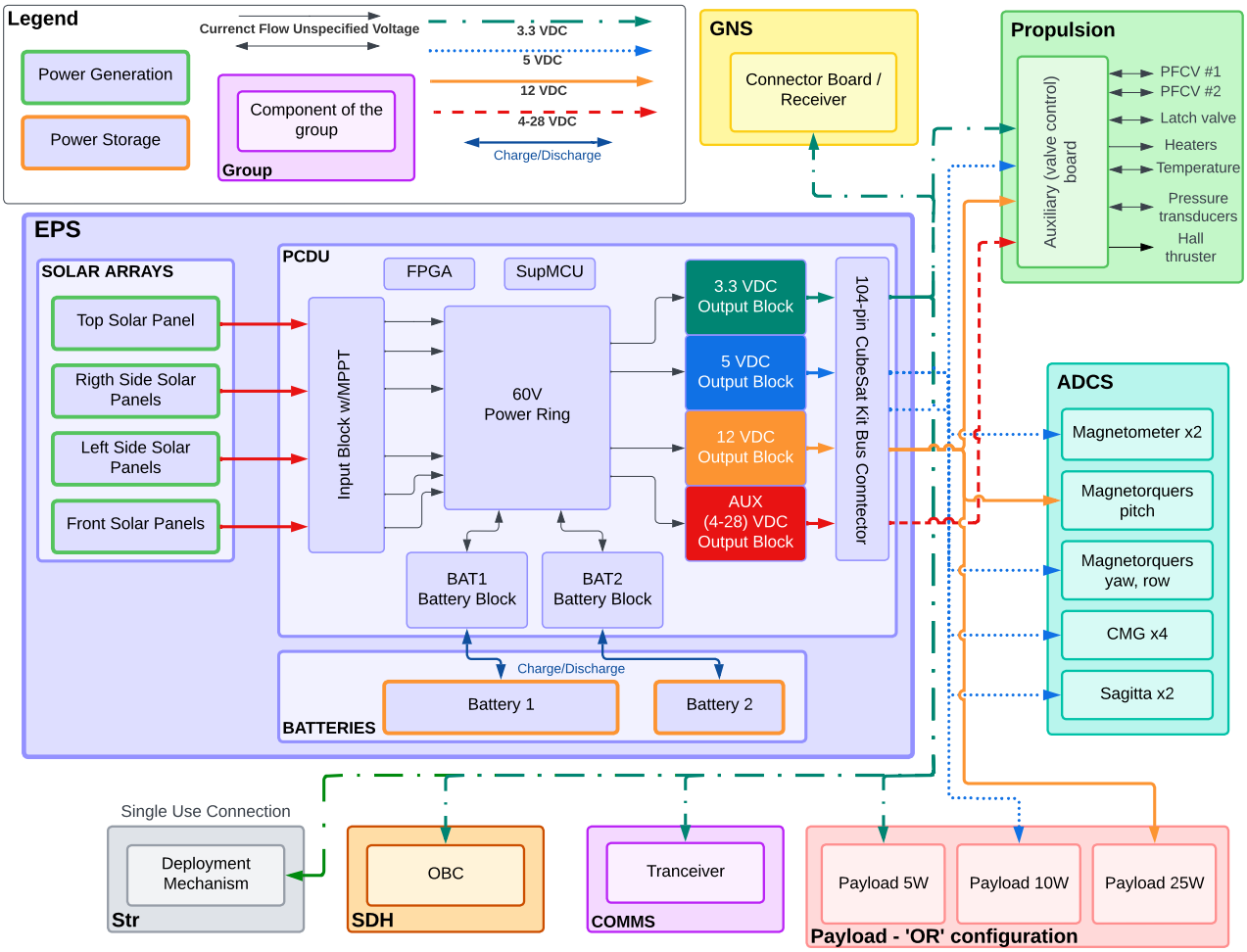

Figure 10.10: *Electrical block diagram*

10.4. System performance

A summary of the EPS system performance is presented in Table 10.8.

Table 10.8: *Summary of EPS component performance*

Item	Capacity [Wh]	Cost [€]	Mass [kg]	Volume [U]
Battery 1	155	16250	1.24	0.88
Battery 2	77	10000	0.61	0.44
Item	**Mass [kg]**	**Number of cells**	**Max. P Generated [W]**	**Cost [€] (cell + structure)**
Top Panel	0.689	26	35.8	5200 + 1733
Side Panels	1.696	64	88.3	12 800 + 4000
Side Panels	1.590	60	82.8	12 000 + 4267
Item	**Mass [kg]**	**Efficiency [%]**	**Volume [U]**	**Output blocks support**
PCDU	0.3	96	0.2	Supports [3.3V, 5V, 12V, (4-28V)], max 8A

Furthermore, with the chosen configuration in Table 10.8, there is a margin to increase the continuous power budget of the payload during certain $LTAN$ as follows:

- 8 W of continuous power can be added to the budget of both payload scenarios 2 and 3 for $LTAN = 6$ h without affecting the overall sizing.

- 8 W of continuous power can be added to the budget of both payload scenarios 2 and 3 for $LTAN < 9$ h but the overall battery pack size increase to 2 kg and 1.5 U, which is the maximum allowable value.

10.5. EPS numerical model verification

The numerical model for the EPS can be found on the GitHub[11] under the EPS branch. In order to verify the simulation a combination of unit tests, system tests, and visual tests were performed on the five main portions of the simulation, i.e. input reading and formatting, operational timeline and power need assembly, power generation computation, battery sizing computations, overall mass and volume computations.

The input reading consists of the orbital parameters from the astrodynamical simulation output file. Only the eclipse boolean, eclipse fraction and incidence angle efficiency from the astrodynamical simulation were used as input for the EPS simulation. The verification of these values is performed in the astrodynamical simulation. The formatting functions responsible to slice and assemble the input data into usable arrays were tested using pytest on smaller arrays of the same construction. All the tests returned nominal performance.
For the timeline and power need assembly functions, they were first tested on a smaller scale (arrays of 100 nodes), in order to ensure the correct insertion of sub-arrays, and operational data is executed, this was done by comparing the wanted/expected result to the function output, and showing that they were identical. The next step was scaling the experiment over the entire nominal operational timeline of LAMP, and visually inspecting continuous power, maximum power peaks, and eclipse timeline compliance. Finally, 4 random samples of the timeline of 100 seconds (two in eclipse with/without propulsion, and two in sun with/without propulsion) were compared to the manually derived scenarios. Results were comparable to machine epsilon error for the power need value. On the other hand, the start of the thrusting can sometimes begin one second before or after the intended start time, but this was judged irrelevant as the thrusting time was always of 870 s.
Testing the battery sizing function was done by comparing the output of the simulation based on a fixed input energy need value to a manually computed counterpart. For capacity, mass, and volume the results were within 0.5 mW h, 0.5 g and 0.5 mU from the manually computed data, due to the rounding performed upon display of the results. Furthermore, the simulation eliminates options based on the feasibility criteria for the batteries (total $< 2kg, < 1.5U$). Testing this was done by compiling a list of 5 input scenarios from which 3 were feasible, and 2 unfeasible. The simulation correctly removed the unfeasible options before moving on to the next stage.
Overall mass and volume computations were compared to manually updated data and the results were within 0.5 g and 0.5 mU (the difference originates from the rounding during the manual computations). This level of accuracy was judged acceptable.
The overall simulation results were first compared qualitatively with the outputs of the verified midterm EPS simulation [12], to check the order of magnitudes. This in combination with all the test of all the unit tests performed, increases the confidence in the simulation. Finally, the complete model was tested using only one solar panel configuration at $LTAN = 6$ h, and the total mass and volume were within 10 g and 10 mU from the manually computed data (the difference is expected to be caused by the rounding used in the manually computed data, and to a much smaller scale the machine epsilon error).

No validation has been performed on the EPS simulation, and is left for future stages. The main reason is that gathering all the necessary input parameters such as nominal operational timelines, power distribution map or the different PCDUs, battery, and solar panel efficiencies/parameters for a mission with similar environmental conditions (i.e. VLEO, sun-synchronous orbit) was deemed too time-consuming for the scope of the current design phase.

[11] https://github.com/DSE/tree/EPS, EPS simulation

11

Communications Subsystem

To transmit the payload data to a ground station on Earth, an antenna and transceiver must be chosen. In this chapter, the requirements Section 11.1, system selection Section 11.2, architecture Section 11.3, and performance of the communications subsystem Section 11.4 will be discussed.

11.1. Comms subsystem requirements

The user requirements for the communications subsystem were previously stated in Table 3.2. In Table 11.1, the system requirements for the communications subsystem can be found.

Table 11.1: *List of system requirements. Description of the requirement with a specific ID, a rationale and the verification method are provided*

ID	Description	Rationale	Verif.M	
Sys-COMMS-01	The Comms shall have the ability to receive data sent from earth when in view of a ground station or relay satellite.	The Comms needs to be able receive and relay uplink data. This is a functional requirement.	Demo Ana	✓
Sys-COMMS-01-I	The Comms shall have a data uplink budget of 50Mb over one orbit.	Per orbit, the satellite needs to be able to receive commands or software updates of a finite amount of bits from the ground station.	Ana	✓
Sys-COMMS-02	The Comms shall have the ability to transmit data to a ground station when in view of the corresponding ground station or relay satellite.	This is a functional requirement.	Ana	✓
Sys-COMMS-02-I	The Comms shall have a data downlink budget of 22.5Gb over one orbit.	The satellite has to downlink both telemetry and payload data when in view of a ground station as dictated by *U-COMMS-01*.	Ana	✓
Sys-COMMS-03	The signal transmitter shall be able to send data while the payload is operational.	No interference should be present between payload and Comms operations. This functional requirement is dictated by *U-Ops-02*.	Demo	✓
Sys-COMMS-03-I	~~The Comms shall have a pointing accuracy need of less than <*TBD*> deg~~	~~Provides the maximum pointing accuracy which can be expected for the Comms~~.	~~Ana~~	-

Sys-COMMS-04	The Comms shall have a channel capacity of 150 Mbit/s when using a direct link, or a capacity of 5Mbit/s when using a relay system with constant connection.	Provide the maximum rate at which information can be transmitted and received.	Test	✓
Sys-COMMS-05	The Comms shall be able to modulate generated data when in orbit.	The Comms needs to transmit digital data to the ground station. This is a functional requirement.	Demo, Ana	✓
Sys-COMMS-06	The Comms shall be able to demodulate received data.	The Comms needs to retrieve digital uplink data to handle by the SDH subsystem. This is a functional requirement.	Demo, Ana	✓

Since the midterm report, several slight adjustments to the requirements have been made: For requirement *Sys-COMMS-01*, *Sys-COMMS-02* and *Sys-COMMS-04* the option of transmitting via relay satellite has been added. Requirement *Sys-COMMS-03-I* has been removed, since this is antenna specific and does not apply to the entire communication subsystem. In the case of using a pointed antenna, a derived requirement will have to be created.

11.2. Comms subsystem design

In the midterm report, a choice for a dual patch antenna was made. Due to iterations in the power subsystem, the solar panels will no longer be rotatable at will. Because of this, the dual patch antenna system will no longer be sufficient.
To have a working communications subsystem, a new analysis of antennas must be performed. For the new analysis, the data transmitted will be simulated over 90 days. This gives a more fair representation and will therefore give a more substantiated choice. In this new analysis, the use of different modulation schemes and relay systems will also be considered.
The new design and choice of the antenna are split up into 5 subsections: The simulation of data capacity for direct link antennas, the verification of the simulation used, the analysis of relay satellite communication, the trade-off between all options, and finally a sensitivity analysis of the choices made.

11.2.1. Simulation

The calculation of the data capacity for every antenna is done in 4 steps: First, the antenna gain is graphed for different angles. Secondly, the data rate is calculated for different angles of elevation. Thirdly, the data rate vs elevation graph is transformed into a data rate vs time graph and integrated, and finally, the data accumulation and data capacity over 90 days is graphed and calculated. For all link-budget calculations, a DVBS-2x demodulator and the accompanying required signal-to-noise ratio (SNR) for each modulation is used. The python code used can be found on GitHub.[1]

Antenna Gains

In Figure 11.1, all the considered antennas and their gains can be found. It should be noted, that the gain distributions of specific antenna types can still vary and if a type is chosen, multiple antennas of the same type with slightly different gain distributions should be analysed to find the best fit. The antenna systems analysed can be split into two groups: the first being fixed antennas that will always point in the same direction as the DST, and the pointed antennas, which are always pointed at the ground station when communicating. The isoflux, low-gain patch, and phased array antennas are assumed as fixed antennas, whilst the high-gain patch, reflect array and parabolic antennas are assumed to be gimballed at the ground station.

[1] Github Comms simulation

Data rate vs elevation

Next to the antenna specifications, the data rate that can be transmitted depends on multiple factors, including the elevation angle of the satellite, the modulation scheme used and the maximum amount of bandwidth that is available. To eventually end up with a set amount of data that can be sent over a number of days, the first thing that must be calculated is the maximum data rate for different elevation angles. This can be done using link budget calculations. In Figure 11.2, the maximum data rate for different elevations for all antennas can be seen. For this graph, the modulation scheme used is 16APSK 2/3-L, and the available bandwidth is set to 100MHz. The effect of the limited bandwidth can clearly be seen for the pointed, high-gain antennas, which reach the bandwidth limit quite quickly, whilst the low-gain fixed antennas do not. This means the high-gain pointed antennas could benefit from a higher order modulation, whilst the fixed, low-gain antennas could benefit from a lower order modulation when having an available bandwidth of 100MHz.

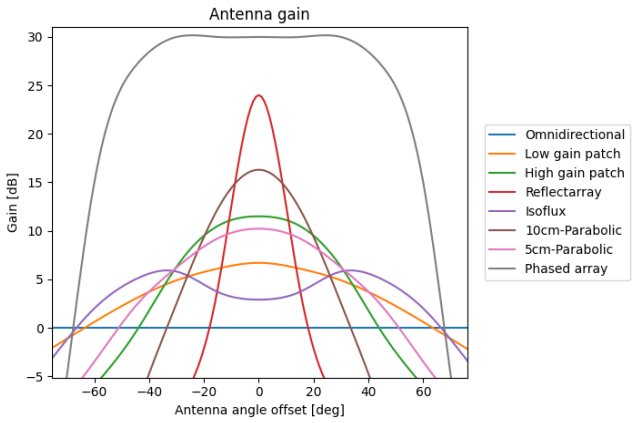

Figure 11.1: *Gain plots of all antennas*

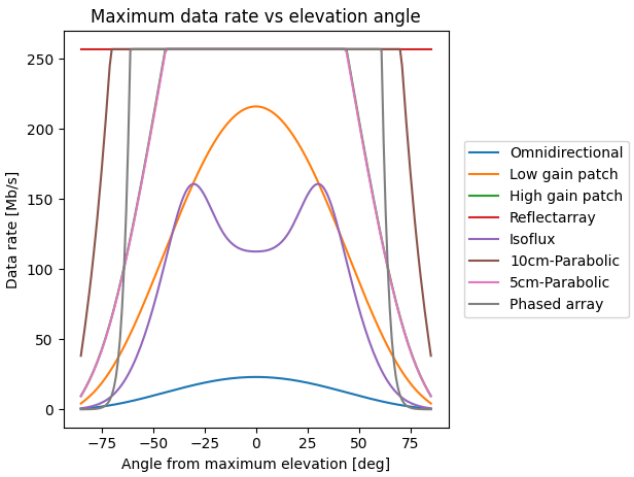

Figure 11.2: *Data rates for different elevations for all antennas (bandwidth=100MHz)*

Data rate vs time

To be able to calculate the total amount of data sent over a pass, the data rate vs time graph must be integrated. To transform the data rate vs elevation graph into a data rate vs time graph, the duration between specific elevations of a pass must be known. To estimate this, Equation 11.1 is used.[66] Here ω_s is the angular velocity of the satellite, ω_E the angular velocity on earth due to the rotation of the earth, i the orbit inclination angle, r_E the earth radius, r the orbit radius, θ_c the minimum elevation angle and θ_{max} the maximum elevation angle of the pass.

$$t_{pass} = \frac{2}{\omega_s - \omega_E \cos i} \cdot \arccos\left(\frac{\cos\left(\arccos\left(\frac{r_E}{r}\cos\theta_c\right) - \theta_c\right)}{\cos\left(\arccos\left(\frac{r_E}{r}\cos\theta_{\text{max}}\right) - \theta_{\text{max}}\right)}\right) \tag{11.1}$$

This can then be used to transform the data rate vs elevation graphs into data rate vs time graphs by discretising the elevation range and using the lower and upper bound in Equation 11.1. The result can be seen in Figure 11.3 and Figure 11.4. These graphs can be integrated over time to calculate the maximum amount of data that can be sent over a specific pass.

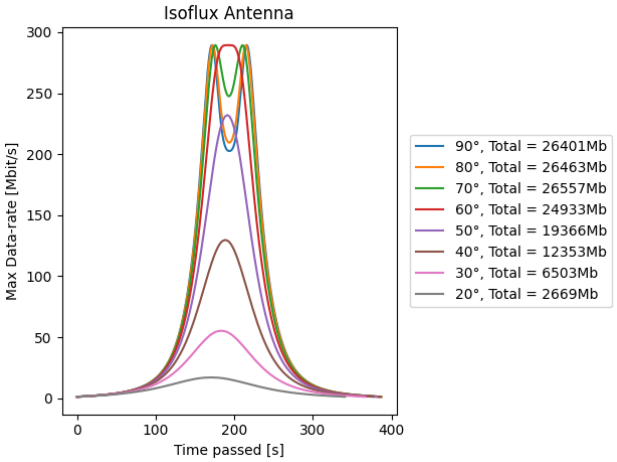

Figure 11.3: *Data rates for isoflux antenna (bandwidth=100MHz)*

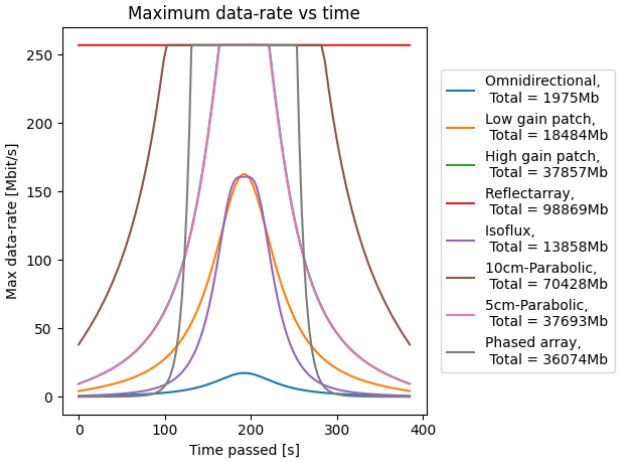

Figure 11.4: *Data rates for all antennas (max elevation =60° , bandwidth=100MHz)*

Data accumulation and modulation

With the amount of data that can be sent over a certain pass, the data that can be sent over 90 days can be calculated using ground station pass data (see Section 6.2 for orbital information) which is needed to get a fair comparison between antennas. Plotting the data that is in storage that still has not been sent against time also gives a visual representation of how long it takes to get all the data to the ground station. In Figure 11.5, the data accumulation plot can be seen for the phased array antenna, with a ground station at 60 degrees latitude and a bandwidth of 150MHz. The plot was made for different modulations of 16- and 32APSK, and it can be seen that in this case, a 16APSK 4/5 Modulation would work best with a theoretical maximum of 6997Gbit that can be sent. It should be noted that the amount of data that needs to be transmitted within 90 days is 6411Gbit.

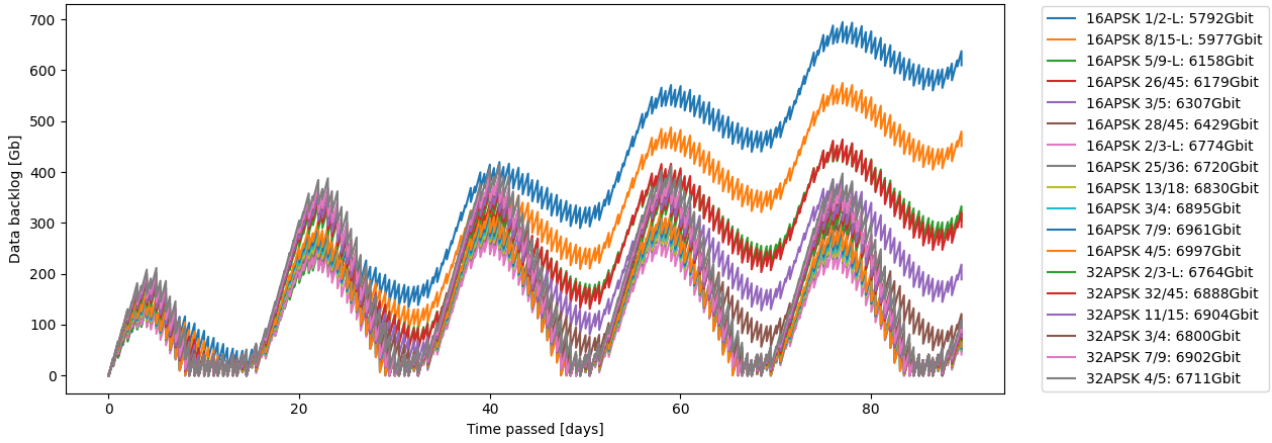

Figure 11.5: *Phased array data accumulation*

In Figure 11.6, the first days of the data accumulation graph can be seen for all antennas with a ground station at 60 and 78 degrees latitude. The bandwidth here is set to a maximum of 50MHz and the best modulation scheme is used for each antenna.

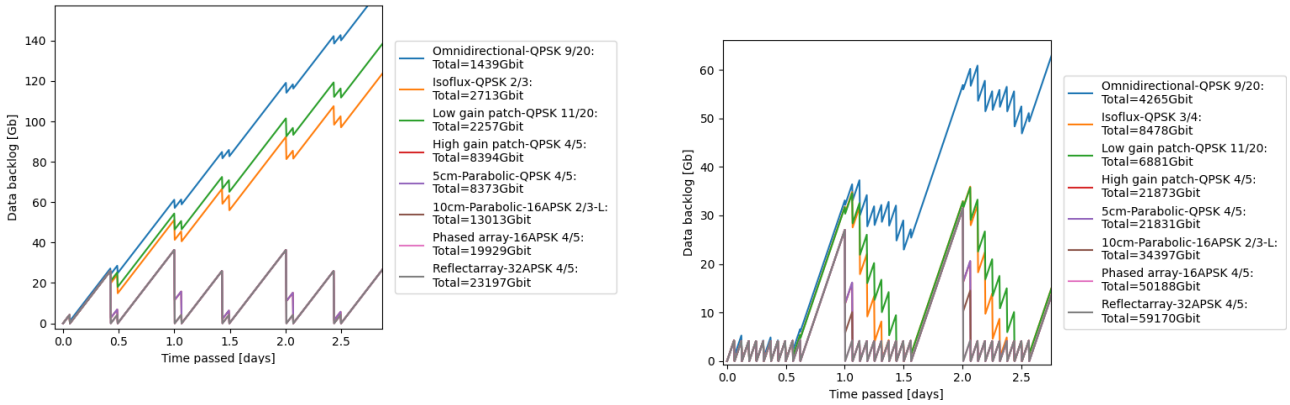

(a) *60 deg latitude* **(b)** *78 deg latitude*

Figure 11.6: *Data accumulation plots of all antennas*

From this, it can be seen that the omnidirectional antenna will not work, and the isoflux and low-gain patch antenna only with a ground station at 78 degrees latitude whilst operating at this frequency and bandwidth.

The omnidirectional, isoflux, 10cm parabolic and reflect array will no longer be considered from this point onwards. The omnidirectional antenna does not perform well enough to meet the requirements. It should be noted that it could benefit from operating at a different frequency than 8GHz, however, an omnidirectional antenna does not perform well enough at other frequencies either. The isoflux takes up a lot more volume than the low gain patch, whilst not performing significantly better, and is therefore excluded. The 10cm parabolic antenna is not needed, considering that the 5cm parabolic antenna already is capable of transmitting the data. Finally, the reflect array will no longer be considered due to the fact that the whole satellite or solar panel, in the case of an integrated reflectarray, will need to be pointed at the ground station whilst other antennas do not have this limitation.

11.2.2. Simulation verification & validation

To verify the simulation used to generate the accumulation graphs and calculate the total amount of data that can be sent with a certain antenna, 28 Unit tests were created. All functions were verified by comparing with hand calculations. The visibility time calculation was also validated by calculating the visibility times of passes from both the ISS and Tiangong and comparing them with online available data. All unit tests passed successfully, and the visibility time was accurate to around 1%.

11.2.3. Data relay satellites

Next to having a direct link with a ground station, using a relay satellite is also possible. For example, 99% of NASA's mission is transmitted via Tracking and Data Relay Satellites (TDRS)[2]. For now, two relay systems are considered: TDRS from NASA and Starlink from SpaceX. The main advantage of using a relay system is the nearly constant connection and the ease of antenna positioning, considering the antenna can then be put on top of the satellite instead of being positioned in a way that the antenna does not interfere with the lower half being reserved for payload.

TDRS

For TDRS, the gains of the receiving antenna are around 37, 54 and 59dB for S-, Ku- and Ka-band respectively[3]. To be able to transmit the 4Mbit per second needed for a live link, the gain of the antenna on LAMP would have to be a high 20dB for all frequency bands. This is due to the high free-space losses, considering TDRS is around 32000km away. The only antennas that have such a high gain are the reflectarray and phased array antennas (see Figure 11.1). The phased array antenna would work best here, considering the entire satellite or a solar array would not have to be pointed towards TDRS. Using a phased array antenna and a QPSK 13/45 modulation, a maximum stable

[2]www.nasa.gov, last accessed on 19/06/2023
[3]ntrs.nasa.gov, last accessed on 21/06/2022

data rate of 35Mbit/s can be achieved. This would require a 0.35W transmitted power to transmit 4.14Mbit/s.

Starlink

At the time of writing, 4491 Starlink satellites have been launched into orbit, of which 3710 are active, and another 7500 satellites have recently been approved[4]. At the current rate of bringing Starlink satellites in operation, SpaceX will have its aimed 10000 Starlink satellites at 550km altitude in around 4 years[5]. A Ku-band antenna on LAMP can replicate the transmission from Starlink user ground stations, using the same 14.5GHz transmission frequency.

Although Starlink has not been used for satellite communication before, Starlink has been used to communicate with drones: the company RDARS has reportedly successfully integrated Starlink into its drones[6], and the Ukrainian army has also used Starlink to control aerial and naval drones, although this use of Starlink was later curbed by SpaceX[7]. The connection with LAMP via Starlink will happen in a very similar manner, where the customer could either be directly connected to LAMP via Starlink or receive the data and transmit commands via a Starlink ”Gateway” ground-station. The biggest hurdle to allow connectivity with a satellite would be the speed at which the satellite moves. Although Starlink is able to connect with fast-moving vehicles such as aircraft[8], the speed of the satellite is around 24 times as high. This means that in a worst-case scenario, the connection would have to be switched to a different Starlink satellite after only 29 seconds. Due to the high velocities, the Doppler effect can also influence the connection, and Doppler compensation techniques will need to be implemented to reduce its impact [67].

Due to the lack of atmospheric losses and the shorter distance, the antenna on LAMP also does not need to have a gain as high as the Starlink ground stations. Assuming 10000 Starlink satellites and equal spacing, the distance between the Starlink satellites would equate to 224km. Using a high-gain patch antenna, a QPSK 13/45 modulation and considering nadir and off-nadir pointing, the maximum stable data rate that can be achieved is 46Mbit/s. The link-budget values for this can be found in Table 11.5. Since this already covers the required 4.14Mbit/s, the use of a more expensive, higher gain antenna, such as the phased array and reflectarray antennas is not needed. Due to their increased thickness, a parabolic reflector is also not used. The high-gain patch antenna is therefore chosen as the best antenna to be used in combination with Starlink satellites. To transmit the required 4.14Mbit/s, the average transmitted power needs to be around 0.07W and the bandwidth that is required is 7.5Mhz.

11.2.4. Communications system trade-off

After analysing all the different antennas and relay systems, a trade-off can be made between the different systems. The trade-off criteria are as follows:

- Mass (15%) - the mass of the antenna system, including a deployment system if needed. Based on the mass budget, a reference value of 300g is used.
- Data Capacity (30%) - The data that can be transmitted within 90 days at full power capacity. The reference value is 6.4Tb, based on U-COMMS-01 and the DST data generation. The power required is also directionally proportional to this, due to the ability to scale down the power when more data rate capacity is available than needed.
- Volume (20%) - The Volume that is needed for the antenna system, including a deployment system if needed. A reference value of 0.4U was used, based on the volume budget.

[4] www.fcc.gov, last accessed 19/06/2023
[5] satellitemap.space, last accessed on 20/06/2023
[6] pcmag.com, last accessed on 20/06/2023
[7] reuters.com, last accessed on 20/06/2023
[8] starlink.com, last accessed on 21/06/2023

- Complexity (20%) - The complexity of the antenna system. This includes added complexity due to deployment systems or low technological readiness levels. An explanation of the complexity of each antenna system can be found after the trade-off table.
- Cost (15%) - The financial cost of the system. This includes the costs of extra deployment systems if needed. A cost between 5000€ and 20000€ is used as ”medium”, corresponding with the financial budget. Exact numbers are not given, since this would depend on the choice to buy the system off-the-shelf and where or to build it in-house.

	Mass [15%]	**Data Capacity [30%]**	**Volume [20%]**	**Complexity [20%]**	**Cost [15%]**
Low-gain Patch	Green 50g	Yellow 6.8Tb	Green 0.003U	Green Low	Green Low
High-gain Patch	Yellow 230g	Yellow 22Tb	Yellow 0.19U	Yellow Medium	Yellow Medium
5cm Parabolic	Orange 407g	Yellow 22Tb	Yellow 0.26U	Yellow Medium	Yellow Medium
Phased Array	Orange 500g	Green 50Tb	Green 0.06U	Orange High	Orange High
TDRS relay	Orange 500g	Green 272Tb	Green 0.06U	Yellow Medium	Orange High
Starlink relay	Green 50g	Green 358Tb	Green 0.003U	Yellow Medium	Green Low

For complexity: The complexity of the high-gain patch and 5 cm parabolic antennas are set to medium due to the added deployable boom system, which increases the complexity. The TDRS relay antenna systems' complexity is set to medium due to the complexity of a phased array antenna, and the phased array antenna without using a relay system complexity is set to high, because the phased array antenna would have to be integrated within the bottom of a solar panel, and the solar panel would need rotation capability as well to make sure it does not point away from the ground station. The Starlink relay antenna system's complexity is set to medium due to the lower technological readiness level of using Starlink satellites as relay satellites. It should also be noted that except for the relay systems and the low-gain patch antenna, the use of a secondary omnidirectional antenna for TT&C communication might be necessary.

As can be seen from the trade-off, the low-gain patch antenna and Starlink relay systems are the best options with their lower complexity, cost, mass and volume. Whilst the low-gain patch has a higher TRL and would therefore be a safer option, using a relay system with Starlink satellites increases the maximum data that can be sent by a factor of 50. Due to the increased marketability of having such a high data transmission capacity and the ability to almost always receive the data within a second, the Starlink relay system is chosen as the communication system. The high data rate capacity of using this system gives the ability to stably send 55 DST or around 2 4K images per second using lossless compression. When using a video camera as a payload and lossless video compression, a 1920x1080p video can be transmitted at around 28 frames per second.

11.2.5. Transceiver

Since the communication with Starlink uses the Ku band, a transceiver that can operate for this band is needed. Due to the limited availability of small transceivers in this band, it has been decided that

the transceiver will be developed and produced in-house. The requirements for this transceiver can be seen in Table 11.2. In Table 11.4, the expected values of power and mass are shown. These are based on existing transceivers that can operate at the Ku band, and by extrapolating mass/power vs frequency graphs for CubeSat transceivers.

Table 11.2: *Transceiver Requirements*

Requirement	Value
Transmit frequency	14-14.5 GHz
Receiving frequency	10.7-12.7 GHz
Output power	>3 W
Modulation	QPSK 13/45
Data rate capacity	>46 Mb/s

11.2.6. Sensitivity analysis

To review the validity of the design choices made, a sensitivity analysis is performed. This is split up between a sensitivity analysis of the simulation, Starlink and the antenna trade-off.
For simulating the data capacity of the direct link antennas, several variables could still influence and change the final values. As stated before, the exact antenna could be slightly different from the gain plot used in Figure 11.1. Secondly, for calculating the data capacity, the antennas are assumed to be operating at a perfect variable data rate. Since this will probably not be perfect in the real world, the final capacities could be slightly lower. This means that the data capacity for the low-gain patch could fall below the required 6.4Tb. That said, designing an antenna with a higher power output could solve this problem.

As stated before, the assumed Starlink satellites equate to 10000. Whilst this is an expected amount before the development of LAMP can be finished, it is not set in stone and if SpaceX decides to not expand any further and the satellite count stays at 4400, the maximum stable data rate that could be achieved would equate to around 9Mbit/s. It should be noted that this is still above the 4.14Mbit/s that is required. In the case of staying under 5000 satellites, the low-gain patch antenna might become a better choice due to the lower complexity, depending on how high the constant connection that Starlink enables is valued.

For the antenna trade-off, the effect of assigning different weights, reference values and the assigned values for complexity must be analysed.
Due to the added benefit of having a very high capacity, the Starlink relay system will stay the best option when changing the weights, unless the complexity of the satellite must be drastically reduced. Changing the reference values will not significantly affect the choice made, since the mass, volume and cost of the low-gain patch and the Starlink relay system are extremely similar and the best when compared to the other antennas.
For the complexity value assignment, the complexity of the low-gain patch could be argued to be Medium due to the attachment on the sun shield. Depending on the development of a phased array antenna, the complexity of the phased array antenna and TDRS relay system could be lowered or increased.
Considering the points discussed above, the sensitivity of the choice made is very low, and the choice to use a Starlink relay system is very unlikely to change.

11.3. Comms subsystem architecture

In Figure 11.7, the communications flow diagram can be seen. This shows the different data- and command links, the encoding- and modulation processes and the gathering of the payload data.

11.4. Comms subsystem performance

The performance values of the final design can be found in Table 11.3 and Table 11.4. The power needed to transmit 4.14Mbit/s is also shown since this is the data rate needed to have a live link with the DST. For the electrical subsystem, a constant power used of 1.8W is assumed, since this is the power needed for 20Mbit/s and the constant use of a data rate higher than this is not expected. In Table 11.5, the final link budget values that were used to calculate the 46Mb/s stable data rate can be found.

Table 11.3: *Antenna performance*

Performance Characteristic	Value
Modulation used	QPSK 13/45
Peak data rate	$180\,\mathrm{Mb/s}$
Stable data rate	$46\,\mathrm{Mb/s}$
Maximum antenna Power	$3\,\mathrm{W}$
Avg. antenna power for 46Mbit/s	$0.82\,\mathrm{W}$
Avg. antenna power for 4.14Mbit/s	$0.07\,\mathrm{W}$
Bandwidth needed for peak	$372\,\mathrm{MHz}$
Bandwidth needed for 46Mbit/s	$83.6\,\mathrm{MHz}$
Bandwidth needed for 4.14Mbit/s	$7.5\,\mathrm{MHz}$
Antenna mass	$59\,\mathrm{g}$
Antenna volume	$0.003\,\mathrm{U}$

Table 11.4: *Transceiver performance*

Performance Characteristic	Value
Maximum transceiver power	$18\,\mathrm{W}$
Avg. transceiver power for 46Mbit/s	$4.92\,\mathrm{W}$
Avg. transceiver power for 4.14Mbit/s	$0.42\,\mathrm{W}$
Transceiver mass	$300\,\mathrm{g}$
Transceiver volume	$0.25\,\mathrm{U}$

Table 11.5: *Link Budget Values*

Characteristic	Value
Max angle offset on antenna	$32.4°$
Max distance to Starlink	370.9km
Data rate	$45.5 \cdot \frac{1}{13/45}$Mb/s
Power output	34.77dBm
Line and connector loss	-1.0dB
Antenna directivity (at 32.4°)	5.29 dBi
Transmitted EIRP	9.06dBW
Path loss	-167.06 dB
Starlink receiver directivity[68]	41.0dBi
Polarization mismatch and line loss	-4.0 dB
SNR power density	83 dBHz
SNR	1.0dB
Required SNR for QPSK 13/45[9]	-2.0dB
Link margin	3.0dB

[9] datumsystems.com - DVBS-2X Dual-Demod Datasheet

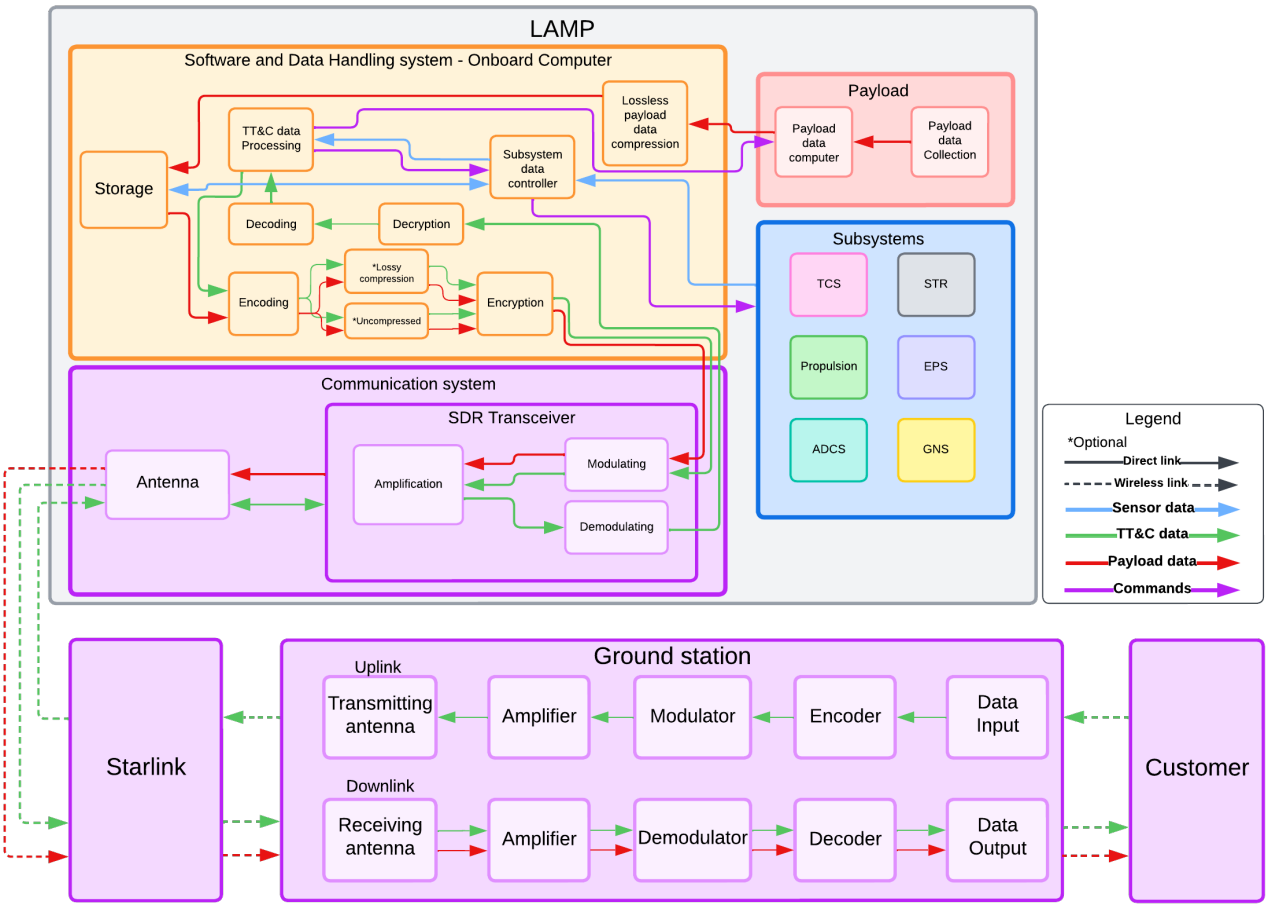

Figure 11.7: *Communications Flow-diagram*

12

SDH

In this chapter, the requirements, design and development for the onboard computer (OBC) and the block diagrams for the data handling and software are discussed and shown.

12.1. SDH requirements

Table 12.1: *Data Handling subsystem requirements.*

ID	Description	Rationale	Verif. M.	
Sys-SDH-01	The SDH shall manage all data originating from all subsystems throughout the satellite's lifetime.	Functional requirement of the SDH.	Demo	✓
Sys-SDH-01-I	The SDH shall be able to receive data from the payload	All payload generated data needs to be sent to the SDH to handle, store and transmit it.	Demo	✓
Sys-SDH-01-II	The SDH shall be able to send the encoded data to the Comms	The SDH provides an interface between the payload and Comms to transmit payload data to the ground station and receive commands from the ground station.	Demo	✓
Sys-SDH-02	The SDH shall be able to issue commands to all subsystems of the satellite	Functional requirement of the SDH.	Demo	✓
~~*Sys-SDH-03*~~	~~The SDH shall be able to encode the data of the payload to a digital format~~	~~The data output of the payload can be in an analogue format, hence, it needs to be digitized to handle and manipulate. Functional requirement of the SDH.~~	~~Demo~~	-
Sys-SDH-04	The SDH shall be able to encrypt the data of the payload	Prevent interception of data interception. Functional requirement of the SDH.	Demo	✓
Sys-SDH-05	The SDH shall be able to control the payload.	SDH needs to collect, handle, and distribute data as well as issue commands to the payload. Functional requirement of the SDH.	Demo	✓
Sys-SDH-06	The satellite shall be able to decrypt received telemetry data	Functional requirement of the SDH, and safety requirement.	Demo	✓

Sys-SDH-07	The satellite shall be able to discern between authorised/secure grounds stations and insecure/unauthorised ground stations	Safety requirement to avoid interception of sensitive payload data and control by unwanted parties.	Demo	✓

Requirement *Sys-SDH-03* has been removed from the list of system requirements as it has been decided that the payload is expected to have its own computer to encode its data.

12.2. SDH design

In the following subsections, the OBC technology will be chosen and sized, followed by a discussion and elaboration on the final OBC design.

12.2.1. SDH choice of technology

In the Midterm report [12], the main focus for selecting the OBC was put on the amount of available storage provided by COTS solutions. This resulted in only two viable solutions that appeared to both be very oversized in available computing power and total power consumption. This resulted in the possibility of further considering in-house development of the OBC in the final report.

12.2.2. OBC sizing

For the OBC there are two available options, a COTS product or an in-house built solution. In order to select the best solution, the general use case must first be understood, specifically the:

- Required storage capacity
- Required computing power
- The interfaces needed per subsystem
- Power availability
- Volume availability
- Mass availability

Required storage capacity

The DST generates 4.14 Mb/s of data during normal operation, with the user requirement *U-SDH-01* stating that LAMP needs to be able to store one month's worth of the total amount of data gathered this equates to a minimum storage capacity of 1360 GB or 1.36TB. If deemed necessary this could be decreased by compressing the data with either lossy (some data is lost) or lossless compression. For lossy compression this could decrease the size by a factor of more than 10, for lossless the decrease can be close to a factor of 2 [15]. Storing the data like this would also increase the amount of data that could be send during transmission.

Required computing power

The required OBC computing capacity and the minimum size of the RAM needed can depend on multiple factors. One of these factors is whether or not the payload processes the gathered data with its own dedicated computer. If this is not the case, the computing requirements of the OBC will likely increase significantly. Other factors depend on the amount of computing capacity needed to operate LAMP itself. The subsystems will be connected to and controlled by the OBC so the required computing power depends on how many subsystem components will be installed in LAMP and how much computing power they require.

For the DST study, it has been decided that the payload itself is required to process and compute the gathered data, so that this can be delivered to the OBC and put into the OBC storage without any extra payload data processing required. This has been decided as the platform will be able to house a variety of different payloads that will all have different interface and processing requirements, so in order to simplify and optimise the OBC, only LAMP's own dedicated subsystems will be controlled directly by the OBC. The payload data will of course still be handled by the OBC when being sent to

and retrieved from the storage but this will primarily only consist of data throughput.

Other than the payload, the next subsystem that will need the most computing power is the ADCS, it is not uncommon for the ADCS to have a dedicated CPU [69]. The ADCS algorithm needs the OBC to process large quantities of sensor data.

Required interfaces per subsystem

The OBC will be used to control the subsystems and their respective components (actuators, sensors, etc.), and each component that is connected to the OBC utilises an interface-specific connector. These interfaces can differ per component and can be divided into low-speed and high-speed data interfaces. Low-speed data interfaces such as I2C, RS422 or RS485 (max 10Mb/s) are commonly used by subsystem components, as these components do not create or require much data to be utilised. High-speed data interfaces such as Ethernet (>1000Mb/s) are less necessary for the utilisation of subsystem components and are more likely to be used for the link between the OBC (storage) and the communications subsystem transceiver. This is because this link will be used to transport the payload data to the transceiver which will require higher data rates.
LAMP houses a large number of actuators and sensors, which results in a large number of different interfaces the OBC needs to support, as can be seen in Table 12.2. With this number of required connections, there are already fewer available COTS OBC solutions that have sufficient connection capabilities, influencing the necessity for building a custom-fit OBC in order to ensure all interfaces can connect to the OBC. It should be noted that for for example I2C or RS-485 it is possible to have multiple nodes connected to the same wire in order to decrease the required connectors.

Table 12.2: *Interface connectors and amounts*

Connector type	Number of times required
I2C	7
RS-485	7
RS-422	2
RS-232	2
RJ45 (Ethernet)	1

Power availability

The power consumption of the OBC depends primarily on the CPU and its computing capabilities. This could be as low as 0.05 W and can go up to over 100 W. Generally, for COTS CubeSat OBCs, the actual value lies closer to the range of 0.5-25 W. In the case of LAMP the available power budget for peak power is 5 W, which needs to be considered when selecting or building the OBC.

Volume availability

Generally, the size/volume of COTS OBC is relatively small, when looking at different available options that range from low to high computing power the volume ranges from 0.1-0.6U. the available volume for the OBC in LAMP is yet to be determined.

Mass availability

Typically the mass of the OBC is relatively low, with larger OBCs weighing around 250 g[1] and smaller OBCs weighing less than 100 g[2], the stringent mass budget for CubeSats makes it important to keep the mass of the OBC as low as possible. This needs to be considered when selecting or building the OBC.

[1] satsearch.co, last accessed on 16/06/2023
[2] satcatalog.com, last accessed on 16/06/2023

12.2.3. OBC selection

Finding a suitable COTS OBC that complies with the requirements and criteria discussed before has shown there are solutions that provide enough storage and computing capacity. However as these OBC's are generally very oversized for the use case of LAMP they are larger, heavier and use considerably more power than is available. This is why it has been decided that developing and building the OBC in-house is the best solution. The reason for this, other than the reasons named before is that the COTS OBC are expensive and building it in house can have a positive impact on the monetary budget. Added benefits of this are better integration possibilities and that the OBC can be tailored to the specific requirements of LAMP. The components needed to build the OBC in-house include, among others, the CPU, PCB and storage units.

For the CPU selection there are many possible solutions. One would be to pick a CPU that is capable of processing all of LAMP's data needs, however, this will have implications on the amount of required power as bigger CPUs require more power. Furthermore, this will also result in a lower reliability, as the entirety of LAMP's processing will be done by just one chip.

Therefore, it was decided that multiple smaller CPUs will be used, in order to divide the larger data streams from subsystems like the ADCS and the lower data streams over multiple different smaller chips. This provides the opportunity to add redundancy by adding extra chips that can either be utilised when more computing capacity is required or in the case of a chip failure.

The selection has been made to include one larger chip that is used primarily for processing the ADCS algorithms. This chip includes a margin as it is likely oversized for just the ADCS processing, this could be further worked out when specifically looking at the computing power the algorithms need in future studies. For now, with the given power availability, a chip that is at least comparable to the ARM Cortex-A9[3] was considered. For the smaller microprocessors, a chip comparable to the ARM Cortex-A7[4] is considered. Three of these chips will be added to the OBC as they are considerably smaller, cheaper and provide redundancy in case of a chip failure.
It is crucial both selected CPUs are compatible with all interfaces discussed in Table 12.2, which for these two options they are. If another similar CPU ends up being selected this should be kept in mind. Lastly, again it should be noted that it is likely the CPUs are oversized but as the exact required computing power has not been estimated the sizing has been performed with the available power in mind.

Table 12.3: *Microprocessor specifications*

	Cores	**Max Clock Frequency [MHz]**	**Normal Power Consumption [mW]**	**L1 Cache [kB]**	**L2 Cache [MB]**
ARM Cortex-A9	4	1000	∼400	128	1
ARM Cortex-A7	2	800	∼100	64	0.5

With the CPU's options selected, there are still some further considerations for the OBC, namely the PCB design and the required interface connection pins, the possible need for radiation hardening and the possibility of using a new standard for the interfaces between the OBC and the subsystems.

For the storage, the most important consideration is that it must have the capacity to store enough data in order to comply with requirement *U-SDH-01*. In the Midterm report [12], it was concluded that SSD storage is the best solution as it is relatively lightweight, small and inexpensive. At this moment, the largest available M.2 SSD drives can store up to 8TB of data. As only 1.36TB are, required but

[3] mouser.com, last accessed on 26/06/2023
[4] mouser.com, last accessed on 26/06/2023

the size of these drives generally increases with increments of 1TB, a drive of 2TB will be selected to act as LAMP's main storage. This will also ensure that there is a large redundancy in storage and ample space for housekeeping and other data to be stored for longer amounts of time.

Radiation hardening the OBC and storage of a satellite is a necessity, as the ionising radiation in space can cause a number of issues. However, in the case of LAMP which will operate in VLEO at an altitude of 300 km the levels of ionizing radiation that it will receive in 5 years is substantially lower at 3 krad compared to 100 krad at an altitude of 1000 km [70]. This means that the measures that need to be taken are less stringent and limiting but do need to be considered during production nonetheless.

While designing the PCB and selecting the layout of the interface connection pins and busses, it is likely that the PC/104 bus standard will be used, although this is an older standard, the EPS, GNS and propulsion boards still use this bus simplifying the integration of the OBC with the rest of the subsystems. Another possibility would be to consider the use of a new type of bus interface (PQ9 and CS14) specifically designed for CubeSats, which can help improve power consumption, connectivity and save volume but integration capabilities need to be considered[71].

12.3. SDH architecture

The data handling block diagram is shown in Figure 12.1, showing the different interfaces and connections between the subsystems; and the OBC, for the payload and communication subsystem the amount of data that can flow through the system is also shown. In turn, Figure 12.2 shows the different software modes for LAMP from before launch until end-of-life.

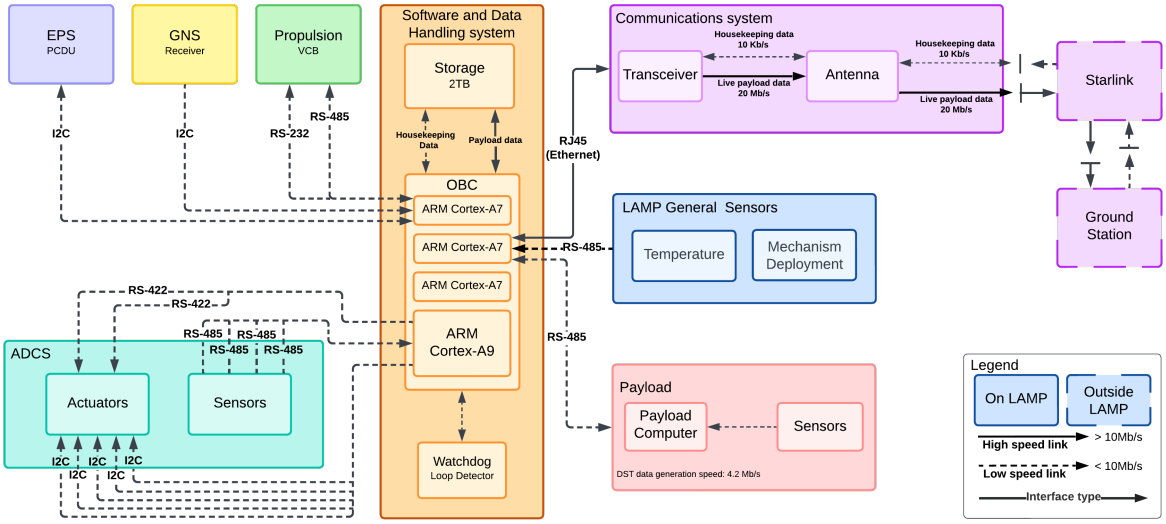

Figure 12.1: *Data Handling block diagram*

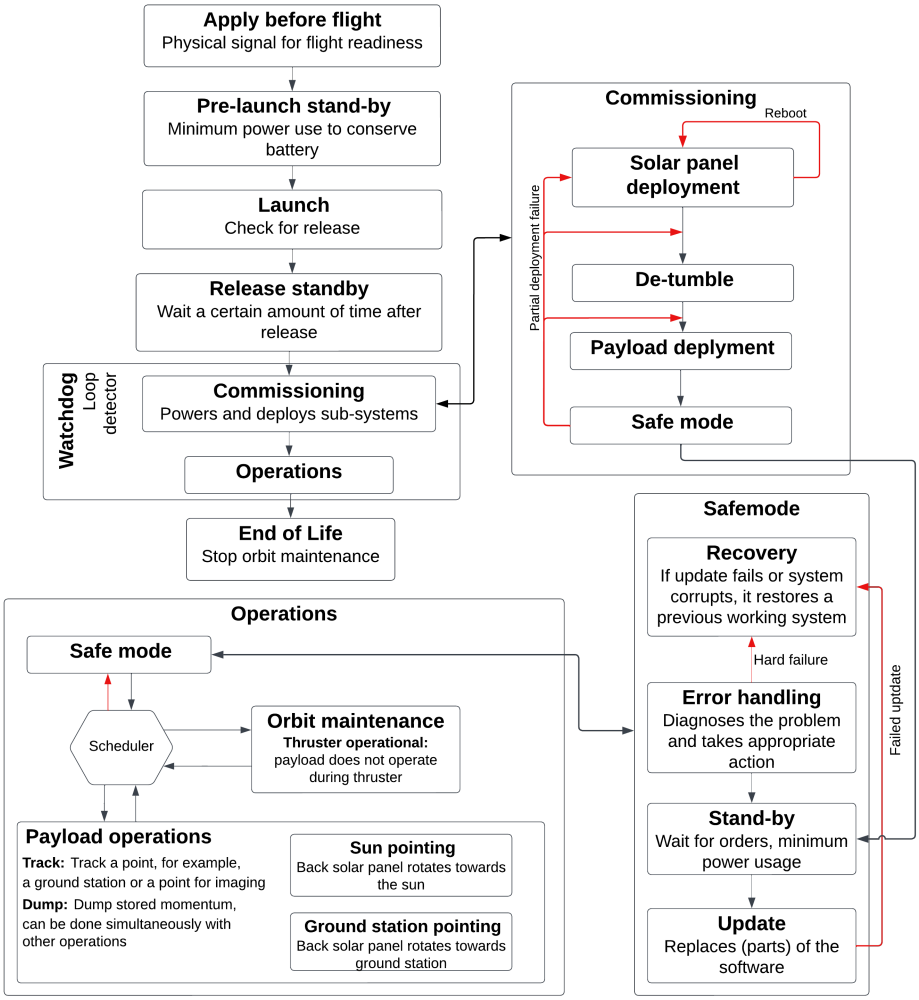

Figure 12.2: *Software block diagram*

12.4. SDH performance

The final design of the OBC will include the components and parameters shown in Table 12.4 below. These options are still open to be changed during further design stages but do give a clear overview of the performance and configuration of the OBC.

Table 12.4: *OBC overview*

OBC Parameters	
CPU 1	Similar to ARM Cortex-A9
CPU 2-4	Similar to ARM Cortex-A7
Storage	2TB SSD
Available interfaces	I2C, RS-232, RS-422, RS-485, RJ45 (Ethernet)
Volume	<0.25 [U]
Mass	<250 [g]
Normal operations Power	2 [W]
Peak Power	4 [W]

13 Structures

The structure is responsible for carrying external loads, like loads during launch and deployment, while maintaining structural integrity. Additionally, the structural subsystem provides mounting points for all subsystems. In this chapter, the structures are designed, first, the system requirements are presented in Section 13.1. Next, the choice of technology is discussed in Section 13.2, and the integration with a CubeSat deployer is discussed in Section 13.3 which provides the geometrical constraints required for the sizing as discussed in Section 13.4. With the outline of the structures sized, structural analysis is performed in Section 13.5 in order to determine the panel thickness and to select the most suitable alloy.

13.1. Structures requirements

The structural subsystem shall comply with the subsystem requirements as shown in Table 13.1, in addition to the user requirements.

Table 13.1: *Structures subsystem requirements.*

ID	Description	Rationale	Verif. M.	
Sys-Str-01	The structure shall provide the attachment points for all subsystems.	Functional requirement of the structures.	Demo	✓
Sys-Str-02	The structure shall not be compromised by radiation exposure in orbit during the lifetime of the satellite	In VLEO, high levels of ionizing radiation can be expected which have negative impact on structural integrity of materials.	Ana, Test	○
Sys-Str-03	The structure shall not be compromised by any impacts in orbit during the lifetime of the satellite.	In VLEO collision with debris is possible, the structures should ensure a safe life in the event of debris.	Ana	○
Sys-Str-04	The satellite shall be able to withstand the g loads during launch	Structural integrity needed for the satellite platform to survive launch	Ana	✓
Sys-Str-05	The eigenfrequency of the satellite shall be higher than 35 Hz	Safety constraints for the satellite platform to survive induced vibrations.	Ana	✓

13.2. Structures choice of technology

For the structures of LAMP, a monocoque concept was selected consisting of load-carrying side panels and stiffeners. During the mid-term phase, the monocoque was shown to be preferred over a structure consisting of beam elements, as the monocoque allows for a larger internal volume which

is advantageous for a modular platform. Next to that, the monocoque is an enclosed structure which is beneficial in terms of stiffness. The structure is made of hard anodised aluminium as prescribed by [72] to prevent cold welding with the deployer.

Magnesium is a suitable material as well as suggested by Slejko, Gregorio, and Lughi[73]. This is due to the fact that the material is suitable for 3D printing and since it has a lower melting temperature than aluminium alloys, it will demise faster during re-entry. However, the use of a material other than aluminium has to be communicated with and approved by the launch provider [72]. To avoid integration issues with the launch vehicle, aluminium is selected as the structural material.

13.3. Deployer integration

As indicated by *U-Str-02*, LAMP has to be deployed by commercially available deployers. Currently, the only deployer for a 27U CubeSat is hosted by the SLS Block-1B [3]. The document describes the maximum payload dimensions and the centre of mass range. A schematic layout of the deployer is shown in Figure 13.1a including the maximum body dimensions of the satellite in the deployer.

The satellite will interface with the deployer using two tabs along the sides of the bottom xy-face. In the configuration where the DST is mounted, the tabs will run along the upper sides of the bus of LAMP. As a result, the DST will point in the positive y-direction of the deployer when stowed inside as shown in Figure 13.1b where the black box indicates the payload envelope for the deployer with the DST in yellow and the bus in grey. The deployer will eject LAMP with the use of a spring and pusher plate system after opening the deployer door.

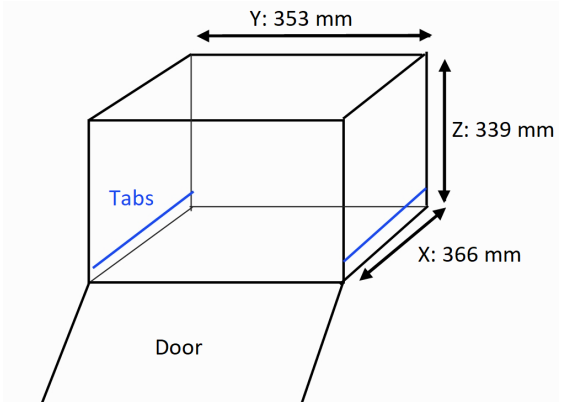

(a) *Deployer reference system with maximum body dimensions [3]*

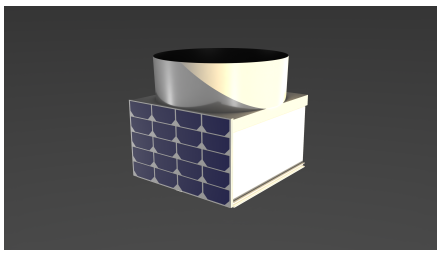

(b) *LAMP with the DST mounted in stowed configuration*

Figure 13.1: *Deployer details and structures integration*

When LAMP is stowed in the deployer, the solar panels and Earth shield are folded to the sides of the bus. The DST's baffle consists of three concentric cones which slide over each other when stowed. The DST includes its own deployment mechanism for the M2 mirror and baffle. The solar panels are deployed using torsion springs in the hinges. The deployment is activated after ejection from the deployer using wires and heat knives. Detailed design of these mechanisms is left for further research post-DSE.

The tabs are used to clamp the satellite in the deployer during launch and to guide the satellite when being deployed. The dimensions of these tabs are obtained from Planetary Science Corporation [74, 75] as they specify the dimensions of the tabs in detail and mention the production of a 27U CubeSat deployer.

The baffle and primary mirror structure of the DST have combined outer dimensions equal to $350 \times 360 \times 150$ mm [50]. These dimensions already reach the deployer envelope, as a result, the M1 mirror structure and baffle will be placed outside of the primary structure which has a maximum height of 189 mm. In the y-direction of the deployer, there is only 3 mm left in total for solar panel folds. As the

solar panels have a thickness between 1.6-2.5mm with two folds required on each side, the panels cannot be folded along the DST to prevent exceeding the payload envelope. Consequently, the width of the primary structure has to be smaller than the width of the M1 mirror structure. The external part of the DST and the geometry of the tabs constrain the area available for solar array folds on the sides to 366$\times$170mm as the tabs have a height of 15 mm with a 4 mm offset from the zenith face to comply with the tab dimensions and placement of the deployer [74].

13.4. Structures sizing

With the geometric constraints from the deployer known, the structures can be sized. The monocoque consists of five main panels, reinforced with stiffeners dividing the panel in 1U-shaped sections as shown in Table 13.2. The stiffeners are added to increase the buckling strength of the side panels and to provide additional mounting points for components. The height of the primary structure is equal to 189 mm as the DST occupies the remaining 150 mm when stowed. The dimensions of the zenith panel are limited to 329.6×360 mm due to the tabs running along the long sides. The cut-outs for the star trackers, antennas and thruster have been determined after making a CAD model.

Table 13.2: *Monocoque panels sizing*

Elements	**Amount**	**Dimension [**mm**]**	**Net area [**mm^2**]**
Nadir panel including cut-out for DST instrument box	1	326×360	108778
Zenith panel including cut-outs for antennas	1	329.6×360	118656
Side panel	2	173.5×360	62460
Back panel with cut-outs for thruster and star tracker	1	188.5×326	50536
Front panel no cut-out	1	188.5×326	62000
tabs	2	$360 \times 15 \times 14.5$	
x-Stiffeners	4	$360 \times 5 \times 5$	
y-Stiffeners	4	$350 \times 5 \times 5$	
z-Stiffeners	12	$189 \times 5 \times 5$	

The nadir panel contains a cut-out to accommodate the instrument box of the DST. The back panel contains a cut-out to accommodate the thruster. In case another payload than the DST is mounted, a dedicated payload structure can be mounted which has a similar design to the primary structure. The payload structure slides over the primary structure to allow for easy integration. The side panels of the payload structure can be modified to accommodate different sensors when required. The Nadir facing panel of the payload structure already contains a large rectangular cut-out of 310×320 mm. The sizing of the payload structure is presented in Table 13.3

Table 13.3: *Payload structure panel sizing*

Elements	**Amount**	**Dimension [**mm**]**	**Net area [**mm^2**]**
Side	2	150×355	54000
Side	2	150×331	52500
Nadir including rectangular cut-out for optical instruments	1	355×331	26800
x-Stiffeners	2	$360 \times 5 \times 5$	
y-Stiffeners	2	$350 \times 5 \times 5$	
z-Stiffeners	12	$150 \times 5 \times 5$	

Figure 13.2a shows the primary structure with the side, front and zenith panels hidden. Figure 13.2b shows the primary structure with side panels removed with the payload structure mounted.

(a) *Primary structure with stiffeners and tabs mounted*

(b) *Primary structure on top of the payload structure*

Figure 13.2: *Overview of the primary structure with and without the payload structure*

13.5. Structural analysis

The monocoque of the main satellite structure is sized for the accelerations and vibrations of the Falcon 9 [76], which is a common launch vehicle for ride-share missions. Additionally, Falcon 9 provides an extensive user guide specifying payload requirements. For this analysis, it is assumed that the deployer specified for the SLS-1B can be hosted by Falcon 9. An overview of the design loads is presented in Table 13.4.

Table 13.4: *Structural design loads*

Design load	Magnitude	Unit
Axial acceleration	8.5	g
Lateral acceleration	4	g
Safety factor	2	-
Min. axial natural frequency	35	Hz
Min. lateral natural frequency	35	Hz
Thermal range	50	K

Consequently, the thickness of the panels was sized based on the following analyses.

- Compression buckling
- Shear buckling
- Axial natural vibration
- Lateral natural vibration
- Thermal expansion

13.5.1. Free body diagram

For the analysis of lateral loads, the free body diagram is considered as shown in Figure 13.3a where the double thin line in Figure 13.3a indicates a hinged boundary condition. The dimensions in the figure are as follows: a =360 mm, b =326 mm and a =175 mm. For axial loads, the cross-section as shown in Figure 13.3b is used where the stiffeners are rectangular with a cross-section of 5×5 mm.

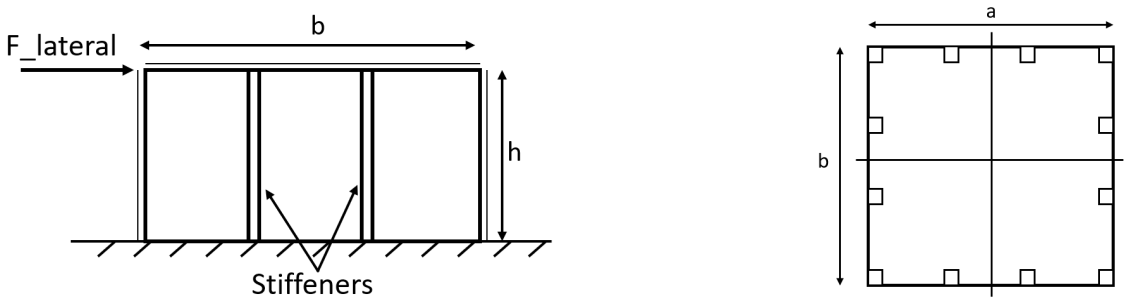

(a) *Free body diagram for lateral loads during launch* **(b)** *Cross section of the box structure*

Figure 13.3: *Free body diagram and simplified section view of the structure.*

13.5.2. Compression buckling

The critical buckling stress can then be calculated using Equation 13.1.

$$\sigma_{cr} = K_{box} \frac{\pi^2 E}{12(1-\nu^2)} \left(\frac{t}{b}\right)^2 \tag{13.1}$$

Where K_{box} is the buckling coefficient for a hollow box, E the Young's modulus of the material, ν the poisson's ratio of the material, t the panel thickness and b the length of the longest side of the box. K_{box} is calculated using Equation 13.2 as presented by Tohamy and Saddek[77].

$$K_{box} = \frac{(\phi^2+1)^2\eta + (\phi^2+\eta^2)^2}{\phi^2\eta(1+\eta^3)} \tag{13.2}$$

Where ϕ is equal to h/b and η is equal to a/b referring to Figure 13.3b
This analysis only takes the box shape into account for determining the critical buckling stress, the effect of the stiffeners is thereby ignored. The stiffeners will have a positive effect on the buckling stress of the structures, by ignoring these, the panels will be overdesigned which is acceptable considering the low-detail analysis performed. In short, ignoring the stiffeners imposes an additional safety factor. The required panel thickness to resist compression buckling was shown to be equal to 1.18 mm

13.5.3. Shear buckling

For the shear buckling analysis, the stiffeners can not be ignored as they divide the side panels into sections subjected to shear. The shear buckling coefficient was obtained from [78] by Abbott which presents the Equation 13.3 considering a panel which is hinged on all sides.

$$K_s = 5.34 + \frac{4}{\left(\frac{h}{d}\right)^2} \tag{13.3}$$

Where h is equal to the height of the panel and d is equal to the largest width of the panel between two stiffeners. The required panel thickness to resist shear buckling was shown to be equal to 0.89 mm which is less than the 1.18 mm for compression buckling. As a result, the panels with a thickness of 1.2 mm are used for further analysis as this is a more standard dimension for which plates can be bought.

13.5.4. Natural frequency

During launch, the payload is subject to random vibrations imposed by the launch vehicle. To prevent adverse effects due to vibration the natural frequency of the satellite has to be computed. For this, the structure is modelled as a massless beam with a lump mass at the end. As LAMP is mounted upside-down in the deployer, the lump mass has contributions in addition to the structure of both the payload, propulsion and ADCS as these are mounted to the bottom plate.

Axial natural frequency

The axial natural frequency is calculated using Equation 13.4 with a clamping factor of 0.160 as proposed by Larson, Wertz, et al. [65]. This clamping factor accounts for the clamping of the top of LAMP by the deployer tabs.

$$\omega_n = 0.160\sqrt{\frac{k_{axial}}{m_{load}}} \tag{13.4}$$

$$k_{axial} = \frac{AE}{L} \tag{13.5}$$

k_{axial} is depends on the cross-sectional area A, the Young's modulus of the material E and the free length L of the structure as mentioned in Equation 13.5. Using the panel thickness as calculated by the buckling requirements, an axial natural frequency of 108.4 Hz was calculated.

Lateral natural frequency

The lateral natural frequency is calculated using Equation 13.6 using a clamping factor of 0.276 [65].

$$\omega_n = 0.276\sqrt{\frac{(k_{shear}}{m_{load}}} \tag{13.6}$$

$$k_{shear} = \frac{A_{shear}G}{L} \tag{13.7}$$

For this, G is the shear modulus of the material and A_{shear} is the cross-sectional area of the side panels loaded in shear. The spring constant for lateral frequency has a contribution of both the side panels loaded in shear. The side panels are assumed to be shearing as the suspended length of the structure of 190 mm is nearly half of the shortest side of 350 mm. This in addition to the clamping by the tabs justifies the assumption that the lateral loads are mainly carried by the shear of the side panels. The impact of this assumption is further discussed in subsection 13.5.6. Next to that, the bending of the stiffeners and side panels perpendicular to the applied load is considered negligible compared to the shear stiffness. The analysis results in a lateral natural frequency equal to 72.3 Hz.

13.5.5. Thermal expansion

Over the lifetime of the satellite, the structure experience 30000 thermal loading cycles when going from sunlight to eclipse, as a result, the structures will be subjected to fatigue. As the structure is made from aluminium, the S,N-curve for zero-mean stress has to be observed. For this analysis, the mounting of a component to a stiffener is considered where the size of the component does not change with temperature while the stiffener does expand. The thermal stress can then be computed as follows, assuming only axial expansion.

$$\sigma_{thermal} = \Delta T \alpha E \tag{13.8}$$

where ΔT is the temperature difference, α the coefficient of thermal expansion of the material and E the Young's modulus. As LAMP is assembled at room temperature while it will operate at a mean temperature of 225 K as shown by the thermal analysis in Section 9.4, the structure will have a mean loading affecting the fatigue life. For 30000 cycles at zero-mean stress, the stress amplitude has to be below 96 MPa[1]. Using the Goodman's Rule [79], the equivalent zero mean stress amplitude for the structure can be calculated to be equal to 72.9 MPa which is less than the fatigue life limit, thereby, the structure complies with the design lifetime.

13.5.6. Verification and validation

The assumption of the side panels carrying all lateral loads in shear can be verified by computing the lateral natural frequency where the side panels are loaded in bending instead of pure shear. Performing the same analysis results in a lateral frequency of 78.8 Hz which is higher than the 72.3 Hz for the case where the side panels are loaded in shear. For launch vehicle integration, the lowest natural frequency is of main interest. Neglecting the effect of the stiffeners for lateral loads already underestimates the stiffness but it still complies with the requirements. Thereby, this analysis is sufficient to justify save launch vehicle integration.

[1] engineersedge.com, Last accessed 16/6/2023

13.5.7. Sensitivity analysis

To analyse the sensitivity of the structural analysis, the following parameters have been varied as shown in Table 13.5. These variables are material parameters which can vary per aluminium alloy, making them uncertain inputs for the analysis.

Table 13.5: *Sensitivity analysis of structures*

Variable	Range	Unit
E	69 - 72	GPa
G	24 - 27	GPa
ν	0.3 - 0.35	-

Performing the sensitivity analysis resulted in the following extremes as shown in Table 13.6

Table 13.6: *Extremes of structural characteristics*

input	**Sheet thickness required [**mm**]**	**Lateral natural frequency [**Hz**]**	**Axial natural frequency [**Hz**]**
E = 72 GPa, G = 24 GPa, ν = 0.35	1.17	70.5	109.5
E = 69 GPa, G = 27 GPa, ν = 0.35	1.21	75.76	108.4

It can be seen from Table 13.6 that the range of results is insignificant and that all requirements regarding structural performance are still complied with. As a result, the structural analysis does not show significant sensitivity towards the properties of different aluminium alloys.

13.5.8. Mechanical stress and material selection

The structure is subjected to a combination of stresses due to mechanical and thermal loading. The Von-Mises stress due to thermal expansion, axial loading and lateral loading is equal to 152 MPa. In combination with the TCS, aluminium 6061-T6 is selected of which the yield stress is equal to 240 MPa[80]. Stronger alloys like 7075 are unnecessary as a higher stiffness or yield strength is not required considering the sensitivity to different material parameters. Additionally, AL 6061-T6 it is a low-cost, widely available and machinable alloy which is beneficial for manufacturing.

14

Propulsion subsystem

This chapter discusses the chosen technology and selected components in detail. First, the subsystem's requirements are listen in Section 14.1. In Section 14.2, a trade-off is established for two of the chosen propulsion systems from the midterm report [12]. Following that, the selection and sizing of various components is discussed. Section 14.3 presents an overview of the designed system. The chapter is concluded with Section 14.4, which presents the main characteristics of the propulsion system designed.

14.1. Propulsion subsystem Requirements

The generated system requirements, in addition to the user requirements in Chapter 3, are tabulated in Table 14.1.

Table 14.1: *Propulsion subsystem requirements*

ID	Description	Rationale	Verif.	M
Sys-Prop-01	The propulsion system shall enable orbit control of the satellite.	The orbit has to be controllable throughout the mission lifetime.	Test	✓
Sys-Prop-01-I	The propulsion subsystem shall enable orbit maintenance.	Propulsion subsystem needs to maintain the platform in orbit throughout the satellite's life time as stated by *U-Ops-01*. Because of the VLEO, the platform without orbit maintenance will decay in the order of months.	Ana	✓
Sys-Prop-01-I-a	Propulsion shall deliver a minimum of 1102.7 m/s delta-V for drag compensation	This stems from the VLEO which implies significant drag.	Ana	✓
Sys-Prop-01-I-b	Propulsion shall deliver 0.4 mN thrust for drag compensation	This stems from the VLEO which causes drag, and thus 0.4 mN is needed for orbit maintenance.	Test	✓
Sys-Prop-01-II	The propulsion system shall enable to change the Δ V of $0.1\,\mathrm{m\,s^{-1}}$ in 5423 s.	Required for collision avoidance.	Ana	✓
Sys-Prop-02	The propulsion unit shall have an arm with the center of mass of no more than 4 cm.	Constraints the disturbance torque using the propulsion system. This is required to prevent stressing the ADCS.	Test	✓
CON-Sus-02	The spacecraft shall use non-toxic methods of propulsion	Ecological considerations	Demo	✓

Sys-Gen-01	All the subsystems shall comply with the mass budget.	Constraint the individual mass of subsystems.	Test	✓
Sys-Gen-02	All the subsystems shall comply with the power budget.	Constraints the individual power requirements of subsystems.	Test	✓
Sys-Gen-03	All the subsystems shall comply with the volume budget.	Constraints the individual volume of subsystems.	Test	✓

14.2. Propulsion subsystem design

The propulsion subsystem design section describes the trade-off used to choose between two propulsion technologies, as well as the sizing of different components involved with the chosen technology.

14.2.1. Propulsion subsystem choice of technology

Various types of electrostatic hall-effect thrusters, electromagnetic radio frequency thrusters, and an electrospray propulsion system were examined in the midterm report [12]. From the trade-off, two hall effect thrusters —the PSAC/SPCS and BHT-100 hall-effect thrusters were selected. The PSAC/SPCS thruster scored nominally for mass and volume criteria as well as for thrust/power efficiency and energy consumption. The BHT-100, on the other hand, is heavier than PSAC/SPCS but has a higher thrust/power efficiency and lower energy consumption. To choose the most effective system for LAMP, further analysis of these two engines is necessary.

A low-power hall thruster electric propulsion system was designed and operated at the Plasma Sources and Applications Centre/Space Propulsion Centre (PSAC/SPC) in the 50 W to 200 W range. The thrust produced by the thrusters is between 2 mN to 5 mN. The most efficient thrust/power ratio was obtained with a thrust of 3.18 mN at 56 W and an ISP of 843 s [81]. It becomes evident that the particular impulse rapidly degrades at low power levels. As a result, another thrust measurement of 5.08 mN was made with a particular impulse of 1106 s seconds at a higher operational power of 120 W [81]. This makes it possible to compare the results more effectively with the BHT-100 hall effect thruster, which operates at a power greater than 100 W.

The BHT-100 was developed at BUSEK Space Propulsion and Systems. It is predicted to have a lifetime of $10\,000$ h, owing to the state-of-the-art magnetic shielding that focuses ions away from the channel walls. It has an efficient operating range of 75 W to 125 W [82]. The BHT-100 is compatible with both xenon and iodine propellants. In the case the engine was to use iodine, it would result in lower tank mass since solid iodine can be stored without the need for large, pressurised tanks. Next to that, the required tank volume is lower because iodine has a storage density of $4.9\,\mathrm{g\,cm^{-1}}$ compared to xenon with a storage density of $1.66\,\mathrm{g\,cm^{-1}}$ at a pressure of 14 MPa [83]. For this, a choice must be made between employing xenon or a (novel) solid iodine as a propellant. To compare the performance between the propellants, the thruster configuration with a thicker outer and central magnetic core that is compatible with iodine was chosen. According to measurement data for the iodine configuration, a force of 8 mN and a specific impulse of 1182 s at a total power of 121 W [82] produced the maximum thruster efficiency.

The criteria used to compare the systems, along with how they are calculated and how much weight each one is given, are listed below.

- **Wet Mass (20%):** The summation of the thruster mass with cathode, propellant mass, and tank mass is taken as the wet mass. The rocket equation from the dry mass estimate, $\Delta V = 1103$ and the specific impulse performance demonstrated by the system are used to estimate the propellant mass. A reference value of 10% of the total CubeSat mass is taken for the propulsion subsystem mass [84] with a 2.5% tolerance margin resulting in a range of 4 kg to 6.75 kg based on the initial mass budgets from the baseline report. For the two different propellants, the methods for sizing the tank are listed:

  - Xenon: The tank is cylindrical with hemispherical caps and needs to be pressurised. A minimum thickness of 1 mm is used. For three different materials (aluminium, titanium and vacuum steel), the tanks are iterated through a list of pressures and densities of Xenon, in which the lightest tank of all combinations is chosen.
  - Iodine: Since it is not pressurised, the sizing is a matter of choosing a shape that holds the volume, a minimum thickness of 1 mm and an appropriate material.

- **Wet Volume (20%):** The summation of the thruster volume with cathode, propellant volume and volume occupied by tank is taken as the wet volume. The propellant volume is calculated by dividing the mass of the propellant by its corresponding density. A reference value of 10% of the total CubeSat volume is taken, similar to the mass estimate for the propulsion system along with a 2.5% tolerance margin resulting in a range of 2 U to 3.4 U.
- **Thrust/Power ratio (45%):** This ratio demonstrates how efficient it is at creating thrust per watt of power. A reference value of 0.05 mN W^{-1} is used based on a reference value of 1 mN for every 20 W for electric propulsion systems [85].
- **Complexity (15%):** Evaluating risk helps ensure mission safety, success, and cost-effectiveness by identifying potential hazards. Risk assessment also addresses system complexity and reliability. Since risk can be managed through various mitigation strategies, thorough testing and redundancy measures, it has the lowest weight compared to other criteria.

The trade-off table is presented in Table 14.2. Each configuration is given a score based on the provided criteria, and colour coded in accordance with the legend as presented in Table 7.5.

Table 14.2: *Trade-off table*

Criteria / Options	**Wet Mass [g] (20%)**	**Wet Volume [U] (20%)**	**Thrust/Power [mN W^{-1}] (45%)**	**Risk (15%)**
PSAC/SPCS - Xe (56 W) [81]	8487 Orange	4.42 Orange	0.057 Yellow	low risk mature system Green
PSAC/SPCS - Xe (120 W) [81]	5456 Yellow	3.39 Yellow	0.043 Orange	low risk mature system Green
BHT-100 - Xe [82]	7034 Yellow	3.23 Yellow	0.067 Green	low risk mature system Green
BHT-100 - I_2 [82]	6675 Yellow	1.28 Green	0.067 Green	corrosive and deposition on structure Yellow

It can be seen that the BHT-100 hall effect thruster configuration using iodine is the best option. Although both Iodine and Xenon show similar performance, the wet mass is lower because the tanks to store solid iodine do not need to be pressurised. Also due to its high storage density, it has the lowest wet volume of all the systems considered. Even though the xenon propellant system is quite mature and has low risk with the only risk being that the tank must be pressurised and there are leakage

possible, the risk of switching to iodine is acceptable because the only risk is that it is corrosive in nature and solid iodine could deposit on the system; therefore, proper precautions must be taken to avoid it, which will be explained in the following sections.

Sensitivity analysis

Power, thrust, and specific impulse measurements are estimated to have an inaccuracy of 2% or less. The trade-off remains unchanged when the best and worst cases in the range are taken into account, proving that it is not sensitive to measurement uncertainty. Changing the weights of the criteria will also have no influence on the final choice because iodine has proven to be effective under all criteria while being an inexpensive propellant. The selection could switch from iodine to xenon propellant if mission reliability becomes most important criteria, as xenon is a well-established and extensively tested propellant for Hall effect thrusters. In contrast to xenon, solid iodine propellant has limited availability, less mature production processes, potentially higher costs, and safety concerns due to its chemical nature, requiring proper safety measures for handling and storage.

14.2.2. Propulsion subsystem sizing

Table 14.3 lists a few of the thruster's physical characteristics. To prevent channel erosion, the thruster is designed to be magnetically insulated by a magnetic shunt across the upstream portion of the discharge channel that focuses ions away from the channel walls [82].

Table 14.3: *BHT-100 Physical Specifications [82]*

Thruster	BHT-100
Diameter	8 cm
Length	5.5 cm
Mass (with Cathode)	1.16 kg
TRL	5
Throughput	15 kg

Tank sizing

For 4.89 kg of iodine propellant at $4.9\,\mathrm{g\,cm^{-3}}$, this would equal 1U of propellant. The tank shape shall be a cylinder, as iodine needs to be heated and wrapping a heating pad around a cylinder distributes the heating evenly. Unlike xenon, the tanks do not need to withstand high pressures, so there is no need for hemispherical ends. A 1 mm wall of Hastelloy C-276 will be used. The thickness could decrease, but 1mm has been chosen for easier manufacturability.

With a fixed radius of 4.5 cm, the length needed to fill one unit of volume is 15.72 cm. LAMP will need two tanks as explained in Section 14.3, which means there are two tanks with the same radius but 7.86 cm length. With a wall of 1 mm and a density of Hastelloy 8.81 grams per centimeter square[1], the tank mass equals 0.31 kg each.

Cathode

The BHT-100 propulsion system incorporates a hollow cathode for neutralisation, and the specific design utilises a 12CaO-$7Al_2O_3$ electride emitter. The advantage of this emitter is that the cathode discharge can be initiated without significant heating, resulting in power savings compared to more conventional cathodes that use BaO-W or LaB_6 emitter materials. While LaB_6 is also compatible with iodine vapor and could be used as a cathode in future iodine-fed missions, it would require more power to initiate a discharge. Therefore, the chosen electride emitter provides a systems-level advantage by reducing power requirements for the cathode discharge initiation in the BHT-100 propulsion system [86].

[1] msestudent.com, last accessed on 13/06/2023

Piping, valves and filter sizing

The piping is designed to use Hastelloy C-276, with and outer radius of 0.635 mm and an inner radius of 0.475 mm and a length of 40 cm. The total weight is 198 g. The length of the tubing can be changed accordingly as the design matures.

The Swagelok model HC-4F2-40 filter, which filters particulates above 40 microns is used to prevent the flow of non-vaporised solid iodine [82]. The filter Swagelok model HC-4F2-40 filter is an adapted Swagelok SS-4F2-40[2] designed for the Iodine Satellite [87]. The Hastelloy version is not listed, but using the same dimensions as the Stainless Steel, the Hastelloy version should weigh 172 g.

The flow in each branch is regulated by a proportional flow control valve (PFCV) as the propellant travels through to the cathode and anode. The PFCVs swiftly alter the flow rate, allowing for dynamic management of the propellant flow rate, which should be kept at 0.689 mg s^{-1} for optimal performance [82]. The PFCVs are also internally heated to keep the wetted surfaces above the gas deposition temperature. The valves have been sized to be similar to the iSat mission [87], which use (non publicly available) Vacco valves with a mass of 100 g and a volume of 250 cm^2.

An auxiliary Power Processing Unit (PPU) is required to supply the energy needed to run the thruster and cathode, and to control the feed system [87]. The PPU must be able to provide power for the main discharge, the magnet circuit, and cathode operation. The PPU for the iSat mission takes input power at a voltage of 28 (+6/ -4) VDC, and has a peak overall efficiency of at least 90% for thruster operation. The EPS system's PCDU chosen in Chapter 10 meets all of these criteria because it contains all of the voltage inputs and outputs, meaning no auxiliary PPU is needed, leaving only an additional valve control board to be added.

14.2.3. Verification and validation

Following the creation of a simple excel model for calculations of wet mass and volume, thrust/power efficiency, and energy, conditional colour scale formatting with three colour scale was used to evaluate the best configuration in terms of thrust, power, and delta V. The values of delta V and drag estimation are obtained from Section 6.2 which have been verified and validated as mentioned in the section. In order to confirm that all of the input values, including thrust, power, and specific impulse, as well as calculations for propellant mass and thrusting time and safety factors for solar maxima, side winds, and conflict resolution, were correct and that the results were what was expected, a visual inspection and hand calculations were carried out.

14.3. Propulsion subsystem architecture

Figure 14.2 depicts the overall architecture of the propulsion subsystem. Several considerations have been taken into account for the system architecture. To start off, the use of two tanks was selected for balance and integration within the internal volume. A single tank symmetric across the centre of gravity is not possible. By having the tanks separate and symmetrical, the centre of gravity will not shift laterally.

Iodine is corrosive to metals. Aluminium in particular is affected by iodine vapour at any temperature. For that reason, both the iodine pipes and the iodine tank is made out of Hastelloy C-276, a Nickel-Chromium-Molybdenum alloy that has good corrosion resistance [87]. Titanium alloys, like nitinol, have generally good corrosion resistance[3], however no literature was found for its corrosive properties on space applications and specifically iodine corrosion, and should be tested in lab for its viability. Polymers are immune to corrosion, however, the thermal conductivity is too low for propellant heating[4].

[2] swagelok.com, last accessed on 13/06/2023
[3] matthey.com, last accessed on 19/06/2023
[4] professionalplastics.com, last accessed on 19/06/2023

Regarding the flow of iodine, a diagram can be observed in Figure 14.1. To start the firing process, the propellant tanks need to be above 90°C, which means patch heaters will be used around the cylindrical tanks. After the iodine has sublimated, it pressurises itself at around 0.067 bar[86] and flows through the fuel pipes. It then encounters the particulate filter after which it divides into two pipes, with 2 proportional flow control valves (PFCV) which regulate the flow to both the cathode and anode. In order to prevent iodine vapour from depositing, blocking the propellant lines, the entire feed system must be kept at a high temperature. Hence, all the pipes from the tanks to the thruster must be heated to 120°C constantly [46]. If iodine builds up on the pipes or valves, it might make the valves malfunction, and thus it is of utmost importance to keep the pipes heated constantly.

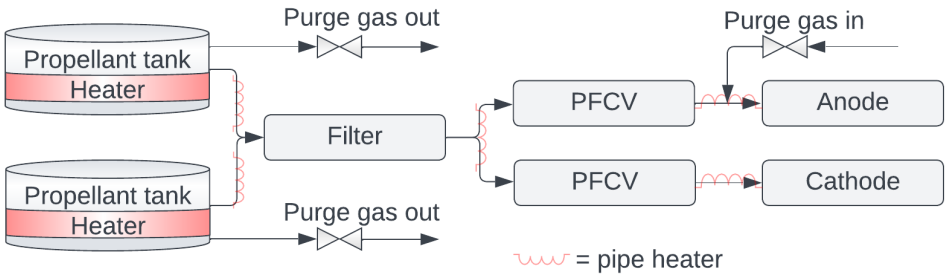

Figure 14.1: *Block diagram of fuel pipes*

Thruster angling

A need to angle the thruster was found during the design of LAMP. This is due to two effects, the torque generated by the offset of the thrust vector and the c.g. and a need to compensate for the average effect of the wind acting on LAMP.

To compensate for the torque due to operating the thruster, the thruster will be angled in the plane consisting of the nadir-pointing axis and the flight-path axis. The thrust vector will be angled with $10.6°$ relative to the flight-path axis such that there is a component of thrust pointing nadir. More explanation of how this angle was determined can be found in Section 15.2. At beginning and end of life, thruster operation will cause a torque of $0.006\,18$ mN m with the direction depending on the propellant level in the tanks.

When the thruster is angled, the effective thrust relative to the flight path axis decreases from 8 mN to 7.85 mN. However, this change is minor and only affects the thrusting time since the thruster will need to operate for a longer period of time, which increases from 853.5 s to 869.4 s, which is not a significant increase. To compensate for any perturbance that might push the platform sideways, such as side-winds, 1% of Fuel was added.

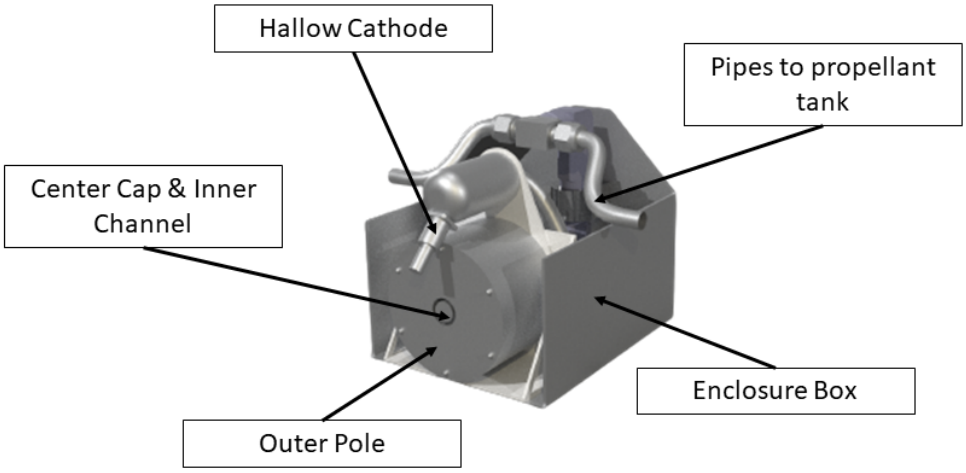

Figure 14.2: *Configuration of BHT-100*

14.4. Propulsion subsystem performance

To summarise, Table 14.4 lists the key performance characteristics of the propulsion subsystem of LAMP.

Table 14.4: *BHT-100 Performance [82]*

Performance Characteristic	Value
Total flow rate	$0.689\,\mathrm{mg\,s^{-1}}$
Total Power	$121\,\mathrm{W}$
Measured Thrust	$8.00\,\mathrm{mN}$
Specific impulse	$1182\,\mathrm{s}$
Thrust/Power ratio	$0.0661\,\mathrm{mN\,W^{-1}}$
Total thruster efficiency	38.3 %
Propellant Mass	$4894\,\mathrm{g}$
Total Mass	$6054\,\mathrm{g}$
Total Volume	$1.28\,\mathrm{U}$
Energy Consumption	$29.3\,\mathrm{W\,h}$

15

System Design

15.1. Hardware block diagram

The hardware block diagram can be found in Figure 15.1.

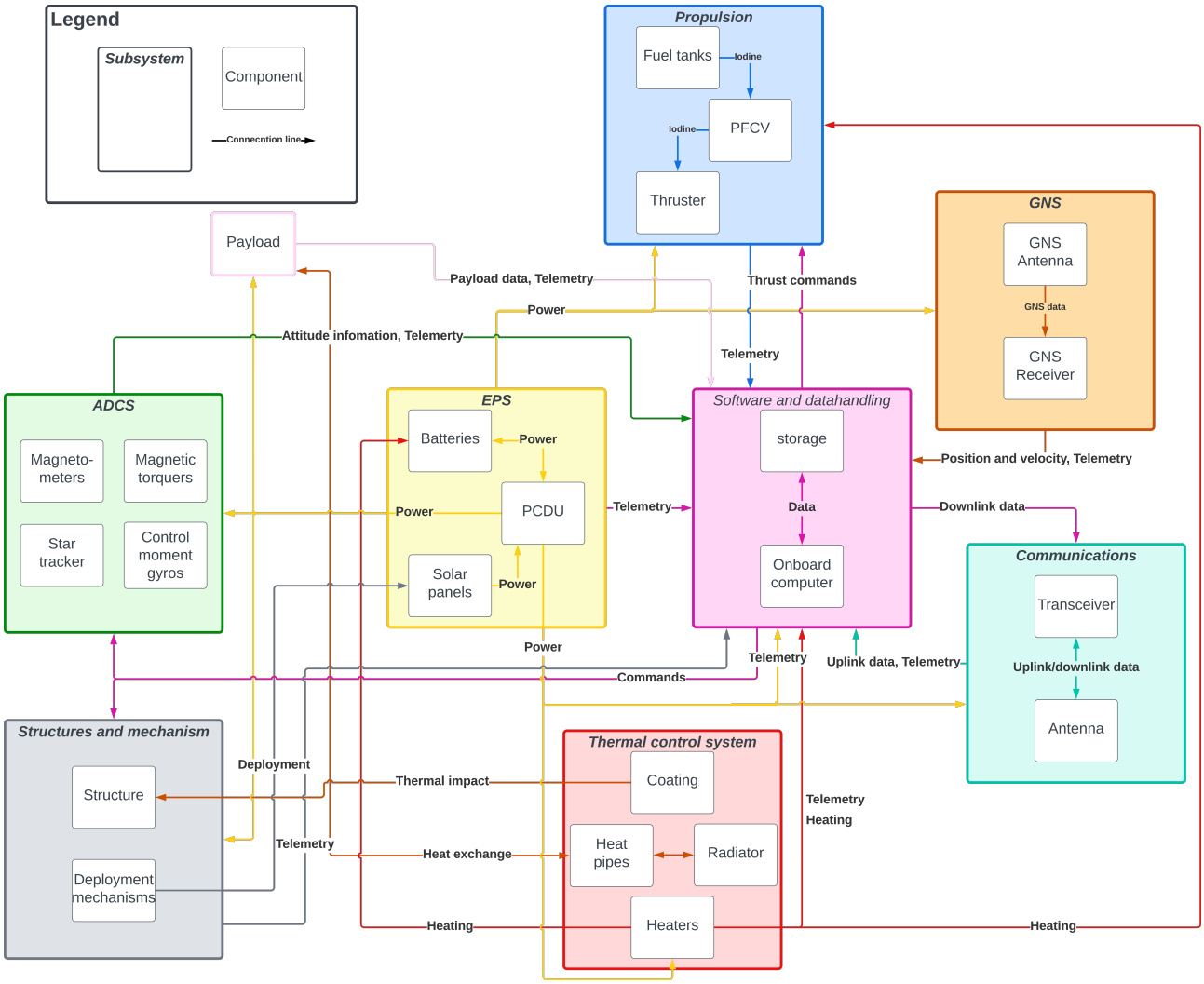

Figure 15.1: *Hardware block diagram of LAMP platform including generic payload*

The hardware block diagram (Figure 15.1 summarises the components of the LAMP platform and how they interact with each other. As becomes evident from the diagram, both the EPS and SDH subsystem have the most interfaces with other subsystems. EPS because every other subsystem

needs power at some point and SDH because it mainly monitors all other subsystems as well as handling the internal data and flow between subsystems.

15.2. Configuration determination

With all the required hardware known, a CAD model can be created to determine the internal configuration of all elements. Additionally, the CAD model was used for validation of the volume budget. The internal configuration is shown in Figure 15.2.

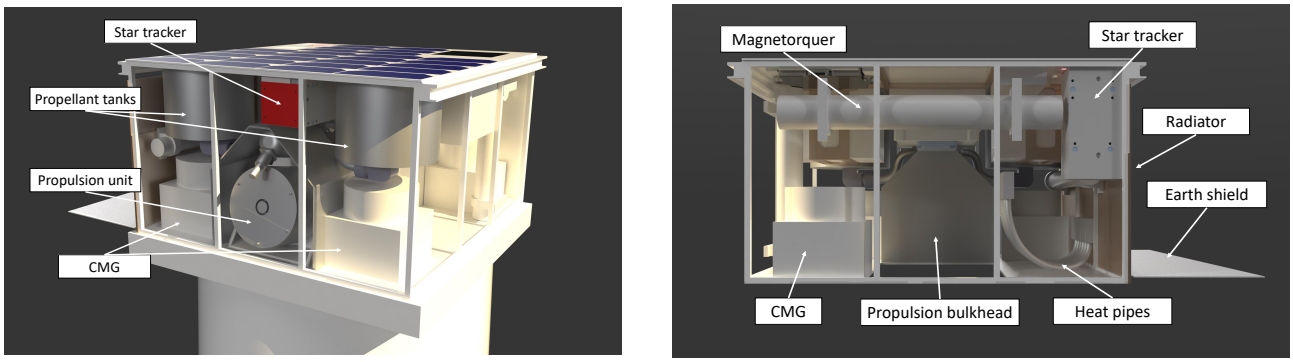

(a) *Internal view of LAMP from thruster side (back)*

(b) *Front view of LAMP's internals*

Figure 15.2: *Internal views of LAMP*

The structural subsystem consists of three sub-assemblies, the zenith panel assembly, the side panel assembly and the bottom plate assembly. In case another payload than the DST is hosted, the modular payload structure can be mounted which is a sub-assembly by itself. Making use of sub-assemblies allows for assembly in parallel which saves overall production time.

As the DST makes up about 56% of the total mass and deploys outside of the CubeSat envelope, it has a large effect on the z-position of the centre of gravity. Therefore, most heavy components such as the propellant tanks and batteries are part of the zenith panel sub-assembly to compensate for this. Additionally, the electronics stack, antennas for GNS and Comms, and the magnetometers are part of the zenith-panel sub-assembly as well. The zenith panel sub-assembly is shown in Figure 15.3.

The side panel assembly consists of the stiffener skeleton, tabs, star tracker, magnetorquers, radiator, Earth shield, and solar panel deployment mechanisms. The bottom panel assembly consists of the Propulsion unit and CMGs.

The propellant tanks are mounted as close to the thruster as possible to limit the length of heated tubing required. The propulsion system is fitted in an enclosed container to limit internal radiation towards other components and to protect LAMP's internals from corrosive Iodine deposition.

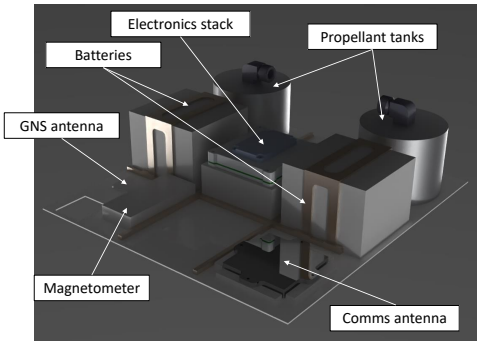

Figure 15.3: *The zenith panel sub-assembly*

The CMGs are placed in an enclosure in a rooftop orientation as discussed in Section 8.2. As the rotating wheels experience some friction, the CMG will produce heat when active. As the Instrument box of the DST has to be kept cool, the CMGs, batteries, and propulsion system are placed as far from the instrument box as possible to limit conduction and radiation effects.

15.2.1. Centre of gravity determination

To estimate the centre of gravity (c.g.), a parts management sheet has been created which specifies the mass and location of each component. The c.g. for the deployed configuration with the DST for beginning and end of life (BOL and EOL) is shown in Table 15.3.

Table 15.1: *LAMP c.g. range in deployed configuration*

mass	x c.g. [mm]	y c.g. [mm]	z c.g. [mm]
BOL: 52.91 kg	4.4	-0.9	169.7
EOL: 48.02 kg	16.5	-0.5	182.6

It can be seen in Table 15.3 that the c.g. especially varies in the x- and z-direction. To limit the torque variation due to the thrust throughout the satellite's lifetime, the thruster is angled as explained in Figure 14.3. The angle is determined based on the c.g. range in the x- and z-direction as shown in Figure 15.4. Where the c.g. at BOL and EOL are highlighted with red dots. The location and direction of action of the thruster is highlighted in blue. Considering the location of the thruster and the c.g. range, an angle of $10.6°$ was calculated at which the thruster has been placed with respect to the x-axis.

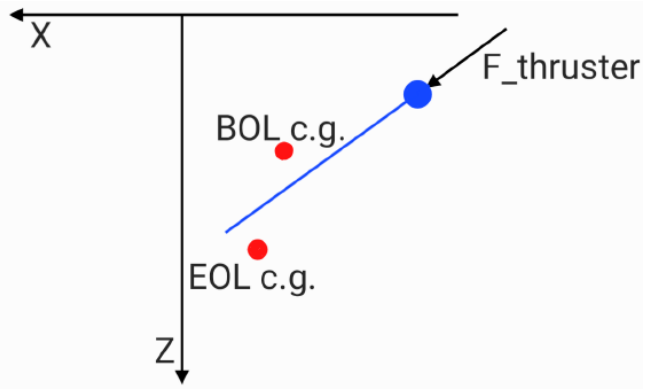

Figure 15.4: *C.G. range between BOL and EOL on the x,z-plane*

When LAMP is stowed in the deployer, the location of the c.g. is constrained to limit the effect on launch vehicle dynamics. The constraints imposed by the deployer [3] and c.g. for the stowed configuration is shown in Table 15.2.

Table 15.2: *C.G. range of satellite when stowed in the deployer*

	x-range [mm]	y-range [mm]	z-range [mm]
Max	53	60	180
Min	-47	-60	100
LAMP	-4.48	-2.54	154

It can be concluded that the c.g. of LAMP in the stowed configuration meets the requirements of the deployer hence LAMP is save to be launched and deployed.

15.2.2. Moment of inertia

The moment of inertia was calculated using the same parts management sheet as used for the c.g. estimation. The basis of the moment of inertia estimation was the parallel axis theorem with the use of point masses of several systems complemented with the moment of inertia of the solar panels, batteries, thruster and DST. These values were of primary importance for the ADCS design.

Table 15.3: *LAMP moment of inertia*

mass	I_{xx} [kg m^2]	I_{yy} [kg m^2]	I_{zz} [kg m^2]
BOL: 52.91 kg	0.776	0.754	1.537
EOL: 48.02 kg	0.732	0.698	1.441

The fact that point masses were used however underestimates the theoretical total moment of inertia.

However, including the individual contribution of all elements would only cause an increase of around 10% as especially heavy components, placed far away from the centre of gravity are most significant for the moment of inertia. Each filled propellant tank, for example, has a total mass of 2.76 kg, a diameter of 48.5 mm, with a length of 78.6 mm resulting in a moment of inertia of I_{xx}, I_{yy} = 2952 kg mm^2, and I_{xx} = 3247 kg mm^2. The parallel axis contribution with respect to the centre of gravity, considering the internal placement of the tanks, equals to I_{xx} = $41\,811$ kg mm^2, I_{yy} = $51\,396$ kg mm^2, and I_{zz} = $36\,015$ kg mm^2. As a result, the shape contribution with respect to the parallel axis contribution is equal to 7 %, 5.7 %, and 9 % respectively. Neglecting this contribution thereby introduces an error of up to 9%. The consequence of this can be found in Equation 8.2.2.

16

Technical Risk Analysis

To adhere to the reliability requirement of 95%, stated in requirements (*U-ReS-01*), a risk analysis is performed to identify potential threats. By identifying, assessing and mitigating technical risks, the design can be made more reliable.

16.1. Risk identification and mitigation

In Table 16.2, LH is the likelihood and S is the severity, both on a scale from 1 to 5. In Table 16.1 the scale definition can be found. The total risk, T, is calculated as the product of likelihood and severity. The accompanying matrix for this table can be found in Figure 16.1.

Table 16.1: *Risk scale definition*

Likelihood		Severity	
1	Extremely unlikely (<0.5%)	1	No impact
2	Very unlikely (0.5-2%)	2	Small impact / Manageable
3	Unlikely (2-5%)	3	Reduced performance
4	Likely (5-30%)	4	Partial mission failure
5	Very likely (>30%)	5	Complete mission failure

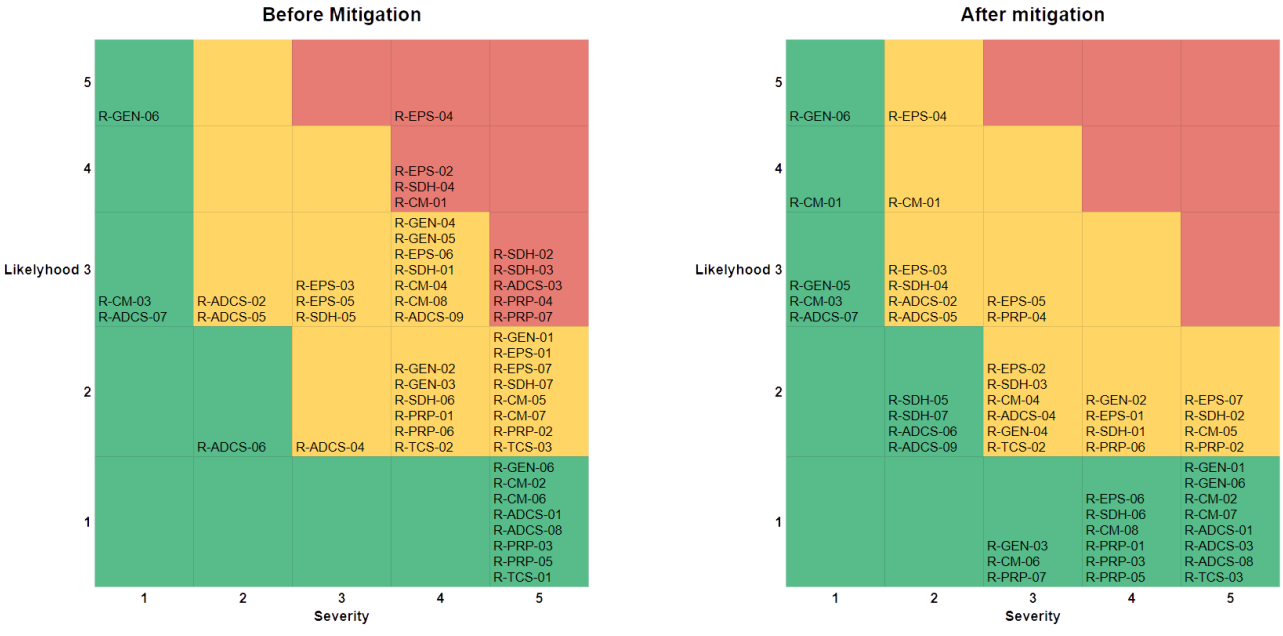

Figure 16.1: *Risk matrix for before and after mitigation*

Table 16.2: *Risk Identification & Mitigation*

Risk ID	Risk	LH	S	T	Likelyhood Mitigation	Impact Mitigation	Mitiagtion Strategy	NL	NS	NT
General										
R-GEN-01	Launch failure	2	5	10	Use a reliable launch vehicle		Reduce	1	5	5
R-GEN-02	Solar storm	2	4	8			Accept	2	4	8
R-GEN-03	Micro meteorites or debris	2	4	8	Active debris avoidance	Double walls to protect important components	Reduce	1	3	3
R-GEN-04	Damage from radiation	3	4	12	Radiation protection	Software backups if possible	Reduce	2	3	6
R-GEN-05	Production failure	3	4	12		Outsourcing V&V	Transfer	3	1	3
R-GEN-06	Physical Attack	1	5	5			Accept	1	5	5
Electrical										
R-EPS-01	Battery Failure	2	5	10		Split the battery into 2 seperate batteries	Reduce	2	4	8
R-EPS-02	Depletion of battery life	4	4	16	Reducing DoD or increased capacity	Adjusting the power budget by software update	Reduce	2	3	6
R-EPS-03	Incorrect power budget	3	3	9		Software updating capability	Reduce	3	2	6
R-EPS-04	Sensor failure	5	4	20		Sensor redundancy	Reduce	5	2	10
R-EPS-05	Single solar panel failure	3	3	9			Accept	3	3	9
R-EPS-06	Solar panel deployment failure	3	4	12	Use of multiple/redundant springs		Reduce	2	4	8
R-EPS-07	PCDU failure	2	5	10			Accept	2	5	10
SDH										
R-SDH-01	Going into hibernation	3	4	12	Outsourcing V&V		Transfer	2	4	8
R-SDH-02	Commissioning failure	3	5	15	Outsourcing V&V		Transfer	2	5	10
R-SDH-03	OBC flight loop error	3	5	15	Outsourcing V&V	Watchdog in combination with a boot counter	Transfer + Reduce	2	3	6

R-SDH-04	Software has faults	4	4	16	Outsourcing V&V	Software updating capability with multiple boot slots	Transfer + Reduce	3	2	6
R-SDH-05	Storage failure	3	3	9	Radiation hardened storage	Multiple seperate storage units	Reduce	2	2	4
R-SDH-06	Watchdog failure	2	4	8	Outsourcing V&V		Transfer	1	4	4
R-SDH-07	CPU failure	2	5	10		Transfer operation tasks to backup CPU	Reduce	2	2	4
Comms										
R-CM-01	Upload failure	4	4	16		Start and finished code to each upload	Reduce	4	1	4
R-CM-02	Patch antenna failure	1	5	5			Accept	1	5	5
R-CM-03	Starlink satellite failure	3	1	3			Accept	3	1	3
R-CM-04	Download failure	3	4	12	Having a high signal to noise ratio	Keeping data stored in case of download failure	Reduce	2	3	6
R-CM-05	Transciever failure	2	5	10			Accept	2	2	4
R-CM-06	Starlink ceases operations	1	5	5		Switch to another relay system, such as OneWeb	Reduce	1	3	3
R-CM-07	Hostile sakeover	2	5	10	Checking recieved data for malware		Reduce	1	5	5
R-CM-08	Interception of communication	3	4	12	Encription of the downlink		Reduce	1	4	4
ADCS										
R-ADCS-01	Magnetorquer failure	1	5	5			Accept	1	5	5
R-ADCS-02	CMG failure	3	2	6			Accept	3	2	6
R-ADCS-03	CMG instabillity	3	5	15	Oursource V&V		Transfer	1	5	5
R-ADCS-04	Star tracker failure	2	3	6			Accept	2	3	6
R-ADCS-05	Star tracker blinded	3	2	6			Accept	3	2	6
R-ADCS-06	Magnetometer failure	2	2	4			Accept	2	2	4
R-ADCS-07	Attitude information loss	3	1	3			Accept	3	1	3
R-ADCS-08	Excessive tumbling	1	5	5			Accept	1	5	5

R-ADCS-08	CMG Singularity point	4	3	12	Use software with singularity avoidance	Use magnetorquers to get out of the singularity point	Reduce	2	2	4
Propulsion											
R-PRP-01	Orbit determination failure	2	4	8	Multiple orbit determination methods		Reduce	1	4	4
R-PRP-02	Thruster failure	2	5	10			Accept	2	5	10
R-PRP-03	Propellant tank failure	1	5	5		Seperate feed system for each tank	Reduce	1	4	4
R-PRP-04	Feed system valve failure	3	5	15		Parallel valves for redundancy	Reduce	3	3	9
R-PRP-05	Propellant tube leak	1	5	5		Seperate feed system for each tank, valves to isolate	Reduce	1	4	4
R-PRP-06	Neutralizer failure	2	4	8			Accept	2	4	8
R-PRP-07	Propellant feed clogged	3	5	25	Constantly heat up propellant pipes	Try to unclog by heating the pipes up even more	Reduce	1	3	3
Thermal											
R-TCS-01	Radiator failure	1	5	5			Accept	1	5	5
R-TCS-02	Electric heater failure	2	4	8		2 seperate battery packs with their own heater	Reduce	2	4	8
R-TCS-03	Earth-shield deployment failure	2	5	10	Use of multiple/redundant springs		Reduce	1	5	5
GNS											
R-GNS-01	GNS Antenna failure	1	4	4			Accept	1	4	4
R-GNS-02	GNS Receiver failure	1	4	4			Accept	1	4	4

16.2. Critical Risks

In this section, recommendations for the most critical risks present after mitigation will be listed. It should be noted that these mitigations are not included in the previous section due to their small impact on likelihood or severity, their impact on the design or because they are deemed unnecessary for now.

- R-EPS-04: Due to the high likelihood of sensor failure, this risk is still high. If deemed needed, more redundant sensors could be added to reduce impact even further.
- R-EPS-05: Due to the high importance of solar panels, high reliability is required and must be analysed and tested extensively.
- R-EPS-07: Mission failures due to PCDU failures are relatively common, and the PCDU should therefore be reliable and extensively tested.
- R-SDH-02: The risk for commissioning failure is hard to estimate in this phase, however, to reduce this risk, more testing can be performed.
- R-CM-05: Just like the PCDU, the transceiver is a critical component that is also a single point of failure. An analysis of the reliability of the component and testing must be performed in later stages
- R-PRP-02: Just like with other single points of failures, a reliability analysis and extensive testing should be performed in a later stage.
- R-PRP-04: If deemed necessary after a reliability analysis and testing, multiple (redundant) feed lines could be used to reduce the impact of valve failure.

16.3. Risk influence on design choices

In this section, a small summary of changes made to the design to decrease risk can be found.

- For the electrical system, safety factors ranging from 5 to 20% were added to reduce the impact of anomalies within the power generation and distribution. In addition to this, to account for unexpected solar cell failure due to for example micro-meteorites, the solar panel design includes 7 redundant solar cells.
- For the structure, a safety factor of 2 was used to account for extra unexpected forces during the launch.
- From the thermal management subsystem, instead of using an active deployment mechanism for earth shield deployment, a passive actuation mechanism is used to decrease the likelihood of failure.
- A safety factor of 1.5 was added to the ADCS, to account for unexpected external forces. Moreover, there are 2 magnetometers and 2 star-trackers included in the design to add redundancy and the CMGs were placed in a rooftop cluster instead of a pyramid cluster to reduce the severity of R-ADCS-09.
- The SDH contains 4 CPUs instead of the required 3, to add redundancy. For the communications system, the complexity, and thus risk, of different systems was taken into account in the trade-off.

17

Sustainable Development Strategy

Focusing on sustainability has become a growing trend when considering development and production in the aerospace industry[1]. LAMP should likewise place focus on the strategies to improve its sustainable development. Using novel sustainability ratings such as the Space Sustainability Rating (SSR)[2], can aid in assessing the overall sustainability of the mission, though it must be noted that the SSR is a very recently developed platform, having only been implemented in early 2023, hence other methods should be employed. This chapter focuses on those strategies, namely sustainability in manufacturing, data sharing, trackability and detectability, minimising space debris, and collision avoidance in Section 17.1 and 17.2. The social and regulatory aspect of sustainability is also assessed in Section 17.3.

17.1. Sustainability in manufacturing

While designing and manufacturing the satellite, certain decisions must be taken to comply with modern sustainability standards. Firstly, the use and sourcing of materials and components must be accounted for. For example, the use of toxic materials should strictly be controlled, also to comply with *CON-Sus-02*, and as such no hydrazine shall be used. Likewise, radioactive materials should be avoided, not only for the damage they could cause to workers during manufacturing but also due to deorbiting considerations, as radioactive materials might not fully disintegrate. Moreover, rare and precious materials should be avoided in the production of the platform itself, as the sourcing of such materials can have serious consequences for both the environment and human health and safety.

An exception to this guideline could be in the case of the possible payloads, semiconductors and solar cells[3], in case it may be unfeasible not to include such materials. Another exception to this, regards the iodine propellant used. In humans, elemental iodine is toxic when orally ingested or when inhaled in moderate doses, as well as being a skin irritant[4]. Therefore, extreme care should be taken when loading the propellant tanks before launch, but also while testing the propulsion system on the ground, as workers should be properly protected. Iodine also has other considerations during manufacturing, especially due to its corrosiveness (further explained in Chapter 18). Care should be taken when handling the iodine for the propellant tans, to make sure there are no major leaks which could corrode other materials and increase the manufacturing waste.

During manufacturing, strategies can be employed to reduce waste, thus improving the sustainability of the mission. For example, designing effective testing strategies can result in reduced waste, as fewer prototypes need to be created and destroyed for testing. Likewise, selecting launch providers that are able to provide reusable launches should be preferred, as this greatly reduces the waste

[1] bsr.org/en, last accessed on 15/05/2023
[2] spacesustainabilityrating.org, last accessed on 15/05/2023
[3] echa.europa.eu, last accessed 05/06/2023
[4] labchem.com, last accessed 19/06/2023

needed to place a satellite in orbit. Also, when purchasing off-the-shelf components from other companies, the CO_2 emissions of such components should be accounted for and minimised where possible.

During the operational phase of the satellite, sustainability remains important, hence it should be designed and manufactured to ensure this. One example where it can be made more sustainable is in the power generation of the satellite. Using solar panels which provide renewable energy instead of non-renewable chemical generators or nuclear energy (which poses its own sustainability issues as previously discussed) should be preferred. Even though solar panels mounted on the outside of the spacecraft can have a greater probability of creating orbital debris on collision with micro-meteoroids, they should still be preferred in terms of sustainability, as this risk can be mitigated.

17.2. Space debris and collision avoidance

Once the satellite is in orbit, the issue of space debris must be taken into consideration. Launching into a very Low Earth Orbit (VLEO) is a clear advantage in this sense, as it is much less crowded than other orbital altitudes (such as LEO) [88], meaning that the probability of impact with space debris is considerably lower. As more commercial and non-scientific space missions appear, the number of satellites orbiting at low altitudes has greatly increased, especially with the growth in popularity of satellite constellations [89].

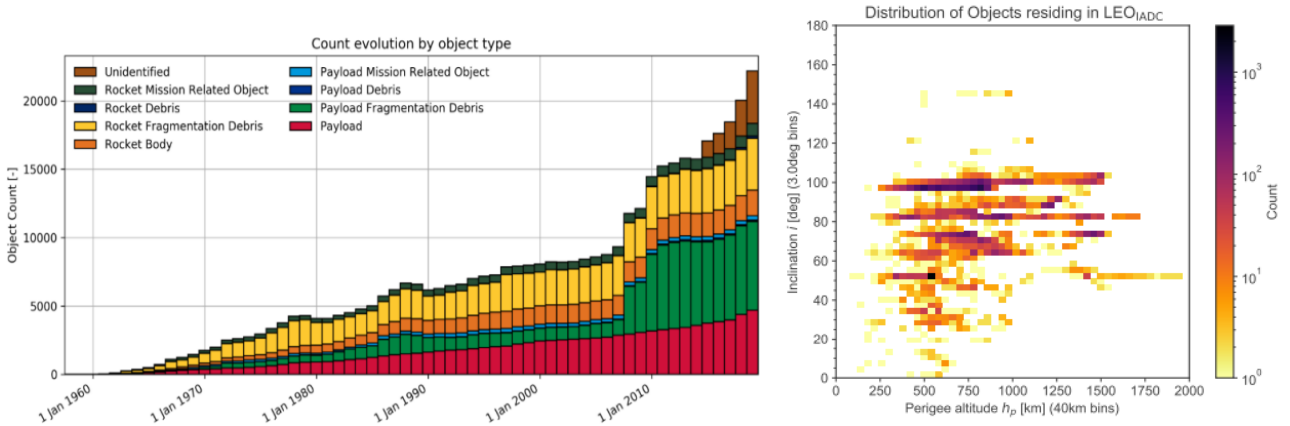

(a) *Orbital evolutions by object type [90]*

(b) *Distribution of objects residing in LEO [90].*

Figure 17.1: *Debris and other objects orbiting Earth.*

As can be seen in Figure 17.1, the amount of orbital debris has been greatly increasing in the past years, and likewise, the number of objects in LEO (and especially at a Sun-synchronous orbit) is very large. With these two considerations in mind, if any collision is predicted to happen, there should be provisions in place such that a collision is avoided, as it can prevent the creation of further space debris (on top of causing the mission to be preemptively ended). Specifically, the ADCS and propulsion system should be able to handle additional fast movements of the satellite to circumvent any incoming debris (as specified in requirement *Sys-Prop-01-II*). Having the capability to predict and avoid debris collisions greatly improves the SSR. An example of a product which could be used to improve collision avoidance is ECOSMIC's SAFE-H[5], which is a 'plug-and-play' software that uses on-board sensors to provide collision avoidance probabilities and suggest possible manoeuvres. Using the simulation of collision likelihood from Section 6.2 (seen in Figure 17.2), the probability of colliding with an object is 6×10^{-8}, considerably lower than that of higher altitudes, as described by Zhang et al. [91] - thus showing the higher sustainability of VLEO in terms of lower collision probability.

[5]ecosmic.nl, last accessed 19/03/2023

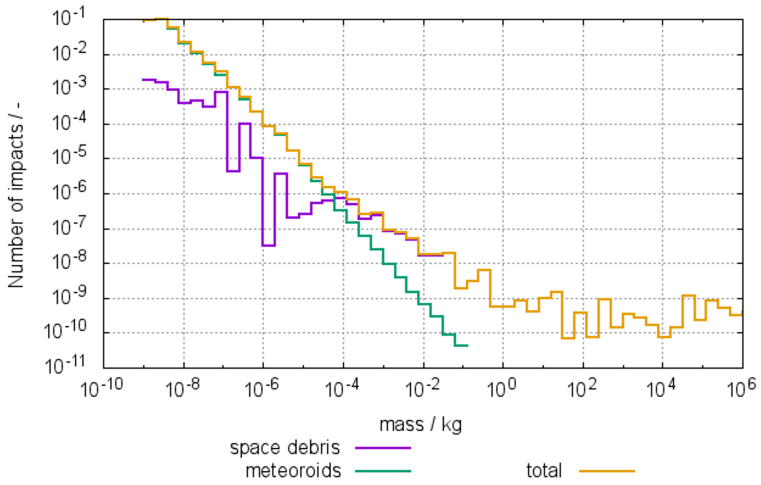

Figure 17.2: *Collision likelihood estimation for a one-month duration.*

Another advantage of orbiting in VLEO pertains to the high-drag environment that the spacecraft experiences, where it can be used for its EOL strategy. This greatly aids in the deorbiting of the spacecraft, as it will naturally decrease in altitude, and eventually burn up in the high altitude. Again, this improves the sustainability of the satellite as no extra orbital debris should be created, as all components must burn up in the atmosphere (according to the requirements *U-ReS-03* and *U-ReS-04*). Linked to the sustainability in manufacturing, the spacecraft should aim to not use any radioactive components, as it would complicate deorbiting procedures as those components may not fully burn up in the atmosphere, but also they could become toxic to wildlife or people if they reach the ground.

17.2.1. Trackability and detectability

Another category of the SSR concerns the trackability and detectability of a satellite in orbit. This is important to reduce the probability of collisions between spacecraft and with existing debris, as the satellite's position can be tracked by independent observers. Working in VLEO already reduces the possibilities of collisions, however, detectability can pose a challenge for CubeSats, as they are usually launched in 'rideshare' programs in multiple bundles, causing some confusion in tracking the correct satellite [7]. Good coordination with tracking agencies before launch can greatly improve detectability and trackability, though the best method would be to use tracking aids on the satellite, to aid in detection by external parties. This can be in the form of high-reflectance surface coatings around the satellite to increase radar visibility - which is already the case for the thermal control system in Chapter 9.

17.2.2. Data sharing

Data sharing is yet another category of the SSR that should be taken into consideration when discussing the sustainability of the mission. Data regarding the spacecraft's position should always be shared, to provide collision avoidance coordination information to other companies that have satellites in a similar orbit. Moreover, if the mission is of a scientific nature, data could be shared with other interested parties (such as universities or research groups), though this cannot be fully enforced on the customers of the CubeSat platform. Finally, to improve the SSR, spacecraft characteristics could be published, namely the mass, manoeuvrability capability and the satellite's operational status throughout the mission. Such characteristics can help in the prediction of conjunction events between satellites by third parties.

17.3. Compliance with regulation

Even though the vast majority of space sustainability related regulation is non-binding, compliance with such regulation should be construed as highly appealing, due to its growing trend in the aerospace industry [92]. An example of such a regulatory body is the Committee on Space Research (COSPAR) Planetary Protection Policy guidelines [93], which are a list of ethical principles including: promoting

scientific research in space and its dissemination, reducing contamination of Earth and promoting diversity and gender equality in all activities.

Other regulation comes from the UNOOSA European Code of Conduct for Space Debris Mitigation [94], defining measures for the management, design and operational phases of a mission. This code of conduct aims to ”preserve outer space from the uncontrolled growth of space debris”, which is greatly applicable for the LAMP mission, as it is a requirement to fully burn-up in the atmosphere creating the least amount of space debris possible. The mission should especially comply with the design measures SD-DE-11 to SD-DE-12 of the code of conduct, which refer to the reduction of space debris and the minimisation of atmospheric contamination on re-entry.

Furthermore, the UN sustainable development goals could be analysed in the context of the LAMP mission, and in the context of space[6]:

- **SDG-3 Good Health and Wellbeing**: the social sustainability of the team can be assessed, as teams members should maintain a healthy work balance, taking regular breaks and not working later than required, to avoid fatigue and sustain an efficient working environment.
- **SDG-7 Affordable and Clean Energy**: the use of clean energy throughout all stages of the mission should be considered, including transportation to the launch sites, transportation of components to manufacturing facility, selecting reusable launch vehicle providers, among others.
- **SDG-8 Decent Work and Economic Growth**: LAMP is a mission that makes Earth observation more accessible to the private sector and also to the scientific sector, due to its competitive pricing and modularity - this can generate new work opportunities and stimulate the economy, but also generate new scientific research and stimulate education (linking with **SDG-4 Quality Education**).
- **SDG-12 Responsible Consumption and Production**: as previously mentioned, the CO_2 impact of COTS components used in the mission should be minimised, by choosing providers of said components carefully (lowering the environmental impact of the mission). With respect to the components developed in-house, a lean manufacturing approach should be taken, minimising waste as much as possible in all stages of production and adding value. Using the concept of *kaizen*[7] to continuously improve productivity would also contribute to the improved sustainability in production as less waste could be produced.

[6] unoosa.org, last accessed 20/06/2023
[7] kaizen.com, last accessed 20/06/2023

18

Manufacturing, operations and logistics

In this chapter, the manufacturing, operations and logistics considerations of LAMP are discussed. The project design and development logic is discussed in Section 18.1, manufacturing considerations in Section 18.2 to 18.2, while the mission operations and logistics are developed in Section 18.3. Finally, the RAMS characteristics are described in Section 18.4.

18.1. Project design & development logic

On Figure 18.2, all the post-DSE activities are planned. During the testing and certification phase, environmental tests can be performed such as a vibration test and thermal vacuum bake-out test. Both these tests can be requested by the launch provider [72], and are important validation tests for the platform, as will be discussed in Section 18.5.

In Figure 18.2 the project design and development logic can be seen. During the early development stages, it is suggested to assemble a qualification model for the vibration test to prevent unexpected test results to destroy hardware. However, this does add to the development cost as an additional structure with dummy weights, to represent the different subsystems, needs to be produced. Nevertheless, every flight model has to perform the same vibration test before integration with the deployer and launch vehicle.

Using the project design and development flow diagram as a guide, the project Gantt chart can be created, where the high-level planning of the coming phases of the project can be charted. The project Gantt chart can be seen in Figure 18.1

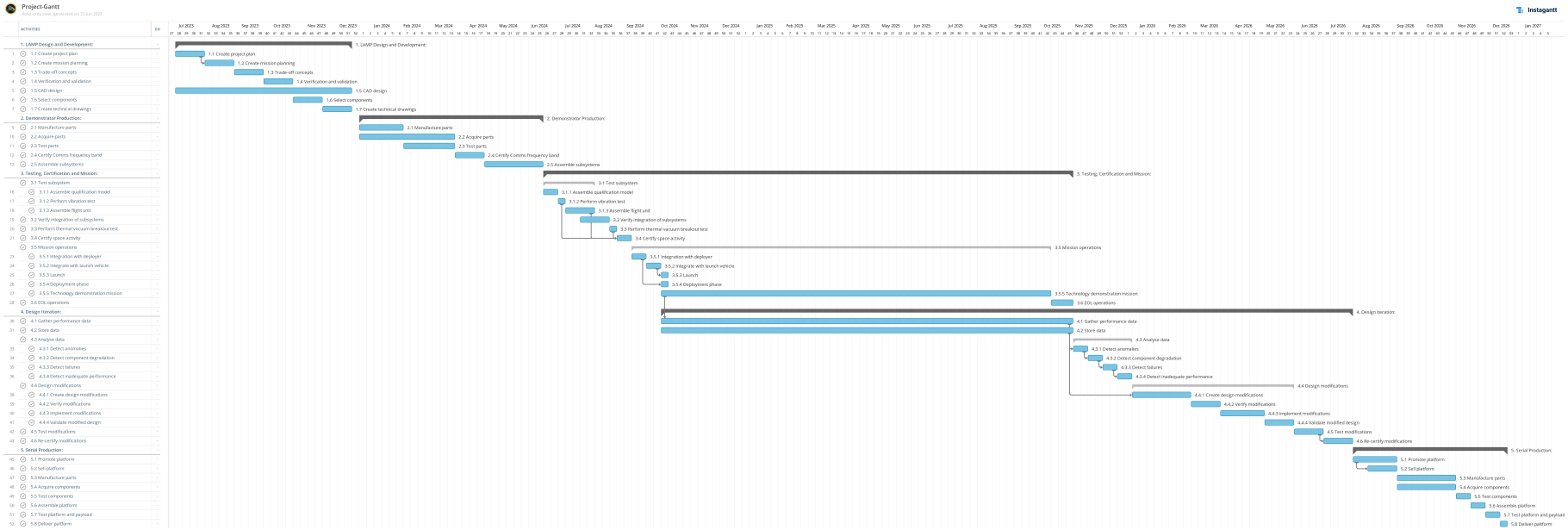

Figure 18.1: *Post-DSE project Gantt chart.*

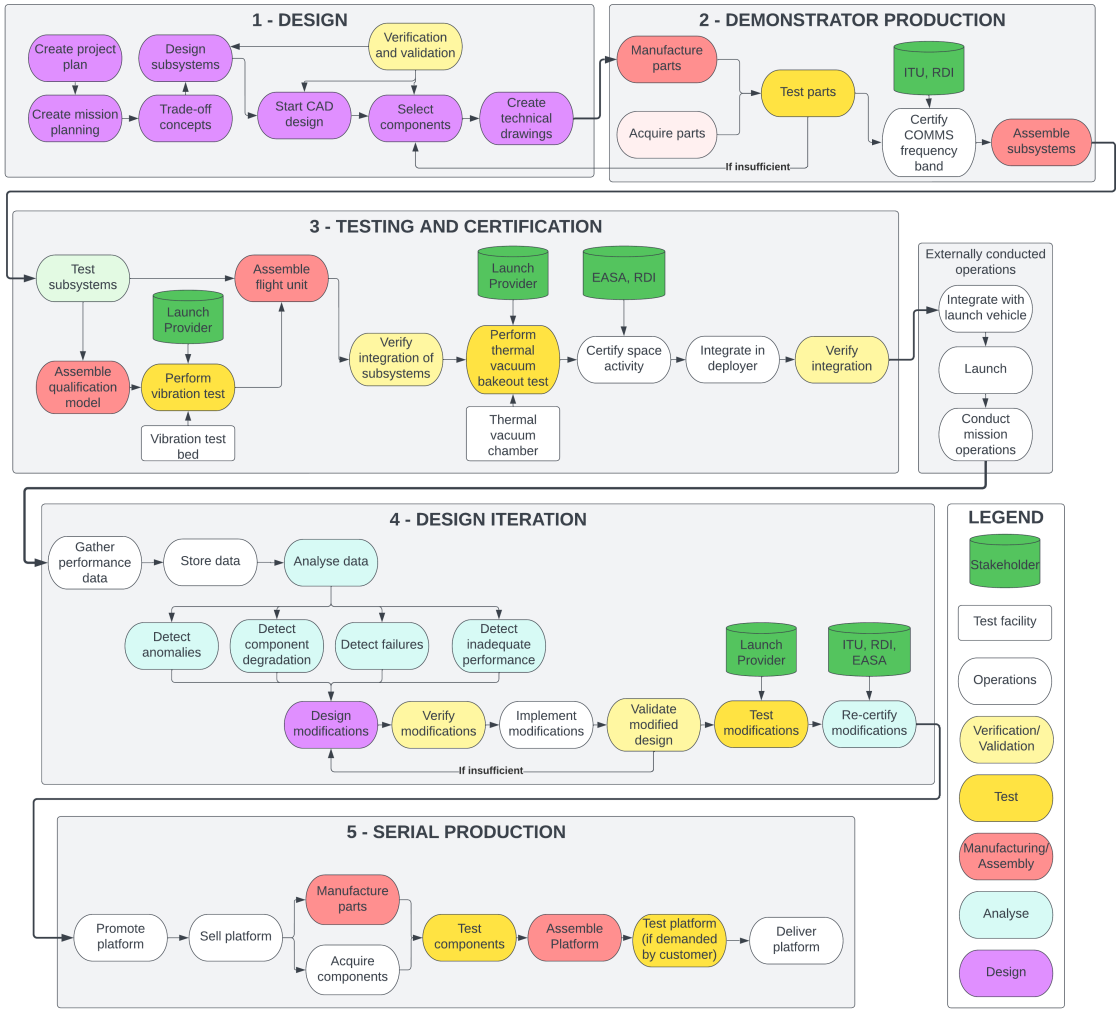

Figure 18.2: *Project design and development logic design flow diagram*

18.2. Manufacturing method

As LAMP expects to produce dozens of spacecraft, demand-driven batch production has been selected as the manufacturing method. The reasoning for this is the number of platforms the team plans to build (50+) is more akin to the aircraft industry than the more custom, single-unit, 'one-of-a-kind' spacecraft industry.
In batch production, an assembly line is used to move the products from one station to the next. This is in between the dock-like system that ships and spacecraft commonly use, and the mass-production systems used by the automotive industry, where a continuous moving line is used.

One of the important defining factors of batch production is the part batch size. When the parts fall below a certain critical number, a new order is placed. Since most manufacturers take weeks to months to deliver their products, a preemptive 6-month inventory has been placed. This means that when the order is placed, there are still enough parts to build platforms for the next 6 months. This number, however, might change for some components as the lead times become known.

Another advantage of batch production is worker experience. As workers do not change from station to station, they become increasingly efficient at their tasks, thus reducing the working hours required to finish the product. This means that the assembly chart presented in Table 18.2 will evolve over time.

Components procurement

Each subsystem produced a list of required components and with their respective mass, volume, power, cost (if found), and if it will be produced in-house or bought off the shelf (COTS). In Table 18.1, this component list is shown.

Table 18.1: *In-house vs COTS and lead times of components.*

Part		Part	
PROP: BHT-100	COTS	THERMAL: White coating	COTS
PROP: Iodine	COTS	THERMAL: Radiator	In-house
PROP: Valves	COTS	THERMAL: Earth shield	In-house
PROP: Filter	COTS	THERMAL: Heat straps	COTS
PROP: Enclosure	In-house	THERMAL: MLI	COTS
PROP: Piping	In-house	THERMAL: Patch heater	COTS
EPS: Batteries	In-house	THERMAL: Pipe heater	COTS
EPS: PCDU	COTS	COMMS: Patch antenna	In-house
EPS: Solar cells	COTS	COMMS: Transceiver	In-house
EPS: Solar panels	In-house	ADCS: Star-trackers	COTS
EPS: Harness	In-house	ADCS: Magnetometer	COTS
Str: Panels	In-house	ADCS: Magnetorquer	COTS
Str: Stiffeners	In-house	ADCS: CMG	In-house
Str: Hinges	COTS	GNS: Patch antenna	COTS
Str: Fasteners	COTS	GNS: GNSS receiver	COTS
Str: Deployment mechanism	COTS	SDH: OBC	In-house
Str: Payload structure	In-house		

The reasoning behind COTS or In-house production is a balance between component costs and development costs. Easy to develop and custom parts such as the structural elements, solar panels and radiator/earth shield are developed in house to save on costs. Some components, such as the CMGs and the OBC are also developed in-house, due to the specific requirements and sizing needed. The CMGs in-house will also save around 40,000€ to the cost of the platform. Complex parts that would increase the development costs significantly are bough COTS, such as the star trackers, the thruster and the solar cells. The COTS price for these is quite high and will be discussed in Chapter 19. Finally, components that are economic and reliable can be bought off-the-shelf, such as the fuel, heaters and coatings.

Assembly chart

An assembly chart has been created in Figure 18.3. This chart presents a timeline of each product. Every second month, the spacecraft moves to the next station, giving way to a new sub-assembly. A total of three platforms will be worked on at the same time. With three stations and six months for every platform, the expected delivery interval is one platform per two months, or 6 a year.

Since demand-driven batch manufacturing is used, production could halt until there is demand. This means that the delivery time for the first product of the platform would be 6 months, and the subsequent platforms would have a delivery interval of two months.

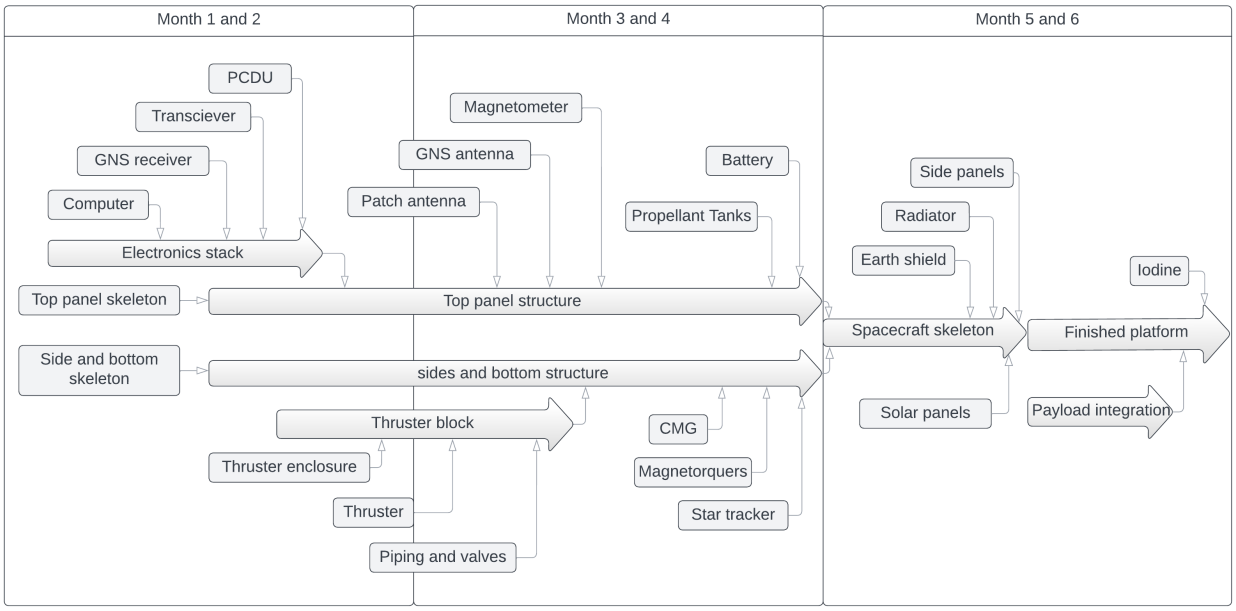

Figure 18.3: *Assembly chart.*

The assembly follows a similar structure to an aircraft assembly, in which several sub-assemblies are worked on in parallel, while heavy, expensive or voluminous components are mounted as late as possible.
Some component considerations are:

- Many components mounted to the inside of the platform will be covered with MLI or thermal tape before being mounted to the structure.
- Some components need to be mounted with non-conductive washers in order to not conduct heat to the spacecraft, such as the thruster block.
- In some orbits, such as the 6h and 18h orbit, the solar panels are rotated at opposite angles, meaning the Earth-shield collides with the solar panel. In this case, the radiator and Earth-shield can be installed on the opposite side of the spacecraft.
- Since the platform can accommodate several payloads, the centre of gravity can shift. This means the thruster needs to be angled at a different angle depending on the payload.
- Regarding the thermal coatings (both white and black coatings), after application to the structure, they must be cured at 70 °C.

Regarding propellant loading, several steps are needed. [87]

1. The satellite is placed in a vacuum chamber for 12h, to remove any residual humidity.
2. The vacuum is lifted, and the powdered propellant is loaded into the two tanks. This should be done as quickly as possible.
3. The satellite is placed inside the vacuum chamber again.
4. A noble gas (for example argon or xenon) is pumped at 100 Torr across a solenoid valve, which will flow backwards towards the tank and purge through another solenoid valve on the tank. This step should last for 2h, or longer if there was prolonged exposure to humid air.
5. The inlet valve is closed first, and then the purge valve is closed.
6. The vacuum is lifted again, completing the propellant loading.

Payload integration

Payload integration requires close contact with the customer, as the integration needs to be designed before the platform (and sometimes the payload) is fully built. The following steps should be taken:

1. **Payload definition and requirements:** The payload provider sends the payload description, CAD files, characteristics and requirements to the LAMP team. This will include mass, shape, power use, power voltage, data interface, etc.
2. **Payload integration design:** A proper mechanical interface is designed, analysed and built. It needs to be designed to withstand the launch and environmental conditions, while safely securing the payload.
3. **Mechanical and electrical integration:** The payload is integrated into the platform and the cabling is connected.
4. **Software integration and testing:** The link between the payload and the OBC is tested. Simulations are performed and all modes of operation are verified to work as intended. The payload is also tested to meet the customers' requirements.
5. **Functional and environmental testing:** The final physical tests are performed. Environmental tests are also needed for the launch provider.

Following the integration, the iodine is loaded and the platform is delivered to the launch provider.

18.3. Mission operations and logistics concept description

Since LAMP is a platform, the post-launch operations and logistics are handled by the buyer. However, since there is a demonstration mission planned, the ground operations will be handled by the LAMP team and thus must be accounted for. There is also the possibility that a customer does not buy the platform, but instead wants the LAMP team to choose a payload, integrate it and fly the mission, while the customer only receives the payload results. In this case, the LAMP team handles the mission operations. In Figure 18.4, the flow of operations can be seen for both a customer terminal (bottom path) and a LAMP terminal (top path).

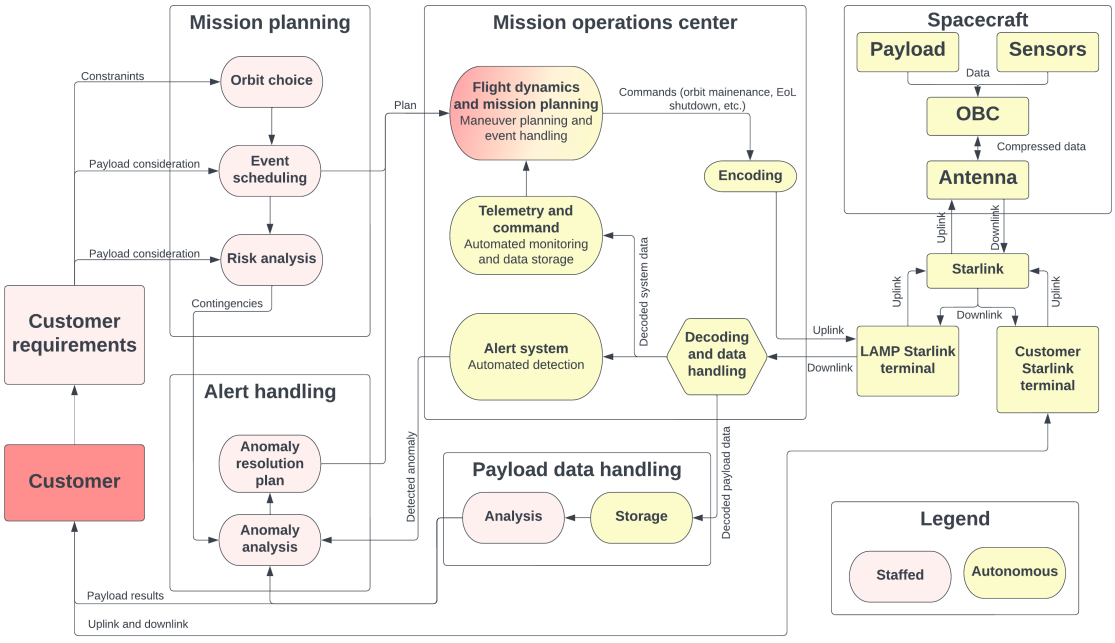

Figure 18.4: *Mission operations diagram.*

18.4. RAMS characteristics

The RAMS characteristics refer to the system's reliability, availability, maintainability and safety. These characteristics can at first be analysed, in the coming subsections, by comparing them with previous missions, to be refined in later reports.

Reliability

According to *U-ReS-01*, the reliability of the system should be above 95 % for the duration of the mission. Bus reliability can be first estimated by considering the product of the reliability of the individual subsystems, tabulated in Table 18.2. Reliability can also be calculated from statistics, by considering the failure rates of previous missions, shown in Figure 18.5 and Figure 18.6.

Table 18.2: *Reliability estimate per subsystem [95, 96, 97]*

Subsystem	Reliability	Subsystem	Reliability
EPS	0.96	GNS	0.99
SDH	0.93	TCS	0.97
Propulsion	0.99	Comms	0.96
ADCS	0.94	Struct ures	0.96
	Total	0.73	

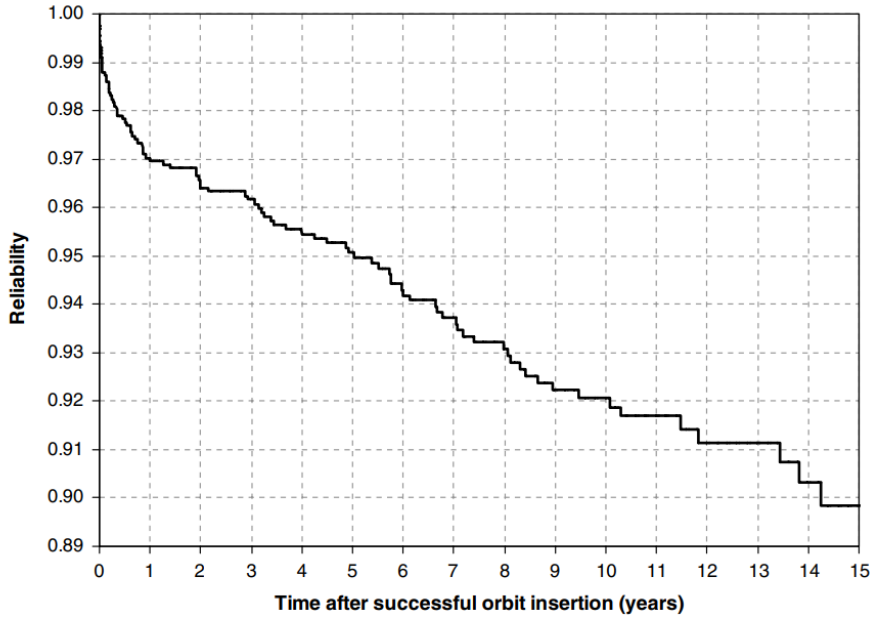

Figure 18.5: *Plot of spacecraft reliability [98]. After five years, reliability is 95%.*

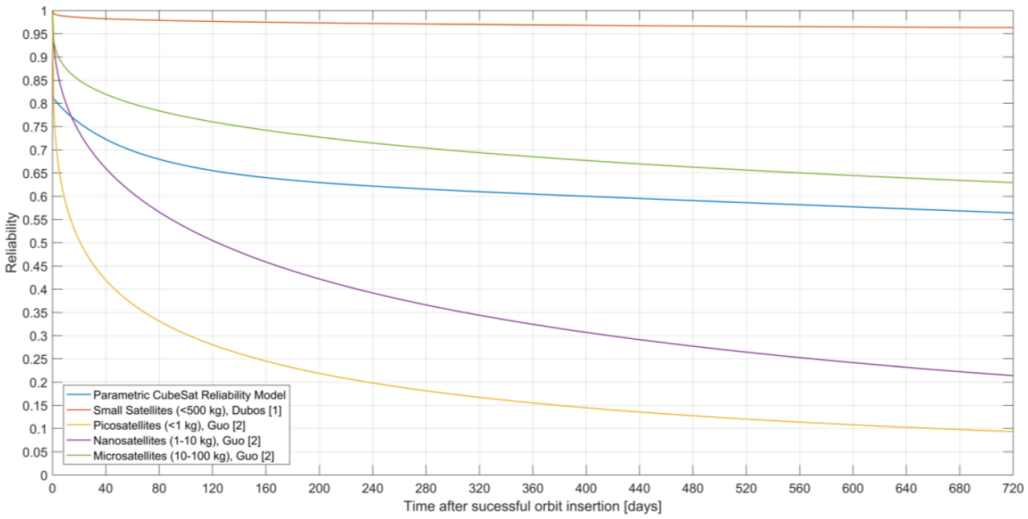

Figure 18.6: *Plot comparing reliability for different satellite classes [95]. After two years, reliability is 63% for microsatellites.*

Considering the different statistical approaches shown in Table 18.2, one can observe that the reliability calculated using a per-subsystem 'bottom-up' approach does not meet the requirement of 0.95, which can be attributed to the coarseness of the estimation. Another possible approach would be to consider statistical data on the failure rate of CubeSats, proposed by Langer and Bouwmeester[95]. However, even after just two years, this method yields an estimated reliability of solely 65%, not meeting requirements. This may be explained by the fact that CubeSats are not usually designed for relatively large mission duration, as well as the fact that the CubeSat failure data is skewed by Dead-On-Arrival satellites and the relatively high immaturity of the systems used [95]. Using instead the approach from Castet and Saleh[98], general satellites' failure rates were used to calculate the reliability (not limited to CubeSats), which leads to an appropriate reliability value after five years. More of the satellites used were designed for relatively longer mission duration, hence as a preliminary reliability estimation, this approach shall be used - leading to a reliability value of 0.95 (complying with the requirement *U-ReS-01*). Likewise, as there shall be a demonstration mission for the satellite, the immaturity factor associated with the systems used can be reduced, hence increasing the reliability compared to the average CubeSat[95]. One should note that this is a coarse initial estimate based on data of which the applicability is up for debate. However, it does provide proof that *U-ReS-01* is possible to comply with.

As a recommendation for further design, a bottom-up approach regarding reliability should be undertaken. This would entail considering the reliability of each component used in the spacecraft, by both collecting this data from the producers of COTS components and designing tests to verify the reliability of components built in-house. Then, the overall bus reliability can be calculated from the product of all the individual reliabilities, including a relevant degradation factor for five years. This proved to be beyond the scope of this report due to the unavailability of data on component reliability.

When estimating reliability, one must take into consideration the redundancy philosophy used for each subsystem. Considering the ADCS, there shall be redundant sensors (i.e. one redundant magnetometer). There shall be no redundancy for the magnetorquers due to the large volume they occupy. The use of redundant components will increase the reliability of the respective subsystem as shown by Equation 18.1.

$$R = 1 - (1 - R_c)^n \tag{18.1}$$

where R is the reliability of the subsystem, R_c the reliability of a single component and n the number of components present in the system.

Another subsystem with some redundancy is the propulsion subsystem. Due to the relatively high thrust chosen compared to the estimated drag values (7.86 Ncompared to 0.277 N), if the thrust were to be reduced (caused by solid iodine build-up in the propellant lines causing a decrease in propellant mass flow rate for example), the spacecraft would still be able to operate, though the lifetime would be reduced due to increased propellant use to achieve the required amount of impulse.

Availability

To optimise the availability of a connection with LAMP throughout its orbit, the Starlink communications network will be used. Starlink is a constellation of communication satellites at a 550 km altitude, which is above LAMP's orbit. The increasing density of the constellation improves the availability of the connection with LAMP. A user can receive the downlink from LAMP either by using one of Starlink's User Terminals or by using existing Starlink 'Gateway' ground stations [1]. Section 11.2 goes into further detail on the availability and the analysis of the use of this network.

[1] starlinkinsider.com/starlink-gateway-locations/, last accessed 21/6/2023

Maintainability
Considering that LAMP is a space mission, physical maintainability of the spacecraft is impossible, due to the difficulty and cost of in-orbit maintenance missions [99]. Other aspects of the spacecraft can be maintained however, namely the software, as updates can be sent to the spacecraft if bugs or failures appear. Regular commands can also be sent to the spacecraft to ensure that it is able to overcome unforeseen conditions.

Safety
For this mission, certain safety-critical functions must be addressed (which could lead to the termination of the mission). Some of these functions are further expanded on in Chapter 16, but others are stated below:

- **Solar panel deployment** - if this fails to deploy, LAMP will not have full or any power generation capabilities. Leading to a shortened mission life and decreased power capabilities. If deployment completely fails it will result in catastrophic failure
- **Propulsion failure** - if there is a reduction of thrust, the propulsion system can still operate, though with a reduced mission lifetime, however, if the propulsion system completely fails, it will lead to instant mission failure.
- **Spacecraft Deployment failure** - if the deployer fails, the spacecraft will not be able to proceed in its mission.

18.5. Product Verification & Validation
Post-design, the components, systems and full assembly needs to be verified, certified and validated (Table 18.3). The results of the tests need to comply with the requirements and some of these tests can also be used to validate the software. Finally, a full product launch will be used as a full-scale validation test.

Table 18.3: *Verification and validation tests applied to the product.*

Type	Test	Description
Verification		
Analysis	Simulations	Thermal, electrical, control, aerodynamic, etc. Simulations. These simulations can go very in depth, be very time consuming and create a big monetary expense in man-hours. In the case of LAMP, the complexity of them can be reduced due to the *Full product launch*, which ends up being a more economical option than a very extensive analysis on the ground.
	Mechanical analysis	Finite element analysis, modal analysis, strength, fatigue, thermal stress, buckling, etc. These tools are usually available in CAD software and provide a good analysis to predict how the platform will respond to the environment, possibly identifying failure points, stress concentrations and deformation patterns.
	RAMS	Discussed in Section 18.4
	Speciality analysis	Ground operators training and ease of production. It is important to train personnel that will work with the platform before the product is finalised. This means ease of production and operations can be streamlined and no product changes need to be done after the production has started.
	Functional and operational analysis	Testing if the spacecraft responds correctly at any moment of time in the mission, as well as testing the failure detection and recovery modes. It is performed on the software, before the spacecraft is built, and tests the interaction of the subsystem between each-other. This analysis ensures that the spacecraft's design meets the mission objectives and functional requirements.
Structural	Limit loads	The structure is checked to not deform permanently under launch conditions.

	Stiffness	Full assembly stiffness needs to be checked, as joints change the stiffness of the assembly compared to the empty structure.
Integration	Mechanical	Mass, volume, tolerances, alignment, build quality, etc. are checked to ensure the build quality is sufficient.
	Electrical	Power consumption, ground planes, delivery, etc. are checked to work as intended. The subsystem must provide the correct voltage and the specified current to all the components to pass the test.
	Mission simulation	A simulated environment is used to test all the modes of the spacecraft. It includes all operating scenarios of the spacecraft and is used to check the operational readiness of the spacecraft.
Functional	Deployment test	Solar panels/antennas deployment testing. It also tests any sensors, actuators, valves or switches for their correct operation and functionality.
	Control test	In a simulated environment, the ADCS is checked to respond correctly to disturbances and commands.
	Communication test	The antennas and transceivers are tested to ensure they work according to specifications.
Qualification and acceptance		
	Flight model	Less stringent tests on the flight model. They are used to verify the user and performance requirements.
	Qualification testing	A structural, thermal, electrical and engineering model are tested to a margin above expected conditions.
	Documenting and reporting	Throughout the acceptance tests, the procedures and results are documented, including any issue or non-compliance encountered. This documentations is then used to determine the flight readiness of the platform.
Payload verification	Calibration	The payload is calibrated to it's standards of accuracy and precision. This is usually done by comparing the readings of the instruments to reference values.
	Performance	It tests the payload sensitivity, resolution, dynamic range, etc. The performance reading should comply with the criteria necessary to achieve the mission objectives.
	Integration and interface	This tests checks for the integration of the payload with the other subsystems, such as the data flow between the payload and the computer, or the electrical integration.
Validation		
Full product launch	Demonstration mission	A mission with a (dummy) payload to do a full test of every subsystem and their interaction, as well as degradation observations.
Environmental	Vibrations	Check for resonances by loading the spacecraft with sine and random vibrations. It must resist launch loads. This test is required by the launch provider and is of upmost importance.
	Thermal	Thermal balance and thermal vacuum tests are performed to make sure the thermal control subsystem works correctly under a vacuum.
	Acoustics	During launch, the spacecraft experiences high-intensity acoustic waves. The built platform is placed on an acoustic chamber and the structural integrity, the functionality of the components and the vibration response are checked.

19

Financial analysis

This section breaks down the financial aspects of LAMP. In Section 19.1, the requirements of lamp can be reviewed, and in Section 19.2, the costs are broken down. Finally, in Section 19.3, the operational profits are presented.

19.1. Requirements

Table 19.1: *Financial requirements.*

ID	Description	Rationale	Verif. M.	
CON-Res-Ct-01	The first mission shall cost no more than 5 million euros (2023) including development costs, excluding launch, operations and maintenance	Budgetary constraint	Ana	✓
CON-Res-Ct-02	A single satellite shall cost no more than 500k euros (2023) excluding development, launch, operations and maintenance.	Required to ensure advantageous market position.	Ana	×

19.2. Cost breakdown

The requirements *U-Ops-03* and *U-Ops-04* are related to the financial costs. This means that the design and demonstration mission will have to be accounted for in the break-even point. It is expected, however, that there will be around 2,500,000€ allocated for extra iteration after the demonstration mission and around 2.5M in initial installations and production investment. By taking everything into account, the budget for each satellite after the demonstration mission should be 300,000€. By selling them at 500,000€, the break even point will be 50 platforms. Table 19.2 shows the costs of different subsystems, which add up to the overall cost of LAMP, which includes all COTS components that would need to be bough. Since LAMP would produce many units, a 15% discount was assumed for all the COTS components. All components and their procurement method (in-house or COTS) were presented in Chapter 18.

Table 19.2: *Cost Breakdown of COTS for LAMP*

Subsystem	Cost ($)	Source/reasoning
Thermal	2,554	COTS for heaters and aluminium
Electrical	66,250	Price per cells (200€), approximated solar structure costs, available batteries
Structures	10,000	Similar COTS structures
Propulsion	34,500	Similar thrusters and iodine price
ADCS	133,400	Main contributor COTS star trackers, magnetorquer price sized from smaller magnetorquers price
Comms	4,000	Patch antenna price
GNS	7,967	Quote from selected component
SDH	0	Not COTS
Payload	0	-
Total	258,671	
With 15% discount	219,870	

In Table 19.3, an estimate of the budget breakdown is presented. In order to reduce development costs, rapid prototyping can be achieved by using novel processes like additive manufacturing[100]. This can decrease the work time greatly in final design, subsystem design and component design. To reduce costs of manufacturing, rental of equipment can be used for the demonstration mission, however, for serial production, a budget is allocated to buy equipment and installations. The man hours also reduce greatly from the first platform, as the workers gain experience building the same platform repeated times. A budget is also allocated to iterate on the demonstration mission, as to achieve a mature platform very quickly. In this way, the first satellite platform will serve as the means to test things thoroughly on the most realistic scenario. This mission should then be seen as an investment, as it will save money on ground testing.

Table 19.3: *Budget breakdown*

Group	Item	Man hours/units	Cost [€]
Development	Final design	4000h(150€ p/h)	600,000
	Component design	12000h(150€ p/h)	1,800,000
	Component testing, verification and validation	3000h(150€ p/h)	450,000
	Assembly testing	2000h(150€ p/h)	300,000
Manufacturing 1st platform	Material cost	1 unit	258,671
	Equipment and facilities	-	100,000
	Man hours	2000(150€)	300,000
	Operations budget	-	1,000,000
Total demonstration mission			4,808,671
Iteration	Design changes	3000h(150€ p/h)	450,000
	Component changes	6,000h(150€ p/h)	900.000
	Extra testing	3,000h(150€ p/h)	450.000
	Extra V&V	3,000(150€ p/h)	450,000
Total iteration			2,250,000
Total production investment			2,500,000

Total platform investment			9,450,000
Manufacturing after the first satellite			
	COTS cost	per platform	219,870
	In-house component cost	per platform	30,000
	Equipment wear and tear	per platform	2,000
	Man hours	1000(150€)	150,000
Total per satellite			401,870

Unfortunately, the predicted price for each platform is around 400000€, this means at least one requirement will not be met.The team is presented with two choices. The platform price could be raised to 600,000€, meaning part of *U-Ops-03* would not be met, but the break even point would still be at 50 missions. The second choice is to keep the platform price at 500,000€, achieving part of that requirement, but instead having the break-even point at 100 platforms sold. Both choices do not meet all the requirements, however, the team decided to sell the platform at 600,000€. This means the break even point will be achieved much earlier in production.

It is important to note that estimating costs early in development is a complicated task. Many companies do not share COTS components prices, while estimating worker hours is also difficult. This means there is a big uncertainty on both the unit price and the development costs. Future analysis should use more accurate methods to estimate costs.

Cost sensitivity

Since cost is very uncertain, the sensitivity of it is also very high. For example, cost of two star trackers alone is 90000€. Adding 13,950€ for the magnetometer, it is clear that the ADCS costs are expensive. If these components were to be developed in-house, the price of the spacecraft could be lowered below 500,000€, fitting the requirement (25% decrease in platform costs, or 16,67% of the price). However, developing minituarised star-trackers with the capabilities of available COTS could become very expensive, most likely going over the 5,000,000€ allocated for the development. For this reason, a better cost estimate method is recommended for the following stages of development.

19.3. Operational profit

When in full production, 6 platforms could be built per year. By selling them at 200,000€ profit each, the company will generate 1.2 million Euro per year in profits. With an initial investment of 10 million Euro, the company would break even after 8.3 years.

It is possible that the production of lamp accelerates with time. This is due to the manufacturing method chosen, where workers gain experience and work faster after each platform built. If the company is able to produce one extra platform per year, every year, the break even can be shrunk to 5.9 years (at which point the profits would be 2.2 Million Euro per year). It is possible to accelerate this even further by adding a second line of production, however, there needs to be enough demand for the platforms, while new workers need to be trained and acquainted with the product. This would temporarily increase the costs, but would achieve twice the output after a few years.

20 Conclusion

LAMP is a modular platform that was created with the aim to develop a 27U micro-satellite platform which can host different Earth observation payloads from a very low altitude (300 km), cost-effectively. Hence, LAMP is entering into a market that does not have significant competition and with its bigger size is positioned perfectly to capitalise on the increase of interest in bigger CubeSats. Potential customers range from science institutions, military, and civil to general commercial ventures.

For the design of LAMP several particularly distinctive elements were selected, which are currently not used or not commonly used for similar size satellite platforms. For the communication subsystem, Starlink was identified as a very desirable option for data transfer giving the possibility for far greater data transfer than alternative systems. For ADCS, control moment gyros were selected which can give LAMP a competitive edge for earth observation customers due to a decrease in jitter, an odd choice at the size of the system. The ADCS further provides accuracy unparalleled by competing platforms. For propulsion, iodine was selected for its excellent volume efficiency giving more space for other subsystems, and therefore making an increase in performance possible. Additionally, an earth shield that makes low-temperature payloads possible increases the capabilities of LAMP.

The cost of LAMP is reported to be 254,000€(only for the components). At a price of 600,000€and with 6 platform sales a year. The team expects to achieve a profit of 200,000€per platform. The company is projected to generate 1.2 million €annually. With an initial investment of 10 million €, the company is expected to break even after 8.3 years.

LAMP sustainable development strategy for the LAMP mission prioritises sustainability in manufacturing, data sharing, trackability and detectability, minimisation of space debris and collision avoidance. Compliance with regulations and standards, such as the Space Sustainability Rating and the UNOOSA European Code of Conduct for Space Debris Mitigation, is of utmost importance for the project.

Table 20.1: *Key Characteristics of LAMP*

Characteristic	Value	Characteristic	Value
Total Mass	52.98 kg	ΔV budget	$1093.5\,\mathrm{m\,s^{-1}}$
Total Volume	22.84 U	Peak Thrust	8 mN
Selling price	600,000€	Data Rate	46 Mb/s
Average Power	57 W	Peak Power	173 W
Sun-synchronous Orbit	300 km	Pointing Accuracy	0.002°

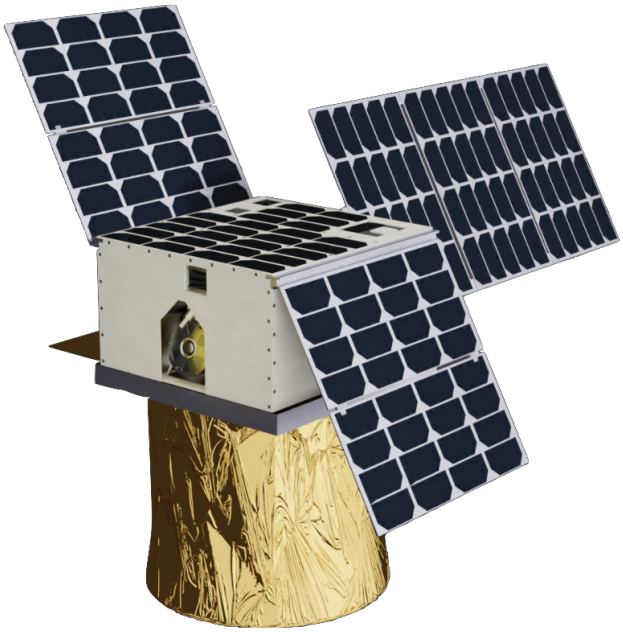

Figure 20.1: *LAMP*

Recommendations

The accuracy of cost estimation can be improved by gathering more detailed data on COTS component prices and a better estimation of worker hours could be made for in-house design. This will provide a more precise understanding of the project's financial aspects. Further work is required on thorough testing, verification, and validation to ensure that the LAMP platform is designed and built to withstand the harsh conditions of space, including radiation, temperature extremes, and mechanical stresses. Redundancy and fault-tolerant mechanisms must be investigated to enhance overall system reliability. Collision avoidance capabilities can be improved by conducting a detailed analysis to determine the altitude range within which the LAMP satellite can safely operate and manoeuvre. For the structure, a more thorough vibrational analysis based on FEM to confirm the natural frequency of the platform is advisable. For the inter-satellite link with Starlink, it is recommended to contact SpaceX to further work out the link. For the propulsion, it is recommended to investigate further how the tank heating would change in the case the iodine powder is floating on the tank, as well as if it has dispersed evenly through the tank, as it affects how well the heat is conducted from the tank to the propellant. The flow of iodine should also be studied further, as low-pressure feed systems are susceptible to backward flow, especially taking into consideration there are two tanks, which might heat up unevenly. A final remark is that LAMP has over one unit of useful volume left available in the bus. This space becomes an opportunity that could enhance the design even more. The empty space could be filled with additional fuel (increasing mission duration) or could be used to host a secondary payload. This payload could be combined with many different primary payloads, and thus could be used to gather information through many missions.

Bibliography

[1] Jasper Bouwmeester. “DSE Project Guide 2022-2023 - A low-flying small satellite platform for Earth Observation”. In: (Apr. 2023). issue 10.

[2] Jasper Bouwmeester and Hans Kuiper. *Enabling cost-effective high-resolution Earth observation with deployable space telescopes*. Jan. 2020.

[3] National Aeronautics and Space Administration. *Space Launch System (SLS) Block 1B Secondary Payloads: ESPA-Type and 27U Cubesat Potential Accommodations*. Tech. rep. Marshall Space Flight Center, Apr. 2019.

[4] Bill Doncaster et al. “SpaceWorks’ 2016 Nano/Microsatellite Market Forecast”. In: *30th Annual AIAA/USU Conference on Small Satellites* ().

[5] James Richard Wertz, David F. Everett, and Jeffery John Puschell. *Space mission engineering : the new SMAD*. Space technology library 28, 2011.

[6] Rainer Sandau. “Status and trends of small satellite missions for Earth observation”. In: *Acta Astronautica* 66.1-2 (Jan. 1, 2010), pp. 1–12. DOI: 10.1016/j.actaastro.2009.06.008. URL: https://doi.org/10.1016/j.actaastro.2009.06.008.

[7] Small Spacecraft Systems Virtual Institute. *State-of-the-Art Small Spacecraft Technology 2023*. Ames Research Center, 2023.

[8] Craig Burkhard and Sasha Weston. “The Evolution of CubeSat Spacecraft Platforms”. In: *AVT-336 Specialist’Meeting*. 2021.

[9] Thyrso Villela et al. *Towards the thousandth CubeSat: A statistical overview*. 2019. DOI: 10.1155/2019/5063145.

[10] Jasper Bouwmeester and Hans Kuiper. “Enabling cost-effective high-resolution Earth observation with deployable space telescopes”. In: *TU Delft* ().

[11] Yong Xue et al. “Small satellite remote sensing and applications – history, current and future”. In: *International Journal of Remote Sensing* 29.15 (July 17, 2008), pp. 4339–4372. DOI: 10.1080/01431160801914945. URL: https://doi.org/10.1080/01431160801914945.

[12] Lodewijk Bakker et al. *LAMP Midterm Report*. Apr. 2023.

[13] Thyrso Villela et al. “Towards the thousandth CubeSat: A statistical overview”. In: *International Journal of Aerospace Engineering* 2019 (2019).

[14] Anton V. Dolgopolov et al. “Analysis of the Commercial Satellite Industry, Key Indicators and Global Trends”. In: *ASCEND 2020*. DOI: 10.2514/6.2020-4244.

[15] Lodewijk Bakker et al. *LAMP Baseline Report*. Apr. 2023.

[16] Luciana Sinpetru et al. “ADBSat: Verification and validation of a novel panel method for quick aerodynamic analysis of satellites”. In: *Computer Physics Communications* 275 (June 1, 2022), p. 108327. DOI: 10.1016/j.cpc.2022.108327. URL: https://doi.org/10.1016/j.cpc.2022.108327.

[17] Nicholas H. Crisp et al. *D2.2 VLEO EO Satellite Aerodynamic Control Techniques and Mechanisms*. Tech. rep. Sept. 2019.

[18] Hermann Lühr et al. “Average thermospheric wind patterns over the polar regions, as observed by CHAMP”. In: *Annales Geophysicae*. Vol. 25. 5. Copernicus Publications Göttingen, Germany. 2007, pp. 1093–1101.

[19] Arjun Berera and Daniel J Brener. “On the force of vertical winds in the upper atmosphere: consequences for small biological particles”. In: *Proceedings of the Royal Society A* 478.2257 (2022), p. 20210626.

[20] Casper Versteeg and David L Cotten. *Preliminary Thermal Analysis of Small Satellites*. Small Satellite Research Laboratory, The University of Georgia, 2018.

[21] Luciana A. Sinpetru et al. “ADBSat: Verification and validation of a novel panel method for quick aerodynamic analysis of satellites”. In: *Computer Physics Communications* 275 (2022), p. 108327. ISSN: 0010-4655. DOI: https://doi.org/10.1016/j.cpc.2022.108327. URL: https://www.sciencedirect.com/science/article/pii/S0010465522000455.

[22] Oliver Montenbruck and Eberhard Gill. *Satellite Orbits*. Jan. 2000. DOI: 10.1007/978-3-642-58351-3.

[23] *World Geodetic System, 1984 (WGS-84) Manual*. International Civil Aviation Organization, Jan. 2002.

[24] Günther March et al. “Gas-surface interactions modelling influence on satellite aerodynamics and thermosphere mass density”. In: *Journal of Space Weather and Space Climate* 11 (2021). ISSN: 21157251. DOI: 10.1051/swsc/2021035.

[25] Chantal. Cappelletti, Simone. Battistini, and Benjamin K. Malphrus. *Cubesat handbook : from mission design to operations*. Academic Press, 2021. ISBN: 9780128178843.

[26] *SARA: a Solar Array Drive Assembly for small satellites*. Rev.5, Date Accessed 16/04/2023. REVOLV.

[27] Daniel Oltrogge and Kyle Leveque. “An Evaluation of CubeSat Orbital Decay”. In: *The 25th Annual AIAA/USU Conference on Small Satellites American Institute of Aeronautics and Astronautics (AIAA)* (Aug. 1, 2011). URL: http://www.agi.com/downloads/resources/white-papers/20110808_SmallSat_CubeSat_Orbit_Lifetime_10.pdf.

[28] Nicholas Crisp, Katharine Smith, and Peter M. Hollingsworth. “Launch and deployment of distributed small satellite systems”. In: *Acta Astronautica* 114 (Sept. 1, 2015), pp. 65–78. DOI: 10.1016/j.actaastro.2015.04.015. URL: https://doi.org/10.1016/j.actaastro.2015.04.015.

[29] J. M. Picone et al. “NRLMSISE-00 empirical model of the atmosphere: Statistical comparisons and scientific issues”. In: *Journal of Geophysical Research* 107.A12 (Dec. 1, 2002), SIA 15–16. DOI: 10.1029/2002ja009430. URL: https://doi.org/10.1029/2002ja009430.

[30] Vitali Braun et al. “DRAMA 2.0 - ESA’s space debris risk assessment and mitigation analysis tool suite”. In: Sept. 2013.

[31] Saika Aida and Michael Kirschner. “Accuracy Assessment of SGP4 Orbit Information Conversion into Osculating Elements”. In: *6th European Conference on Space Debris* 723 (Apr. 2013), pp. 160–. URL: https://conference.sdo.esoc.esa.int/proceedings/sdc6/paper/41/SDC6-paper41.pdf.

[32] Daniele Mortari and Matthew P. Wilkins. “On Sun-Synchronous Orbits and Associated Constellations”. In: 2004.

[33] Frank Stephen Tromp Van Diggelen. *A-GPS*. Artech House, Jan. 2009.

[34] Oguz Kagan Isik et al. “Integrity Analysis for GPS-Based Navigation of UAVs in Urban Environment”. In: *Robotics* 9.3 (2020), p. 66. ISSN: 2218-6581. DOI: 10.3390/robotics9030066.

[35] Vincenzo Pesce, Andrea Colagrossi, and Stefano Silvestrini. *Modern Spacecraft Guidance, Navigation, and Control*. Elsevier, Nov. 2022.

[36] Christian Tiberius. *Lecture notes in Satellite Positioning: Principle and performance of GPS receivers*. Feb. 2011.

[37] B. Rama Rao and W. Kunysz. *GPS/GNSS Antennas*. Artech House, Jan. 2013.

[38] Willem Herman Steyn. “Stability, Pointing, and Orientation”. In: *Handbook of Small Satellites: Technology, Design, Manufacture, Applications, Economics and Regulation*. Ed. by Joseph N. Pelton. Cham: Springer International Publishing, 2019, pp. 1–43. ISBN: 978-3-030-20707-6. DOI: 10.1007/978-3-030-20707-6_8-1.

[39] Almat Raskaliyev et al. “GNSS-Based Attitude Determination Techniques—A Comprehensive Literature Survey”. In: *IEEE Access* 8 (2020), pp. 24873–24886. DOI: 10.1109/ACCESS.2020.2970083.

[40] Willem Herman Steyn. “Stability, Pointing, and Orientation”. In: *Handbook of Small Satellites: Technology, Design, Manufacture, Applications, Economics and Regulation*. Ed. by Joseph N. Pelton. Cham: Springer International Publishing, 2019. ISBN: 978-3-030-20707-6. DOI: 10.1007/978-3-030-20707-6_8-1. URL: https://doi.org/10.1007/978-3-030-20707-6_8-1.

[41] Erik Mumm et al. “Miniature Control Moment Gyroscope development”. In: *2014 IEEE Aerospace Conference*. 2014, pp. 1–9. DOI: 10.1109/AERO.2014.6836474.

[42] Nobuo Sugimura, Toshinori Kuwahara, and Kazuya Yoshida. “Attitude determination and control system for nadir pointing using magnetorquer and magnetometer”. In: *2016 IEEE Aerospace Conference*. 2016, pp. 1–12. DOI: 10.1109/AERO.2016.7500665.

[43] Abhilash Mony, Hari B. Hablani, and Aditya A. Paranjape. “Angular-Momentum-Based Sizing of Control Moment Gyro Cluster for an Agile Spacecraft”. In: *Journal of Guidance, Control, and Dynamics* 45.9 (2022), pp. 1627–1643. DOI: 10.2514/1.G006461. eprint: https://doi.org/10.2514/1.G006461. URL: https://doi.org/10.2514/1.G006461.

[44] Barbara McKissock, Patricia Loyselle, and Elisa Vogel. *Guidelines on lithium-ion battery use in space applications*. Tech. rep. NASA, 2009.

[45] ISISpace. *ISIS On board computer brochure*. 2020.

[46] Stephanie Mauro. *Thermal Analysis of Iodine Satellite (iSAT) from Preliminary Design Review (PDR) to Critical Design Review (CDR)*.

[47] Craig Underwood. “Thermal Design”. In: 2017.

[48] David G Gilmore, David G Gilmore, and Martin Donabedian. *Spacecraft thermal control handbook*. Vol. 1. Aerospace Press El Segundo, CA, 2002.

[49] Murat Bulut et al. “Battery thermal design conception of Turkish satellite”. In: *6th International Energy Conversion Engineering Conference (IECEC)*. 2008, p. 5787.

[50] JM Kuiper, D Dolkens, and Víctor Villalba. “The Delft deployable space telescope project”. In: *70th International Astronautical Congress, IAC 2019*. 2019.

[51] *Thermal Strap Catalog*. Tech. rep. Thermal Management Technologies, 2019.

[52] *Thermally Efficient Deployable Radiators*. Tech. rep. Thermal Management Technologies, 2019.

[53] Casper van Lierop. “Deployable radiator wing for high performance CubeSats: Designing, analysing, prototyping and testing”. In: (2021).

[54] Jim Prince et al. *Sheldahl - The Red Book*. Tech. rep. Sheldahl - a Flex company, 2020.

[55] Rodrigo Avila de Luis. “Standardized Thermal Control Solutions for PocketQubes”. In: (2019).

[56] *MAP® PCBE (K) Low Outgassing Conductive White Silicon Paint*. MAP Space Coatings. 2022.

[57] Eugenio Urquiza et al. *Folding Elastic Thermal Surface-FETS*. Tech. rep. NASA, 2013.

[58] Lars Ole Valøen, Mark Shoesmith, and E-One Moli. “The effect of PHEV and HEV duty cycles on battery and battery pack performance”. In: 2007.

[59] Kevin R. Mallon, Francis Assadian, and Bo Fu. “Analysis of on-board photovoltaics for a battery electric bus and their impact on battery lifespan”. In: *Energies* 10 (7 2017). ISSN: 19961073. DOI: 10.3390/en10070943.

[60] *PCDU power board*. Rev. B. GAUSS Srl. Apr. 2021.

[61] Sami Ekici and Mehmet Ali Kopru. “Investigation of PV system cable losses”. In: *International Journal of Renewable Energy Research (IJRER)* 7.2 (2017), pp. 807–815.

[62] Sioe Yen Go et al. *Mechanical Design and Arrangement of nanosatellite Delfi-n3Xt Exam committee: Chair of Space Systems Engineering Chair of Space Systems Engineering Chair of Space Systems Engineering*. 2009.

[63] Fabio Santoni et al. “An innovative deployable solar panel system for Cubesats”. In: *Acta Astronautica* 95 (2014), pp. 210–217. ISSN: 0094-5765. DOI: https://doi.org/10.1016/j.actaastro.2013.11.011.

[64] Ernie Eugene Gabriel Alvarez. “Thermal and Power Cubesat Subsystem Integration”. PhD thesis. San Jose State University, 2014.

[65] Wiley J Larson, James Richard Wertz, et al. *Space mission analysis and design*. Vol. 3. Springer, 1992.

[66] I. Ali, N. Al-Dhahir, and J.E. Hershey. “Predicting the visibility of LEO satellites”. In: *IEEE Transactions on Aerospace and Electronic Systems* 35.4 (1999), pp. 1183–1190. DOI: 10.1109/7.805436.

[67] Mohamed Elbahaay et al. “5G and Satellite Network Convergence: Survey for Opportunities, Challenges and Enabler Technologies”. In: Oct. 2020. DOI: 10.1109/NILES50944.2020.9257914.

[68] Inigo del Portillo, Bruce G. Cameron, and Edward F. Crawley. “A technical comparison of three low earth orbit satellite constellation systems to provide global broadband”. In: *Acta Astronautica* 159 (2019), pp. 123–135. ISSN: 0094-5765. DOI: https://doi.org/10.1016/j.actaastro.2019.03.040. URL: https://www.sciencedirect.com/science/article/pii/S0094576518320368.

[69] Sara Mohamed et al. “Design and Implementation of an ADCS for a CubeSat”. In: *Journal of Engineering Research* 7.Issue 2 (2023), pp. 15–21. ISSN: 2356-9441. DOI: 10.21608/erjeng.2023.197719.1160. eprint: https://erjeng.journals.ekb.eg/article_292905_785d31f10db8ca81cf7eb15157743b9a.pdf. URL: https://erjeng.journals.ekb.eg/article_292905.html.

[70] Fujian Ma et al. “Hybrid constellation design using a genetic algorithm for a LEO-based navigation augmentation system”. In: *GPS Solutions* 24 (Mar. 2020). DOI: 10.1007/s10291-020-00977-0.

[71] Jasper Bouwmeester. *PQ9 and CS14 Electrical and Mechanical Subsystem Interface Standard for PocketQubes and CubeSats*. Version V1. 2018. DOI: 10.34894/6MVBCZ.

[72] Alicia Johnstone. “CubeSat Design Specification”. In: vol. 14. 14.1. The CubeSat Program, Cal Poly SLO. 2022.

[73] Emanuele A. Slejko, Anna Gregorio, and Vanni Lughi. “Material selection for a CubeSat structural bus complying with debris mitigation”. In: *Advances in Space Research* 67.5 (2021), pp. 1468–1476. ISSN: 0273-1177. DOI: 10.1016/j.asr.2020.11.037.

[74] *Canisterized Satellite Dispenser, Payload Specification for 3U, 6U & 12U*. 2002367F. PSC by RocketLab. 2018.

[75] Ryan Hevner et al. “An Advanced Standard for CubeSats”. In: vol. SSC11-II-3. Annual AIAA/USU Conference on Small Satellites 25. AIAA/USU. 2011.

[76] *Falcon User’s Guide*. Space Exploration Corporation. Sept. 2021.

[77] Sedkyabdellah Tohamy and Amr Saddek. “Elastic buckling of steel box column under uniaxial compressive loads”. In: (Mar. 2015).

[78] Richard Abbott. *Analysis and Design of Composite and Metallic Flight Vehicle Structures*. Georgetown: Abbott Aerospace SEZC Ltd, 2019.

[79] S Van der Zwaag. *Lecture 8: Fatigue*. Lecture slides. Lecture series AE1108: Materials Science, Delft University of Technology. 2019.

[80] Salomons Metalen B.V. *Technische Gegevens Aluminium*. https://salomons-metalen.nl/datasheets/aluminium.pdf. 2021.

[81] George-Cristian Potrivitu et al. “A Review of Low-Power Electric Propulsion Research at the Space Propulsion Centre Singapore”. In: *Aerospace* 7.6 (2020). ISSN: 2226-4310. DOI: 10.3390/aerospace7060067.

[82] James J Szabo et al. “Characterization of a one hundred Watt, long lifetime Hall effect thruster for small spacecraft”. In: *53rd AIAA/SAE/ASEE Joint Propulsion Conference*. 2017, p. 4728.

[83] James Szabo et al. “Performance evaluation of an iodine-vapor Hall thruster”. In: *Journal of Propulsion and Power* 28.4 (2012), pp. 848–857.

[84] Moerel J.L.P.A. et al. “Development of Micro Propulsion System Technologies for Minisatellites in the Netherlands”. In: May 2008.

[85] Mirko Leomanni et al. “Propulsion options for very low Earth orbit microsatellites”. In: *Acta Astronautica* 133 (2017), pp. 444–454. ISSN: 0094-5765. DOI: 10.1016/j.actaastro.2016.11.001.

[86] *The iodine Satellite (iSAT) 7 th Annual Government CubeSat TIM 5/12/2015 John Dankanich Category A*.

[87] Kurt A Polzin et al. *Propulsion System Development for the Iodine Satellite (iSAT) Demonstration Mission*.

[88] Chan Yuk Chi, Indraji Ushantha Wanigaratne, and David Dubinsky. “HOW LOW CAN YOU GO: ADVOCATING VERY LOW EARTH ORBIT AS THE NEXT FRONTIER FOR SATELLITE OPERATIONS”. In: 8th European Conference on Space Debris (virtual), Darmstadt, Germany. 2021.

[89] Abid Murtaza et al. “Orbital debris threat for space sustainability and way forward”. In: *IEEE access* 8 (2020), pp. 61000–61019.

[90] Francesca Letizia and Stijn Lemmens. *ESA’S Annual Space Environment Report*. Tech. rep. European Space Agency, 2023.

[91] Yan Zhang et al. “An analysis of close approaches and probability of collisions between LEO resident space objects and mega constellations”. In: *Geo-spatial Information Science* 25.1 (2022), pp. 104–120.

[92] Thomas Cheney et al. “Planetary protection in the new space era: science and governance”. In: *Frontiers in Astronomy and Space Sciences* (2020), p. 90.

[93] JD Rummel et al. “COSPAR’s planetary protection policy: A consolidated draft”. In: *Advances in Space Research* 30.6 (2002), pp. 1567–1571.

[94] Flury Alby and Luciano Anselmo and. *European Code of Conduct for Space Debris Mitigation*. Tech. rep. United Nations Office for Outer Space Affairs, 2004.

[95] Martin Langer and Jasper Bouwmeester. “Reliability of cubesats-statistical data, developers’ beliefs and the way forward”. In: (2016).

[96] Barry Zandbergen. *AE1222-II: Aerospace Design & Systems Engineering Elements I - Spacecraft (bus/platform) design and sizing*. Tech. rep. TU Delft, 2020.

[97] Jean-Francois Castet and Joseph H Saleh. “Satellite and satellite subsystems reliability: Statistical data analysis and modeling”. In: *Reliability Engineering & System Safety* 94.11 (2009), pp. 1718–1728.

[98] Jean-Francois Castet and Joseph H Saleh. “Satellite reliability: statistical data analysis and modeling”. In: *Journal of Spacecraft and Rockets* 46.5 (2009), pp. 1065–1076.

[99] Andrew Tatsch, Norman Fitz-Coy, and Svetlana Gladun. “On-orbit servicing: A brief survey”. In: *Proceedings of the IEEE International Workshop on Safety, Security, and Rescue Robotics (SSRR’06)*. 2006, pp. 276–281.

[100] Reid R. et al Michael S. Matt B. “ALTAIR™ : Millennium’s DARPA SeeMe Satellite Solution Technical (R)evolution”. In: *28 th Annual AIAA/USU* (2014).